

**Characterising the association of CCR5  
with *Leishmania donovani* infection and  
the protein composition of the *Leishmania*-  
containing intracellular phagolysosome**

Christopher Saunders

Doctor of Philosophy

University of York  
Biology

September 2016

# Abstract

*Leishmania* parasites infect macrophages where they reside within phagolysosomal compartments but the mechanisms of entry and intracellular survival are not fully understood. The chemokine receptor CCR5 may facilitate *L. donovani* infection but whether this is through roles in individual macrophages or in coordinating the immune response is unclear. We aimed to determine the association between *L. donovani* LV9 amastigotes and CCR5 both *in vivo* and *in vitro* using an established infection model. We also performed comparative proteomics on isolated phagolysosomal compartments from cells infected with live and heat-inactivated (HI) parasites to better characterise the compartment and determine whether CCR5 was associated with it.

Parasite burden between mice and macrophages either possessing or lacking CCR5 did not differ. However, CCR5<sup>-/-</sup> mice had a transient decrease in leukocyte recruitment to hepatic granulomas. *In vitro*, we observed a dose- and contact-dependent *Leishmania*-specific reduction in CCR5 cell surface expression during a short time-course of infection. CCR5 decreases were maintained when using the antagonist ligand Met-RANTES. When combined with reductions seen in CCR5 mRNA levels, the cell surface decrease was likely caused by gene down-regulation rather than pure receptor internalisation.

*Leishmania* parasites were made magnetisable and then isolated from infected cells; we found that CCR5 was not associated with these compartments. Combined use of iTRAQ-labelled LC-MS/MS and mathematical techniques identified a number of protein groups differentially expressed on phagolysosomes isolated from cells infected with live or HI parasites, including those related to actin dynamics, phagosome maturation and intracellular signalling. Overall, these findings demonstrate that CCR5 has a subtle role in the immune response to *L. donovani* infection and give new insights into how the live parasite exploits its phagolysosomal compartment to fine-tune the host cell's response to infection.

# Table of Contents

<b>Abstract</b> .....	<b>2</b>
<b>Table of Contents</b> .....	<b>3</b>
<b>List of Figures</b> .....	<b>10</b>
<b>List of Tables</b> .....	<b>14</b>
<b>List of Accompanying Material</b> .....	<b>16</b>
<b>Acknowledgements</b> .....	<b>17</b>
<b>Author's declarations</b> .....	<b>18</b>
<b>1. INTRODUCTION</b> .....	<b>19</b>
<b>1.1 <i>Leishmania</i></b> .....	<b>19</b>
1.1.1 Leishmaniasis: a spectrum of clinical disease .....	19
1.1.2 The <i>Leishmania</i> lifecycle .....	20
1.1.3 <i>Leishmania donovani</i> .....	23
1.1.4 The immune response to <i>Leishmania</i> infection .....	24
<b>1.2 Chemokine receptors</b> .....	<b>27</b>
1.2.1 Definition and nomenclature .....	27
1.2.2 CCR5 expression and regulation .....	28
1.2.3 The differences between murine and human CCR5.....	32
1.2.4 The role of CCR5 during chronic inflammatory conditions and infections.....	34
1.2.5 The association between <i>Leishmania</i> and chemokine receptors .	36
<b>1.3 The <i>Leishmania</i>-containing intracellular compartment</b> .....	<b>39</b>
1.3.1 Endocytic pathway .....	39
1.3.2 Phagocytosis and the phagolysosome .....	42
1.3.3 Techniques used to characterise intracellular pathogen-containing compartments .....	44
1.3.4 Characterisation of the protein composition of the <i>Leishmania</i> - containing intracellular compartment .....	47

1.3.5 Functional roles of the <i>Leishmania</i> -containing intracellular compartment.....	50
<b>1.4 Project aims .....</b>	<b>51</b>
<b>2. GENERAL MATERIAL AND METHODS .....</b>	<b>54</b>
<b>2.1 Reagents, buffers and solutions.....</b>	<b>54</b>
<b>2.2 Antibodies .....</b>	<b>56</b>
<b>2.3 Tissue culture .....</b>	<b>58</b>
2.3.1 Cell lines .....	58
2.3.2 Cryopreservation of cells .....	58
<b>2.4 Primary cells, mice and parasites.....</b>	<b>59</b>
2.4.1 Mice .....	59
2.4.2 Genotyping of mice.....	59
2.4.3 Isolating bone marrow cells .....	59
2.4.4 Generating bone marrow-derived macrophages .....	60
2.4.5 Isolation of <i>Leishmania donovani</i> amastigote parasites .....	60
2.4.6 Culturing promastigote <i>Leishmania donovani</i> parasites .....	61
<b>2.5 Immunofluorescent imaging .....</b>	<b>61</b>
2.5.1 Preparation of coverslips .....	61
2.5.2 Immunofluorescent staining.....	61
2.5.3 Mounting of coverslips onto slides.....	62
2.5.4 Microscopy and image analysis.....	62
<b>2.6 Electron microscopy.....</b>	<b>62</b>
<b>2.7 Protein quantification.....</b>	<b>63</b>
<b>2.8 Western blotting .....</b>	<b>63</b>
2.8.1 SDS-PAGE .....	63
2.8.2 Membrane transfer.....	63
2.8.3 Membrane immunoblotting .....	64
<b>2.9 Flow cytometry .....</b>	<b>64</b>
2.9.1 Flow cytometry cell surface expression of CCR5 assay.....	64
2.9.2 Flow cytometry processing .....	64
2.9.3 Flow cytometry analysis.....	65
2.9.4 CFDA-SE labelling of cells.....	65
2.9.5 Transwell infection assay.....	65

2.9.6 Translocation infection assay.....	66
<b>2.10 Enzyme-linked immunosorbent assay (ELISA) .....</b>	<b>66</b>
<b>2.11 PCR.....</b>	<b>66</b>
2.11.1 DNA amplification by PCR.....	66
2.11.2 Agarose gel electrophoresis .....	67
2.11.3 qRT-PCR of mRNA levels.....	67
<b>2.12 Mass spectrometry.....</b>	<b>67</b>
2.12.1 In-gel deglycosylation and digestion .....	67
2.12.2 iTRAQ labelling and peptide fractionation .....	68
2.12.3 LC-MS/MS .....	69
2.12.4 Database searching .....	70
<b>2.12 Statistical analyses .....</b>	<b>70</b>
<b>3. THE EFFECT OF <i>L. DONOVANI</i> INFECTION ON CCR5</b>	
<b>EXPRESSION <i>IN VITRO</i> .....</b>	<b>71</b>
<b>3.1 Chapter-specific background and rationale .....</b>	<b>71</b>
3.1.1 Techniques available for investigating the role of chemokine receptors during infection.....	72
3.1.2 Objectives .....	74
<b>3.2 Chapter-specific methods .....</b>	<b>75</b>
3.2.1 Generating antibodies against murine CCR5 .....	75
3.2.1.1 Primer design and plasmid generation.....	75
3.2.1.2 Transforming bacteria with target plasmid.....	75
3.2.1.3 Protein production .....	76
3.2.1.4 Purifying GST-CCR5 recombinant proteins.....	76
3.2.1.5 Polyclonal antibody production in rabbits .....	76
3.2.1.6 Affinity purification of anti-CCR5 antibodies .....	77
3.2.2 Culturing <i>E. coli</i> and <i>R. equi</i> for infection assay .....	77
3.2.3 CCR5 blockade using Met-RANTES .....	77
<b>3.3 Results.....</b>	<b>79</b>
<b>3.3.1 Characterising the parasite preparation.....</b>	<b>79</b>
<b>3.3.2 Genotyping of wild-type and CCR5<sup>-/-</sup> mice .....</b>	<b>82</b>
<b>3.3.3 Testing of available murine CCR5 antibodies.....</b>	<b>82</b>

3.3.3.1	Flow cytometry for CCR5 expression .....	82
3.3.3.2	Immunofluorescent staining for murine CCR5 .....	85
3.3.3.3	Western blotting for murine CCR5.....	85
<b>3.3.4</b>	<b>Making an anti-mouse CCR5 antibody .....</b>	<b>85</b>
3.3.4.1	Making GST-CCR5 recombinant proteins for injection into rabbits .....	88
3.3.4.2	Testing and purifying anti-CCR5 antibody .....	88
<b>3.3.5</b>	<b>Cell surface CCR5 expression during <i>L. donovani</i> infection .</b>	<b>91</b>
3.3.5.1	Live <i>L. donovani</i> parasites induce a greater decrease in CCR5 cell surface expression compared to heat-inactivated parasites .....	91
3.3.5.2	Decrease in CCR5 cell surface expression is dose- dependent and specific to <i>L. donovani</i> .....	93
3.3.5.3	Direct contact with an intact parasite is necessary.....	95
3.3.5.4	Chemokine response in <i>L. donovani</i> -infected cells .....	97
<b>3.3.5</b>	<b>CCR5 mRNA levels for J774.2 cells infected with <i>L. donovani</i> amastigotes .....</b>	<b>98</b>
<b>3.4</b>	<b>Chapter-specific discussion.....</b>	<b>102</b>

<b>4. THE EFFECT OF CCR5<sup>-/-</sup> ON <i>L. DONOVANI</i> INFECTION <i>IN VIVO</i> .....</b>	<b>109</b>
<b>4.1 Chapter-specific background and rationale .....</b>	<b>109</b>
4.1.1 CCR5 <sup>-/-</sup> mice .....	109
4.1.2 Objectives .....	112
<b>4.2 Chapter-specific methods .....</b>	<b>113</b>
4.2.1 Wild-type and CCR5 <sup>-/-</sup> mice infections .....	113
4.2.2 Chimera generation and infection .....	113
4.2.3 Preparation of liver and spleen material .....	113
4.2.4 Calculating parasite burden using Leishman Donovan Units .....	114
<b>4.3 Results.....</b>	<b>115</b>
<b>4.3.1 Wild-type vs CCR5<sup>-/-</sup> experiments .....</b>	<b>115</b>
4.3.1.1 Repeating experiments with tdTomato <i>L. donovani</i> parasites .....	119

4.3.1.2 Detailed screening of splenic cell populations.....	119
<b>4.3.2 Chimera experiments .....</b>	<b>123</b>
4.3.2.1 Experimental overview .....	124
4.3.2.2 Weights and LDUs.....	124
4.3.2.3 Immunofluorescent analyses.....	124
<b>4.3.4 Wild-type vs CCR5<sup>-/-</sup> BMDM infection rates .....</b>	<b>127</b>
<b>4.4 Chapter-specific discussion.....</b>	<b>132</b>

<b>5. ISOLATING INTRACELLULAR <i>L. DONOVANI</i>-CONTAINING COMPARTMENTS FOR QUALITATIVE PROTEOMIC MEMBRANE CHARACTERISATION .....</b>	<b>139</b>
<b>5.1 Chapter-specific background and rationale .....</b>	<b>139</b>
5.1.1 Objectives .....	141
<b>5.2 Chapter-specific methods .....</b>	<b>142</b>
5.2.1 Assessing parasite viability .....	142
5.2.2 Colloidal iron dextran (FeDex) production .....	142
5.2.3 Lysosome isolation .....	143
5.2.4 $\beta$ -hexosaminidase assay .....	143
5.2.5 Protocol for parasite isolation.....	144
5.2.6 Nitric oxide production .....	144
5.2.7 Determining subcellular localisation of proteins.....	145
<b>5.3 Results.....</b>	<b>146</b>
<b>5.3.1 Isolating lysosomes from uninfected cells .....</b>	<b>146</b>
5.3.1.1 Isolation of lysosomes .....	146
5.3.1.2 Proteomic data from isolated lysosomes.....	146
<b>5.3.2 Isolating parasite-containing compartments from infected cells .....</b>	<b>148</b>
5.3.2.1 Making magnetisable <i>Leishmania</i> parasites .....	150
5.3.2.2 Optimising the isolation of <i>L. donovani</i> -containing compartments.....	155
5.3.2.3 Qualitative proteomic characterisation of isolated parasite-containing compartments .....	162
<b>5.4 Chapter-specific discussion.....</b>	<b>171</b>

<b>6. QUANTITATIVE PROTEOMIC CHARACTERISATION OF THE PARASITE-CONTAINING COMPARTMENT.....</b>	<b>178</b>
<b>6.1 Chapter-specific background and rationale .....</b>	<b>178</b>
6.1.1 Quantitative proteomics .....	178
6.1.2 Exploring high dimensional proteomic datasets .....	180
6.1.3 Objectives .....	186
<b>6.2 Chapter-specific methods .....</b>	<b>187</b>
6.2.1 Gene Ontology annotation of biological processes .....	187
6.2.2 Statistics.....	187
6.2.3 Pathway and network analyses .....	187
<b>6.3 Results.....</b>	<b>189</b>
<b>6.3.1 Summary of iTRAQ-labelled samples .....</b>	<b>189</b>
6.3.1.1 iTRAQ-labelling of samples .....	189
6.3.1.2 Global analysis of identified proteins .....	191
<b>6.3.2 Data pre-processing .....</b>	<b>191</b>
<b>6.3.3 Hierarchical cluster analysis shows clear differentiation between live and heat-inactivated samples .....</b>	<b>196</b>
<b>6.3.4 Initial exploration of datasets using principal component analysis.....</b>	<b>196</b>
<b>6.3.5 Univariate comparisons between live and heat-inactivated parasite-fed compartments.....</b>	<b>206</b>
<b>6.3.6 Analysing proteins based on subcellular location .....</b>	<b>208</b>
<b>6.3.7 Global characterisation of the parasite-containing compartment.....</b>	<b>210</b>
6.3.7.1 IPA analysis of proteins.....	213
6.3.7.2 Differentially expressed canonical pathways.....	213
<b>6.3.8 Relevant dynamic protein networks .....</b>	<b>216</b>
<b>6.4 Chapter-specific discussion.....</b>	<b>220</b>
<b>7. GENERAL DISCUSSION .....</b>	<b>235</b>
<b>7.1 The parasite-containing compartment as a signalling platform.</b>	<b>237</b>
<b>7.2 Active manipulation of intracellular processes by the live parasite .....</b>	<b>239</b>



7.3 Balance at the host-pathogen interface .....	241
7.3 Fine-tuning, rather than dramatic shifts, in host cell processes	243
7.3 Future directions .....	244
7.4 Concluding remarks.....	248
<b>APPENDIX A: CCR5<sup>-/-</sup> mice.....</b>	<b>249</b>
<b>APPENDIX B: Detailed analysis of splenic populations from infected cells.....</b>	<b>250</b>
<b>APPENDIX C: Dynamic networks generated by IPA.....</b>	<b>252</b>
<b>ABBREVIATIONS.....</b>	<b>257</b>
<b>REFERENCES.....</b>	<b>263</b>

# List of Figures

<b>FIGURE 1.1</b> The lifecycle of the <i>Leishmania</i> parasite .....	21
<b>FIGURE 1.2</b> Schematic representation of the differences in primary structure between murine and human CCR5.....	29
<b>FIGURE 1.3</b> Schematic representation of the endocytic trafficking and degradation pathways for agonist-stimulated CCR5.....	31
<b>FIGURE 1.4</b> Schematic representation of the process of endocytosis and phagocytosis .....	40
<b>FIGURE 1.5</b> Summary of our current understanding of the proteins comprising the <i>Leishmania</i> -containing intracellular compartment and its interaction with other organelles .....	49
<b>FIGURE 3.1</b> Within parasite preparations, host cell membranes can be found both surrounding parasites and freely in suspension.....	80
<b>FIGURE 3.2</b> Membranes surrounding parasites are LAMP1+ve and significantly reduced after leaving parasites in culture overnight.....	81
<b>FIGURE 3.3</b> Absence of CCR5 expression at the gene and protein level in CCR5 <sup>-/-</sup> macrophages .....	83
<b>FIGURE 3.4</b> Characterising three monoclonal antibodies against murine CCR5 .....	84
<b>FIGURE 3.5</b> Assessing antibodies available to track murine CCR5 expression and localisation in mouse cells .....	86
<b>FIGURE 3.6</b> The design of the vector used to produce GST-CCR5 recombinant proteins.....	87
<b>FIGURE 3.7</b> GST-CCR5 recombinant proteins were successfully produced	89
<b>FIGURE 3.8</b> Mouse CCR5 was not detected via western blotting using new rabbit antibodies.....	90
<b>FIGURE 3.9</b> CCR5 cell surface expression decreased with <i>L. donovani</i> infection over a 48 hr time-course of infection .....	92
<b>FIGURE 3.10</b> Decrease in CCR5 cell surface expression is dose-dependent and specific to <i>L. donovani</i> .....	94

<b>FIGURE 3.11</b> Decrease in CCR5 cell surface expression required direct contact of intact <i>L. donovani</i> parasites.....	96
<b>FIGURE 3.12</b> The secretion of CCR5 specific chemokines was altered in <i>L. donovani</i> -infected J774.2 cells but blocking CCR5 did not inhibit the decrease seen with <i>L. donovani</i> .....	99
<b>FIGURE 3.13</b> mRNA levels of CCR5 were decreased at 24 hr in cells infected with <i>L. donovani</i> LV9 amastigotes compared to non-infected control cells .....	100
<b>FIGURE 4.1</b> Overview of CCR5 <sup>-/-</sup> vs control wild-type (CCR5 <sup>+/+</sup> ) infection experiments.....	116
<b>FIGURE 4.2</b> Lack of CCR5 does not influence parasite burden during <i>in vivo</i> infection with <i>L. donovani</i> LV9 amastigotes .....	117
<b>FIGURE 4.3</b> Overall time-course summaries of the LDU counts and organ weights in wild-type and CCR5 <sup>-/-</sup> mice during <i>L. donovani</i> LV9 amastigote infection.....	118
<b>FIGURE 4.4</b> Method used for granuloma quantification .....	120
<b>FIGURE 4.5</b> CCR5 <sup>-/-</sup> mice showed subtle differences in granuloma scores at day 28 post-infection .....	121
<b>FIGURE 4.6</b> The same results for organ weight, parasite burden and granuloma formation at day 28 were seen when infections used tdTomato <i>L. donovani</i> amastigotes .....	122
<b>FIGURE 4.7</b> Overview of chimera experiments .....	125
<b>FIGURE 4.8</b> Overall summary of parasite burdens in chimeric mice.....	126
<b>FIGURE 4.9</b> Appearance of infection foci in liver sections taken from chimeric mice.....	128
<b>FIGURE 4.10</b> There was no difference in the uptake of <i>L. donovani</i> parasites by macrophages either possessing or lacking CCR5 .....	129
<b>FIGURE 4.11</b> There was no difference in infection rates between wild-type and CCR5 <sup>-/-</sup> BMDMs infected with <i>L. donovani</i> .....	131
<b>FIGURE 5.1</b> Lysosomes can be isolated from J774.2 cells .....	147
<b>FIGURE 5.2</b> Not all dextran-filled compartments contain <i>L. donovani</i> parasites.....	149

<b>FIGURE 5.3</b> Magnetisable <i>L. donovani</i> parasites can be retained within a magnetic field .....	151
<b>FIGURE 5.4</b> Parasites survive exposure to FeDex and have unaltered infection uptake and intracellular survival .....	152
<b>FIGURE 5.5</b> FeDex likely binds to the outer surface of <i>L. donovani</i> amastigote parasites .....	154
<b>FIGURE 5.6</b> Analysis of mouse proteins identified from each sample preparation for preliminary rounds of unlabelled LC-MS/MS .....	158
<b>FIGURE 5.7</b> Alteration of the lysosome isolation technique can be used to isolate the parasite-containing compartment .....	160
<b>FIGURE 5.8</b> The total mouse proteins identified from each sample preparation (either using live or heat-inactivated parasites) for preliminary proteomics round C.....	161
<b>FIGURE 5.9</b> Summary of proteins identified from four samples made using the final parasite-containing compartment isolation protocol .....	163
<b>FIGURE 5.10</b> The majority of mouse proteins were found in all 4 samples for both live and heat-inactivated preparations, and those that were not were predominately low abundance proteins represented by a low number of peptide identifications.....	165
<b>FIGURE 5.11</b> Live <i>Leishmania</i> parasites were able to attenuate nitric oxide production by J774.2 cells.....	168
<b>FIGURE 6.1</b> Quantitative summary of the peptides identified using iTRAQ-labelled LC-MS/MS on 4 live and 4 heat-inactivated phagolysosome preparations .....	190
<b>FIGURE 6.2</b> Summary of protocol used for data pre-processing to facilitate valid comparison between samples .....	194
<b>FIGURE 6.3</b> Data pre-processing was required to prevent high abundance proteins from dominating the samples .....	195
<b>FIGURE 6.4</b> After normalisation and scaling, live and heat-inactivated (HI) preparations differentiated into two distinct clusters .....	197
<b>FIGURE 6.5</b> Exploratory data analyses showed differentiation along principal component 1 for live and heat-inactivated samples.....	198

<b>FIGURE 6.6</b> The PLS model could correctly predict the class of the live and heat-inactivated preparation from sample 4.....	200
<b>FIGURE 6.7</b> Several proteins disproportionately represented the variation seen between live and heat-inactivated (HI) parasite intracellular compartments .....	202
<b>FIGURE 6.8</b> There was greater differentiation between samples when phagolysosomal and 'other' proteins were explored separately .....	209
<b>FIGURE 6.9</b> A number of interconnected canonical pathways were represented within the parasite-containing compartment samples .....	214
<b>FIGURE 6.10</b> Protein groups relating to phagocytosis, cytoskeleton signalling, protein translation and metabolism were well represented and differentially expressed between live and HI parasite-containing compartments .....	215
<b>FIGURE 6.11</b> Proteins related to phagosome maturation had lower expression in live parasite-containing compartment samples.....	217
<b>FIGURE 6.12</b> The two most biologically relevant networks generated by IPA were related to actin cytoskeletal dynamics and transporters .....	219
<b>FIGURE 7.1</b> Schematic representation of the overall effects that infection with live <i>L. donovani</i> LV9 amastigotes had on J774.2 cells.....	236
<b>FIGURE A1</b> Strategy adopted by Kuziel et al. 2003 to make CCR5 <sup>-/-</sup> mice	249

# List of Tables

<b>TABLE 2.1</b> Composition of buffers and solutions used in this project.....	54
<b>TABLE 2.2</b> Primary and secondary antibodies and isotype controls used in this project.....	56
<b>TABLE 4.1</b> The overall effect of CCR5 <sup>-/-</sup> on <i>L. donovani</i> LV9 amastigote infection <i>in vivo</i> was minimal with the only difference observed being a transient difference in liver granuloma progression .....	132
<b>TABLE 5.1</b> The only treatment found to fully inhibit the ability of amastigote <i>L. donovani</i> parasites to transform into promastigotes was heat inactivation at 56°C for 30 minutes .....	156
<b>TABLE 5.2</b> Proteins identified in all 4 live samples that were either entirely absent from heat-inactivated samples or only present in one sample .....	166
<b>TABLE 5.3</b> Proteins identified in all 4 heat-inactivated samples that were either entirely absent from live samples or only present in one sample .....	169
<b>TABLE 6.1</b> Overall biological processes of proteins represented within <i>L. donovani</i> -containing compartments .....	192
<b>TABLE 6.2</b> Proteins (identified from either any number of peptides or at least 2 peptides) contributing to the greatest variation between the live and heat-inactivated parasite samples, as determined by principal component analysis (PCA) .....	203
<b>TABLE 6.3</b> Proteins (identified with 3 or more peptides) contributing to the greatest variation between the live and heat-inactivated parasite samples, as determined by PCA .....	204
<b>TABLE 6.4</b> Individual proteins with statistically significant differences between live and heat-inactivated (HI) parasite-fed compartments .....	207
<b>TABLE 6.5</b> Phagolysosomal-specific proteins (identified with ≥2 peptides) contributing to the greatest variation between the live and heat-inactivated parasite samples, as determined by PCA .....	211

**TABLE 6.6** Proteins (identified with  $\geq 2$  peptides) categorised as 'other' for subcellular localisation contributing to the greatest variation between the live and heat-inactivated parasite samples, as determined by PCA ..... 212

# List of Accompanying Material

## **DVD** (*attached to back of thesis*)

### **./Curated lists of proteins**

Lists of proteins that were literature searched to identify their subcellular location.

### **./LC-MSMS data**

Raw data for all unlabelled LC-MS/MS analyses. iTRAQ-labelled data is provided as raw and preprocessed (normalised) data.

### **./Scripts**

The C code used for preprocessing and Python script used for checking subcellular locations was written by Dr Julie Wilson (University of York).

### **./Thesis**

An electronic version of this thesis.



# Acknowledgements

I would like to thank all of my supervisors (Dr Nathalie Signoret, Dr Paul Pryor and Dr Julie Wilson) for their support and guidance over the course of my PhD. I am particularly grateful for your help in developing my critical analysis skills, for helping me develop as a person, and for telling me to be concise.

I am thankful to the Wellcome Trust for funding my PhD and providing opportunities for personal development, and Prof Paul Kaye and Dr Sean Sweeney as members of my thesis advisory panel for helping to guide my research.

I am also grateful to the many other people who have helped me over the last four years with special mention needed for: Dr Naj Brown, for help with *in vivo* experiments; Dr Adam Dowle, for help with proteomic data acquisition; Dr James Hewitson, for informative discussions; Dr Pegine Walrad and Dr Luis Miguel de Pablos, for guidance with promastigote work; Dr Allison Green, for advice for bone marrow-derived macrophage work; Dr Ana Pinto, Dr Olivier Preham and Dr Johannes Doehl, for advice and help with parasite work; Dr Helen Ashwin and Dr Rebecca Wiggins, for general help and advice; members of the Pryor and Signoret groups past and present who have been good friends; Daniel Yee, for guidance with qRT-PCR; and members of the Technology Facility for general guidance and support.

Most importantly, I thank my partner Jenny and daughter Emily, both of who have been understanding and supportive throughout my PhD even when this required sacrificing time together.

## Author's declarations

All data presented in this thesis are original and have not previously been presented for an award at this or any other university. All work was performed by Christopher Saunders, with the following exceptions (clearly stated in the text):-

- In Chapter 3, rabbit polyclonal antibodies were made against the N- and C-terminal GST recombinant proteins using a third party provider (Dundee Cell Products, UK). Another researcher of the Pryor laboratory (Adam Rofe) supplied *Rhodococcus equi* for one experiment.
- In Chapter 4, injection of *L. donovani* amastigotes into mice and the production of chimeric mice with mixed populations of bone marrow cells was performed by Dr Naj Brown (University of York). The screening of splenic cell populations was performed by Dr James Hewitson (University of York).
- In Chapter 6, the C code used for pre-processing and Python script used for checking subcellular locations was written by Dr Julie Wilson (University of York).
- Processing for electron microscopy and mass spectrometry was performed using the University of York Biology Department's in-house Technology Facility.

# 1. Introduction

## 1.1 *Leishmania*

Protozoan parasites of the genus *Leishmania* are unicellular eukaryotes of the Kinetoplastida order, so called because of the presence of an extensive mass of mitochondrial DNA (the 'kinetoplast') that can be easily identified under a light microscope after staining. *Leishmania* are dimorphic organisms with both a long flagellated promastigote form and short flagellated (sometimes incorrectly referred to as 'aflagellated') amastigote form. There are six major *Leishmania* species: *Leishmania donovani*, *L. major*, *L. mexicana*, *L. amazonensis*, *L. braziliensis* and *L. infantum* (Kaye & Scott 2011), but there are at least 20 different species of clinical importance that can infect human macrophages resulting in a range of symptoms, from minor self-resolving cutaneous lesions to potentially fatal visceral disease.

### 1.1.1 Leishmaniasis: a spectrum of clinical disease

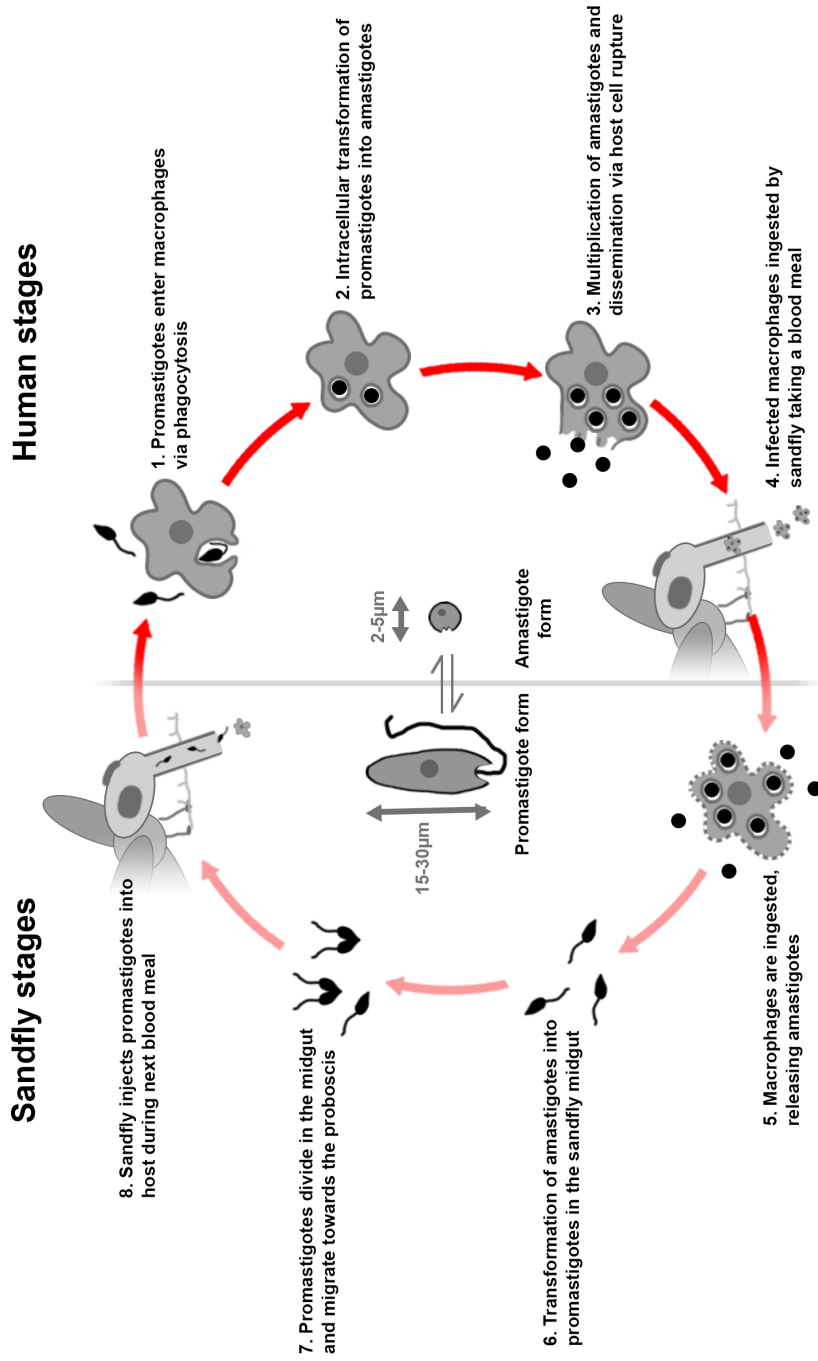
The leishmaniasis spectrum of disease has a prevalence of 12 million cases and an incidence of 1-2 million new cases per year across 98 countries and 5 continents (Alvar et al. 2012), causing significant morbidity and approximately 50,000 deaths per annum. After malaria, leishmaniasis has the highest mortality among all parasitic diseases (Pace 2014). Despite this, it has been largely neglected by policy-makers because of the complex ecology of the parasite, the lack of effective clinical screening and treatments and incomplete information on the disease's epidemiology (Alvar et al. 2012). This has led the World Health Organization to define it as a "neglected tropical disease" to highlight the impact and severity that this understudied disease has on some of the world's least economically developed countries (Feasey et al. 2010).

There are several different clinical manifestations of leishmaniasis. The most common is called cutaneous leishmaniasis (CL), primarily caused by *L.*

*major*, *L. mexicana*, *L. tropica*, *L. amazonensis* and *L. braziliensis*, and is characterised by ulcerative lesions forming on the skin. Up to 75% of the cases of CL are found within Syria, Afghanistan and Brazil (Savoia 2015). Although not lethal, these disfiguring scars are associated with social stigma and considerable psychological stress for the individual (Kassi et al. 2008). Diffuse mucocutaneous leishmaniasis has widespread destruction of oro-naso-pharyngeal tissues and occurs mainly in South America with up to 35,000 cases occurring annually (Pace 2014). Visceral leishmaniasis, caused by *L. donovani* and *L. infantum* (known as *L. chagasi* in South America) affects internal organs such as the spleen, liver and bone marrow and there are up to 400,000 cases worldwide (Pace 2014). Mainly affecting young children, the disease is associated with severe wasting, multi-organ failure, haemorrhagic diathesis, opportunistic infections and ultimately death. The vast majority of these cases occur in India, Ethiopia, Brazil, Sudan and Bangladesh, where mortality is up to 20% (Savoia 2015). The disease is often accompanied by post kala-azar dermal leishmaniasis, a post-infection chronic dermatosis that can occur years after the initial infection has been treated. There are as yet no effective and safe vaccines available to prevent leishmaniasis so current interventions focus on treating the disease. These treatments include pentavalent antimonials, miltefosine and amphotericin B, the latter of which is now the treatment of choice in most regions. However, treatment is often expensive and becoming increasingly ineffective due to the spread of drug resistance (Moradin & Descoteaux 2012), highlighting the importance of finding new therapeutic targets.

### **1.1.2 The *Leishmania* lifecycle**

Although our current understanding of the host-pathogen interaction is incomplete, the lifecycle of the dimorphic *Leishmania* parasite has been well characterised (**Figure 1.1**). Parasites enter the human host when a female sand fly (*Phlebotomus* species (spp.) and *Lutzomyia* spp.) inoculates infective non-dividing metacyclic promastigotes into the dermis. Once transmitted, they are phagocytosed by macrophages (McCall et al. 2013). Although the macrophage is their primary target, other cell types can be



**FIGURE 1.1. The lifecycle of the *Leishmania* parasite.** Infective non-dividing metacyclic promastigotes enter macrophages via phagocytosis (1), where they transform into the intracellular amastigote form (2). Amastigotes reside and multiply within the phagolysosomal compartment of macrophages before dissemination and infection of vicinal macrophages (3). When a sand fly takes a blood meal, infected macrophages are transferred to the insect vector (4) where they break down and release their parasites (5). These parasites then transform into procyclic promastigotes and reside in the sand fly midgut (6). Parasites then transform into metacyclic promastigotes and can be found in the sand fly proboscis (7). During the sand fly's next blood meal, metacyclic promastigotes are transferred into a new host to complete the cycle (8). Adapted from an image by the Centers for Disease Control and Prevention Division of Parasitic Diseases (2015).

infected with *Leishmania* parasites, including fibroblasts, monocytes and dendritic cells (Kaye & Scott 2011). In macrophages, phagocytosis is thought to be initiated either by the opsonised parasites using the Fc and complement receptors (Ueno & Wilson 2012), or the parasite displaying phosphatidylserine (PS) and gaining access to the cell via the PS receptor (Leary et al. 2000; de Freitas Balanco et al. 2001; Wanderley et al. 2006), although the exact mechanisms of intracellular entry are still unknown. Indeed, many other receptors have been implicated in *Leishmania* phagocytosis, including mannose receptors (Ueno & Wilson 2012). In reality, this could reflect a complex multi-receptor system for parasite internalisation or that the parasite is able to utilise a number of different receptors with differing efficiency of uptake.

Once inside the macrophage, promastigote parasites differentiate to the amastigote form, a process which begins within hours of phagocytosis but can take much longer to complete (De Pablos et al. 2016). During this process, the flagellum undergoes significant remodelling with the structure changing from having 9-fold microtubule symmetry with two microtubules in the core (9 + 2) into a 9 + 0 structure through disassembly of the central pair of microtubules (Wheeler et al. 2015). The flagellum is also considerably shortened until it is almost completely contained within the flagellar pocket with only a small portion exposed to the contents of the parasite-containing compartment (Gluenz et al. 2010). The presence of this shortened flagellum in contact with host cell contents has led to suggestions that it could be ideally placed to function as a sensory organelle with key roles in the host-parasite interaction (Gluenz et al. 2010), and is consistent with the sensory and signalling roles found with 9 + 0 axonemes in eukaryotic cells (Gerdes et al. 2009). During this transformation process, amastigotes proceed to their terminal compartment widely believed to be the acidic and hydrolase-rich phagolysosome (Kaye & Scott 2011; Liévin-Le Moal & Loiseau 2016). It is thought that the lipophosphoglycan (LPG) on the promastigote's outer surface gets transferred to the phagosomal membrane (Winberg et al. 2009) and restricts the fusion of the parasite-containing compartment with late endosomal compartments, perhaps giving the promastigote time to

differentiate into the amastigote form, which is more suited to the acidic and hydrolase-rich intraphagolysosomal environment (reviewed by Liévin-Le Moal & Loiseau 2016). Once inside the phagolysosome, *Leishmania* parasites multiply and destroy the host cell resulting in the dissemination of amastigotes throughout the vascular and lymphatic system. More recently, this process of parasite egression has been suggested to be mediated by macrophage extrusions, with parasites being transferred to surrounding recipient macrophages in zeiotic structures from donor macrophages undergoing imminent apoptosis (Real et al. 2014). This could help parasites avoid the host immune system because they are surrounded by host cell components throughout the transfer process.

When the sand fly next takes a blood meal from an infected host, parasitised macrophages present in the skin or circulation can infect the insect to continue the cycle. Within the insect host, they differentiate into their dividing non-infective procyclic promastigote form and attach to the sand fly midgut epithelium to avoid being excreted. Through the process of metacyclogenesis, they then differentiate into the mammalian-infective metacyclic promastigote form that detaches from epithelial cells and migrates towards the anterior end of the sand fly's digestive tract where it can be transferred into the next mammalian host during the sand fly's subsequent blood meal (reviewed by Dostálová & Volf 2012).

### **1.1.3 *Leishmania donovani***

The differences between individual *Leishmania* species are still relatively unknown despite the strikingly different pathologies induced by each. *L. donovani* parasites form single, tight-forming compartments rather than the multi-parasite containing compartments of species such as *L. mexicana*. Visceralising species of *Leishmania* can also readily grow at the 37°C found within internal organs, in contrast to *L. mexicana* and *L. panamensis* where such temperatures can kill parasites (Gupta et al. 2001). *L. donovani* parasites were also shown to elicit a relatively subdued immune response during early infection compared to *L. major* (Matte & Olivier 2002). Indeed,

macrophages infected with *L. donovani* have unique gene expression profiles compared to other species of *Leishmania* (Gregory et al. 2008), showing that different species can induce distinct macrophage responses. Despite this, much of our understanding of individual species is extrapolated from a number of different *Leishmania* species, with the molecular mechanisms unique for each species currently unknown.

This is complicated further by the observation that within the *L. donovani* species, there are distinct strains found in different regions of the world. For example, LV9 and 1S are common strains in East Africa whereas the AG83 strain originated in India. Although each of the *L. donovani* strains are broadly similar, studies have found that there are differences between the overall infection kinetics for each (Ghosh et al. 1998; Basu et al. 2007). Furthermore, the genomic profile of *L. donovani* shows significant intraspecies variation (El Tai et al. 2001). This could manifest as phenotypical variation as has been seen for *L. infantum*, which has intraspecies differences in surface LPG (Coelho-Finamore et al. 2011).

#### **1.1.4 The immune response to *Leishmania* infection**

Intracellular parasitism, particularly within cells of the immune system, is a common strategy utilised by pathogenic viruses, bacteria and protozoan parasites to hide from host defenses. Whilst this strategy is used successfully by *Leishmania* parasites, it is important to note that the host immune system is still able to mount a response to the parasite. The overall response to *Leishmania* infection depends on host, vector and parasite determinants that work together to influence the immune response and overall clinical manifestation (McCall et al. 2013). This response is often orchestrated by differential secretion profiles of cytokines, which are small molecules involved in cell signalling that play an important role in allowing cells to coordinate immune responses and signal sites of infection.

The literature for the immunological response mounted against *Leishmania* during infection often has conflicting data, in part due to different *Leishmania*



species, different host species or different tissues being examined (for example, footpad versus ear). For many species of *Leishmania*, infection in mice brings about a number of immune responses and is a careful balance between type 1 T helper (Th1) cell-mediated protection and type 2 (Th2) disease susceptibility (Sacks & Noben-Trauth 2002; Tripathi et al. 2007; McCall et al. 2013). For cutaneous *Leishmania* species, mice with a prominent Th1 response to parasitic challenges characterised by high levels of interferon- $\gamma$  (IFN- $\gamma$ ) develop a resistant phenotype to *Leishmania* infection, whereas mice with a prominent Th2 response associated with high levels of interleukin (IL)-4 are susceptible to infection (reviewed by Maspi et al. 2016). However, for visceralising *Leishmania* species, such as *L. donovani*, this Th1/Th2 dichotomy does not seem to be as influential because the Th1 response is significantly suppressed by parasite-induced production of IL-10 and transforming growth factor  $\beta$  (TGF- $\beta$ ) (Somanna et al. 2002; Tripathi et al. 2007; Kaye & Scott 2011). This was demonstrated by Kaye et al. (1991) who showed that adjusting the production of Th1 and Th2 cytokines in murine visceral leishmaniasis does not control the rate of cure.

After initial infection, the release of chemokines such as CC-chemokine ligand (CCL) 3, 4 and 5 is thought to facilitate the recruitment of natural T regulatory (nTreg) cells to infection foci (Yurchenko et al. 2006). With the onset of chronicity, these cluster of differentiation (CD)4<sup>+</sup> CD25<sup>+</sup> IL-10-producing nTreg cells, which preferentially express C-C chemokine receptor type 5 (CCR5), begin to accumulate at the sites of infection and suppress the Th1 anti-parasitic response (Yurchenko et al. 2006). The mechanisms by which IL-10 is able to support parasite persistence are unclear, although Yurchenko et al. (2006) suggest that it may be due to the ability of IL-10 to reactivate macrophages and make them unresponsive to IFN- $\gamma$ . These cells, either alone or in the presence of effector T cells, secret or induce the production of more chemokines that in turn recruit further nTreg cells to areas of infection (Yurchenko et al. 2006). This response is thought to be the major immunosuppressive mechanism involved in visceral leishmaniasis (McCall et al. 2013).

In contrast, Th2 responses (such as IL-4 and IL-13) have been described as possessing a protective role during *L. donovani* infection (reviewed by Jain & Jain 2014). At the same time, infected macrophages release small amounts of IL-12 that help to promote the Th1 response (Afonso et al. 1994; Engwerda et al. 1998; McCall et al. 2013). The importance of this feedback mechanism was highlighted by the observation that mice immunised with *Leishmania* antigens alone established a parasite-susceptible phenotype, whereas those also given IL-12 developed a parasite-resistant Th1 response (Afonso et al. 1994). Other cytokines produced by antigen-presenting cells help to support the Th1 response, such as TNF- $\alpha$  and IFN- $\alpha/\beta$ , which help to clear parasites by activating macrophages and stimulating nitric oxide production (Tripathi et al. 2007; McCall et al. 2013).

Although *Leishmania*-specific immunity is predominately facilitated by T cells (Tripathi et al. 2007), the actual destruction of parasites is controlled by macrophages. Normally, recruitment of macrophages, as the main target cell for *Leishmania* infection, is crucial for parasite persistence and survival. With the expansion of Th1 IFN- $\gamma$ -producing effector CD4<sup>+</sup> CD25<sup>-</sup> T cells (Yurchenko et al. 2006), there is an increase in local concentrations of IFN- $\gamma$ . This stimulates nitric oxide production, a critical component of the anti-parasitic machinery present within phagocytes, but also causes more monocytes/macrophages to migrate into the area (Kaplan et al. 1989). However, *L. donovani* parasites have been shown to suppress host macrophage responses to IFN- $\gamma$  (McMahon-Pratt & Alexander 2004), thereby promoting parasite persistence and the emergence of chronic infection.

At the macroscopic level, the immune response to *Leishmania* infection in the liver is characterised by the formation of granulomas. These anatomically circumscribed functional structures help to contain and eliminate invading *Leishmania* parasites but can also result in considerable destruction of the local hepatic tissue architecture. These structures largely consist of CD4<sup>+</sup> and CD8<sup>+</sup> T cells and blood monocytes surrounding a core of infected liver macrophages (Kupffer cells) (Murray 2001). These cells are recruited to infection foci through the sustained release of endogenous cytokines,

principally IL-12, IL-2, IFN- $\gamma$  and tumour necrosis factor (TNF), the latter two of these cytokines also helping to activate incoming Kupffer cells and stimulate leishmanicidal nitric oxide production (Jain & Jain 2014), as described previously. Over time, these structures start to impinge on the surrounding hepatocytes and the size of the granuloma increases leading to liver enlargement and dysfunction. The final outcome of whether the parasite is cleared or persists within these structures relies on host and parasite determinants, in particular whether the recruited cells are present within an appropriate cytokine milieu to potentiate antimicrobial activity (Murray 2001; Jain & Jain 2014).

## **1.2 Chemokine receptors**

### **1.2.1 Definition and nomenclature**

The chemokine signalling system consists of an important family of cell surface receptors that are involved in the trafficking of leukocytes, as well as angiogenesis, haemopoiesis and development (Bachelierie et al. 2014). First discovered in the seventies (Walz et al. 1977), chemotactic polypeptides called chemokines (for chemotactic cytokines) have since been classified based on the arrangement of their first two cysteine residues: either CXC ( $\alpha$ ), CC ( $\beta$ ), C ( $\gamma$ ), or CX<sub>3</sub>C ( $\delta$ ), or a single conserved N-terminal cysteine for XC (Bachelierie et al. 2014). Chemokine receptors, which belong to the superfamily of seven transmembrane domain-spanning G protein-coupled receptors (GPCRs), are the effector targets of secreted chemokines and are primarily involved in immune cell recruitment via the process of chemotaxis, triggering directed cell movement up a chemokine gradient towards the source of release. Chemokine receptors are broadly classified as homeostatic or inflammatory based on whether they have a role in basal leukocyte trafficking or in guiding leukocytes to sites of inflammation, respectively. With each chemokine receptor having a unique spatiotemporal expression profile and often a large repertoire of chemokine ligands, fine tuning of leukocyte trafficking needs to be achieved to ensure proper functioning of the chemokine system during both homeostatic and disease conditions (Bachelierie et al. 2014).

### 1.2.2 CCR5 expression and regulation

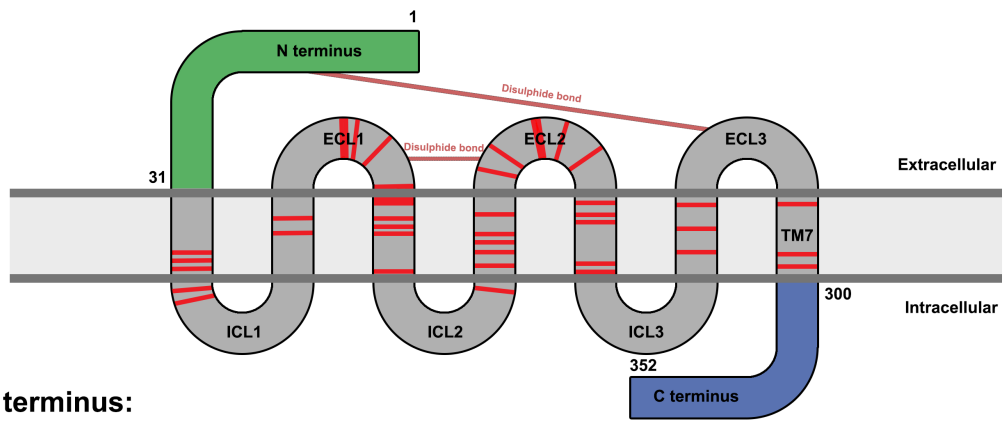
CCR5 is the most studied chemokine receptor after it was shown to be a co-receptor aiding human immunodeficiency virus (HIV)-1 entry into CD4<sup>+</sup> target cells (Samson et al. 1996; Dean et al. 1996) and is classified as an inflammatory chemokine receptor because of its significant role in guiding leukocyte trafficking during inflammation. It is expressed on a number of cells of haemopoetic origin and on some non-haemopoetic cells. More specifically, the receptor has been characterised on subsets of T cells, monocytes and macrophages, but has also been found to be present on cancer cells (Bachelier et al. 2014), endothelial cells (Edinger et al. 1997), epithelial cells (Dwinell et al. 1999), neurons (Galasso et al. 1998) and vascular smooth muscle cells (Schechter et al. 2000). Possible CCR5 expression has also been reported for adipocytes by immunohistochemistry (Hazan et al. 2002) and fibroblasts by immunofluorescence (Mueller & Strange 2004; Wu et al. 2008).

CCR5 has a wide repertoire of CC chemokine ligands, including CCL2, 3, 4, 5, 6, 7, 11, 13, 14 and 16 (Barmania & Pepper 2013). There are two principal regions of the receptor involved in ligand binding: the second extracellular loop (ECL2), and motifs of hydrophobic and negatively charged residues in the extracellular N-terminal region (**Figure 1.2**). This binding region interacts with the N terminus of chemokines, leading to receptor activation (Samson et al. 1997). Interestingly, the presence of these hydrophobic and negatively charged residues, rather than the exact sequence of the N-terminus, is more important for binding (Samson et al. 1997). However, the ECL2 of CCR5 has been shown to be particularly important when considering ligand specificity (Samson et al. 1997).

Upon ligand activation, the receptor undergoes phosphorylation by a G protein receptor kinase (GRK) at threonine and serine residues within the third intracellular loop (ICL3) and C-terminal region (Marchese et al. 2008). This induces conformational changes that dissociate the G protein from the receptor, causing intracellular signalling cascades.  $\beta$ -arrestin is recruited to

**N terminus:**

Human: <sup>1</sup> **M** <sup>S</sup> **D** **Y** **Q** **V** **S** **S** **P** - - **I** **Y** **D** **I** **N** **Y** **Y** **T** **S** **E** **P** **C** **Q** **K** **I** **N** **V** **K** **Q** **I** **A** **A** **R** <sup>31</sup>  
 Mouse: **M** **D** **F** **Q** **G** **S** **V** **P** **T** **Y** **S** **Y** **D** **I** **D** **Y** **G** **M** **S** **A** **P** **C** **Q** **K** **I** **N** **V** **K** **Q** **I** **A** **A** **Q**



**C terminus:**

Human: <sup>300</sup> **V** **G** **E** **K** **F** **R** **N** **Y** **L** **L** **V** **F** **F** **Q** **K** **H** **I** **A** **K** **R** **F** **C** **K** **C** **C** **S** **I** **F** **Q** **Q** **E** **A** **P**  
 Mouse: **V** **G** **E** **K** **F** **R** **S** **Y** **L** **S** **V** **F** **F** **Q** **K** **H** **M** **V** **K** **R** **F** **C** **K** **R** **C** **S** **I** **F** **Q** **Q** **D** **N** **P**

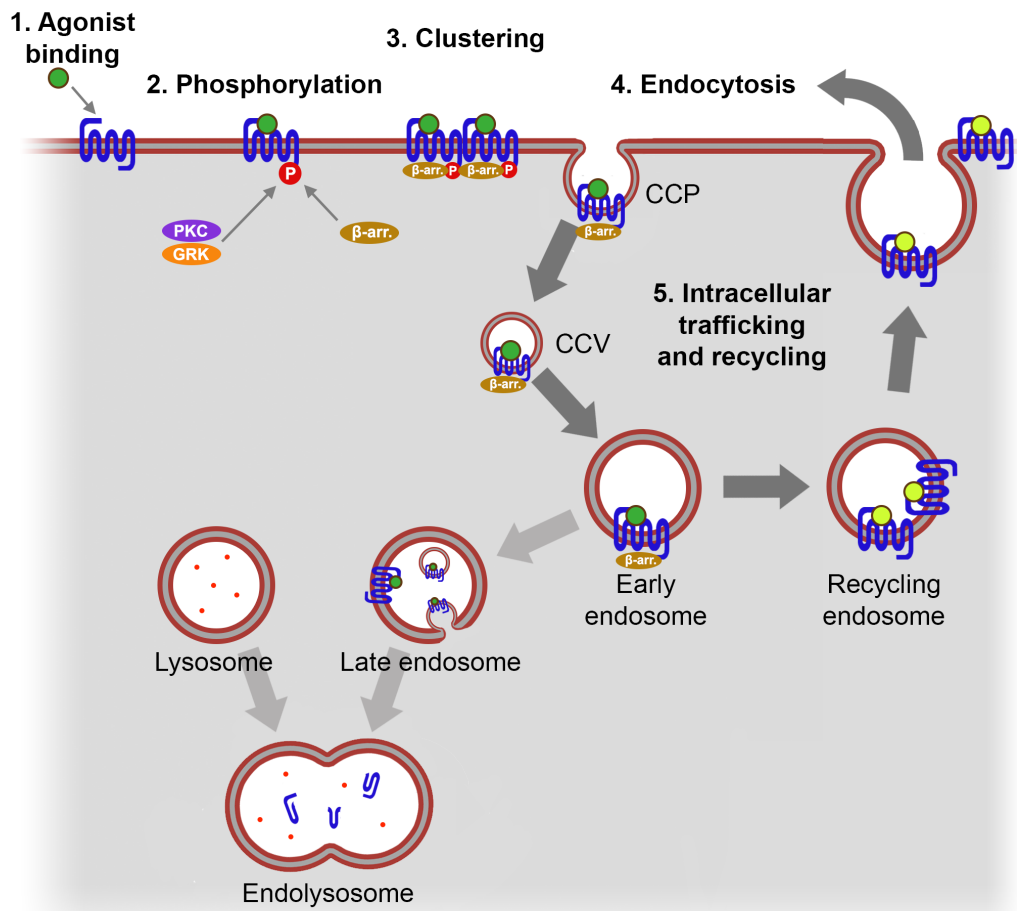
Human: <sup>352</sup> **E** **R** **A** **S** **S** **V** **Y** **T** **R** **S** **T** **G** **E** **Q** **E** **I** **S** **V** **G** **L**  
 Mouse: **D** **R** **A** **S** **S** **V** **Y** **T** **R** **S** **T** **G** **E** **H** **E** **V** **S** **T** **G** **L**

**FIGURE 1.2. Schematic representation of the differences in primary structure between murine and human CCR5.** The amino acid sequence for N and C terminal regions were aligned for human and mouse CCR5 (Golding et al. 2005); differences are highlighted with red on the CCR5 diagram. Red bands show approximate regions where the amino acid sequence differs between mouse and human CCR5. Regions of post-translational modification for human CCR5 are highlighted with blue circles. S = tyrosine sulphation; G = O-glycosylation; P = phosphorylation.

the phosphorylated receptor and acts as a scaffold for their internalisation via clathrin-coated pits (Mueller et al. 2002; Signoret et al. 2005), and caveolae in certain circumstances (Venkatesan et al. 2003). Once inside, CCR5 is sorted to early endosomes (Signoret et al. 2000) and the trans-Golgi network (Escola et al. 2010), causing a down-modulation of the receptor from the cell surface. Regardless of whether bound ligand is removed, the re-sensitised receptor returns to the plasma membrane via recycling endosomes (Signoret et al. 2000). This process is summarised in **Figure 1.3**, which also highlights the pathway of degradation for this receptor.

The process of chemokine receptor internalisation can also be stimulated by agonist-independent cross-phosphorylation mechanisms, often mediated by protein kinase C (reviewed by Bennett et al. 2011). This can occur through the formation of homomers or heteromers where multiple receptors structurally interact with each other, with only one receptor needing agonist binding for both to be internalised. It can also occur through indirect cross-talk with intracellular signalling cascades resulting from activation of other receptors without a physical interaction between receptors. As an example, chemokine receptor down-modulation has been seen in response to Toll-like receptor (TLR)-2 agonist stimulation for CCR1, 2 and 5 (Fox et al. 2011). These mechanisms could reflect additional means by which the immune system is able to alter the behaviour of individual leukocytes based on their specific micro-environment, allowing cells to uncouple the CCR5-CCL5 axis in response to appropriate external cues.

Longer term regulation of CCR5 can be controlled via changes in gene expression and protein degradation (reviewed by Bennett et al. 2011). For receptor degradation specifically, sorting motifs and post-translational modifications can direct vesicles containing internalised receptor towards degradative pathways that terminate with the lysosome. This can be achieved through so called PDZ (“Post synaptic density protein PSD95, Drosophila disc large tumor suppressor Dlg1, and zonula occludens-1 protein zo-1”) ligand motifs on the receptor, which delay lysosomal sorting (Delhaye et al. 2007) or via ubiquitination, which labels GPCRs for degradation by the



**FIGURE 1.3. Schematic representation of the endocytic trafficking and degradation pathways for agonist-stimulated CCR5.** In response to agonist binding, CCR5 is phosphorylated on its cytoplasmic tail by a G protein receptor kinase (GRK); phosphorylation can also be triggered by protein kinase C (PKC). Phosphorylation uncouples the G protein, allowing the receptor to interact with  $\beta$ -arrestin triggering receptor clustering and internalisation of the receptor mainly via a clathrin-dependent pathway. Most internalised receptors will return to the cell surface via recycling pathways and ligand occupied receptors can be re-internalised, but they can also be sent for lysosomal degradation. Of note, there is no active ligand-induced degradation of CCR5.  $\beta$  arr. =  $\beta$ -arrestin; P = phosphorylation; CCP = clathrin-coated pit; CCV = clathrin-coated vesicle.

addition of a ubiquitin tag, although this latter mechanism has not yet been demonstrated for CCR5.

The most common mutation of CCR5, called CCR5 $\Delta$ 32, was first discovered in 1996 (Dean et al. 1996; Samson et al. 1996) and results in individuals with no functional CCR5. The deletion involves a 32 base-pair region that causes a frameshift mutation and introduces a stop codon. This results in a protein that is 215 amino acids long rather than the full-length 352 amino acid protein; the truncated protein is restricted to the ER, resulting in the complete loss of functional CCR5 (Benkirane et al. 1997). CCR5 $\Delta$ 32 has an allelic frequency of between 1-15% depending on the population studied (Bachelierie et al. 2014). These individuals appear healthy with no overt pathology attributable to the lack of CCR5 during homeostatic conditions; this finding is replicated in CCR5<sup>-/-</sup> mice with pathology only being noticeable during chronic inflammation (Zhou et al. 1998).

### **1.2.3 The differences between murine and human CCR5**

Owing to the relative ease of access of haematopoietic cells and the specificity of HIV-1 to infect human cells, the mouse has regularly been bypassed in favour of more clinically relevant human cells. This has resulted in the generation of a plethora of antibody tools to use to follow human CCR5 expression and localisation, targeting many different domain regions of the receptor allowing for intricate studies of intracellular receptor trafficking. However, some studies, such as *in vivo* knockout experiments, are only possible using mouse models. Until recently, many mouse chemokines and chemokine receptors were assumed to be equivalent to their human counterparts. However, with improving technology it is becoming clear that there is considerable inter-species variation in the chemokine system. As examples of this inter-species variation, it has been found that a number of chemokines are exclusive to either mice or humans (Zlotnik & Yoshie 2012). In comparison, chemokine receptors are more well conserved between human and mouse species with all human chemokine receptors having a



mouse counterpart (Nomiya et al. 2011), although these may be structurally distinct (Carmo et al. 2006).

As well as differences in structure there are also variations in the function of the immune system in general and, as a result, the chemokine system specifically. The blood composition of haemopoietic cells is different between the two species: in humans, peripheral blood consists of 30-50% of total lymphocytes, whereas in mice that figure is almost doubled at 75-90% (Doeing et al. 2003). For macrophages, the transcriptome and proteome of murine and human macrophages have been compared under basal conditions and after activation (Martinez et al. 2013). They found that in the basal state, approximately 50% of human and mouse macrophage expression profiles were conserved at protein and mRNA levels. However, after activation there was considerable intra- and inter-species variation for macrophages, suggesting that there may be many differences in how macrophages become activated and respond to stimuli between mice and humans.

For CCR5 specifically, the amino acid sequences for human and mouse CCR5 have been aligned (Golding et al. 2005), as shown in **Figure 1.2**. This has revealed some similarities: for example, the Asp-Arg-Tyr (DRY) motif remains conserved and large regions, particularly for intracellular portions, have considerable sequence identity between the two species. However, the N terminus is significantly different with several key tyrosine sulphation and O-glycosylation sites missing in the mouse sequence. Unfortunately, sites of tyrosine sulphation and O-glycosylation have not been confirmed experimentally for murine CCR5. However, by comparing to human CCR5, it is likely that Y12 and Y16 are sites of tyrosine sulphation as they are both conserved between mouse and human CCR5. There may also be an additional murine tyrosine sulphation site at Y10. For O-glycosylation, S6 is likely to remain a key site because this site has been shown to be glycosylated in human CCR5. There may also be an additional site at S11 but that has not yet been confirmed experimentally. The overall structure of murine CCR5 is likely to be similar to human CCR5 because of the high

degree of sequence identity (83%) (Golding et al. 2005); however, this again has not been confirmed through crystal structures. These differences, particularly for the N terminal region, illustrate why most antibodies targeting human CCR5 do not work against murine CCR5 and the likely extensive post-translational modifications of this region introduce challenges to antibody production.

In addition to differences in the primary, secondary and tertiary structure of murine CCR5, there are differences in the expression of the receptor compared to human CCR5. For example, Mack et al. (2001) found CCR5 to be highly expressed on murine natural killer (NK) cells, whereas only a small number of NK cells express CCR5 in humans, and in much lower quantities (Mack et al. 1999). There are also differences in how these receptors respond to ligands. For example, the chemically modified CCL5 analog aminooxypentane (AOP)-regulated on activation, normal T cell expressed and secreted (RANTES) is very efficient at internalising human CCR5 (Mack et al. 1998) but was found to only weakly internalise murine CCR5 (Mack et al. 2001). In contrast, the chemokine analog methionine (Met)-RANTES is a partial agonist able to activate intracellular signalling in humans but a blocking antagonist that inhibits intracellular signalling in murine cells (Mack et al. 2001). Encouragingly, murine and human CCR5 are present in comparable expression levels in T cells and monocytes and have comparable T cell behaviour in inflammatory conditions (Mack et al. 2001).

#### **1.2.4 The role of CCR5 during chronic inflammatory conditions and infection**

CCR5's role in leukocyte recruitment during inflammatory states results in the receptor being involved in a number of chronic inflammatory conditions. As an example, CCR5 has been implicated in the pathophysiology of the central nervous system (CNS) disease multiple sclerosis where the receptor has increased expression on a number of different cell types (reviewed by Martin-Blondel et al. 2016) and increased CCR5 ligand secretion (Simpson et al. 1998); this was shown to be functionally relevant when Sapir et al. (2010)

made a receptor-based fusion protein to selectively bind and neutralise CCL3-5, thereby reducing the severity of a mouse-model of multiple sclerosis.

The process of atherosclerosis causes arterial wall thickening via the accumulation of leukocytes; it is responsible for the majority of deaths from cardiovascular disease and has been linked to several chemokine receptors, including CCR5 (Jones et al. 2011). However, it has been shown that CCR5<sup>-/-</sup> was not protective during the early stages of atherogenesis, suggesting that CCR5 may only be important for the chronic stages of atherosclerosis (Kuziel et al. 2003). In addition to cardiovascular disease, mice lacking CCR5 were also found to have lower incidence of hepatocellular carcinoma, a chronic inflammation-induced cancer (Barashi et al. 2013). This was attributed to impairment of macrophage recruitment and trafficking to the liver causing less inflammation overall.

CCR5 has also been implicated in a number of infections. Individuals with the CCR5Δ32 mutation are protected against HIV-1 because the virus needs the receptor to gain entry to target CD4<sup>+</sup> T cells (Samson et al. 1996; Dean et al. 1996) and against Hepatitis C virus, although data for the latter are controversial (Coenen & Nattermann 2010). In contrast, the mutation has been shown to be a strong risk factor for West Nile virus infection (Glass et al. 2006). Furthermore, CCR5<sup>-/-</sup> mice have reduced clearance of: *Listeria monocytogenes* likely due to altered macrophage function (Zhou et al. 1998), herpes simplex virus type 2 caused by reduced NK cell proliferation and activity (Thapa et al. 2007), *Chlamydia trachomatis* by reducing T cell homing to infection sites (Olive et al. 2011), encephalomyocarditis virus through interruption of inflammatory gene expression in response to viral infection (Christmann et al. 2011), and *Neospora caninum* via reduced dendritic cell migration and activation (Abe et al. 2015).

From these studies, it is clear that CCR5 has a complex, multi-faceted role during infection. At the cellular level, CCR5 has a known role in facilitating entry of certain pathogens into target cells (Samson et al. 1996; Dean et al.

1996), modulates macrophage anti-microbial activity via the generation of nitric oxide (Bhattacharyya et al. 2002) and controls macrophage activation (Zamilpa et al. 2011). In addition, CCR5 has a role in orchestrating the overall immune response to infection, triggering leukocyte recruitment to sites of infection. Dissecting these two levels and building a complete picture of the role played by each for a specific infection is therefore difficult.

### **1.2.5 The association between *Leishmania* and chemokine receptors**

The release of chemokines and expression of chemokine receptors is crucial in determining the composition of leukocyte infiltrates at sites of infection. The interaction between *Leishmania* and the chemokine system is less clear, often with differing effects between *Leishmania* species (Oghumu et al. 2010). For example, infection with *L. major* significantly induces gene expression of the CCR5 chemokines CCL3-5 in T regulatory (Treg) cells (Yurchenko et al. 2006). Higher expression of CCL2, CCL4, CCL5, CCL21 and CXCL8 have also been reported in canine infection with *L. infantum* (Menezes-Souza et al. 2012). In comparison to *L. major*, infection with *L. amazonensis* results in a delayed and reduced expression of CCL3-5 (Ji et al. 2003). In contrast, evidence demonstrates that other species down-regulate chemokine genes to avoid detection by the host immune system (Matte & Olivier 2002), particularly after the early stages of the infection (Steigerwald & Moll 2005; Pinheiro et al. 2006). This is complicated further by the finding that *L. donovani* promastigotes can respond directly to CCL3-5 and move up a chemotactic gradient towards the site of release (Roychoudhury et al. 2006), making the causative link between chemokines and *Leishmania* harder to establish. Despite this, it has been suggested that the up-regulation of chemokines may be beneficial to the host, as CCL5 blockade resulted in higher susceptibility to *L. donovani* infection (Murray et al. 2017). Indeed, chemokines have been linked to anti-leishmanial activity by inducing respiratory bursts in murine macrophages (Bhattacharyya et al. 2002), and the administration of CCL2 or CCL3 has been shown to reduce

parasite burdens during *in vivo* models of *L. donovani* promastigote infection (Dey et al. 2005).

These studies highlight the interspecies variation in the dynamic chemokine response profiles for cells infected with *Leishmania*, a variation also seen at the receptor level. Studies have reported that certain chemokine receptors are increased, like CCR1-3 during infection with *L. major* and *L. donovani* promastigotes (Matte & Olivier 2002). CCR1 has been suggested to promote a Th2 response that favours parasite persistence with CCR1<sup>-/-</sup> mice having significantly lower *L. major* parasite burdens (Rodriguez-Sosa et al. 2003). In contrast, protein expression of CCR1 has been shown to decrease during infection of human macrophages with the visceralising parasite *L. infantum* (Panaro et al. 2004). CCR2 knockout mice have markedly increased parasite burdens during *L. major* infection, suggested to be caused by defects in dendritic cell (DC) functioning (Sato et al. 2000); this is in contrast to *L. donovani* infection where mice lacking the receptor have smaller liver granulomas, but with no change in parasite burdens compared to wild-type control mice (Sato et al. 1999). It has also been observed that mice infected with *L. donovani* amastigotes had splenic DCs with lowered expression of CCR7 and reduced migration (Ato et al. 2002).

Thus, the effect of *Leishmania* infection is different depending on the chemokine receptor studied. For CCR5, it has been reported that mice lacking the receptor may have an enhanced ability to control parasite load in *L. major* metacyclic promastigote infection by reducing the migration of regulatory T cells to infection foci, thereby increasing the number of CD4<sup>+</sup> T cells (Yurchenko et al. 2006). This resulted in significant reductions in parasite numbers and a lack of overt pathology. For *L. donovani* specifically, infection with AG83 promastigotes has been suggested to up-regulate CCR5 in human mononuclear phagocytes and THP1 cells, as evident from reverse transcriptase-polymerase chain reaction analysis (Dasgupta et al. 2003). This has also been suggested to occur on mouse macrophages with *L. donovani* AG83 promastigotes as shown by western blotting (Bhattacharyya et al. 2008), although appropriate loading controls were missing. Perhaps in

conflict with this, this same group also found that the chemotactic index, a measure of movement up a chemokine gradient in response to specific chemokines, was attenuated in *L. donovani* promastigote-infected peritoneal macrophages stimulated with CCL3 (Dey et al. 2005). CCR5<sup>-/-</sup> mice infected with *L. donovani* 1S promastigotes have reduced parasite burden in the liver at day 64 post-infection in a non-resolving model of infection (Sato et al. 1999), which was attributed to reduced intracellular replication and/or decreased parasite uptake, although a role for the wider immune response cannot be excluded. In an attempt to attribute this effect to CCR5 at the macrophage-level, Bhattacharyya et al. (2008) used RNA interference techniques to knock-down CCR5 on *in vitro* peritoneal macrophages and J774A.1 cells; they found that there was a decrease in parasite burden when expression of the receptor was reduced. More recently, research by the same group (Majumdar et al. 2014) has suggested that there may be a facilitating interaction between CCR5 and TLRs, the latter of which has previously been shown to help the host macrophage detect invading *L. donovani* promastigotes (Tuon et al. 2008) and plays a role in both initiating pro-inflammatory responses and controlling phagocytosis. They suggest that both CCR5 and TLR2 are involved in regulating the entry of the promastigote parasite into the host cell (Majumdar et al. 2014). However, the reduction in parasites observed could also be due to decreased intracellular survival or reduced replication, not just reduced parasite entry.

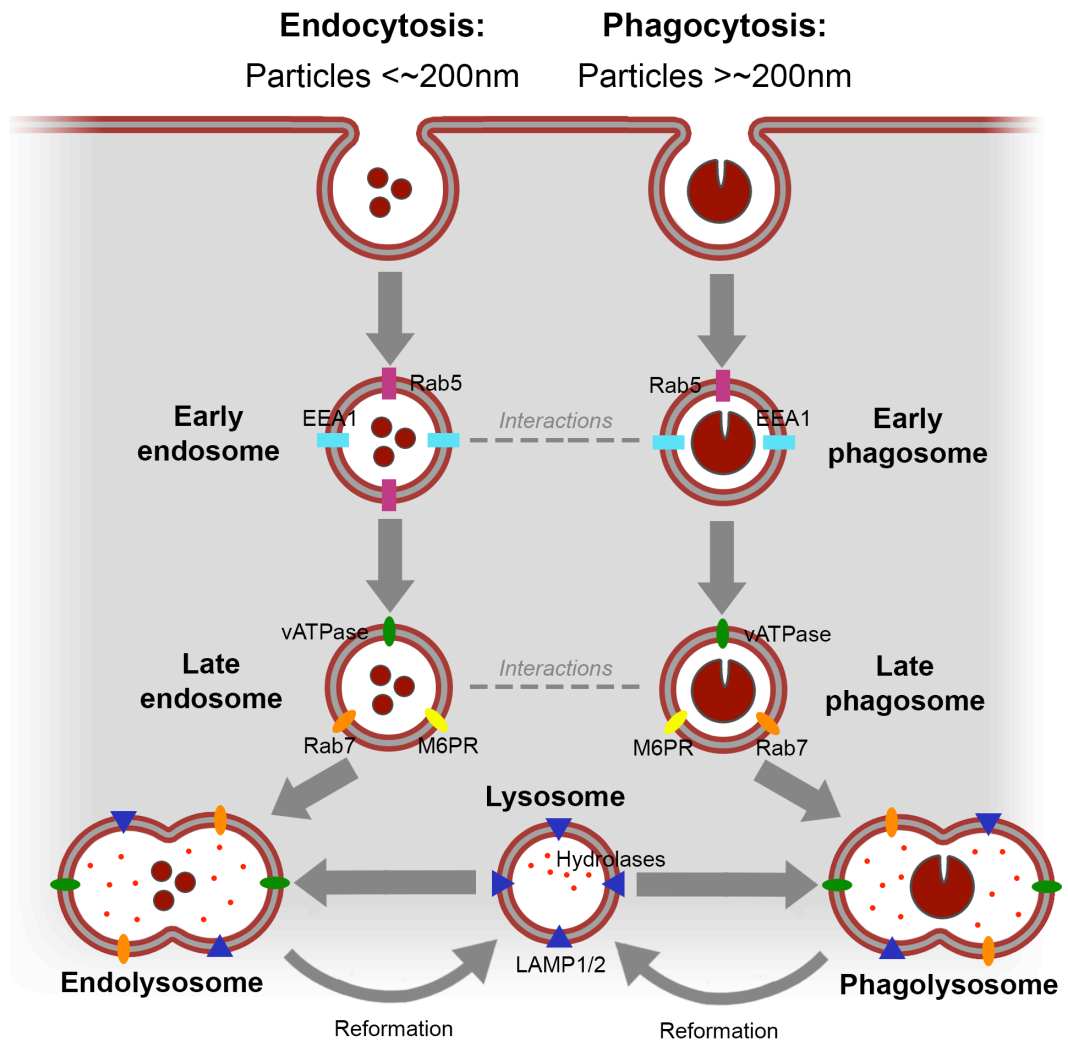
Collectively, these studies have shown that *Leishmania* species have complex and individual interactions with the chemokine system. They also highlight the issue of combining the results from different *Leishmania* species, varying forms of the parasite and distinctive host models to generate a complete picture of the role of individual chemokine receptors during infection.

## 1.3 The *Leishmania*-containing intracellular compartment

### 1.3.1 Endocytic pathway

Endocytosis is the process by which cells are able to engulf material less than ~200nm in size suspended in the extracellular fluid into *de novo* internal membrane-bound compartments. It is involved in a number of essential cellular processes such as allowing nutrient uptake and modulating intracellular signalling through the internalisation of receptors. Solutes can also be taken up via this process, where it is termed fluid-phase endocytosis. At each stage of the pathway, there are a number of intermediates with each being spatiotemporally distinct and possessing characteristic markers. A number of trafficking mechanisms exist to regulate the flow of material through this pathway, such as the differential recruitment of Rab family guanosine triphosphate (GTP)-ases to intracellular compartments. Rab GTPases can function as “molecular switches” alternating between an active GTP-bound and inactive guanosine diphosphate (GDP)-bound states. They play an important role in structurally and functionally identifying an organelle (Ohya et al. 2009); thus, it is clear that appropriate spatiotemporal regulation of their activity is paramount. Furthermore, a number of sorting machinery proteins are involved in diverting incoming traffic to the correct intracellular location. Such proteins include sorting nexins, endosomal sorting complexes required for transport (ESCRT) machinery, homotypic fusion and vacuole protein sorting (HOPS), and soluble N-ethylmaleimide-sensitive factor-attachment protein receptor (SNARE) complexes, all helping to regulate membrane fusion and overcome the free energy barrier involved in this process (Luzio et al. 2010; Elkin et al. 2016). The process of endocytosis, including markers often used to characterise each of the main compartments, is summarised in **Figure 1.4**.

Early endosomes are the first main structures to which incoming endocytic vesicles are delivered and are characterised by the presence of early endosome antigen 1 (EEA1) and Rab 5. This is the stage at which it is decided whether the contents of the vesicle continues along the path to



**FIGURE 1.4. Schematic representation of the process of endocytosis and phagocytosis.** Particles are taken up by invaginations of the plasma membrane that form membrane-bound compartments and rapidly acquire markers like Rab5 and EEA1. These early compartments mature into late compartments that acquire Rab7, M6PRs and vATPase. These late compartments mature further by transient fusion events with lysosomes, acquiring LAMP1/2 and hydrolases from terminal storage lysosomes. Membrane retrieval and condensation events then lead to lysosome reformation from endolysosomes or phagolysosomes.



degradation or are recycled via the tubular sorting endosome (van Meel & Klumperman 2008). This is commonly mediated by receptor-ligand dissociation (Mellman 1996), with receptors that dissociate from their ligand at an early-endosomal pH of ~6.5 able to rapidly recycle back towards the plasma membrane, with examples of such receptors including the transferrin receptor. Receptors can also be recycled through this route via pH-independent mechanisms, as has been seen for CCR5 (Signoret et al. 2000; Signoret et al. 2004). In addition to any remaining ligand-bound receptors, the cargo from fluid-phase endocytosis is usually transported onwards towards the lysosome (Hsu et al. 2012).

The next structurally and functionally unique components of the degradation pathway are late endosomes. These structures are also known as multivesicular bodies (MVBs) because of the presence of internal vesicular membranes in their lumen. The process of surface invagination allows the extracellular portion of membrane proteins to be exposed to the degradative conditions present within this compartment. Maturation of early endosomes into late endosomes is mediated by compartment conversion, whereby Rab5 can recruit a guanine nucleotide exchange factor (GEF) that can recruit and activate Rab7; Rab 7, in turn, can then recruit a GTPase-activating protein (GAP) that can remove Rab5 (Elkin et al. 2016). This results in these late endosomal structures characteristically expressing Rab 7; they also have decreasing pH caused by the incorporation of v-type vacuolar H<sup>+</sup> ATPase (vATPase) into their membrane. The two main subunits of vATPase are the cytoplasmic V<sub>1</sub> subunit and membrane-incorporated V<sub>0</sub> subunit (Forgac 2007). Dissociation of the ligand from its receptor at this point typically results in retrograde transport of the compartment towards the trans-Golgi network, as seen with the mannose-6-phosphate receptor (M6PR) (Hirst et al. 1998).

The final destinations for this pathway are lysosomes, which are multifunctional organelles with roles in degradation, autophagy, energy metabolism, antigen processing and organelle biogenesis (Saftig & Klumperman 2009). Interaction between the late endosome and lysosome has been described as a series of fusion-fission events often termed “kiss-

and-run” fusion (Storrie & Desjardins 1996). However, the formation of a hybrid organelle, termed the endolysosome, from late endosome and lysosome fusion is now the current favoured model, with lysosomal compartments later being reformed by selective and dynamic retrieval from these hybrid organelles (Luzio et al. 2007; Bright et al. 2016). Our current understanding of these organelles is changing. Recent data from Bright et al. (2016) demonstrated that acid hydrolases are only active in endolysosomes with terminal lysosomes being hydrolase-inactive and non-acidic. This helps to explain the previous observation of protein degradation and hydrolase activity within compartments with endosomal characteristics (Casciola-Rosen et al. 1992). In addition, recent research by Johnson et al. (2016) has shown that lysosomes can have different pHs depending on their position within the cell, likely mediated by decreased vATPase and H<sup>+</sup> leakage. These data confirm the structural and functional heterogeneity that has often been documented for lysosomes (Saftig & Klumperman 2009). Regardless, lysosomes have traditionally been characterised by their lack of M6PR and high proportions of lysosomal membrane proteins, of which many have been described but the most characteristic are lysosome-associated membrane proteins (LAMPs) (Callahan et al. 2009; Saftig & Klumperman 2009).

### **1.3.2 Phagocytosis and the phagolysosome**

In contrast to endocytosis, phagocytosis is the process by which a cell is able to internalise particles larger than ~200nm into membrane-bound compartments called phagosomes. These intracellular structures interact extensively with the major organelles of the endocytic pathway, ultimately delivering material to a hybrid compartment called the phagolysosome (**Figure 1.4**). In addition to extracellular material, the process of phagocytosis plays a major role in autophagy, receiving subcellular components destined for degradation in structures termed autophagosomes. These subcellular components are most often mitochondria, endoplasmic reticulum, ribosomes and peroxisomes (Wang & Klionsky 2011). Professional phagocytes are cells specialised in phagocytosis with the aim of engulfing and destroying invading microorganisms; they include macrophages, neutrophils and dendritic cells.

Phagocytosis is initiated when a particle, which could be anything from a large macromolecule to a pathogen, interacts with distinct plasma membrane-receptors that help the phagocyte recognise the type of particle and initiate the appropriate intracellular processes. The large diversity of phagocytic material has necessitated the evolution of many different groups of phagocytic receptors, many of which are often co-expressed on an individual phagocyte and collaborate in the process of phagocytosis. Receptors considered phagocytic receptors include Fc receptors, complement receptors, pattern-recognition receptors (such as the mannose receptor), scavenger receptors, PS receptors and apoptotic corpse receptors, with each recognising unique molecule patterns and responding through distinctive mechanisms (Freeman & Grinstein 2014). In addition to these receptors, there are a plethora of accessory receptors that help to modulate and fine-tune the phagocytic process, such as GPCRs and TLRs (Freeman & Grinstein 2014).

Phagocytic receptors become activated when their local density increases in response to stabilising interactions with specific ligands; often, multiple receptors are activated in response to a single external stimulus, which can result in significant receptor cross-talk that can synergise or antagonise the response (Freeman & Grinstein 2014). This accumulation of phagocytic and accessory receptors causes disruption of the resting membrane-associated cortical cytoskeleton. This helps liberate G-actin monomers that can then be used to initiate F-actin polymerisation and pseudopodia extension. The subsequent plasma membrane invagination encompasses the target particle until it is enclosed, thereby forming a particle-containing phagosome. This process involves a range of signaling pathways, principally Ras-related C3 botulinum toxin substrate 1 (Rac1), cell division control protein 42 homolog (Cdc42) and Ras homolog gene family member A (RhoA), that act together to maintain and orchestrate actin cytoskeleton dynamics (Freeman & Grinstein 2014). Complex interactions of these signaling pathways with other actin-related proteins, including the actin-related protein (Arp)2/3 complex (Rotty et al. 2013) and coronins (Yan et al. 2005), also influence F-actin networks and help control the formation of phagosomes.

Intracellular phagosomes are dynamic in nature and undergo a complex series of interactions with endomembranous structures where they acquire new membrane proteins and luminal contents in a process known as phagolysosome biogenesis (Goyette et al. 2012), as summarised in **Figure 1.4**. Progressively, this hybrid compartment becomes increasingly acidic, hydrolytic and hostile to any microorganisms inside it, eventually fusing with endolysosomal and lysosomal compartments. In most cases, containment of an invading microorganism within a phagosome results in its effective killing. However, there are a number of important exceptions to this rule with pathogens known to either arrest phagosome maturation, as seen with *Mycobacterium tuberculosis*, or alter the normal pathway route, as seen with *Legionella pneumophila* (Kumar & Valdivia 2009). Some pathogens actively seek out phagocytes where intracellular survival within a phagosome is an important part of their lifecycle. Within this compartment, they are able to avoid immune responses mediated by circulating antibodies and components of the complement system while receiving a constant supply of nutrients from incoming endocytic cargo (McConville et al. 2015). This is the case for *Leishmania*, where the parasites appear to be able to survive within the degradative conditions found within endolysosomal compartments. However, the *Leishmania*-containing compartment has not yet been fully characterised so whether the parasite makes more subtle changes to its intracellular compartment to aid its own survival within this inhospitable environment is not known.

### **1.3.3 Techniques used to characterise intracellular pathogen-containing compartments**

Previous methods commonly used to isolate endocytic and phagocytic subcellular compartments from cells have taken a variety of approaches. When a cellular organelle is found to possess unique proteins specific for that structure, immuno-affinity purification can be performed where an antibody against the target is covalently coupled to a retrievable tag, such as magnetic material. This has been used previously for lysosomes with antibodies that targeted specific vATPase targets (Nylandsted et al. 2011),

but has the potential disadvantage of artificially biasing for a particular subpopulation of compartments where the target protein is highly expressed. Care must also be taken to ensure that the protein targeted by antibodies is not present in other structures of the cell.

Alternatively, endocytic and phagocytic organelles can be filled with magnetic particles and subsequently isolated within a magnetic field. Small magnetic nanoparticles less than 200nm in size can be used to isolate lysosomes. This has been done by different laboratories (Rodriguez-Paris et al. 1993; Diettrich et al. 1998; Rofe & Pryor 2015) using supraparamagnetic iron oxide nanoparticles (SPIONs), with each group taking a different approach to cell lysis. These methods can provide significant enrichment for lysosomal compartments using a physiologically relevant method of cargo delivery. For phagosomes, whole magnetic beads (>200nm) can be fed to cells and afterwards isolated (described by Pryor & Rofe 2015). However, although it can give us important information about the general processes of phagocytosis, the use of magnetic beads negates the significant contribution made by the surface properties of engulfed micro-particles (de Chastellier & Thilo 1997; Li et al. 2010) making the results from these studies less relevant to invading microorganisms.

Density-gradient centrifugation is another common technique that can be used to isolate lysosomes and phagosomes from cells. For phagosomes, this is most often done using latex beads. The low density of latex beads allows them to be isolated on single step sucrose gradients rather than the multiple steps often required for density-based ultracentrifugation of pathogen-containing phagosomes. Most often, macrophages are exposed to latex beads and homogenised at a particular time-point post-exposure (Li et al. 2010). The homogenate is then usually passed through needles and separated using a sucrose gradient. This technique was used by Garin et al. (2001) and Goyette et al. (2012) to produce some of the best early proteomic datasets for phagosomes thus far. However, the use of this technique in combination with latex beads again has the disadvantage of lacking the surface antigens found with real pathogens. Furthermore, the sucrose used

for density-gradients can cause significant osmotic stress to isolated compartments, potentially disrupting the protein composition of vulnerable proteins prior to analysis.

Attempting to isolate pathogens from infected cells is considerably more challenging (reviewed in Li et al. 2010). Other groups have previously attempted to isolate the *Leishmania*-containing compartment from infected cells. For example, Kima & Dunn (2005) produced a methodology paper detailing a technique using RAW 264.7 macrophages for isolating *L. pifanoi* promastigote parasites, which are part of the *L. mexicana* complex of parasites that produce large multi-parasite containing vacuoles. Here, they exploit the observation that phagosomes have calnexin (Gagnon et al. 2002) and use immunoaffinity selection to select phagosomes over other host cell vesicles. Calnexin should be absent from late endosomal vesicles that have comparable density, thus helping to purify the sample. They show electron micrographs to support their claims of successfully isolating the compartment; however, these images show significant damage to the parasites suggesting that the samples had been exposed to significant stress. Unfortunately, the authors of this study do not proceed to sending these isolated compartments for liquid chromatography-tandem mass spectrometry (LC-MS/MS) proteomic analysis so detailed protein composition data are not available. This technique also has the disadvantage that it is selecting for compartments rich in calnexin; this is particularly a problem with *Leishmania* because others have suggested that, in neutrophils at least, there are two different parasite containing compartments, only one of which is calnexin-positive (Gueirard et al. 2008).

The group of M. Desjardins has also worked on developing techniques to recover parasite-containing compartments from infected cells (Dermine et al. 2005). This involved infecting J774 cells with *L. donovani* (1S strain) promastigotes and using a dounce homogeniser to homogenise the sample in an appropriate buffer. After removing intact cells, the sample was processed through a density gradient (Desjardins et al. 1994; Dermine et al. 2005; Goyette et al. 2012). For these earlier studies, they were principally

interested in the distribution of phagosome microdomains (Dermine et al. 2005) without proteomic characterisation. Later, as supplementary data for work done to characterise phagosomal membrane microdomains using proteomics, Goyette et al. (2012) hypothesise that a number of phagosomal functions could be altered by *Leishmania* promastigotes interacting with membrane microdomains, such as membrane fusion, lipid metabolism, transmembrane transport and actin remodelling. However, proteomic characterisation of this parasite-containing compartment remains to be performed.

With advances in the sensitivity of mass spectrometry coupled with new methods of isolating intracellular organelles, proteomic characterisation of both lysosomes and phagosomes has improved significantly over the last decade. Despite this, obtaining a highly purified homogeneous phagosome preparation from real pathogen infected cells is difficult because of extensive and complex interactions of the phagosome with other cytoplasmic organelles and a lack of suitable isolation methods (Li et al. 2010). Thus, the need for novel techniques to isolate intracellular phagosomes to better understand these pathogen-containing compartments is evident, with each new addition helping to strengthen the knowledge base on phagosome composition.

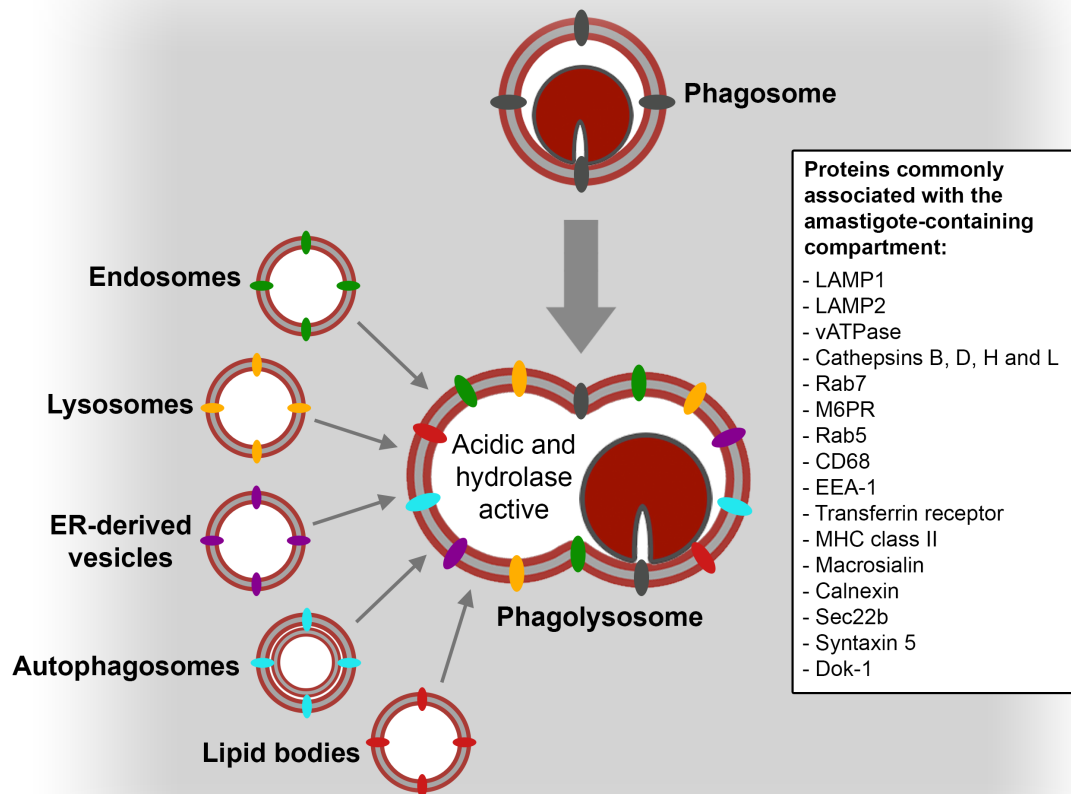
#### **1.3.4 Characterisation of the protein composition of the *Leishmania*-containing intracellular compartment**

The importance of understanding the composition of the *Leishmania*-containing intracellular compartment to better understand *Leishmania*-induced pathology has long been appreciated. As with all *Leishmania* studies, a plethora of studies have been reported using different species and forms of the parasite, and there are differences in the compartment composition and morphology between each. As an example, *L. mexicana* amastigotes reside in large communal intracellular compartments whereas *L. infantum* amastigotes have a tightly bound, single parasite-containing compartment (Liévin-Le Moal & Loiseau 2016). The protein composition of

such divergent intracellular compartments is therefore likely to be different. Furthermore, as one might expect from the dynamic nature of phagocytosis, there are also differences in the compartment composition depending on the time-point studied post-infection (as summarised by Liévin-Le Moal & Loiseau 2016).

Previous studies aiming to characterise the compartment have primarily used immunofluorescence techniques on fixed *Leishmania*-infected cell samples to determine compartment composition, as summarised in **Figure 1.5**. From such studies, it is now well established that a number of proteins with a traditional lysosomal localisation have been identified on this compartment, such as LAMP1 and LAMP2 (Lang et al. 1994). Lang et al (1994) also suggested that the compartment acquires lysosomal proteases such as cathepsins B, D, H and L. However, although there is clear evidence for lysosomal proteins within the *Leishmania*-containing compartment, other proteins not traditionally associated with lysosomes have been found suggesting that this compartment is better viewed as a hybrid organelle composed of lysosomal, late endosomal and ER components. For example, Lang et al (1994) found that the parasite-containing compartment also contained the proteins macrosialin, M6PR and Rab7p, which are markers of the late endosome/prelysosomal compartments (Chavrier et al. 1990; Rabinowitz et al. 1992; Courret et al. 2002). There have also been multiple reports of a range of resident ER molecules such as calnexin (Ndjamen et al. 2010), syntaxin V (Canton et al. 2012) and Sec22b (Ndjamen et al. 2010) being present on the *Leishmania*-containing intracellular compartment. However, after several years of debate on whether ER-related proteins are present on phagosomes (Gagnon et al. 2002; Desjardins 2003; Gagnon et al. 2005; Touret et al. 2005), it is now accepted that at least some proportion of the ER likely plays a role in the general process of phagocytosis (Campbell-Valois et al. 2012). More recent investigations into sites of ER interactions suggest that the ER may have multiple contact sites with components of the endocytic pathway (recently reviewed by Eden 2016; Henne 2016), so whether individually identified ER proteins are specific to *Leishmania*-





**FIGURE 1.5. Summary of our current understanding of the proteins comprising the *Leishmania*-containing intracellular compartment and its interaction with other organelles.** Amastigote *Leishmania* parasites are internalised into invaginations of the plasma membrane called phagosomes. During phagocytosis, *Leishmania*-containing phagosomes interact with several other intracellular organelles and acquire proteins from each. Several proteins have been localised to the *Leishmania*-containing intracellular compartment using various experimental techniques (Lang et al. 1994; Courret et al. 2002; Liévin-Le Moal & Loiseau 2016). CD68 = cluster of differentiation 68; MHC = major histocompatibility complex.

containing phagosomes or a more general property of phagocytosis is unknown.

### **1.3.5 Functional roles of the *Leishmania*-containing intracellular compartment**

As might be expected with the differences in protein composition compared to normal phagosomes, there are also differences in the functionality of these parasite-containing compartments. In addition to the LPG-dependent mechanisms of delayed phagosome maturation discussed earlier, it has been shown that phagosomes containing *Leishmania* do not fuse as well with phagosomes containing zymosan particles (Veras et al. 1992) and that they are poorly accessible to fluid phase tracers (Harris et al. 1994). This suggests that the parasite is able to alter fusion and fission events for its intracellular compartment.

The phagolysosome also provides a platform by which the parasite can receive the nutrients it requires for survival and replication. Indeed, the parasite is unable to use the fatty acids within endosomes as a major carbon source: the parasite's genome lacks key enzymes required for converting acetyl-CoA into useable sugar (Ivens et al. 2005; Naderer et al. 2006). This makes them unable to utilise the high lipid levels within the early endosome and the low levels of sugars and amino acids here are insufficient for *Leishmania* metabolism (Lorenz et al. 2004; Muñoz-Elías & McKinney 2005). Instead, the parasites must progress to the phagolysosome compartment, which contains higher levels of readily available amino acids supplied by degraded macromolecules and subcellular organelles (Rubin-Bejerano et al. 2003; Lorenz et al. 2004). It is likely that the parasite is able to exploit and divert other systems involved in host nutrient transport, but these processes remain to be elucidated (Liévin-Le Moal & Loiseau 2016).

A study has reported that the phagolysosome may also play a role in helping the parasite travel from cell to cell. It has been suggested by Real *et al* (2014) using live cell imaging and electron microscopy on bone marrow-

derived macrophages (BMDMs) infected for 20 days with *L. amazonensis* amastigotes that parasites are released from apoptotic cells within LAMP1 and Rab7 rich membranes, and that these structures are readily taken up by vicinal macrophages. Whether this is a property used by the parasite for increased protection and avoiding exposure to the host immune system is currently not known.

It is not only the immediate surroundings of the phagolysosome that the parasite can manipulate to its own advantage; it has been suggested that *Leishmania* can also induce remote changes for a wide-range of signalling pathways via the incorporation of parasite-derived exosomal material into the phagolysosomal membrane (Liévin-Le Moal & Loiseau 2016). As an example of this remote manipulation of host cell receptors, some *Leishmania* species are able to induce macrophages to express CD200 ligand (Cortez et al. 2011), which binds to the CD200 inhibitory receptor that dampens macrophage microbicidal activity, thereby increasing intracellular survival of the parasite. Furthermore, the *Leishmania* virulence factor zinc-metalloprotease glycoprotein (GP)63 is able to localise to the host macrophage nuclear envelope where it can alter the activity of nuclear transcription factors such as NFκB, thereby reducing pro-inflammatory signalling pathways (Isnard et al. 2015).

Together, these studies suggest that *Leishmania* parasites reside in an intracellular compartment that has altered protein composition and functional activity, but as yet this compartment has not been fully characterised.

## **1.4 Thesis aims**

Much of our current understanding of how *Leishmania* parasites interact with the host macrophage is incomplete, with both the mechanisms of entry and intracellular survival not fully understood.

To date, there have been several sporadic studies looking at the interaction between the chemokine receptor CCR5 and *Leishmania*, each using different

species of *Leishmania* and distinct models of infection making it difficult to obtain a complete picture. A clearer understanding of the role that CCR5 plays during *L. donovani* amastigote infection would be gained by performing *in vivo* and *in vitro* experimentation using an established model of *Leishmania* infection to dissect the role of CCR5 both at the level of individual target cells (macrophages) and the wider immune system response to infection. Much work has already been done within the Signoret laboratory in characterising human CCR5 regulation and intracellular trafficking in human macrophages and T-cells. No cell biology tracking of CCR5 has thus far been performed in murine cells so we aimed to build on this knowledge to characterise the interaction between clinically relevant *L. donovani* LV9 amastigotes and murine CCR5.

CCR5 relies extensively on intracellular trafficking pathways and *Leishmania* parasites may interact with these same pathways when phagocytosed by their host cell. Incomplete characterisation of the *Leishmania*-containing intracellular compartment and a lack of antibody tools to track murine CCR5 means that whether CCR5 interacts and remains associated with this compartment is currently unknown. These compartments have previously been characterised as being phagolysosomal based on the presence of only a few markers. However, the endocytic pathway is now well recognised as possessing plasticity and dynamic cycling meaning that endocytic and lysosomal compartments cannot be characterised based on a limited number of markers alone. We aimed to develop a new method to isolate this intracellular compartment from *L. donovani*-infected cells for further characterisation, particularly with regard to CCR5 expression. Thus, we took an interdisciplinary approach and the specific aims of the current project were to:-

- A) Determine whether *L. donovani* LV9 amastigote infection affects CCR5 expression using an *in vitro* model of infection.
- B) Determine if (and the mechanisms by which) murine CCR5 is required for *L. donovani* LV9 amastigotes using *in vivo* infections.

- C) Develop a protocol to isolate intracellular *L. donovani* amastigote-compartments from J774.2 cells for subsequent LC-MS/MS analysis of membrane proteins.
- D) Perform comparative proteomics on these intracellular *L. donovani*-containing compartments using statistical approaches, comparing compartments from live parasite-infected cells to those from dead (heat inactivated) parasite-infected cells.

## 2. General materials and methods

### 2.1 Reagents, buffers and solutions

All chemicals were purchased from Sigma (Gillingham, UK) unless otherwise specified. The complete protease inhibitor cocktail was from Roche Diagnostic Ltd (Burgess Hill, UK). Tissue culture medium and supplements were purchased from GIBCO (Life Technologies, Paisley, UK) unless otherwise stated. Foetal calf serum (FCS) was purchased from HyClone (Thermo Fisher Scientific, Hemel Hempstead, UK) and heat inactivated (HI) at 56°C for 30 mins. Purified lipoteichoic acid (LTA) from *Staphylococcus aureus* was purchased from Invivogen (Toulouse, France) and murine CCL5 from PeproTech (London, UK). Buffers and solutions were made according to **Table 2.1**.

**TABLE 2.1 Composition of buffers and solutions used in this project.**

Buffer / solution	Composition
<b>Complete Dulbecco's Modified Eagle's medium (DMEM)</b>	500mL DMEM, 2mM L-glutamine, 100U/mL penicillin, 100µg/mL streptomycin, 10% (v/v) HI FCS.
<b>Complete Grace's media</b>	1L Grace's Insect Medium (Sigma, Gillingham, UK), 4µM NaHCO <sub>3</sub> , 10% (v/v) HI FCS, 100U/mL penicillin, 100µg/mL streptomycin, 0.5% (v/v) Basal medium Eagle (BME) vitamins, pH 5.5.
<b>Complete M199 media</b>	500mL M199, 20% (v/v) HI FCS, 40mM HEPES, 100U/mL penicillin, 100µg/mL streptomycin, 100µM adenine, 0.005% (w/v) hemin.
<b>Complete Roswell Park Memorial Institute (RPMI) media</b>	500mL RPMI 1640, 2mM L-glutamine, 100U/mL penicillin, 100µg/mL streptomycin, 10% (v/v) HI FCS.
<b>Coomassie solution</b>	0.1% (v/v) Phast Gel™ Blue K (Healthcare, Buckinghamshire, UK) in 30% (v/v) methanol, 10% (v/v) acetic acid.
<b>Fluorescence-</b>	1% (v/v) FCS, 0.05% (w/v) sodium azide in phosphate-

<b>activated cell sorting (FACS) buffer</b>	buffered saline (PBS).
<b>FACS blocking solution</b>	10% (v/v) mouse/goat serum (as appropriate) in FACS buffer.
<b>Glutathione elution buffer</b>	20-50mM reduced glutathione, 100mM Tris-HCl, pH 8.0, 120mM sodium chloride.
<b>IF blocking solution</b>	1% (v/v) FCS, 5µg/mL purified rat anti-mouse CD16/CD32 (BD Bioscience, UK) in PBS.
<b>Liquid broth (LB)</b>	10g/L tryptone, 10g/L NaCl, 5g/L yeast extract in dH <sub>2</sub> O.
<b>LB agar</b>	17.5g/L agar, 10g/L tryptone, 10g/L NaCl, 5 g/L yeast extract in dH <sub>2</sub> O.
<b>Lysis buffer</b>	20mM TRIS, pH 8, 150mM NaCl, 2mM EDTA, 1% (v/v) IGEPAL CA-630 and a cocktail of protease inhibitors.
<b>Phosphate-buffered saline (PBS)</b>	One 5g PBS tablet GIBCO (Life Technologies, Paisley, UK) dissolved in 500mL dH <sub>2</sub> O, giving 0.01M phosphate buffer, 0.0027M potassium chloride, 0.137M sodium chloride, pH 7.4.
<b>Ponceau-S solution</b>	0.2% (v/v) Ponceau-S in 3% (w/v) trichloroacetic acid (TCA).
<b>Quenching solution</b>	50 mM NH <sub>4</sub> Cl in FACS buffer.
<b>Sodium dodecyl sulphate polyacrylamide gel electrophoresis (SDS-PAGE) 3x sample loading buffer</b>	188mM Tris, pH 6.8, 6% (w/v) SDS, 30% (v/v) glycerol, 0.03% (w/v) bromophenol blue, +/- 5% (v/v) β-mercaptoethanol.
<b>SDS-PAGE resolving gel</b>	0.375M Tris, pH 8.8, 0.1% (w/v) SDS, acrylamide [between 7.5-15% (v/v) depending on molecular weight of target protein], 0.5% (v/v) ammonium persulphate, 0.05% (v/v) tetramethylethylenediamine (TEMED) in de-ionised H <sub>2</sub> O.
<b>SDS-PAGE running buffer</b>	25mM Tris, pH 8.8, 192mM glycine, 0.1% (w/v) SDS in de-ionised H <sub>2</sub> O.
<b>SDS-PAGE stacking gel</b>	0.125M Tris, pH 6.8, 0.1% SDS, 4% (v/v) acrylamide, 0.5% (w/v) ammonium persulphate, 0.1% (v/v) TEMED in de-ionised H <sub>2</sub> O.

<b>SDS-PAGE transfer buffer</b>	25mM Tris, pH 8.8, 192mM glycine, 20% (v/v) methanol.
<b>TAE (Tris base, acetic acid and EDTA) buffer</b>	40mM Tris, pH 8, 20mM acetic acid, 0.5mM ethylenediaminetetraacetic acid (EDTA).
<b>Tris-buffered saline (TBS)</b>	20mM Tris, pH 7.4, 150mM NaCl.

## 2.2 Antibodies

The antibodies used in this project are shown in **Table 2.2** and were purchased from: Abcam (Cambridge, UK), BD Biosciences (Oxford, UK), BD Pharmingen (California, USA), BioLegend (London, UK), Developmental Studies Hybridoma Bank (University of Iowa, USA), eBioscience (Altrincham, UK), Invitrogen (UK), R&D Systems (Abingdon, UK), Santa Cruz (Dallas, USA) and Sigma (Gillingham, UK). Two non-commercial rat anti-mouse CCR5 antibodies (mc68 and mc69) were a kind gift from Prof Mack (Klinikum Universität Regensburg, Germany), with mc68 given as a purified IgG2b antibody and mc69 provided as non-purified hybridoma supernatant

**TABLE 2.2. Primary and secondary antibodies and isotype controls used in this project.** FC: flow cytometry; IF: immunofluorescence, WB: western blotting; IgG: immunoglobulin G; HRP: horseradish peroxidase.

<b>PRIMARY ANTIBODIES AGAINST CCR5</b>				
<b>Antibody name</b>	<b>Specificity</b>	<b>Species and isotype</b>	<b>Application / concentration</b>	<b>Source</b>
HM-CCR5 (7A4)	N terminal domain CCR5	Armenian Hamster IgG	FC: 2µg/mL	eBioscience
C34-3448	N terminus (amino acids 9-30) of CCR5	Rat IgG2c,κ	FC: 0.5-5µg/mL IF: 0.5-5µg/mL	BD Pharmingen
Clone 645807	N terminus (amino acids 1-32) of CCR5	Rat IgG1	WB: 0.5-10µg/mL	R&D Systems



E-6	Amino acids 62-250 of human CCR5	Mouse IgG1	WB:1-5µg/mL IF: 0.4-5µg/mL	Santa Cruz
D-19	N terminus of CCR5	Goat polyclonal IgG	WB: 1-5µg/mL IF: 0.4-5µg/mL	Santa Cruz
HEK/1/85a	Human CCR5	Rat IgG2a	FC: 5µg/mL	Abcam
CTC5	N terminus of human CCR5	IgG1	WB: 1-5µg/mL FC: 2.5µg/mL	R&D Systems

#### PRIMARY ANTIBODIES AGAINST OTHER TARGETS

Specificity	Antibody name	Species and isotype	Application / concentration	Source
α tubulin	Clone DM 1A	Mouse IgG1	WB: 5µg/mL	Sigma
CD45.2	Clone 104 (Alexa Fluor 647 conjugated)	Mouse IgG2a,κ	IF: 2.5µg/mL	BioLegend
F4/80	Clone BM8 (Alexa Fluor 488 conjugated)	Rat IgG2a,κ	IF: 2.5µg/mL	BioLegend
LAMP1	Clone 1D4B	Rat IgG2a,κ	IF: 0.72- 1.44µg/mL WB: 1.44µg/mL	Developmental Studies Hybridoma Bank
TLR2	Clone 6C2	Rat IgG2b,κ	Neutralising: 10µg/mL	eBioscience

#### SECONDARY ANTIBODIES

Antibody and specificity	Concentration	Source
Alexa Fluor 488 goat anti-mouse IgG	IF: 4µg/mL	Invitrogen
Alexa Fluor 488 goat anti-rabbit IgG	IF: 4µg/mL	Invitrogen
Alexa Fluor 488 goat anti-rat IgG	IF: 4µg/mL	Invitrogen
Alexa Fluor 555 goat anti-rat IgG	IF: 4µg/mL	Invitrogen

Alexa Fluor 555 goat anti-rabbit IgG	IF: 4µg/mL	Invitrogen
Alexa Fluor 647 goat anti-rat IgG	IF: 4µg/mL	Invitrogen
Alexa Fluor 647 goat anti-mouse IgG	IF: 4µg/mL	Invitrogen
HRP-conjugated goat anti-rabbit IgG	WB: 0.125 µg/mL	Sigma
HRP-conjugated rabbit anti-goat IgG	WB: 0.125 µg/mL	Sigma
HRP-conjugated rabbit anti-mouse IgG	WB: 0.125 µg/mL	Sigma
HRP-conjugated rabbit anti-rat IgG	WB: 0.125 µg/mL	Sigma

<b>ISOTYPE CONTROLS</b>		
<b>Antibody</b>	<b>Concentration</b>	<b>Source</b>
APC Armenian Hamster IgG (Clone: HTK888)	2µg/mL	BioLegend
Rat IgG2bk (Clone: eB149/10H5)	5µg/mL	eBioscience

## **2.3 Tissue culture**

### **2.3.1 Cell lines**

The macrophage-like cell line J774.2, originally derived from murine reticulum cell sarcoma (Ralph et al. 1975), was cultured in monolayers in complete DMEM. Cells were grown in 10cm adherent surface tissue culture dishes (Sarstedt, UK) in a humidified incubator at 37°C, 5% CO<sub>2</sub> and, when almost confluent, were detached using a cell scraper (Sarstedt, UK) for passaging.

### **2.3.2 Cryopreservation of cells**

Cells that were approximately 70% confluent were pelleted and left on ice for 10 mins to slow their metabolism. Cells were then re-suspended in 90% (v/v) heat-inactivated (HI)-FCS, 10% (v/v) dimethyl sulphoxide (DMSO) and aliquotted into Nunc™ cryovials (Life Technologies, Paisley, UK) before being transferred to a Mr Frosty™ container (Life Technologies, Paisley, UK) precooled to 4°C and left in a -80°C freezer for 24 hr. Cryovials were then submerged in liquid nitrogen for long-term storage. When required, cells were quickly thawed and re-suspended in pre-warmed media (complete DMEM or RPMI, as appropriate). Cells were centrifuged at 300 x g and re-suspended in complete media before plating onto 10cm tissue culture dishes.

## **2.4 Primary cells, mice and parasites**

### **2.4.1 Mice**

CCR5<sup>-/-</sup> mice (strain B6.129P2-Ccr5<sup>tm1Kuz</sup>/J; purchased from The Jackson Laboratory (USA); detailed in **Appendix A**) and appropriately matched wild-type mice (strain C57BL/6J) were housed in specific pathogen-free conditions. Female mice were used at 8-12 weeks old from both strains for experiments; male mice were used to isolate bone marrow. All experiments were covered by existing ethical approval and performed under a U.K. Home Office license.

### **2.4.2 Genotyping of mice**

Wild-type and CCR5<sup>-/-</sup> mice were polymerase chain reaction (PCR) screened to confirm the genotype for each group of mice. DNA was extracted from ear punch samples by mixing the tissue with 40µL 25mM NaOH and incubating at 95°C for 15 mins. Then, an equal amount of 40mM Tris-Cl was added to neutralise and 2µL of the mixture used as DNA template. Forward and reverse primers were made for both the wild-type (forward: 5'-CAG GCA ACA GAG ACT CTT GG; reverse: 5'-TCA TGT TCT CCT GTG GAT CG) and CCR5<sup>-/-</sup> (forward: 5'-CTT GGG TGG AGA GGC TAT TC; reverse: 5'-AGG TGA GAT GAC AGG AGA TC) mice, as suggested by The Jackson Laboratory's PCR guidance for these mice. All four primers were used in each PCR mix along with GoTaq® G2 flex enzyme (Promega, UK) and the standard PCR screening programme ran (see Section 2.11).

### **2.4.3 Isolating bone marrow cells**

Primary bone marrow cells were isolated from either wild-type C57BL/6 or CCR5<sup>-/-</sup> mice, as appropriate. Mice were sacrificed by CO<sub>2</sub> suffocation and cervical dislocation and their hind legs removed. Both ends of the femur and the tibia were cut to access the bone marrow cavity, which was then flushed with RPMI 1640 (non-supplemented, 4°C) using a 26-gauge needle. Cells were pipetted up and down to make a single cell suspension before being passed through a 100µm cell strainer and collected into a 50mL tube. The cell strainer was washed with non-supplemented RPMI 1640 several times

and any remaining cells collected. Cells were then centrifuged at 300 x *g* for 5 mins at 4°C and either used immediately or frozen in 90% HI FCS, 10% DMSO at -80°C before submerging in liquid nitrogen for long-term storage.

#### **2.4.4 Generating bone marrow-derived macrophages**

To make bone marrow-derived macrophages (BMDMs), bone marrow cells were cultured in complete RPMI for 3 days at 37°C, 5% CO<sub>2</sub> in a humidified incubator. On day 3, cells were washed once with PBS and the media replaced with complete RPMI supplemented with either 20% supernatant from L929 cells containing macrophage colony stimulating factor (m-CSF) or recombinant m-CSF (Sigma, UK) at 20ng/mL. Cells were then washed every 3 days with PBS and fresh media added (complete RPMI + 20% L929 supernatant). Twenty-four hours before using, the media was changed to complete RPMI (without L929 supernatant) to reduce the risk of vesicles from the supernatant contaminating experiments.

#### **2.4.5 Isolation of *Leishmania donovani* amastigote parasites**

The Ethiopian strain of *Leishmania donovani* (LV9) was used for parasite experimentation along with a transgenic line of *L. donovani* expressing tdTomato fluorescent protein (Beattie et al. 2008). Parasites were maintained by serial passage in B6.RAG1(recombination activating gene 1)<sup>-/-</sup> mice by infection with 3 x 10<sup>7</sup> amastigote parasites injected intravenously via the lateral tail vein. Parasites were harvested 3-9 months later.

For each experiment using *L. donovani* parasites, parasites were taken from an infected mouse. Mice spleens were isolated and processed for parasite isolation as previously described (Smelt et al. 1997). In brief, a glass dounce homogeniser was used to create a single-cell suspension of homogenised spleen in non-supplemented RPMI 1640. Cellular debris was removed by centrifugation at 130 x *g* for 5 mins at 37°C, and the supernatant transferred to a saponin-coated (1.25mg per mL supernatant) tube to lyse erythrocytes. Pellets of parasites were produced and washed by centrifuging three times at 1934 x *g* for 10 mins at 37°C, each time re-suspending in fresh non-supplemented RPMI 1640. A 26-gauge needle was used to break up parasite

aggregates, and parasites counted using a Helber bacteria-counting chamber (Weber Scientific International Ltd, Teddington, UK). Finally, parasites were re-suspended in complete RPMI and left overnight in a humidified incubator at 37°C, 5% CO<sub>2</sub>. The next day, parasites were passed through a 26-gauge needle several times and re-counted on a Helber bacteria-counting chamber (Weber Scientific International Ltd, Teddington, UK). For infections, parasites were added directly to cells with a multiplicity of infection (MOI) of 10 used for all experiments.

#### **2.4.6 Culturing promastigote *Leishmania donovani* parasites**

Amastigote *L. donovani* parasites were isolated from the spleen of infected RAG1<sup>-/-</sup> mice, as detailed in Section 2.4.5. Parasites were then counted using a haemocytometer counting chamber (Marienfeld Superior, Germany) and 1 x 10<sup>5</sup> parasites/mL re-suspended in complete M199 media. Parasites were cultured in a 26°C incubator and passaged 1:10 into fresh complete M199 media every 3 days until passage number 3. Then, 1 x 10<sup>5</sup> parasites/mL were re-suspended in complete Grace's media for 7 days to allow parasites to transform into infective metacyclic promastigotes ready for use.

## **2.5 Immunofluorescent imaging**

### **2.5.1 Preparation of coverslips**

Sterile coverslips were made by dipping 13mm round coverslips (Agar Scientific, Essex, UK) in 70% ethanol and baking at 121°C for at least 2 hr. Where poly-D-lysine coated-coverslips were required, 0.1mg/mL of poly-D-lysine was pipetted onto sterile coverslips and left for 30 mins at 22°C. Coverslips were then washed extensively with distilled H<sub>2</sub>O and left to air-dry.

### **2.5.2 Immunofluorescent staining**

Cells on coverslips were fixed using 3% (w/v) formaldehyde for 20 mins. Free aldehyde groups were then quenched in 50mM NH<sub>4</sub>Cl diluted in PBS and washed 2 x 5 mins, before being washed 1 x 5 mins in PBS. Coverslips were then blocked in IF blocking solution for 30 mins. To permeabilise cells, 0.05% (w/v) saponin was added to this blocking solution and any subsequent

washes. Primary antibody solutions, diluted to appropriate concentrations (see Table 2.2) in IF blocking solution, were then applied and left for 1 hr. Coverslips were washed in PBS (3 x 5 mins), and fluorescently tagged secondary antibodies were applied for 1 hr in IF blocking solution (see Table 2.2). They were then washed in PBS (3 x 5 mins), PBS with 1µg/mL DAPI (4'-6' diamidino-2-phenylindole, Invitrogen; 1 x 5 mins), and then mounted onto slides. Where cryosections were used, a hydrophobic barrier was drawn around cryosections prior to immunofluorescent staining.

### **2.5.3 Mounting of coverslips onto slides**

Coverslips were mounted onto slides using mowiol mounting medium and left to air-dry overnight before long-term storage at -20°C. Mowiol mounting medium was made by adding 6g glycerol and 2.4g mowiol 4-88 (Calbiochem) to 6mL dH<sub>2</sub>O and leaving at 22°C for 2 hr. To this, 12mL 0.2M Tris, pH 8.5, was added and the solution incubated at 50°C for 1 hr. The mixture was then clarified by centrifuging at 5000 x g for 15 mins.

### **2.5.4 Microscopy and image analysis**

Samples were visualised with the use of a Zeiss LSM 510 or 710 confocal microscope with an Axiocam HRC camera and images were taken with a 63x/1.4 NA Plan-apochromat oil objective. Acquired single slices and maximum intensity Z projections were analysed using ZEN imaging software (Zeiss, Cambridge, UK).

## **2.6 Electron microscopy**

The University of York Biology Department's in-house Technology Facility performed electron microscopy processing on collected samples. Cells were fixed in 4% (w/v) formaldehyde, 2.5% (w/v) glutaraldehyde in 100mM sodium phosphate buffer, pH 7.3, for 20 mins. Cells were then washed in 100mM sodium phosphate buffer, pH 7.3, 2 x 10 mins and post fixed with 1% (w/v) osmium tetroxide for 45 mins. After washing, cells were re-suspended with 1% (w/v) tannic acid in 100mM sodium phosphate buffer, pH 7.3, for 10 mins. They were then washed again in sodium phosphate buffer, pH 7.3, 2 x 10

mins and dehydrated through an ethanol series: 25% (v/v) ethanol for 15 mins, 30% (v/v) ethanol with 2% (w/v) uranyl acetate for 1 hr, and 50% ethanol (v/v) for 15 mins. This then switched to an acetone series, with steps of 15 mins for 50%, 70%, 90% and then 100% (v/v) acetone. Cells were then infiltrated with Spurr's resin during 20 mins steps: 25% (v/v) Spurr's resin, 75% (v/v) acetone; 50% (v/v) Spurr's resin, 50% (v/v) acetone; 75% (v/v) Spurr's resin, 25% (v/v) acetone; and 100% (v/v) Spurr's resin. Samples were then left at 70°C overnight for polymerisation. Sections were then visualised using an FEI Tecnai 12 G2 transmission electron microscope fitted with a charge-coupled device (CCD) camera.

## **2.7 Protein quantification**

Protein quantification was performed using a bicinchoninic acid (BCA) protein assay (Life Technologies, Paisley, UK) as per the manufacturer's instructions, except in circumstances where colloidal iron dextran (FeDex) had been used because it has been suggested that this may interfere with the assay as described in Rofe & Pryor (2015). In these cases, a Bradford assay was performed instead (Bio-Rad Laboratories, Hemel Hempstead, UK), as per the manufacturer's instructions.

## **2.8 Western blotting**

### **2.8.1 SDS-PAGE**

Lysed protein samples were prepared as described in subsequent chapters. Sample buffer (+/-  $\beta$ -mercaptoethanol reducing agent) was added to samples and then heated to 95°C for 5 mins, except when blotting for CCR5. Equivalent quantities of protein were loaded and samples analysed by SDS-PAGE using discontinuous polyacrylamide gels (upper SDS-PAGE stacking gel and lower SDS-PAGE resolving gel) on Bio-Rad minigel apparatus (Mini-PROTEAN Tetra cell, Bio Rad Laboratories, Hemel Hempstead, UK).

### **2.8.2 Membrane transfer**

Proteins were transferred onto nitrocellulose or polyvinylidene difluoride (PVDF) transfer membrane using either an iBlot dry blotting system (Life

Technologies, Paisley, UK) using standard programme 6 or a Transblot SD semi dry electrophoretic transfer cell (Bio-Rad Laboratories Ltd, Hemel Hempsted, UK) at 20V for 40 mins in SDS-PAGE transfer buffer. Gels were stained with Ponceau-S solution to visualise proteins on membranes.

### **2.8.3 Membrane immunoblotting**

Membranes were blocked overnight at 4°C using an appropriate blocking agent. As standard, 5% (w/v) Marvel milk powder was used in TBS with 0.1% (v/v) Tween-20 (TBS-T). Other blocking agents were tested for CCR5 western blotting: 10% (v/v) FCS, SEA BLOCK Blocking Buffer (Thermo Fisher Scientific, Hemel Hempstead, UK), 5% (w/v) BSA, or 5% (w/v) gelatin. Membranes were blocked overnight in blocking buffer at 4°C with agitation. The next day, membranes were incubated with the appropriate primary antibody (see Table 2.2) diluted in blocking buffer for 1 hr at 22°C under agitation. Membranes were then washed 3 times in TBS-T and incubated with an appropriate horseradish peroxidase (HRP)-conjugated secondary antibody (see Table 2.2) for 30 mins at 22°C under agitation. Membranes were washed in TBS-T 3 x 5 mins and immunolabelled proteins visualised using enhanced chemiluminescence western blotting reagents and X-ray film.

## **2.9 Flow cytometry**

### **2.9.1 Flow cytometry cell surface expression of CCR5 assay**

J774.2 cells were seeded into wells of a 24 well plates at a density of  $2 \times 10^5$  cells per well. Where necessary, the following day cells were infected with *L. donovani* amastigotes at an MOI of 10 for 24 hr. Cells were then processed for live staining flow cytometry.

### **2.9.2 Flow cytometry processing**

For live staining, cells were placed on ice and kept at 4°C throughout. Cells were scraped using a cell scraper (Sarstedt, UK) and placed into 5mL polystyrene round-bottom tubes (Thermo Fisher Scientific, Hemel Hempstead, UK). For each step, cells were centrifuged at 300 x g for 5 mins



at 4°C. Fc receptors were blocked by re-suspending in FACS blocking solution for 30 mins and then incubated with primary antibody (diluted in FACS blocking solution; see Table 2.2) for 1 hr. Cells were washed with FACS buffer 3 x 5 mins and then fixed with 4% (w/v) formaldehyde in FACS buffer for 20 mins. Free aldehyde groups were quenched using quenching solution 2 x 5 mins and cells washed with FACS buffer 1 x 5 mins. Then, if necessary, cells were incubated with secondary antibody (diluted in FACS blocking solution; see Table 2.2) for 1 hr. Cells were then washed using FACS buffer and kept at 4°C until analysed. For non-live staining, cells were fixed (as above) prior to blocking/antibody steps. Appropriate isotype control antibodies (see Table 2.2) were used to assess background staining.

### **2.9.3 Flow cytometry analysis**

Flow cytometry analysis was performed using a CyAn flow cytometer (Beckman Coulter, UK) where the mean fluorescence intensity (MFI) of each sample was determined by measuring approximately 10,000 events. The main population of cells was always gated to remove cellular debris. Data collected was analysed using Summit 4.0 software (Dako, USA).

### **2.9.4 CFDA-SE labelling of cells**

Cells were labelled in suspension with 5µM carboxyfluorescein diacetate succinimidyl ester (CFDA-SE) in non-supplemented DMEM or RPMI-1640 media for 30 mins at 37°C, 5% CO<sub>2</sub> in a humidified incubator. The labelling reaction was stopped by re-suspending cells in complete DMEM or RPMI media.

### **2.9.5 Transwell infection assay**

Cells were seeded 24 hr prior to infection in the top and bottom chambers of 0.4µm filter transwell inserts (Corning, US) placed into 24 well plates. When necessary, cells were infected at an MOI of 10 using *L. donovani* amastigote parasites, with care taken not to contaminate sample between chambers. Cells were then processed for live flow cytometry staining.

### **2.9.6 Translocation infection assay**

Cells were seeded 24 hr prior to infection into wells of a 24 well plate. The cells in half of the wells were CFSE-labelled and infected with *L. donovani* parasites at an MOI of 10 for 6 hr; the cells in the other wells were left non-CFSE-labelled and non-infected. After 6 hr, all cells were detached using a cell scraper (Sarstedt, UK) and re-seeded into new wells of a 24 well plate. Cells were left for a further 18 hr and then processed for live flow cytometry staining.

### **2.10 Enzyme-linked immunosorbent assay (ELISA)**

Collected cell supernatant was centrifuged at 2000 x *g* for 10 mins at 22°C to remove particulate material. Using the standard manufacturer's protocol, a Multi-Analyte ELISArray Kit (MEM-009A; Qiagen) was performed to determine the fold change in CCR5-specific chemokines compared to uninfected control cells.

### **2.11 Polymerase chain reaction (PCR)**

#### **2.11.1 DNA amplification by PCR**

DNA was isolated using a QIAprep Spin Miniprep Kit (QIAGEN, UK). Appropriate forward and reverse primers were added to PCR reaction mixtures to give a final primer concentration of 0.5µM. A PCR reaction mix consisted of 1 unit GoTaq® G2 flex enzyme (Promega, UK), 1x GoTaq® reaction buffer (Promega, UK), 1.5mM MgCl<sub>2</sub> and 200µM dNTPs. DNA amplification was performed on a Bio Rad PTC-200 DNA engine cycler (Bio Rad Laboratories, Hemel Hempstead, UK). The general PCR cycle used was: 94°C for 45 secs, then 30 cycles of 94°C for 45 secs, (T<sub>m</sub>-5)°C for 45 secs (where T<sub>m</sub> is the temperature at which 50% of the primer is bound to its target template), and 72°C for 1 min (per 1000 bases of PCR product). When all cycles had completed, one final cycle of 72°C for 10 mins was performed and then samples held at 4°C until analysed. All DNA amplifications were performed using appropriate negative controls to detect contamination.

### **2.11.2 Agarose gel electrophoresis of PCR products**

Amplification products were analysed by gel electrophoresis on a 2.5% (w/v) agarose gel and DNA electrophoresed at 60V constant in TAE buffer. DNA was visualised using a blue light transilluminator after being stained with SYBR™ Safe (Invitrogen, UK). PCR products were excised from the gel using a sterile scalpel blade and purified using a gel purification kit (Qiagen, Netherlands), as per the manufacturer's instructions.

### **2.11.3 qRT-PCR of mRNA levels**

Total RNA was extracted from cells using an RNeasy mini kit (QIAGEN, UK), as per the manufacturer's instructions. For cDNA synthesis, 100ng of total RNA was reverse-transcribed using Superscript II reverse transcriptase (Invitrogen, UK). qRT-PCR was performed on cDNA from each sample using 10µL Fast SYBR™ Green PCR Master Mix, 0.6µL 10µM forward primer, 0.6µL 10µM reverse primer and 7.8µL nuclease-free H<sub>2</sub>O, per reaction. All reactions were performed in duplicate. Primers were designed against CCR5 (forward: 5'-AAG AGA CTC TGG CTC TTG CAG; reverse: 5'-GAG CTG AGC CGC AAT TTG TT) and hypoxanthine guanine phosphoribosyl transferase (HPRT) as a loading control (forward: 5'-GCG TCG TGA TTA GCG ATG ATG AAC; reverse: 5'-ATC TCC TTC ATG ACA TCT CGA GCA AGT C). The PCR reactions were performed using a StepOnePlus Real Time PCR System (Applied Biosystems). At the end of the run, a melt curve analysis was performed to monitor non-specific product formation and primer dimers. Relative mRNA levels were calculated using the  $2^{-\Delta\Delta CT}$  method (Livak & Schmittgen 2001), with mRNA levels normalised to HPRT.

## **2.12 Mass spectrometry**

The University of York Biology Department's in-house Technology Facility performed LC-MS/MS on collected samples.

### **2.12.1 In-gel deglycosylation and digestion**

Samples were solubilised in NuPAGE lithium dodecyl sulphate (LDS) sample buffer (Life Technologies, Paisley, UK) with heating at 70°C for 10 mins

before running into a 7cm NuPAGE Novex 10% Bis-Tris Gel (Life Technologies, Paisley, UK) at 200V for 6 mins. Gels were stained with SafeBLUE protein stain (NBS Biologicals, UK) for a minimum of 1 hr before destaining with ultrapure water for a minimum of 1 hr. In-gel deglycosylation and tryptic digestion was performed after reduction with dithioerythritol (DTE) and S-carbamidomethylation with iodoacetamide. Gel pieces were washed twice with 50% (v/v) aqueous acetonitrile containing aqueous 25mM ammonium bicarbonate, then once with acetonitrile and dried in a vacuum concentrator for 20 mins. Proteins were O-deglycosylated with the addition of aqueous 25% (v/v) ammonium hydroxide and incubation overnight at 45°C. Gel pieces were washed with acetonitrile and dried in a vacuum concentrator for 20 mins before N-deglycosylation with 3 units of PNGaseF (Roche) in aqueous 100mM ammonium bicarbonate and incubated overnight at 37°C. Gel pieces were washed in acetonitrile and dried down before addition of trypsin. Sequencing-grade, modified porcine trypsin (Promega) was dissolved in 50mM acetic acid, then diluted 5-fold with 25mM ammonium bicarbonate to give a final trypsin concentration of 0.02mg/mL. Gel pieces were rehydrated by adding 25mL of trypsin solution, and after 10 mins enough 25mM ammonium bicarbonate solution was added to cover the gel pieces. Digests were incubated overnight at 37°C. Peptides were extracted by washing three times with 50% (v/v) aqueous acetonitrile containing 0.1% (v/v) trifluoroacetic acid, before being dried down in a vacuum concentrator and reconstituted in aqueous 0.1% (v/v) trifluoroacetic acid. Samples were buffer exchanged into aqueous 0.5M triethylammonium bicarbonate using Strata C<sub>18</sub>-E cartridges (55mm; 70Å; 50mg/mL) before isobaric tag for relative and absolute quantitation (iTRAQ) labelling.

### **2.12.2 iTRAQ Labelling and Peptide Fractionation**

Peptides were labelled with iTRAQ 8-plex reagents (SCIEX) before being combined and desalted using an iCAT cation exchange cartridge (SCIEX) as detailed in the manufacturer's protocol. Post cation exchange, the samples were dried down in a vacuum concentrator before 300mL of aqueous 0.1% (v/v) trifluoroacetic acid was added. A reverse phase pH-resistant C<sub>18</sub> column (Pierce) was packed, washed and conditioned following the manufacturer's

protocol. Combined labelled peptides were loaded onto the column with centrifugation at 5,000 x *g* for 2 mins before washing with 300mL of liquid chromatography-mass spectrometry (LC-MS) grade water. Peptides were eluted into 8 fractions using increasing concentrations of acetonitrile in aqueous triethylamine, ranging from 10% acetonitrile (v/v) with 0.9% triethylamine (v/v) to 50 % acetonitrile (v/v) with 0.05% trimethylamine (v/v). Peptides were eluted at each solvent composition with centrifugation at 5,000 x *g* for 2 mins. Fractions were dried down in a vacuum concentrator before reconstituting in aqueous 0.1% (v/v) trifluoroacetic acid.

### 2.12.3 LC-MS/MS

High pH C<sub>18</sub> fractions were loaded onto a nanoAcquity UPLC system (Waters) equipped with a nanoAcquity Symmetry C<sub>18</sub>, 5µm trap (180µm x 20mm, Waters) and a nanoAcquity HSS T3 1.8 µm C<sub>18</sub> capillary column (75µm x 250mm, Waters). The trap wash solvent was 0.1% (v/v) aqueous formic acid and the trapping flow rate was 10µL/min. The trap was washed for 5 mins before switching flow to the capillary column. The separation used a gradient elution of two solvents (solvent A: 0.1% (v/v) formic acid; solvent B: acetonitrile containing 0.1% (v/v) formic acid). The flow rate for the capillary column was 300nL/min. Column temperature was 60°C and the gradient profile was linear 2-30% B (98-70% A) over 240 mins then linear 30-50% B (70-50% A) over 5 mins, all runs then proceeded to wash with 95% B (5% A) for 2.5 mins. The column was returned to initial conditions and re-equilibrated for 25 mins before subsequent injections. The nanoLC system was interfaced with a maXis HD LC-MS/MS system (Bruker Daltonics) with CaptiveSpray ionisation source (Bruker Daltonics). Positive ESI-MS and MS/MS spectra were acquired using AutoMSMS mode. Instrument control, data acquisition and processing were performed using Compass 1.7 software (microTOF control, Hystar and DataAnalysis, Bruker Daltonics). Instrument settings were: ion spray voltage: 1,450V, dry gas: 3L/min, dry gas temperature 150°C, ion acquisition range: *m/z* 150-2,000, MS spectra rate: 5Hz, MS/MS spectra rate: 5Hz at 2,500 cts to 20Hz at 250,000 cts, cycle time: 1 s, quadrupole low mass: 300 *m/z*, collision RF: 1,400 Vpp, transfer time 120 ms. The collision energy and isolation width settings were

automatically calculated using the AutoMSMS fragmentation table, absolute threshold 200 counts, preferred charge states: 2 – 4, singly charged ions excluded. A single MS/MS spectrum was acquired for each precursor and former target ions were excluded for 0.8 min unless the precursor intensity increased fourfold.

#### **2.12.4 Database Searching**

Tandem mass spectra were searched against the human subset of the UniProt database (20,259 sequences; 11,329,622 residues) using a locally-running copy of the Mascot program (Matrix Science Ltd., version 2.5.1), through the Mascot Daemon interface (version 2.5.1). Search criteria specified: Enzyme, Trypsin; Fixed modifications, Carbamidomethyl (C) and iTRAQ8plex (N-term, K); Variable modifications, Oxidation (M), Asn->Asp (N), Ser->Dha (S), Thr->DAb (T) and iTRAQ8plex (Y); Peptide tolerance, 10 ppm; MS/MS tolerance, 0.1 Da; Instrument, ESI-QUAD-TOF. Results were passed through Mascot Percolator to achieve a global false discovery rate of 1% and further filtered to accept only peptides with an expect score of 0.05 or lower.

#### **2.13 Statistical analyses**

Unless otherwise stated, unpaired or paired (as appropriate) Student t-tests were performed when 3 or more replicates were available. A p value of  $\leq 0.05$  was considered significant. All statistical analyses were performed in GraphPad Prism 5 software.

# **3. The effect of *L. donovani* infection on CCR5 expression *in vitro***

## **3.1 Chapter-specific background and rationale**

It has been suggested that *in vitro* *L. donovani* infection may influence the expression of CCR5 in macrophages (Dasgupta et al. 2003; Bhattacharyya et al. 2008; Majumdar et al. 2014). To fully characterise the association between CCR5 and the parasite, it is important to consider how the parasite may alter both the expression and intracellular trafficking of the receptor in response to infection. There are a number of established techniques for studying chemokine receptor biology (Kershaw et al. 2009); however, most rely on the use of reliable monoclonal antibodies verified against their target receptor.

Although the GPCR superfamily consists of a considerable number of membrane proteins, GPCRs are notoriously difficult to develop antibody tools for because of a lack of suitable antigens to use as an antibody target. For example, the majority of an individual GPCR is embedded into the lipid bilayer of the plasma membrane making accessibility problematic and overexpression of GPCRs for use in cellular systems is difficult (Hutchings et al. 2010). The linear peptides of the terminal sequences of GPCRs are often used as targets. However, they lack the post-translational modifications and structural features of the *in situ* receptor (Hutchings et al. 2010). Furthermore, GPCRs are often very unstable when purified (Hutchings et al. 2010).

### **3.1.1 Techniques available for investigating the role of chemokine receptors during infection**

There are several methods available to detect and follow expression of chemokine receptors, including flow cytometry, immunofluorescence (IF) imaging, fluorescent chemokines, western blotting, immunoprecipitation and genetic analyses (Kershaw et al. 2009). However, the three most commonly used methods are flow cytometry, IF imaging and western blotting. Flow cytometry is the preferred method used to track CCR5 expression and quantify receptor internalisation (Kershaw et al. 2009), and has been used extensively to characterise both cell surface expression (e.g. Fox et al. 2011) and internalised stores of chemokine receptors, as described in Kershaw et al. (2009). This is important because for chemokine receptors to have a functional role, it is necessary that they be expressed at the cell surface where they interact with ligands and initiate downstream intracellular signalling cascades. Thus, flow cytometry is particularly useful for this application and for providing quantification data that would not be possible with IF staining. However, IF staining has an advantage over flow cytometry in that it can be used to visualise and localise the receptor within individual cells. For determining changes in the total protein levels of CCR5 within a cell, western blotting is the primary method used (Kershaw et al. 2009) and is useful to determine whether a pathogen is inducing overall receptor biogenesis or degradation.

For all three of the aforementioned techniques, the specificity of antibodies is important and may be a particular problem for chemokine receptors with a number of commercially available antibodies having questionable specificity (Bernstone et al. 2012; Ford et al. 2013). Alternatives to chemokine receptor-specific antibodies have been generated. For example, small molecular tags can be added to the N-terminal region of the receptor allowing for other antibodies to be used against the specific tag (Kershaw et al. 2009). These are often more readily available and better characterised than antibodies against chemokine receptors. However, the use of these physical tags may



interfere with the interaction between the receptor and the pathogen, again making this technique unfavourable for studying host-pathogen interactions. As another example, fluorescently labelled chemokines can be used to map where chemokine receptors are located based on ligand-binding (Ford et al. 2013). This can be done on cells cooled to 4°C to label receptors present at the cell surface or at 37°C to follow receptor internalisation. However, owing to the promiscuous nature of many chemokines being able to bind to several different receptors, binding proteoglycan and the ability of some chemokines to be taken up via pinocytosis (Ford et al. 2013), this technique is challenging to use for monitoring specific chemokine receptors. Furthermore, these chemokines often activate the receptor meaning that the receptor cannot be examined in its basal state.

An alternative approach to investigating chemokine receptors is to study the mRNA level rather than protein expression. However, for chemokine receptors it is well established that this method may not truly reflect what is happening with functional forms of the receptor (Ford et al. 2013), particularly when the functional relevance of expressed chemokine receptors is dependent on the presence of receptors at the cell surface. As previously discussed, there are large intracellular reservoirs of chemokine receptors that can greatly influence chemokine-signalling cascades without any change in mRNA expression. Conversely, increases or decreases in mRNA may not necessarily change cell surface expression of the receptor.

Investigations into chemokine receptor function in mouse models of disease have primarily relied on the use of knockout mice and RNA interference because of the relative absence of antibodies against murine chemokine receptors (Mack et al. 2001; Bernstone et al. 2012). However, these techniques also have problems, particularly with regard to chemokine receptors that have traditionally been associated as having compensatory mechanisms to adapt to the lack of a particular receptor (Chen et al. 2003). These techniques allow the receptor's influence on infection to be studied, but not the converse. Thus, it is clear that to be able to properly define the role of murine CCR5 during homeostasis and infection, additional antibody

tools are needed that are specific against the murine form of the receptor. This would also facilitate the translation of mouse chemokine studies into humans, and vice versa, greatly expanding the knowledge of how these receptors work, particularly when they are exposed to pathogenic agents such as *Leishmania*.

### **3.1.2 Objectives**

The literature pertaining to the association between CCR5 and *L. donovani* is often contradictory, likely due to differences in the species of *Leishmania* used and the host species of infection. In this chapter, we aimed to characterise the effect that infection with *L. donovani* LV9 amastigotes had on CCR5 expression and localisation using the same species and form of the parasite that would be used for *in vivo* experiments. Due to the lack of specificity for some chemokine receptor antibodies, we first aimed to check the antibody tools available to follow CCR5-specific expression and localisation in mouse cells. Due to the general lack of antibody tools available for tracking the structurally distinct murine form of the receptor, we then aimed to make our own antibody that could be used for intricate CCR5 tracking studies. Finally, having identified an antibody that we were confident was able to give specific staining for CCR5, we aimed to determine the levels of CCR5 at the cell surface to characterise cell surface expression of the receptor during *L. donovani* LV9 amastigote infection. Together, this allowed us to determine changes in CCR5 associated with infection.

## **3.2 Chapter-specific methods**

### **3.2.1 Generating antibodies against murine CCR5**

#### **3.2.1.1 Primer design and plasmid generation**

The pGEX-3PLX vector system (Long et al. 1995) was used to make recombinant proteins consisting of N or C terminal regions of CCR5 attached to glutathione S-transferase (GST), with GST chosen because it is stable, highly soluble and is known to elicit a strong immune response (Lynne et al. 2006). Forward and reverse primers were designed for both the N terminus (forward primer: 5'-TACCGCGGCCGCTAGCATGGATTTTCAAGGGTCAGTT-3'; reverse primer: 5'-TCGACTGCATGCTAGTTACTGAGCCGCAATTTGTTT-3') and C terminus (forward primer: 5'-TACCGCGGCCGCTAGCATTTTCCAGCAAGACAAT-3'; reverse primer: 5'-TCGACTGCATGCTAGTCATAAACCAGTAGAACTTCATG-3') of CCR5. Using these primers and mouse splenocyte cDNA, PCR was used to produce full-length N- or C-terminus products (as detailed in Section 2.11), and the size of these products was confirmed by agarose gel electrophoresis. After linearising the vector using the Nhe1 restriction enzyme, these products were then inserted into the pGEX-3PLX vector using an In-Fusion HD Cloning Kit (Clontech, USA) as per manufacturer's instructions.

#### **3.2.1.2 Transforming bacteria with target plasmid**

DH5- $\alpha$  bacteria were heat-shock transformed with the pGEX-3PLX vector containing either the N terminal or C terminal construct. This involved cooling bacteria to 4°C for 5 mins, heating bacteria to 42°C using a waterbath for 30 seconds and then cooling to 4°C for a further 5 mins. Bacteria were then streaked onto LB agar plates containing ampicillin (100 $\mu$ g/mL).

Transformation of single colonies was confirmed by PCR screening the following day. Colonies were grown overnight in LB agar plates with ampicillin (100 $\mu$ g/mL). Plasmid DNA was then purified using a QIAprep Spin Miniprep Kit (Qiagen, Netherlands) and correct insertion of the plasmid confirmed by sequencing (Source BioScience, United Kingdom).

### **3.2.1.3 Protein production**

BL21 (DE3) pLysS bacteria were transformed with plasmids and grown on LB agar plates with ampicillin (100µg/mL) and chloramphenicol (25µg/mL). Single colonies were picked and grown overnight at 37°C in a shaking incubator in LB containing ampicillin (100µg/mL) and chloramphenicol (25µg/mL). The following morning, high nutrient LB (1L of distilled water containing 16g tryptone, 10g yeast extract and 5g NaCl) containing ampicillin (100µg/mL) was inoculated with 2mL of overnight culture. When grown at 37°C and in their exponential growth phase, bacteria were then treated with isopropyl β-D-1-thiogalactopyranoside (IPTG; final concentration of 0.2mM) to induce protein expression. After 4 hr of treatment at 37°C, bacteria were re-suspended in lysis buffer (PBS containing 1% (v/v) Triton X-100, protease inhibitors, 1U/mL DNase, lysozyme 1mg/mL and 2mM MgCl<sub>2</sub>) and frozen overnight.

### **3.2.1.4 Purifying GST-CCR5 recombinant proteins**

The lysate was defrosted slowly at 22°C and centrifuged at 47,800 x g for 20 mins. The soluble proteins in the supernatant were removed and mixed with glutathione sepharose beads for 2 hr at 4°C. The mixture was then passed through a plastic column with a frit and the beads washed several times with PBS + 1% (v/v) Triton X-100. Bound protein was eluted by the addition of 20mL of elution buffer (50mM Tris, pH 8.0, 10mM reduced glutathione) and multiple 1mL fractions were collected. Fractions were analysed with Coomassie stain on 3M paper to determine which fractions had the most protein; the most concentrated fractions were then ran on a 10% SDS-PAGE gel. Samples were then dialysed against PBS (using 3.5k molecular weight cut-off (MWCO) tubing).

### **3.2.1.5 Polyclonal antibody production in rabbits**

Rabbit polyclonal antibodies were made against the N- and C-terminal GST recombinant proteins using a third party provider (Dundee Cell Products, UK). For each N- or C-terminus construct, two rabbits were inoculated with 2mg of GST-CCR5 recombinant protein in PBS. Rabbits were immunised 3 times and final bleed sera collected.

### **3.2.1.6 Affinity purification of anti-CCR5 antibodies**

Separate samples of GST protein alone and the two GST-CCR5 recombinant proteins were made using the protein production protocol detailed in Section 3.2.1.3. For each protein, the resulting lysate was then defrosted slowly at 22°C and centrifuged at 47,800 x *g* for 20 mins. The soluble proteins in the supernatant were removed and mixed with glutathione sepharose beads for 2 hr at 4°C. The mixture was then passed through a plastic column with a frit and the beads washed several times with PBS + 1% Triton X-100. Final bleed sera resulting from rabbits inoculated with either GST-CCR5(N) or GST-CCR5(C) recombinant proteins (see Section 3.2.1.5) were then passed through separate GST-bound columns to bind GST-specific antibodies. The flow-through was then passed through either a GST-CCR5(N)- or GST-CCR5(C)-bound column, respectively. CCR5-specific antibodies were then eluted from these columns by the addition of 20mL of 200mM glycine, 0.1% (w/v) gelatin, pH 4.0. The acid was neutralised using 1M Tris, pH 9.0, and multiple 1mL fractions were collected. Fractions were analysed with Coomassie stain on 3M paper to determine which fractions had the most protein.

### **3.2.2 Culturing *E. coli* and *R. equi* for infection assay**

LB was inoculated with *Escherichia coli* and left to grow at 37°C in a shaking incubator until the optical density of the sample measured at a wavelength of 600nm (OD<sub>600</sub>) was 0.3, corresponding to 2.4 x 10<sup>8</sup> bacteria/mL. Bacteria were washed several times in PBS and used to infect J774.2 cells at an MOI of 10. Then, flow cytometry cell surface expression of CCR5 assays were performed as detailed in Section 2.9.1. Another researcher of the Pryor laboratory (Adam Rofe) supplied *Rhodococcus equi*, which was grown from a single colony in brain heart infusion broth (Sigma, UK) overnight at 30°C in a shaking incubator. Cell numbers were estimated using OD<sub>600</sub> values.

### **3.2.3 CCR5 blockade using Met-RANTES**

The CCR5 ligand Met-RANTES (1µg/mL), which has been shown to be an effective antagonist for CCR5 in murine cells (Mack et al. 2001), was added

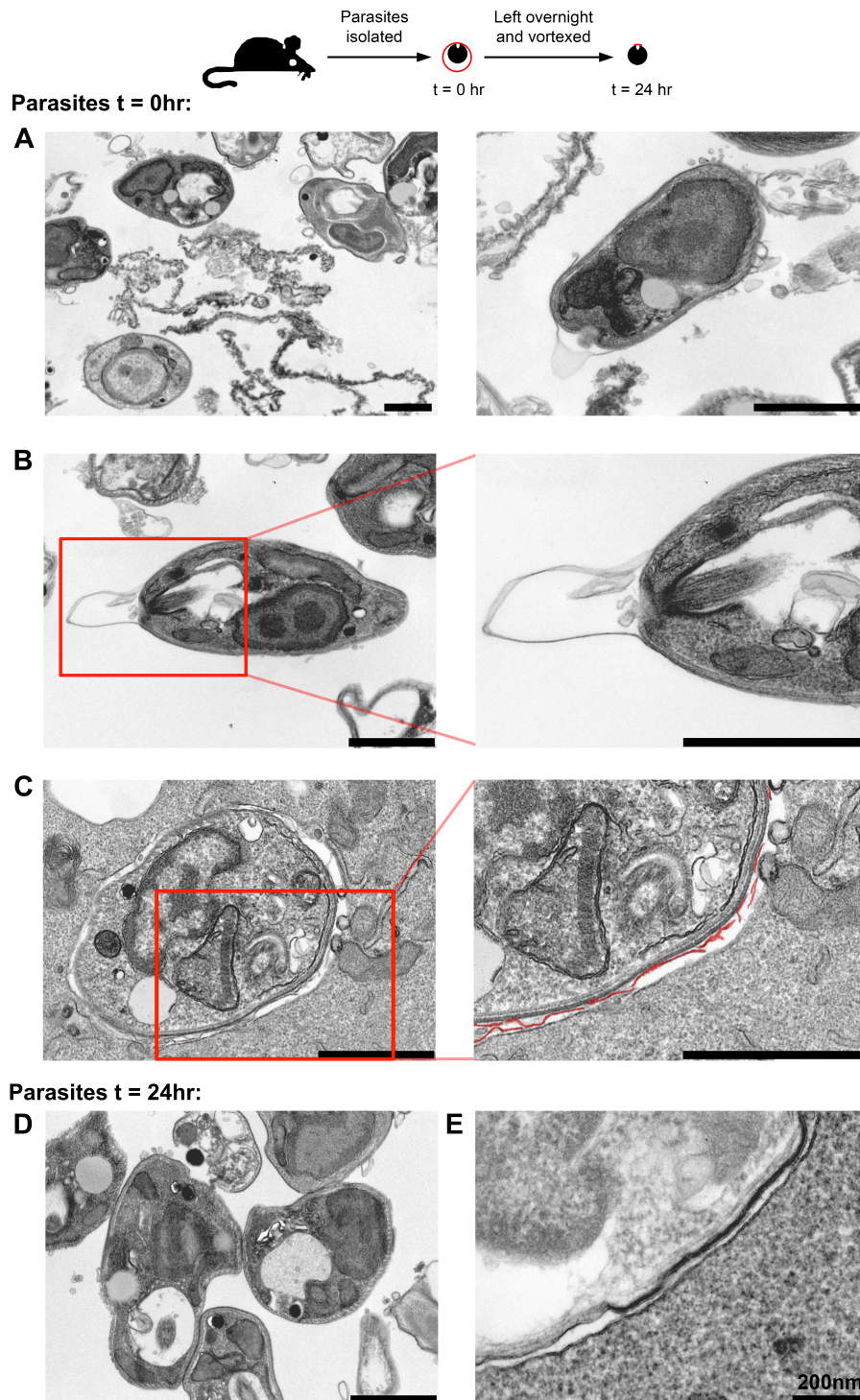
to cells 1 hr prior to *L. donovani* infection. Parasites were added to cells drop-wise without the removal of antagonist. When necessary, 1 hr prior to harvesting cells murine CCL5 (1µg/mL; PeproTech, UK), a CCR5 agonist, was added to wells. Cell surface expression was analysed by flow cytometry, as described in Section 2.9.1.

## 3.3 Results

### 3.3.1 Characterising the parasite preparation

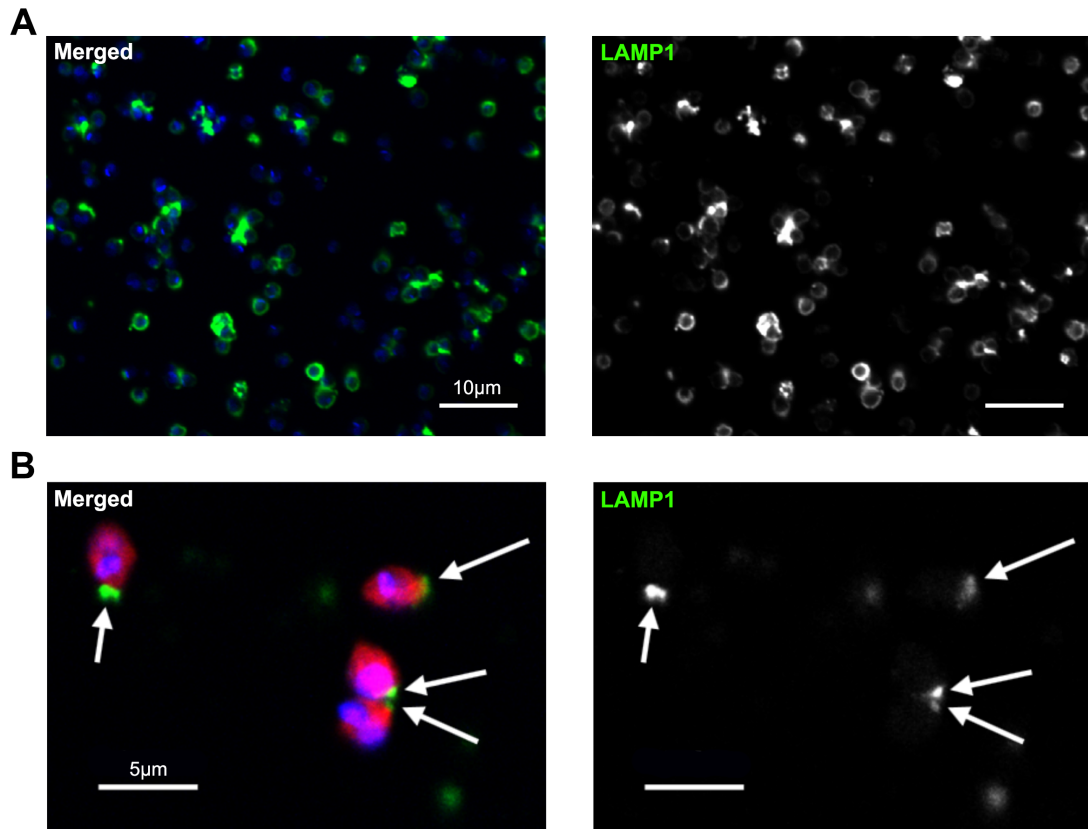
The method detailed in Section 2.4.5 used to isolate amastigote *L. donovani* parasites from an infected mouse spleen may lead to co-contaminants being present within the parasite preparation, which could include membranous material, subcellular debris and even whole cells from the host spleen. This could be a problem for characterising interactions with cell surface receptors because it is harder to attribute any effect seen directly to the parasite. It was therefore important to characterise the contents of these preparations before progressing to *in vitro* experimentation.

To this end, a parasite preparation was made and processed for transmission electron microscopy (TEM). As shown in **Figure 3.1A**, there were numerous examples of membranous material dissociated from parasites and free in the sample. In addition, the majority of parasites in this sample were surrounded by membranous material that often enclosed the entire parasite (**Figure 3.1B**). When these parasites were used to infect J774.2 cells, TEM images showed that many of the parasites that were taken up in a compartment were surrounded by a double membrane, as shown in **Figure 3.1C**. Others have reported that this does not affect parasite uptake by cells (Chang & Dwyer 1978). Leaving parasite preparations in a humidified 37°C, 5% CO<sub>2</sub> incubator overnight removed the majority of membranous material associated with parasites (**Figure 3.1D**), which were remnants from the LAMP1+ve parasite-containing compartment from RAG1<sup>-/-</sup> mouse macrophages (**Figure 3.2**). This remnant material was likely to be the point of attachment of the parasite to the host-cell phagosome which occurs at the posterior pole of the parasite (Benchimol & de Souza 1981). Subsequent experiments were all performed using parasite preparations that had been left overnight to minimise membranous material that could interfere with results.



**FIGURE 3.1. Within parasite preparations, host cell membranes can be found both surrounding parasites and freely in suspension.** Parasites were processed for TEM either immediately after isolating from an infected spleen (t=0hr) or after leaving for 24hr and vortexing. **A)** Fields of view showing multiple t=0hr parasites and surrounding material. **B)** Increased zoom on an individual t=0hr parasite. **C)** Infection of J774.2 cells with t=0hr parasites with membranous material surrounding the internalised parasite highlighted in red. **D)** Field of view showing multiple J774.2 cells infected with t=24hr parasites. **E)** Increased zoom on a t=24hr parasite taken up by a host cell. Scale bar = 1µm unless otherwise stated.





**FIGURE 3.2. Membranes surrounding parasites were LAMP1+ve and significantly reduced after leaving parasites in culture overnight.** Parasites were processed for immunofluorescent staining either immediately after isolation from an infected spleen (t=0hr; **A**) or after leaving for 24hr and vortexing (**B**). Blue = DAPI; red = tdTomato *L. donovani* amastigotes; green = LAMP1.

### 3.3.2 Genotyping of wild-type and CCR5<sup>-/-</sup> mice

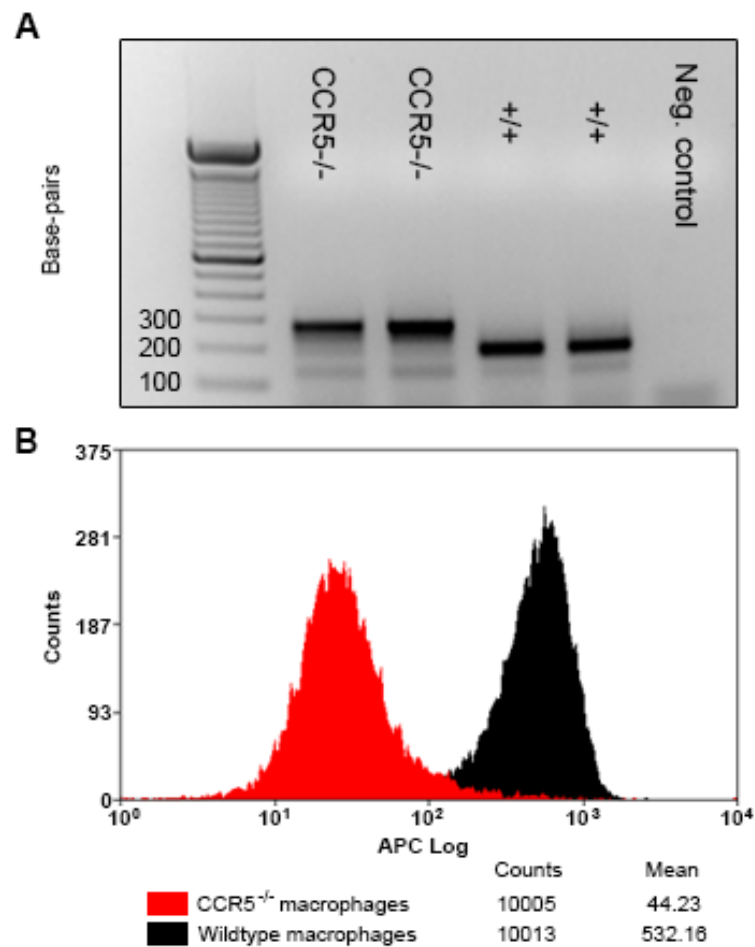
Wild-type and CCR5<sup>-/-</sup> BMDMs were generated to use for testing antibodies and for subsequent flow cytometry experiments. Mice were genotyped using a protocol provided by The Jackson Laboratory and confirmed as homozygote mutants lacking the CCR5 receptor, as shown in **Figure 3.3A**. To confirm that this genotype correlated with a lack of CCR5 at the protein level, bone marrow cells were isolated from CCR5<sup>-/-</sup> and wild-type mice and cultured *in vitro* to produce bone marrow-derived macrophages (BMDMs). The cell surface expression of CCR5 on these BMDMs was then assessed by flow cytometry using mc68, a rat anti-mouse CCR5 antibody gifted to us by Prof Mack (Klinikum Universität Regensburg, Germany). As shown in **Figure 3.3B**, there was a two-log reduction in the mean fluorescent intensity (MFI) associated with anti-CCR5 staining when compared to wild-type BMDMs. Thus, these CCR5<sup>-/-</sup> mice have the correct genotype and phenotype.

### 3.3.3 Testing of available murine CCR5 antibodies

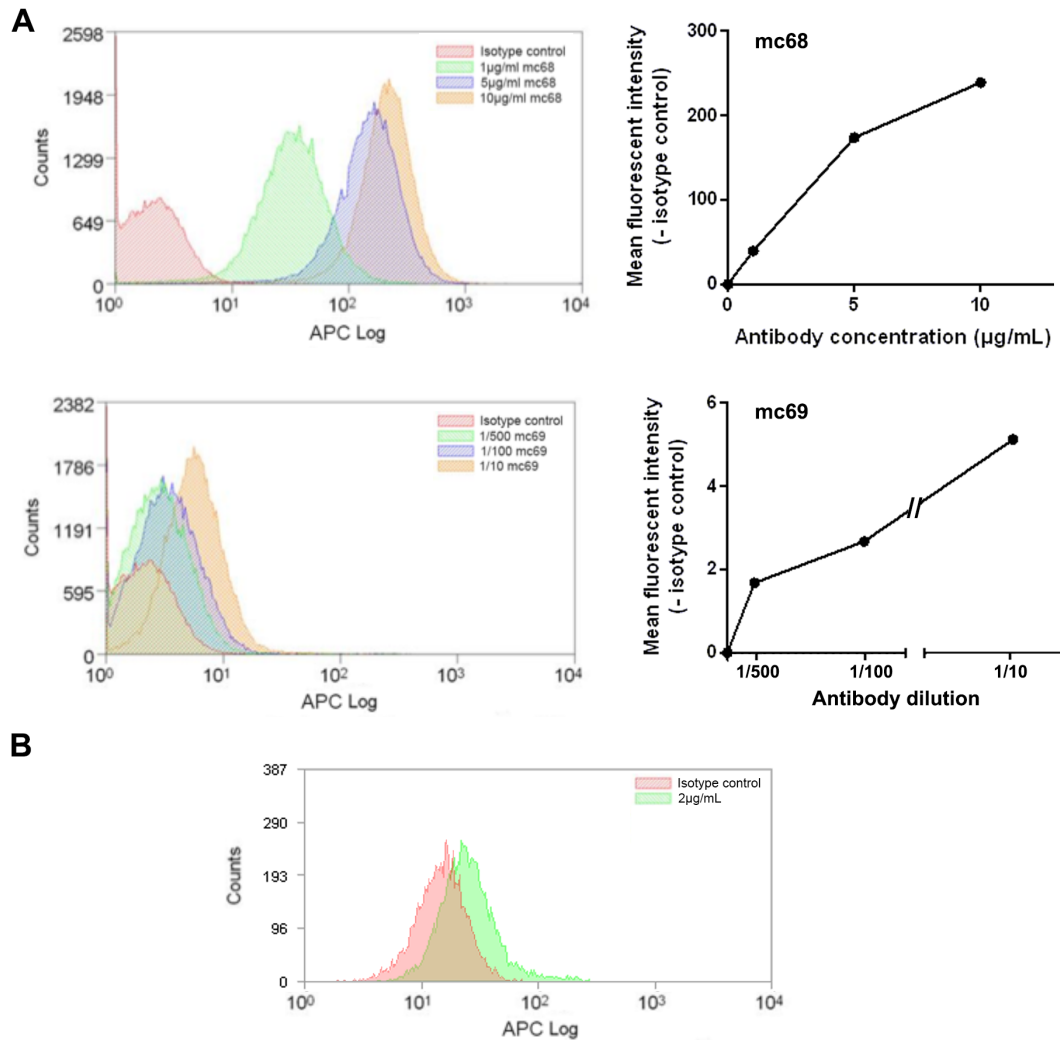
Despite the majority of CCR5 experimentation being conducted on human cells, there were some commercial antibodies that pertain to work against murine CCR5. We also had access to well-defined non-commercial antibodies (mc68 and mc69) targeting murine CCR5, the former of which has been used previously to define CCR5 cell surface expression patterns on murine leukocytes (Mack et al. 2001). We decided to characterise all of these antibodies in a range of different conditions to establish which would be useful for the current study.

#### 3.3.3.1 Flow cytometry for CCR5 expression

As the preferred method for following chemokine receptor expression, we first used flow cytometry to test antibodies against murine CCR5 with 3 suitable antibodies identified. Mc68 and mc69 (**Figure 3.4A**) were tested to determine which gave better staining for CCR5 via flow cytometry; titration curves were produced and mc68 was found to give better staining above the appropriate isotype control. By plotting this as a titration curve, saturation of



**FIGURE 3.3. Absence of CCR5 expression at the gene and protein level in CCR5<sup>-/-</sup> macrophages.** **A)** PCR genotyping of both wild-type (CCR5<sup>+/+</sup>) and CCR5<sup>-/-</sup> mice using the recommended protocol provided by The Jackson Laboratory. Expected band sizes were 280bp for CCR5<sup>-/-</sup> mutant and 203bp for CCR5<sup>+/+</sup> wild-type mice. **B)** Protein expression of CCR5 was assessed by measuring the mean fluorescence intensity for anti-CCR5 staining via flow cytometry on primary bone-marrow derived macrophages from either wild-type (black) or CCR5<sup>-/-</sup> (red) mice, using rat anti-CCR5 mc68 from Prof Mack (Mack et al. 2001).



**FIGURE 3.4. Characterising three monoclonal antibodies against murine CCR5. A)** Mc68, a purified monoclonal antibody directed against mouse CCR5, and mc69, a monoclonal antibody against mouse CCR5 in non-purified hybridoma supernatant, were titrated by flow cytometry to determine saturation point by measuring mean fluorescent intensity. **B)** Cells stained for CCR5 using the commercial antibody HM-CCR5 7A4 (eBioscience) plotted against an isotype control.

staining was seen at an antibody concentration of approximately 10µg/µL. The commercially available HM-CCR5 7A4 (eBioscience) also gave convincing CCR5-specific staining above the isotype control (**Figure 3.4B**).

### **3.3.3.2 Immunofluorescent staining for murine CCR5**

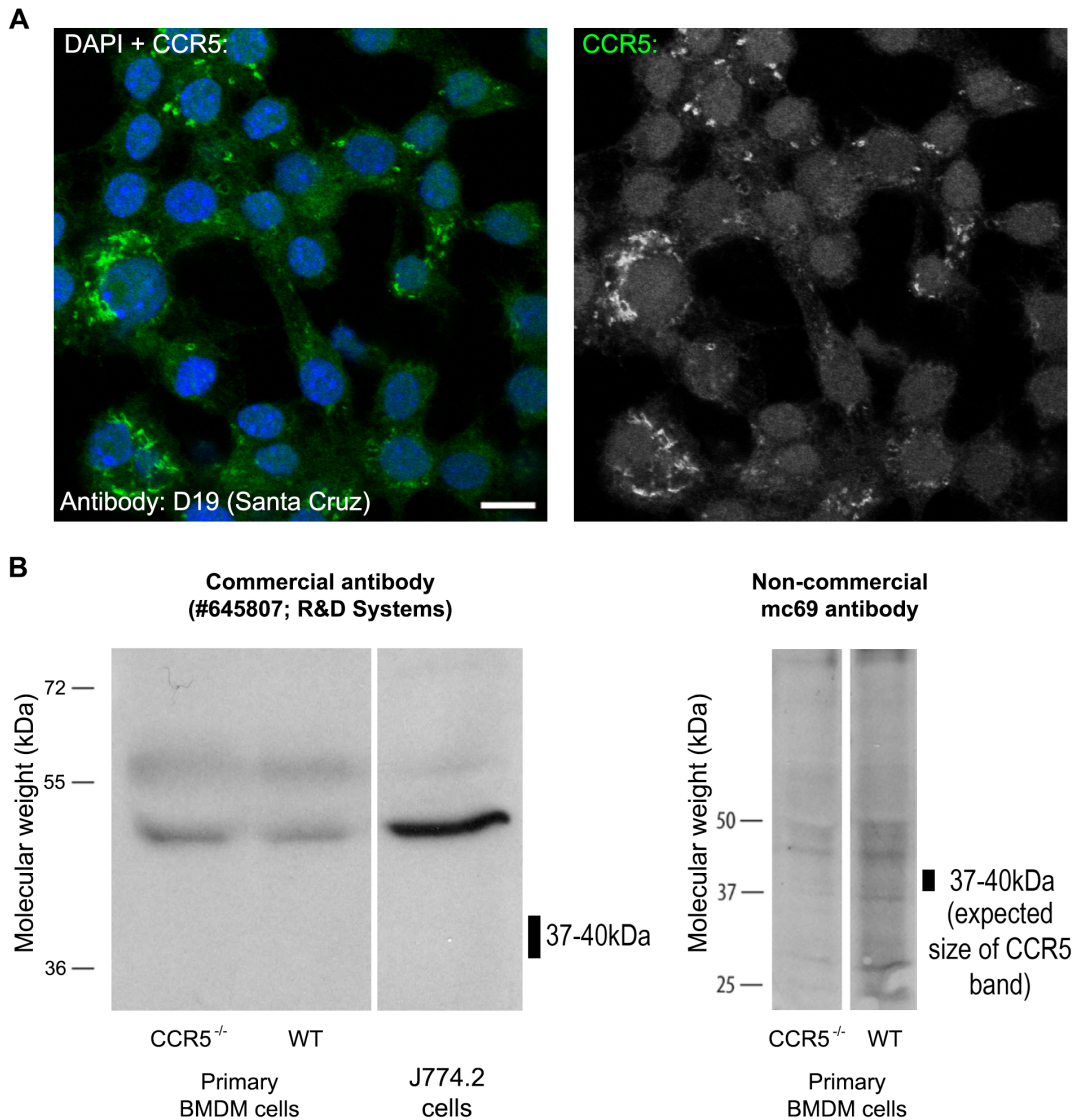
Commercially available antibodies with advertised specificity against murine CCR5 (detailed in Section 2.2) were tested using a plethora of different immunofluorescent staining conditions including different blocking buffers, fixation methods and permeabilisation options. Regardless of the antibody and conditions used, we only observed non-specific staining for CCR5. An example confocal micrograph showing non-specific staining for one of the antibodies tested against murine CCR5 is shown in **Figure 3.5A**.

### **3.3.3.3 Western blotting for murine CCR5**

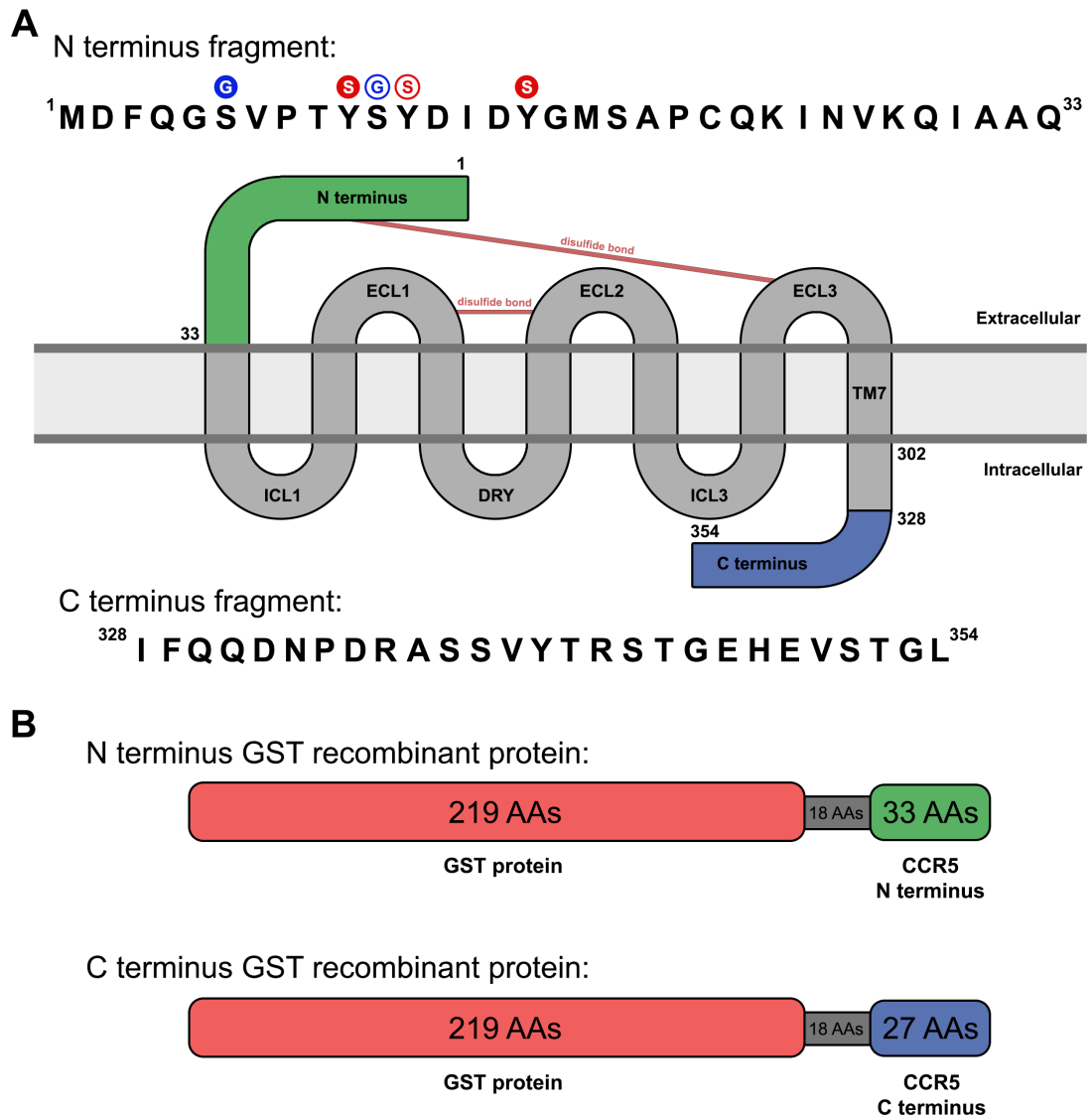
A number of antibodies (detailed in Section 2.2) were also tested for their specificity against murine CCR5 when used for western blotting. Only two of these antibodies gave bands at the expected molecular size for murine CCR5 when tested using the J774.2 mouse cell line (**Figure 3.5B**). However, these antibodies also showed similar bands for lysate from CCR5<sup>-/-</sup> bone marrow-derived macrophages (BMDMs), confirming their lack of specificity.

### **3.3.4 Making an anti-mouse CCR5 antibody**

To address the poor antibody repertoire available to track murine CCR5 expression and localisation, we endeavored to produce our own CCR5 antibody for use in *in vitro* experimentation. A diagram of the structure of CCR5, including likely sites of glycosylation, tyrosine sulphation and disulphide bonding, is shown in **Figure 3.6A**. N and C terminal fragments of CCR5 were fused to GST using the pGEX-3PLX vector system to produce recombinant proteins that are summarised in **Figure 3.6B**.



**FIGURE 3.5. Assessing antibodies available to track murine CCR5 expression and localisation in mouse cells. A)** Example of non-specific staining seen with the commercially available antibody D19 (Santa Cruz) against mouse CCR5 when used on permeabilised J774.2 cells. Scale bar = 10µm. Green = CCR5; blue = DAPI. **B)** Examples of western blotting for CCR5 using either the commercially available #645807 antibody (R&D Systems) or the non-commercial antibody mc69 (a kind gift from Prof Mack) on CCR5<sup>-/-</sup> or wild-type (WT) bone marrow-derived macrophages and J774.2 cells.



**FIGURE 3.6. The design of GST-CCR5 recombinant proteins. A)** Cartoon illustrating the amino acid composition of the N- and C-terminus of CCR5 with the target regions of CCR5 to be fused with GST highlighted. Amino acids that are likely to be post-translationally modified by tyrosine sulphation or O-glycosylation are shown in red or blue, respectively, with filled circles highlighting sites that have been experimental identified for human CCR5. **B)** Schematic representation of the GST-CCR5 recombinant proteins designed with number of amino acids (AAs) shown.

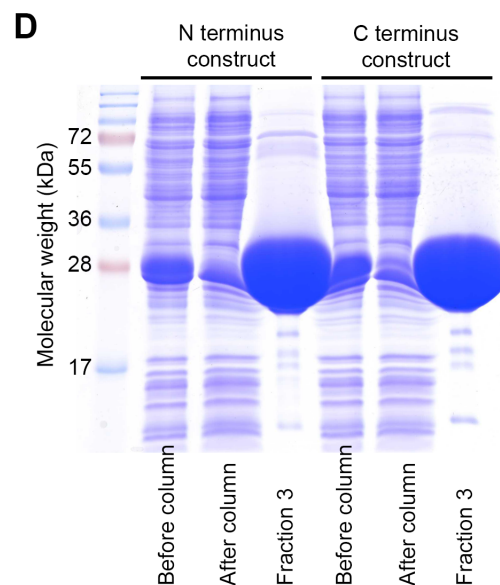
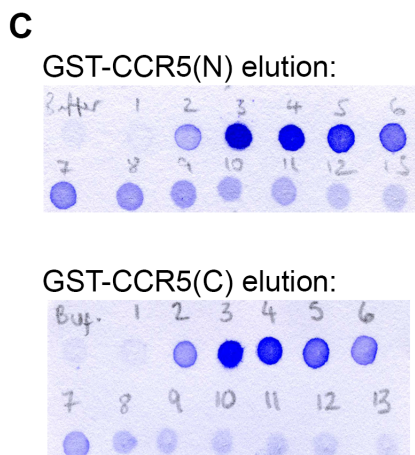
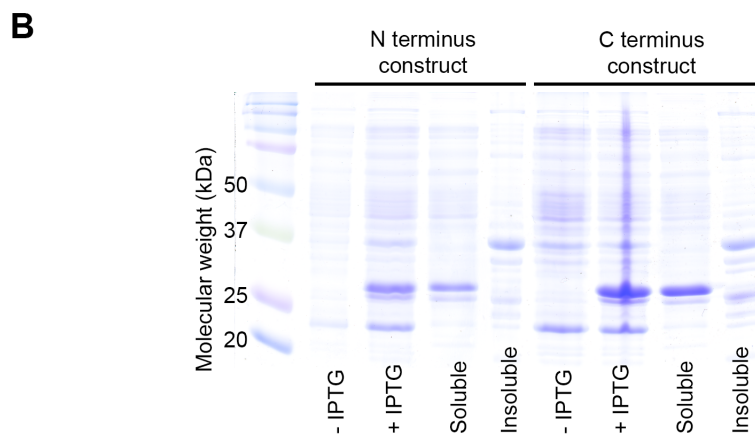
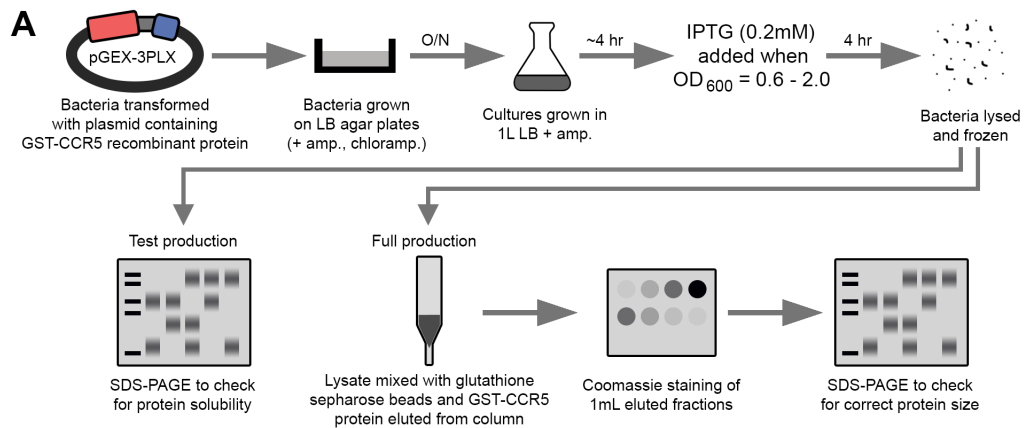
#### **3.3.4.1 Making GST-CCR5 recombinant products for injection into rabbits**

Successfully transformed bacteria, containing the pGEX-3PLX vector with incorporated N and C terminal regions of CCR5, were used to perform a small-scale test production of GST-CCR5 recombinant proteins, as summarised in **Figure 3.7A**. Bacteria were then lysed and soluble and insoluble proteins ran on a 10% SDS-PAGE gel as shown in **Figure 3.7B**. The molecular weights for the GST-CCR5 recombinant proteins were 29.7 kDa and 29 kDa for the N terminus and C terminus recombinant proteins, respectively, and found in soluble fractions demonstrating that the proteins were present within cell lysate supernatant. Protein production was then scaled up to use 1L cultures with the resulting soluble protein fraction from lysed bacteria being mixed with glutathione sepharose beads. After eluting any bound material, 1mL elution fractions were analysed using Coomassie staining and fraction 3 was found to be the most concentrated fraction, as shown in **Figure 3.6C**. Running this fraction on a 10% SDS-PAGE gel confirmed that the protein in this sample was significantly enriched for the 29 kDa or 29.7 kDa proteins of interest, for C and N terminus proteins respectively (**Figure 3.7D**). Fraction 3 was then dialysed against PBS and sent for inoculation into rabbits.

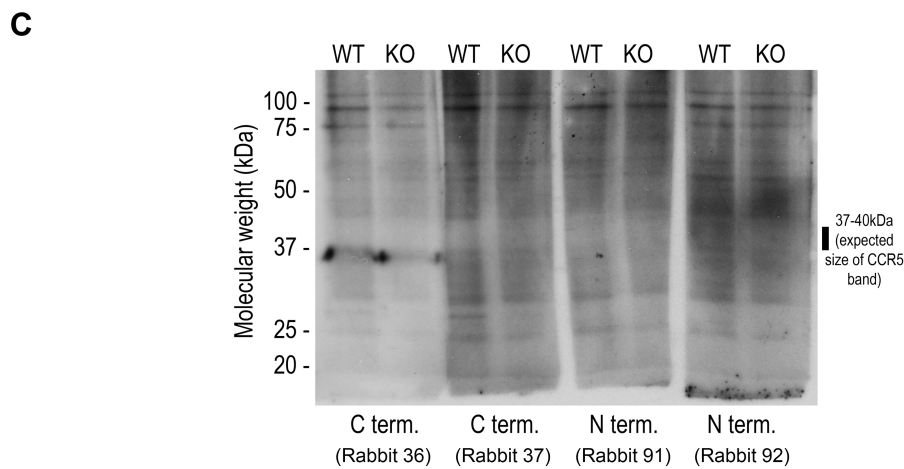
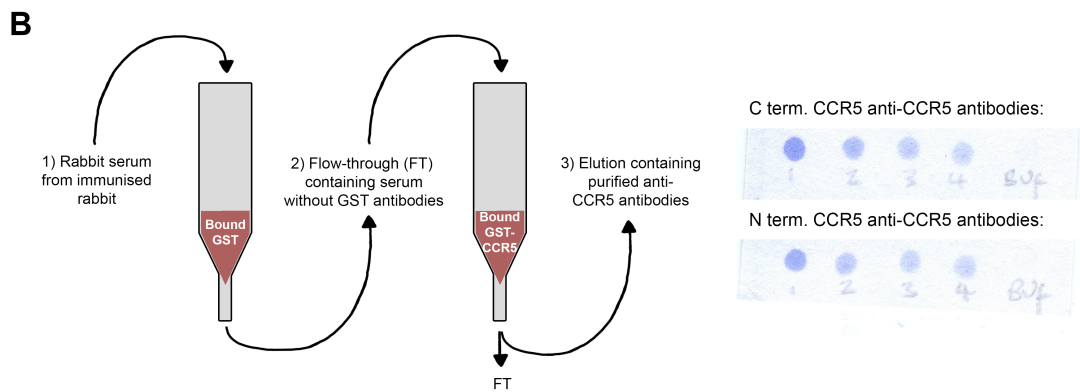
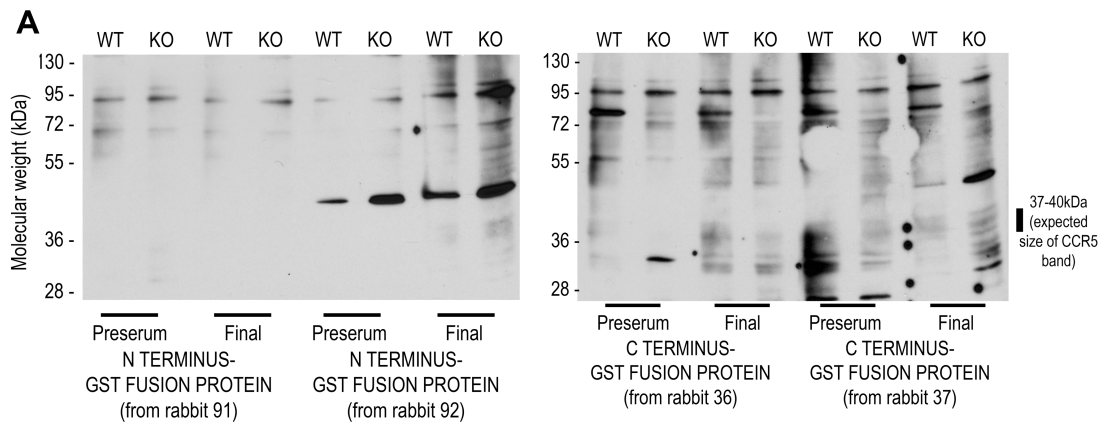
#### **3.3.4.2 Testing and purifying anti-CCR5 antibody**

Sera from rabbits exposed to GST-CCR5 recombinant proteins were tested for CCR5 specificity. This was done by using BMDMs from either wild-type (CCR5<sup>+/+</sup>) or CCR5<sup>-/-</sup> mice and a range of different western blotting conditions, including boiled and non-boiled protein, reduced and non-reduced protein, different blocking conditions and different sera concentrations. An example western blot is shown in **Figure 3.8A**, showing that final bleed sera from all four rabbits gave no convincing band for CCR5 (expected molecular weight of 40.8kDa) compared to the pre-immunisation sera. In addition, all bands were found in both wild-type and CCR5<sup>-/-</sup> BMDMs samples suggesting that none of the antibodies were specific for murine CCR5. Rabbit sera were therefore purified for CCR5-specific antibodies. Affinity purification matrixes were made, bound with either GST alone or one of the GST-CCR5





**FIGURE 3.7. GST-CCR5 recombinant proteins were successfully produced. A)** Overview of GST-CCR5 recombinant protein production after 4hr of isopropylthiogalactoside (IPTG) induction. **B)** Testing solubility of GST-CCR5 recombinant proteins. Soluble and insoluble samples were ran on a 10% SDS-PAGE gel along with whole bacterial samples before and after IPTG treatment, and then Coomassie stained. **C)** 1mL fractions were eluted from glutathione sepharose beads that had coupled the GST-CCR5 recombinant proteins and then Coomassie stained. **D)** The fraction with the highest amount of protein was then ran on a 10% SDS-PAGE gel and Coomassie stained, showing protein in 'before column', 'after column' and 'fraction 3' samples for each construct.



**FIGURE 3.8. Mouse CCR5 was not detected via western blotting using new rabbit antibodies.** **A)** Pre-immunisation rabbit sera (“preserum”) and final sera were used for western blotting of wild-type ( $CCR5^{+/+}$ ) and  $CCR5^{-/-}$  BMDMs to determine whether any of the final sera gave convincing staining for CCR5 (expected molecular weight of 40.8kDa). **B)** Schematic representation of affinity purification process. Sera were passed through columns with affinity purification matrixes bound with either GST or GST-CCR5 recombinant protein to remove GST-specific antibodies and retrieve CCR5-specific antibodies, which were Coomassie stained to check for elution. **C)** Testing of affinity purified CCR5-specific antibodies using western blotting for wild-type (WT) and  $CCR5^{-/-}$  (KO) BMDMs.

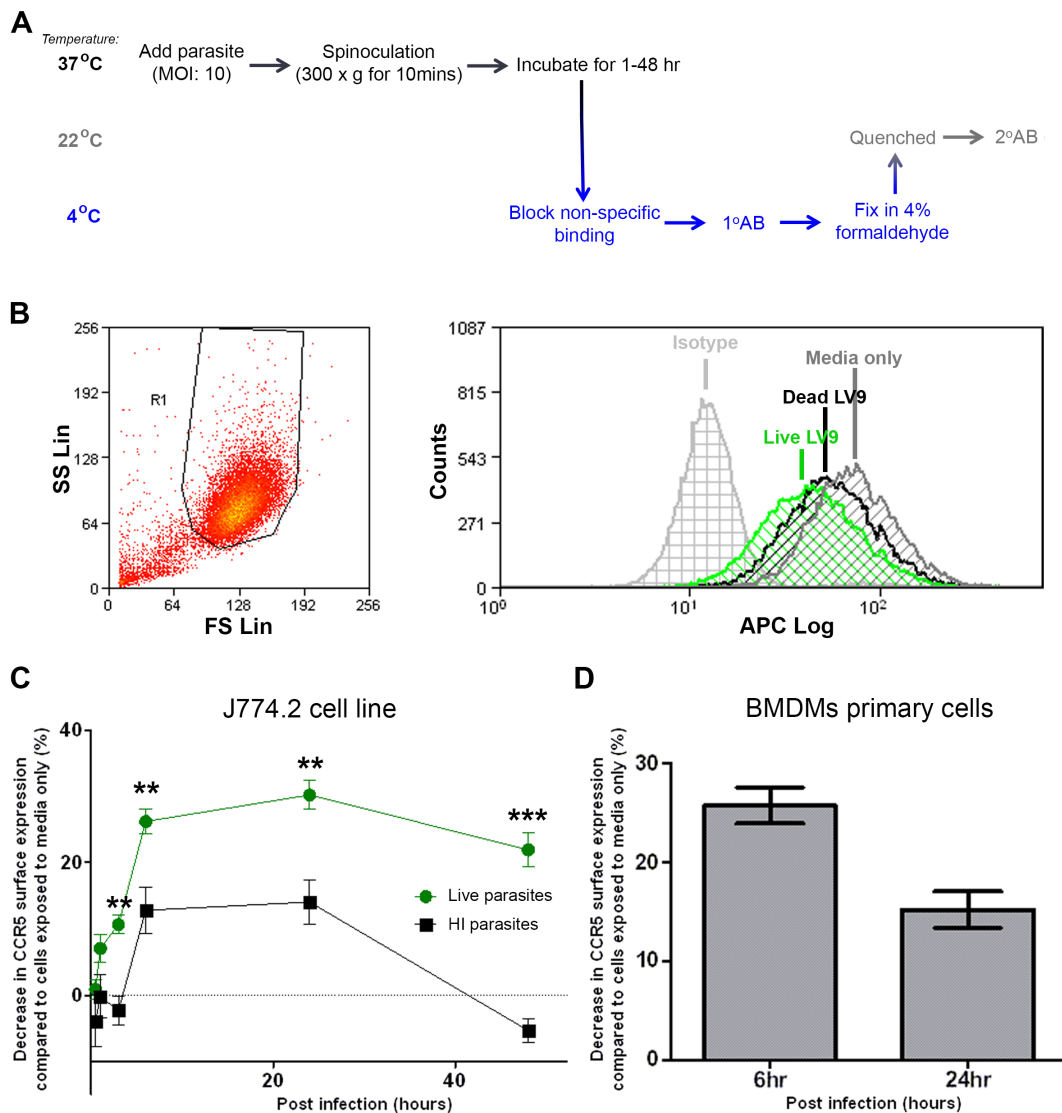
recombinant proteins. Each of the rabbit sera, which contained antibodies against each GST-CCR5 recombinant protein construct, was then passed through a separate GST-bound column to remove antibodies specific to GST. The flow-through from this column was then passed through a GST-CCR5-bound column to remove antibodies specific to the CCR5 fragment, and then those CCR5-specific antibodies collected using elution buffer. A diagram summarising this process is shown in **Figure 3.8B**. When these antibodies were tested using wild-type and CCR5<sup>-/-</sup> BMDMs, again there was no specific staining for CCR5 seen using any of the purified antibody preparations (**Figure 3.8C**).

### **3.3.5 Cell surface CCR5 expression during *L. donovani* infection**

Due to the lack of antibodies available to track murine CCR5 expression and localisation, the extent to which CCR5 could be followed during infection with *L. donovani* parasites was limited. The only antibodies to give specificity against murine CCR5 were the commercial antibody HM-CCR5 7A4 (eBioscience, UK) and the non-commercial antibody mc68 (as detailed in Section 3.3.3.1), both of which could be used for flow cytometry on live non-fixed, non-permeabilised cells. Therefore, levels of CCR5 cell surface expression were measured using flow cytometry to determine the effect of *L. donovani* during infection.

#### **3.3.5.1 Live *L. donovani* parasites induce a greater decrease in CCR5 cell surface expression compared to heat-inactivated parasites**

The effect of live *L. donovani* LV9 amastigotes on CCR5 cell surface expression in J774.2 cells was first tested to characterise expression levels over a 48 hr time-course of infection (as summarised in **Figure 3.9A**); this was compared to cells exposed to HI parasites to determine whether there was an active effect of the parasite. Cells were then processed for flow cytometry analysis using the gating strategy shown in **Figure 3.9B**. To calculate the decrease in CCR5 cell surface expression, the mean fluorescence intensity (MFI) for CCR5 staining for infected cells was



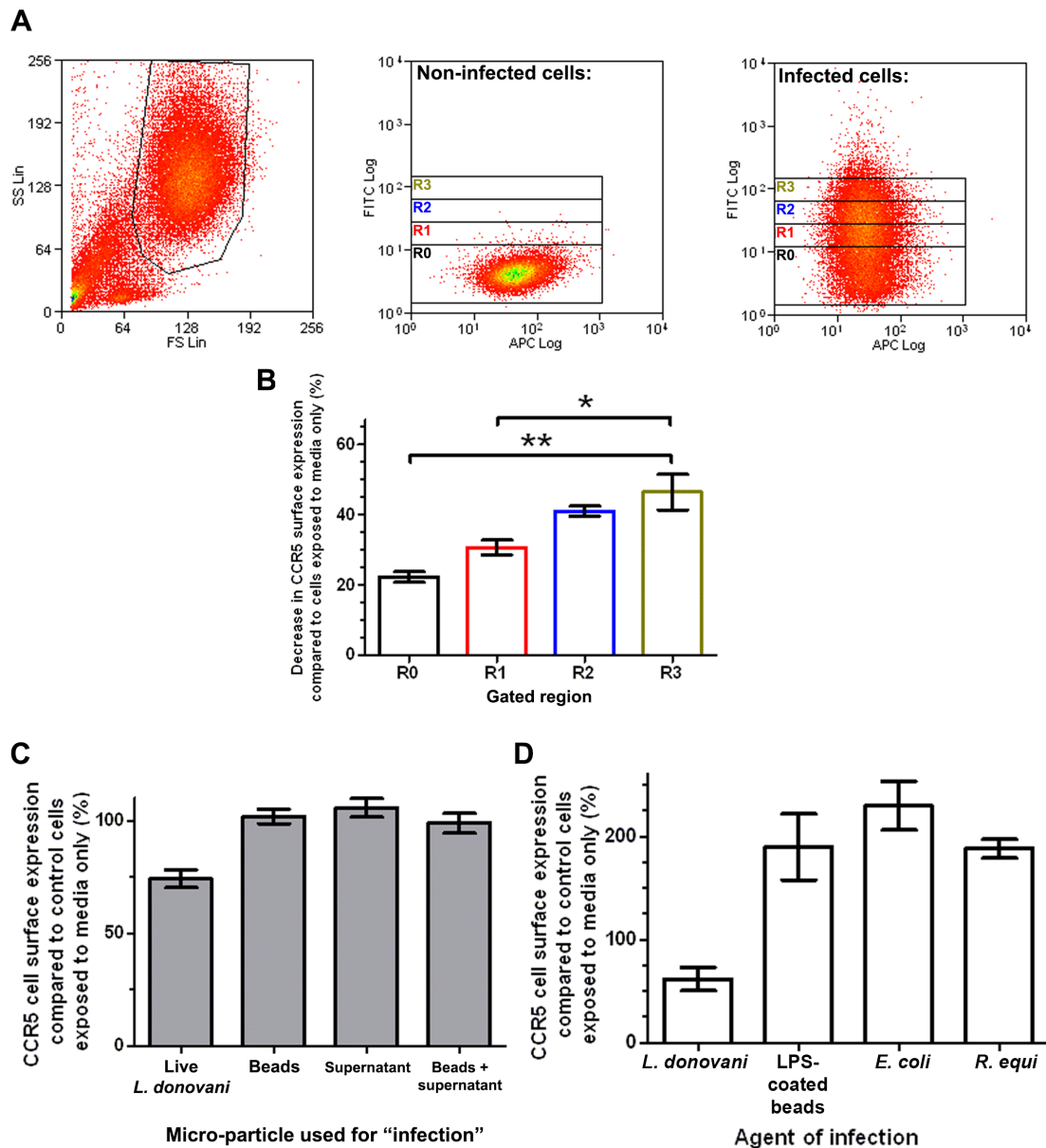
**FIGURE 3.9. CCR5 cell surface expression decreased with *L. donovani* infection over a 48 hr time-course of infection. A)** Experimental overview illustrating the process of fixing cells after incubation with primary antibody (1°AB). **B)** Example gating of J774.2 cells using a flow cytometer. **C)** CCR5 cell surface expression during *L. donovani* amastigote infection seen in J774.2 cells. Unpaired T tests conducted between live parasite sample and heat-inactivated (HI) parasite sample. **D)** CCR5 cell surface expression seen with bone marrow-derived macrophages (BMDMs) during infection with live *L. donovani* amastigote parasites. Data shown as mean  $\pm$  SEM from 3 independent experiments done in triplicate. \*\* p < 0.01, \*\*\* p < 0.001.

compared to the MFI for cells exposed to media only, with isotype control MFI values subtracted from all values before percentages were calculated. A decrease in CCR5 cell surface expression was seen for both live and HI parasites, with the decrease being maximal at 24 hr post-infection (mean decrease of 30% for live parasites and 14% for HI parasites) for the J774.2 cell-line (**Figure 3.9C**). This decrease was more pronounced with live parasites with a statistically significant difference being seen from 3 hr post-infection onwards. Interestingly, those cells infected with HI parasites returned to pre-infection level of receptor cell surface expression whereas live-infected cells remained affected at 48 hr post-infection. We demonstrated that the same effect was also seen in primary BMDMs taken from a wild-type (CCR5<sup>+/+</sup>) mouse, but in this case the decrease in CCR5 cell surface expression was maximal at 6 hr post-infection (**Figure 3.9D**).

### **3.3.5.2 Decrease in CCR5 cell surface expression is dose-dependent and specific to *L. donovani***

Fluorescently labelling parasites with CFSE prior to infection allowed tracking of which J774.2 cells contained parasites. The increase in fluorescein staining could correspond to increasing number of parasites contained within a cell. We therefore designed a gating strategy to investigate whether there was any link between the level of infection and the decrease seen with CCR5 cell surface expression (**Figure 3.10A**). At 24 hr post-infection, there was a statistically significant difference in the decrease of CCR5 between those cells that had highest numbers of parasites in them (gated region R3) compared to those that had the lowest numbers of parasites in them (gated region R0), as shown in **Figure 3.10B**.

The process of phagocytosis utilises small portions of plasma membrane (reviewed by Rougerie et al. 2013); as CCR5 is a transmembrane receptor incorporated into the plasma membrane, one hypothesis could be that this decrease in cell surface expression was caused by large portions of the plasma membrane being used for phagocytosis. To test this, 1µm latex beads of approximate equivalent size to amastigote *L. donovani* parasites were used for mock infections. As shown in **Figure 3.10C**, this failed to



**FIGURE 3.10. Decrease in CCR5 cell surface expression is dose-dependent and specific to *L. donovani*.** **A)** J774.2 cells were infected with CFSE-labelled *L. donovani* parasites and gated on the FITC channel, with R0 identifying non-infected cells and R1, R2 and R3 identifying infected cells. **B)** The gating strategy was used to determine the cell surface expression on J774.2 cells 24 hr post-infection. **C)** To test whether the decrease in CCR5 was due to a general effect of phagocytosis, cells were exposed to live *L. donovani* parasites, latex beads, supernatant from parasite preparations, or latex beads + supernatant. CCR5 cell surface expression assessed at 24hr using a flow cytometer. **D)** To test for the specificity of this decrease, CCR5 cell surface expression was assessed 24 hr post-infection of J774.2 cells with either live *L. donovani*, LPS-coated beads, *Escherichia coli*, or *Rhodococcus equi*. Data shown as mean  $\pm$  SEM; \*\* =  $p < 0.01$ , \* =  $p < 0.05$ .

decrease CCR5 cell surface expression at 24 hr post-infection. Latex beads were further tested by pre-incubating them with supernatant from parasite preparations, and then mock infecting J774.2 cells with a mix of latex beads and parasite preparation supernatant. This again failed to induce the decrease in CCR5 cell surface expression seen with *L. donovani* amastigote infections (**Figure 3.10C**).

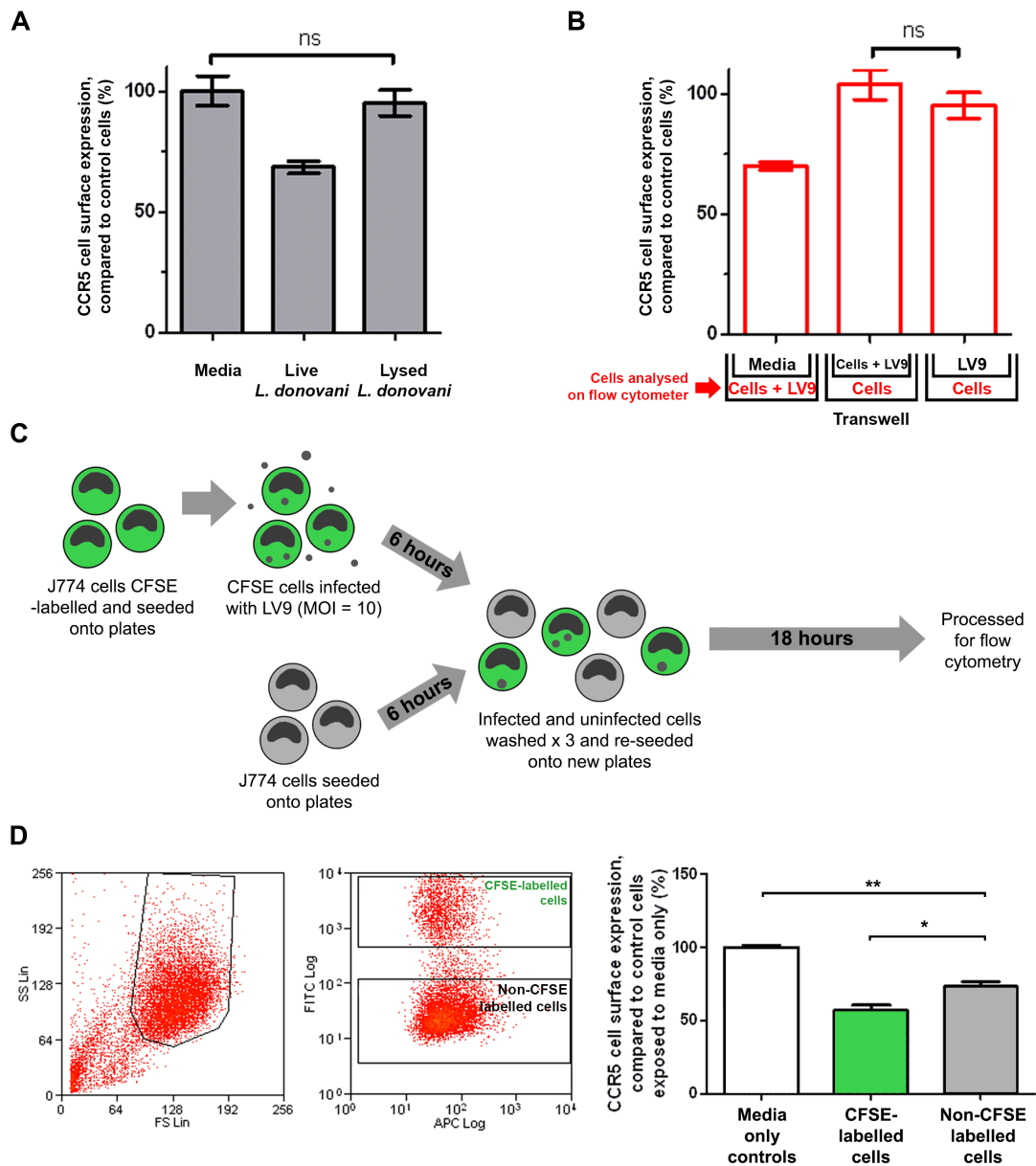
As the general process of phagocytosis did not induce this effect, other pathogens were tested to determine whether this effect might be a characteristic response to infection in J774.2 cells (**Figure 3.10D**).

Lipopolysaccharide (LPS)-coated beads and the Gram-negative bacterium *Escherichia coli* both induced a substantial increase in CCR5 cell surface expression 24 hr post-infection. This was also seen with the Gram-positive bacterium *Rhodococcus equi*, suggesting that decrease in CCR5 expression at the cell surface was a *L. donovani*-specific effect.

### **3.3.5.3 Direct contact with an intact parasite is necessary**

As a decrease in CCR5 cell surface expression was also seen with HI parasites (see Section 3.3.5.1), we next wanted to determine whether an intact parasite structure was necessary for CCR5 to decrease. Parasites were lysed and then exposed to cells at an equivalency of an MOI of 10. At 24 hr post-exposure, the cell surface expression of CCR5 was assessed using a flow cytometer and compared to cells exposed to either media only or to live *L. donovani* parasites (**Figure 3.11A**). Interestingly, the decrease in CCR5 cell surface expression seen at 24 hr post-infection was completely abolished with lysed parasites, suggesting that the parasite needed to be intact for the effect to be seen.

We then asked whether parasites need to be in direct contact with cells to induce this down-modulation or whether the effect could be due to the parasite inducing the secretion of soluble factors. For example, others have shown that extracellular vesicles from *Leishmania*-infected macrophages can induce nearby macrophages to produce pro-inflammatory cytokines (Cronemberger-Andrade et al. 2014). In addition, infection with *Leishmania*



**FIGURE 3.11. Decrease in CCR5 cell surface expression required direct contact of intact *L. donovani* parasites.** **A)** J774.2 cells were exposed to parasites that had been lysed in water and cell surface expression of CCR5 measured 24 hours post exposure using a flow cytometer. Data shown as mean  $\pm$  SEM from 3 independent experiments. **B)** Transwell experiments using J774.2 cells were performed as described and cell surface expression of CCR5 measured 24 hr later for the cells in the lower chamber. Data shown as mean  $\pm$  SEM from 3 independent experiments. **C)** Schematic representation of the translocation of infected cells experiment. J774.2 cells were CFSE-labelled and infected with *L. donovani* parasites. After 6 hr, cells were detached and reseeded onto new plates with J774.2 cells that had not been infected. The infection was allowed to progress for a further 18 hr. **D)** Cells were gated using the FITC channel into “infected” CFSE-labelled cells and “non-infected” non-CFSE-labelled cells and the cell surface expression of CCR5 assessed. Data shown as mean  $\pm$  SEM from 1 experiment.



parasites is known to directly induce the production of inflammatory cytokines and chemokines (Ji et al. 2003; Teixeira et al. 2005; Murray et al. 2017). J774.2 cells were seeded in the top and bottom chambers of a transwell insert, separated by a 0.4µm permeable membrane; cells in the bottom chamber would be assessed on a flow cytometer for CCR5 cell surface expression. Parasites were added to infect cells in the bottom chamber (to mimic the experiment already performed) or to the top chamber that either had or did not have J774.2 cells seeded in it. When the cells in the top chamber were infected with *L. donovani* parasites, there was no corresponding decrease in the cell surface expression of CCR5 for the cells in the bottom chamber at 24 hr post-infection (**Figure 3.11B**). There was also no decrease in CCR5 for cells in the bottom chamber when *L. donovani* parasites alone were in the top chamber (**Figure 3.11B**). This suggested that secreted chemokines and cytokines from infected cells or exosomes from the parasite, all of which should freely diffuse through the membrane, were unlikely to play a role in the effect seen.

Next, we performed a translocation experiment to investigate whether J774.2 cells could have their CCR5 cell surface expression decreased by being co-seeded with infected J774.2 cells, with the experimental setup of this experiment summarised in **Figure 3.11C**. Fluorescently labelling cells that would be infected with CFSE prior to infection allowed tracking of which J774.2 cells originally contained parasites. Both CFSE- (initially infected) and non-CFSE-labelled cells were found to have decreased CCR5 cell surface expression by 24 hr post-infection (**Figure 3.11D**); however, the possibility that parasites were transferred from infected cells to non-infected cells during the 18 hr after co-seeding cannot be excluded.

#### **3.3.5.4 Chemokine response in *L. donovani*-infected cells**

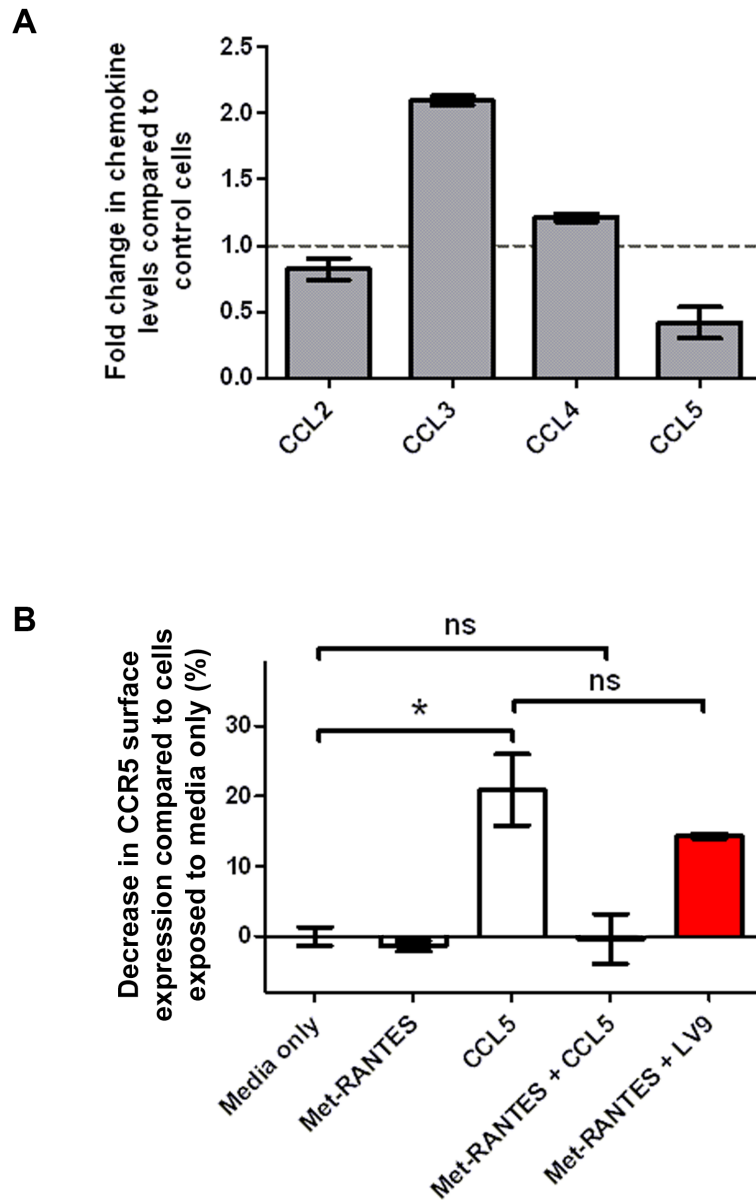
To profile the chemokine response in *L. donovani*-infected cells, an ELISArray was performed on supernatant collected from infected cells 24 hr post-infection. The CCR5 ligands CCL2-5 were of particular interest because they have been shown to increase during infection with *L. major* (Yurchenko et al. 2006), *L. braziliensis* (Teixeira et al. 2005) and *L. amazonensis* (Ji et al.

2003), with subtle differences in the response between different *Leishmania* species. As shown in **Figure 3.12A**, *L. donovani*-infected J774.2 cells produced a two-fold increase in CCL3 whilst secretion of CCL5 was reduced and there was no change in CCL2 and CCL4 levels.

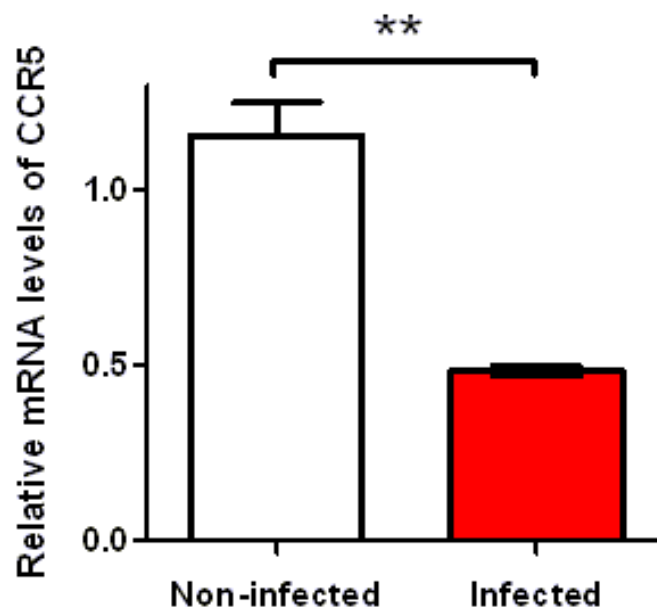
All of these CCR5-specific agonistic ligands induce internalisation of CCR5 and result in a decrease of the receptor at the cell surface (Bachelierie et al. 2014). We thus wanted to determine whether the decrease in CCR5 could still be induced if the receptor was blocked using the CCR5 ligand Met-RANTES, which has been previously shown to be an effective antagonist for CCR5 in murine cells (Mack et al. 2001). When cells were pre-incubated with Met-RANTES and then exposed to *L. donovani* amastigotes, the *Leishmania*-induced decrease in CCR5 cell surface expression still occurred (**Figure 3.12B**) suggesting that this effect did not rely on agonist-induced removal of CCR5 from the plasma membrane.

### **3.3.6 CCR5 mRNA levels for J774.2 cells infected with *L. donovani* amastigotes**

The decrease in CCR5 levels at the cell surface occurred more slowly than is usually seen with down-modulation of the receptor resulting from increased intracellular trafficking of the receptor (e.g. Signoret et al. 2004, Fox et al. 2011). We therefore performed qRT-PCR to determine the levels of CCR5 mRNA in J774.2 cells, for cells infected with *L. donovani* or non-infected control cells at 24 hr post-infection. As shown in **Figure 3.13**, infected cells had a statistically significant reduction in CCR5 mRNA levels compared to non-infected control cells. This suggested that the down-modulation of CCR5 seen could be due to down-regulation of CCR5 at the gene level. Raw data extracted from the transcriptomics study performed by Beattie et al. (2013) also found that CCR5 mRNA levels were decreased in isolated *L. donovani*-infected Kupffer cells (2hr: 0.41 fold change; 12hr: 0.48 fold change), compared to control mice. Interestingly, inflamed cells taken from an infected liver but not infected with parasites also showed a decrease in CCR5 mRNA levels (2hr: 0.38 fold change; 12hr: 0.39 fold change), reminiscent of the



**FIGURE 3.12. The secretion of CCR5 specific chemokines was altered in *L. donovani*-infected J774.2 cells but blocking CCR5 did not inhibit the decrease seen with *L. donovani*.** **A**) An ELISA checking for levels of common chemokines was performed on supernatant collected from J774.2 cells infected with *L. donovani* for 24 hr. Samples analysed in triplicate and data shown as the mean fold change in chemokine expression compared to non-infected control cells  $\pm$  SEM. **B**) The effect of CCR5 cell surface expression on J774.2 cells when exposed to the antagonist ligand Met-RANTES (100nM), the agonist ligand CCL5 (100nM) and *L. donovani* (LV9) parasites at an MOI=10 in the presence of Met-RANTES. \* =  $p < 0.05$ , ns = non-significant.



**FIGURE 3.13. mRNA levels of CCR5 were decreased at 24 hr in cells infected with *L. donovani* LV9 amastigotes compared to non-infected control cells.** qRT-PCR was performed on J774.2 cells infected with *L. donovani* LV9 amastigotes and non-infected control cells exposed to media only. Relative mRNA levels for CCR5 were calculated and CCR5 mRNA levels compared to the loading control hypoxanthine guanine phosphoribosyl transferase (HPRT). \*\*  $p < 0.01$ .

changes in CCR5 seen in non-infected cells with our translocation experiment detailed previously in Figure 3.11.

### 3.4 Chapter-specific discussion

During *in vitro* infection with *L. donovani* LV9 amastigotes, it was observed that CCR5 cell surface expression was significantly decreased by up to 40% in BMDMs and J774.2 cells, peaking 6 and 24 hr post-infection, respectively. This parasite-specific effect was more pronounced using live rather than HI parasites, was dose-dependent, and required physical contact between host cells and intact parasites. Although we initially hypothesised that this was through receptor activation and down-modulation, several factors suggested the interaction was more complex. Firstly, the decrease in CCR5 was not blocked by the antagonist ligand Met-RANTES, suggesting that this decrease may be partly mediated through indirect cross-talk mechanisms regulating CCR5 cell surface expression and not ligand stimulation. Furthermore, the decrease in CCR5 seen through our time-course experiments suggested a slower, more prolonged decrease in CCR5 than is normally seen with receptor down-modulation mediated by increased intracellular trafficking (e.g. Signoret et al. 2004). The later finding that mRNA levels of CCR5 were decreased in *L. donovani*-infected J774.2 cells suggested that the decrease seen in cell surface CCR5 could be caused by down-regulation of the receptor at the gene level.

Levels of the receptor are usually controlled by post-transcriptional adjustments in the intracellular repositories of CCR5 because expression of functional chemokine receptors at the cell surface needs to change rapidly to be able to respond appropriately to external stimuli. Although evidence for changing mRNA levels of CCR5 during infections is limited, there are studies that have shown that infections can alter CCR5 expression at the gene level. Das et al. (2014) found that infection of murine BMDMs with *Mycobacterium tuberculosis* increased CCR5 mRNA and that this correlated with higher expression of CCR5 at the cell surface and total CCR5 levels. IL-10, an important cytokine involved in parasite persistence for visceralising *Leishmania* species, has been shown to increase levels of CCR5 mRNA in mouse cells (Takayama et al. 2001). Thus, it is likely that *L. donovani*

significantly suppresses CCR5 mRNA levels, altering the normal immune response to cytokines. To our knowledge, this is the first time that CCR5 has been targeted for down-regulation at the gene level by an infectious agent.

There are several reasons why the parasite may want to down-regulate the quantity of CCR5 receptors on the surface of infected cells. CCR5 is involved in the recruitment of cells to sites of infection or injury and is therefore classed as an inflammatory, rather than homeostatic, chemokine receptor. Thus, by down-regulating an inflammatory receptor such as CCR5, the infected macrophage is less responsive to activation from external stimuli. Furthermore, a decrease in cell surface CCR5 would inhibit the chemotactic recruitment of infected macrophages, perhaps keeping them isolated from areas of leucocyte foci that could potentially help eradicate the infection. CCR5 activation has also been linked to leishmanicidal nitric oxide production (Bhattacharyya et al. 2002). Alternatively, this pathway may be a normal physiological response to retain infiltrating monocytes at sites of infection, as has been suggested for TLR2-dependent down-modulation of CCR5 (Fox et al. 2011). It may also be logical to hypothesise that the immune system may have mechanisms like this in place to make infected macrophages unresponsive to chemotactic cues in an attempt to isolate infected cells; however, it is interesting that we did not see the same down-modulation of CCR5 when other pathogens were used suggesting that this is not a general response to infection. It is also of note that the live parasite can induce a greater decrease in CCR5 cell surface expression compared to HI parasites, implying that CCR5 may be actively targeted and manipulated by the live parasite.

The decrease in CCR5 cell surface expression and mRNA levels associated with *L. donovani* amastigote infection is in contrast to what others have seen using a different strain of *L. donovani* (AG-83) promastigotes and J774.2 cells (Bhattacharyya et al. 2008; Majumdar et al. 2014). This same group also claimed an overall increase in CCR5 levels associated with infection, based on western blot analysis; this was something that could not be addressed after we found that none of the commercially available anti-CCR5

antibodies were suitable for western blotting. However, in their studies the AG83 strain of *L. donovani* that originates from an Indian Kala-azar patient was used, while in the present study the LV9 strain originating from Ethiopia was used. Others have shown that there are dramatic differences between *Leishmania* species and strains in their chemokine secretion profiles (Ji et al. 2003; Teixeira et al. 2005), so there may be similar disparity between the receptor responses in different *Leishmania* infections. In addition, differences between promastigote and amastigote forms of the parasite could account for these differences.

Although there were changes in the mRNA levels of CCR5, it cannot be assumed that this accounts for all of the changes seen at the cell surface for the receptor, particularly since variations in intracellular trafficking of the receptor extensively alter CCR5 levels at the surface. The observation that cells with more parasites in them had lower cell surface expression of CCR5 led us to hypothesise that the decrease may be due in part to more plasma membrane being used for the process of parasite phagocytosis. This was a particular concern since parasites were spinoculated onto cells to synchronise infections; thus, plasma membrane would be used to form many phagosomes at the same time, potentially with little time for the membrane to be replaced or recycled back to the cell surface. Others have also found plasma membrane proteins and receptors present within phagosomes, suggesting that some receptors may be internalised as bystanders during the process of phagocytosis (Garin et al. 2001; Goyette et al. 2012). However, both latex beads and infections with other pathogens increased levels of CCR5. Garin et al. (2001) also found that significant numbers of particles can be internalised via phagocytosis without the integrity of the plasma membrane being compromised. Thus, these findings strongly suggest that the reduction seen in cell surface CCR5 was not an effect of phagocytosis.

The results from transwell experiments suggest that the parasite needed to be in direct contact with cells to induce a decrease in CCR5 cell surface expression. However, when infected cells were translocated amongst non-infected cells, the latter also saw a decrease in CCR5. This could be



explained by the release of extracellular vesicles (EVs), either from infected macrophages (Cronemberger-Andrade et al. 2014) or from parasites (reviewed by Atayde et al. 2016). The TEM images of parasite preparations demonstrated that there was membranous material associated with parasites, some of which may have included EVs, although leaving parasites overnight reduced this material. EVs up to 1000nm in size have been reported to readily bud off of plasma membranes during cell activation (Zwaal & Schroit 1997) that would not be able to pass through the 0.4µm transwell filter used. These structures have a functional relevance during infection because macrophage-derived EVs have been shown to stimulate the release of pro-inflammatory cytokines and chemokines (Walters et al. 2013). Parasite-derived EVs are thought to contain GP63 (Hassani et al. 2014), a major surface protease of *Leishmania* that has been shown to access the host cell cytoplasm and negatively regulate intracellular signalling pathways (Gomez et al. 2009); however, parasite-derived EVs are unlikely to account for the decrease in CCR5 cell surface expression as there was no effect seen for cells in the bottom chamber when *L. donovani* amastigotes were placed in the top chamber of a transwell chamber. Alternatively, the difference between transwell and translocation experiments could be explained if the cells that were originally non-infected subsequently became infected by *L. donovani* parasites. Real et al. (2014) performed impressive time-lapse high magnification fluorescent microscopy to study the cell-to-cell transfer of *L. amazonensis* amastigotes and found that parasites were readily transferred between neighbouring cells via cellular extrusions. This could occur at the same time as parasite dissemination from apoptosis and cell damage, resulting in non-infected cells becoming infected.

During the course of these experiments, there was an increase in CCL3 released by *L. donovani*-infected J774.2 cells. This was not unexpected because, as described in Section 1.2.5, *Leishmania* can induce chemokine secretion from infected cells, the profile of which is dependent on *Leishmania* species and host cell type. However, the increase in CCL3 is interesting because Bhattacharyya et al. (2002) found that this chemokine, along with CCL2, might inhibit parasite growth through nitric oxide activity, implying that

the cell may use this as a protective mechanism against infection. Despite this, Roychoudhury et al. (2006) demonstrated that parasites respond to bound chemokine via intracellular  $Ca^{2+}$  mobilisation, suggesting that this binding is functional and was found to be greatest with CCL3 (Roychoudhury et al. 2006). Thus, this increase in CCL3 could be exploited by the parasite as a way to home additional parasites to suitable target cells. The decrease we see with CCL5 in infected cells was of interest because it has been suggested that this chemokine can skew the immune response to a type 1 response, up-regulating IL-12 (Aliberti et al. 2000), IFN- $\gamma$  (Makino et al. 2002) and the migration of Th1 cells (Weber et al. 2001), whereas with visceralising forms of *Leishmania* the chronicity-inducing Th2 response is dominant, as described in Section 1.1.4. Again, the parasite may be exploiting the chemokine expression profiles of host cells to facilitate parasite homing and intracellular survival.

Despite the increase in certain CCR5-specific chemokines in response to *L. donovani* infection, the decrease seen in CCR5 cell surface expression was still seen when the receptor was blocked using the antagonist ligand Met-RANTES. This suggests that the decrease of the receptor was not CCR5 agonist-dependent. As mentioned previously, this effect was not merely a result of plasma membrane being used for phagosome biogenesis because latex beads of equivalent size and abundance failed to reduce CCR5 levels. In addition to reducing mRNA levels of CCR5, an alternative explanation for reducing CCR5 cell surface expression could be indirect cross-regulation by another receptor, such as with CXCR4 (Bennett et al. 2011) or TLR2 (Fox et al. 2011), both of which are present on macrophages along with CCR5. We aimed to determine whether a neutralising anti-TLR2 antibody could be used to block the effect seen with *L. donovani* amastigote infection. However, we were unable to find a suitable antibody against murine TLR2 that completely blocked the receptor. Future experiments could study whether the use of CXCL12 (for CXCR4) or lipoteichoic acid (LTA; for TLR2) is able to induce a decrease in CCR5 cell surface expression.

Surprisingly, a number of commercially available antibodies with alleged specificity to murine CCR5 did not give convincing staining for the chemokine receptor by western blotting, flow cytometry or immunofluorescent imaging. This lack of antibody specificity for CCR5 has also been seen with the human receptor, with Bernstone et al. (2012) testing nine commercially available anti-CCR5 monoclonal antibodies and finding that 3 had substantial background binding whilst 3 others had questionable results. Worryingly, these specificity problems remained despite technical assistance from the manufacturers and a number of these antibodies remain on sale (Bernstone et al. 2012). A similar study for murine CCR5 antibodies has not been previously performed but the results from the current study showed strong evidence to suggest that a number of commercially available murine CCR5 antibodies also have poor specificity. Others have published studies using commercially available murine CCR5 antibodies (e.g. Bhattacharyya et al. 2008; Majumdar et al. 2014). The methodology used in these studies for western blotting and immunofluorescent staining was precisely followed but did not give convincing staining for CCR5 in our hands when using CCR5<sup>-/-</sup> for specificity control, despite being tested in a wide range of experimental conditions.

To address the lack of antibodies available to follow murine CCR5, GST-CCR5 recombinant proteins were made to inoculate into rabbits with the resulting antibody response being collected in final bleed sera. However, extensive post-translational modifications, such as N-terminal tyrosine sulphation sites (Liu et al. 2008) and glycosylation (Neel et al. 2005), in addition to a lack of the correct conformation for the truncated peptide sequence inoculated into rabbits, could explain why the resulting rabbit sera did not contain antibodies that recognised CCR5. To help address this problem, we have commissioned the production of a murine CCR5 antibody using phage display to quickly screen large antibody libraries against a post-translationally modified CCR5 molecule. Although this antibody will not be ready in time for use during this project, it will prove useful to other investigators to help better follow CCR5 in mouse models of infection, thus

helping to bridge the gap between human and mouse chemokine receptor studies.

To summarise, an *L. donovani*-specific, dose-dependent decrease in cell surface CCR5 was seen during infection with intact parasites in direct contact with J774.2 cells, greatest for live parasites. Although this may be due to significant down-regulation of the receptor at the transcriptional level, a lack of suitable antibodies meant that we were not able to follow the intracellular trafficking of the receptor. It is possible that the receptor could be interacting with the parasite at the cell surface, facilitating parasite entry into the cell and associating with the parasite-containing compartment. We therefore wanted to determine whether the knockout of CCR5 could have any effect on *L. donovani* infection using *in vivo* and *in vitro* models of infection, either at the level of the macrophage specifically or the whole immune system in general.

## 4. The effect of CCR5<sup>-/-</sup> on *L. donovani* infection *in vivo*

### 4.1 Chapter-specific background and rationale

*In vitro*, we have seen a *Leishmania*-specific reduction in CCR5 cell surface expression during a short time-course of infection. Although this could be explained through reductions in mRNA levels for the receptor, our experiments were unable to address the importance of CCR5 for entry and intracellular survival of *L. donovani* LV9 amastigotes during a typical time-course of *L. donovani* LV9 amastigote infection. In York, there is an established model of *L. donovani* LV9 amastigote *in vivo* infection (Beattie et al. 2011; Owens et al. 2012; Maroof et al. 2012). Infection kinetics for this model of infection have previously been characterised and the standard measurement of parasite burden, namely Leishman Donovan units (LDUs), peaked 14 days post-infection in the liver and was effectively cleared by day 56, although hepatic granulomas persist (Beattie et al. 2011). As the other major target of *Leishmania* infection, the spleen had LDUs that increased throughout a 56 day time-course of infection (Owens et al. 2012). We combined this infection model with the use of mice deficient in CCR5 (Kuziel et al. 2003) to determine whether the absence of CCR5 affects *L. donovani* infection progression.

#### 4.1.1 CCR5<sup>-/-</sup> mice

The B6.129P2-CCR5<sup>tm1Kuz</sup>/J (hereon referred to as CCR5<sup>-/-</sup>) mouse strain has a permanent deletion in the gene for CCR5 generated by insertion of a 9.0kbp XbaI restriction fragment containing the gene for CCR5 into the XbaI site of the pBluescript vector, which also contains a gene for ganciclovir sensitivity (Kuziel et al. 2003). The entire coding region of CCR5, ~550bp of the preceding intron and ~1.1kbp of DNA downstream of the translation stop codon was then removed using BglII and replaced with a 1.8kbp neomycin resistance gene in the opposite transcriptional orientation. The final targeting

plasmid was electroporated into the embryonic stem (ES) cell line E14TG2A, derived from the 129/Ola mouse strain, resulting in the entire coding region of CCR5 being replaced with a neomycin resistance expression cassette. ES cells that had incorporated the vector could then be selected for by treating cells with media containing neomycin and ganciclovir antibiotics. CCR5<sup>-/-</sup> ES cells were injected into a developing mouse embryo at the blastocyst stage to make chimeras (CCR5<sup>+/-</sup>); heterozygotes were then mated together to produce homozygous second generation (F2) CCR5<sup>-/-</sup> mice. CCR5<sup>-/-</sup> mice were then outbred on a C57BL/6J x 129/Ola background resulting in mice that have a permanent deletion of the whole CCR5 coding region.

These knockout mice have been used to study the role of CCR5 in different models of infection, including the 1S strain of *L. donovani*, *L. major*, *Toxoplasma gondii*, and *Chylamdia trachomatis*. Sato et al. (1999) performed a 56 day time-course experiment of *L. donovani* infection using stationary phase promastigotes from the 1S strain. When the parasite burden was subsequently quantified using the method of limiting dilution culture, there was a marginal trend for less of an increase in parasite burden over time compared with wild-type control mice in both spleen and liver tissue in this chronic model of *Leishmania* infection. By 56 days post-infection, the absolute parasite burden was significantly different between the two mice strains in the liver. However, whether this difference in parasite burden was attributable to effects at the level of the macrophage or the immune system in general was not explored. Thus, Sato et al. (1999) were unable to conclude whether the lack of CCR5 affected parasite entry and intracellular survival within macrophages or whether the reduction in parasite burden was caused by an altered immune response.

To follow this up, the same group used these CCR5<sup>-/-</sup> mice to determine whether CCR5 influences DC migration and localisation during *L. major* infection (Sato et al. 2000). Using an ear skin explant model, they noticed a decreased Langerhans cell (skin DC) migration out of ear skin explants. However, they saw no significant difference in parasite burden in the ear, lymph node or spleen at 35 days post-infection, and no deviation of the ear

thickness (a marker of infection) from the wild-type infected control group. Others have also noticed these defective migratory abilities of CCR5<sup>-/-</sup> leukocytes. In uninfected models, Yurchenko et al. (2006) provided evidence to suggest that naturally occurring nTreg cells lacking CCR5 have reduced abilities to respond to chemotactic signals, while the suppressive function of these cells remained unchanged. After infection with *L. major* metacyclic promastigotes, intradermal parasite burden and lesion size were reduced in CCR5<sup>-/-</sup> mice compared to wild-type control. This correlated with an increase in CD4<sup>+</sup> T cell accumulation at the site of intradermal injection, illustrating that nTreg cells were unable to properly migrate to infection areas to suppress parasite-specific effector T cells.

Khan et al. (2006) used these mice to explore the impact on a typical time-course of infection with the intracellular protozoan parasite *Toxoplasma gondii*. They found that CCR5<sup>-/-</sup> mice had higher parasite burdens in the liver than wild-type control mice, although other organs had no significant difference in parasite numbers. This was likely due to impairment of leukocyte migration into infected tissues and they found that adoptively transferring CCR5<sup>+/+</sup> leukocytes into these knockout mice restored the ability to control parasite numbers. A similar effect was seen within the context of *Chlamydia trachomatis* infection. Lymphocytes isolated from the genital tract of *C. trachomatis*-infected mice have been reported to have increased expression of CCR5; when the receptor was knocked out, the bacterial burden was increased eightfold due to problems with T cells homing to appropriate sites of infection (Olive et al. 2011). Nogueira et al. (2015) found that CCR5<sup>-/-</sup> T cells had reduced migration indices suggesting that the receptor played a role in aiding T cell migration into the lung during intranasal infection with the pathogen. They also found that there was no significant difference between the bacterial burden in wild-type and CCR5<sup>-/-</sup> mice, suggesting that the receptor was not involved in clearing the pathogen from sites of infection but may have helped direct the immune response.

### 4.1.2 Objectives

It is possible that CCR5 could be involved during *Leishmania* infection in two distinct roles. Firstly, it could play a role at the local level of the macrophage, either affecting the ability of the parasite to enter its target cell or survive intracellularly within its compartment. Alternatively, CCR5 could play a role in orchestrating the immune system to infection, helping to direct immune cells to sites of inflammation to support the containment and elimination of invading parasites. Thus, the exact role that CCR5 plays during *L. donovani* infection is yet to be fully characterised.

Here, we aimed to determine whether deletion of CCR5 had an effect on *in vivo* *L. donovani* LV9 amastigote infection during a murine time-course of infection of up to 64 days. This was to be achieved through two main experimental approaches:

- a) By performing a time course of infection in CCR5<sup>-/-</sup> mice to determine whether the parasite burden and granuloma formation differed from wild-type C57BL/6 control mice.
- b) By using chimeric mice with mixed bone marrow populations to determine whether there was a difference in the ability of parasites to infect and survive in CCR5<sup>-/-</sup> macrophages compared to CCR5<sup>+/+</sup> macrophages.

This enabled us to assess whether the absence of CCR5 affects normal *L. donovani* LV9 amastigote infection initiation and progression, both at the level of the macrophage and the immune system as a whole. By using the same strain of parasites throughout in an established and published *in vivo* model of *Leishmania* infection, we were able to determine whether the association seen in Chapter 3 between CCR5 and *L. donovani* infection *in vitro* was important for the outcome of infection *in vivo*.



## 4.2 Chapter-specific methods

### 4.2.1 Wild-type and CCR5<sup>-/-</sup> mice infections

Age-matched wild-type control (“CCR5<sup>+/+</sup>”) C57BL/6 mice and CCR5<sup>-/-</sup> mice were infected with either  $3 \times 10^7$  *L. donovani* amastigotes or  $1 \times 10^8$  tdTomato *L. donovani* amastigotes, both suspended in RPMI-1640 (Gibco, UK) and injected via the tail vein. Infections were left for either 14, 28 or 64 days, at which time spleens and livers were isolated and prepared for processing. Mice were housed in specific pathogen free (SPF) conditions.

### 4.2.2 Chimera generation and infection

Age-matched B6.CD45.1 mice (n = 24 females) were given acidified water for 5 days and then irradiated with  $2 \times 550$  rads (24 hr apart) administered using a RS2000 X-ray irradiator (RadSource Inc.). After the second dose,  $2 \times 10^6$  isolated bone marrow cells from B6.CD45.1 (n = 5 females) and CCR5<sup>-/-</sup> (n = 5 females) mice were adoptively transferred by tail vein injection 1:1 into these mice. Mice were given Baytril-treated water for 1 week and left to recover for 6 weeks before being infected with  $1 \times 10^8$  tdTomato *L. donovani* amastigotes (Beattie et al. 2008) suspended in RPMI 1640 (Gibco, UK) by tail vein injection. Mice were then sacrificed at different time points: 6hr, 24hr, 28 days and 56 days post-infection, at which time spleen and livers were isolated and prepared for processing.

### 4.2.3 Preparation of liver and spleen material

When organs were ready to harvest, mice were sacrificed using carbon dioxide asphyxiation followed by cervical dislocation. Freshly removed liver and spleen tissue to be used for cryosectioning were cut into cubes approximately  $5\text{mm}^3$  in size and embedded into optimal cutting temperature (OCT) compound (TissueTek) where it was frozen and stored at  $-80^\circ\text{C}$ . Tissue was also placed into RNeasy and frozen for RNA extraction, and multiple slide impression smears prepared for LDU counting. For cryosectioning, liver and spleen tissue embedded in OCT were cut into  $8\mu\text{m}$  thick sections using a cryostat (Leica, Germany) and placed onto poly-L-lysine-coated slides. Sections were left to air-dry at  $22^\circ\text{C}$  and stored at  $-80^\circ\text{C}$

until needed. For haematoxylin and eosin staining, cryosection slides were fixed in acetone for 5 mins. Sections were then stained with Harris haematoxylin solution (Sigma, UK) for 4 mins and rinsed in cool running water for 5 mins. They were then dipped in 0.5% (w/v) eosin dissolved in 95% (v/v) ethanol 12 times and washed in water until eosin streaking stopped. Sections were put through an ethanol dehydration series from 50% (v/v) to 100% (v/v) ethanol in 10% increments and finally a coverslip was mounted on them using DePeX mounting medium. A light microscope was used for looking at sections at 100x magnification and a Zeiss AxioScan.Z1 slider scanner (Zeiss, Germany) was used to digitally capture slides for granuloma analyses.

#### **4.2.4 Calculating parasite burden using Leishman Donovan Units**

Slide impressions were fixed by submerging in methanol and left to air dry. Slides were then submerged in 10% (v/v) Giemsa stain solution (VWR International, USA) suspended in 4.4mM Na<sub>2</sub>HPO<sub>4</sub> and 1.7mM KH<sub>2</sub>PO<sub>4</sub> in dH<sub>2</sub>O for 30 mins at 22°C, rinsed under running tap water and left to air dry before visualising on a light microscope. LDUs were calculated for both spleen and liver sections of each infected mouse. This was done by multiplying the organ weight by the number of amastigotes present per 1000 host cell nuclei, first detailed by Stauber (1955).

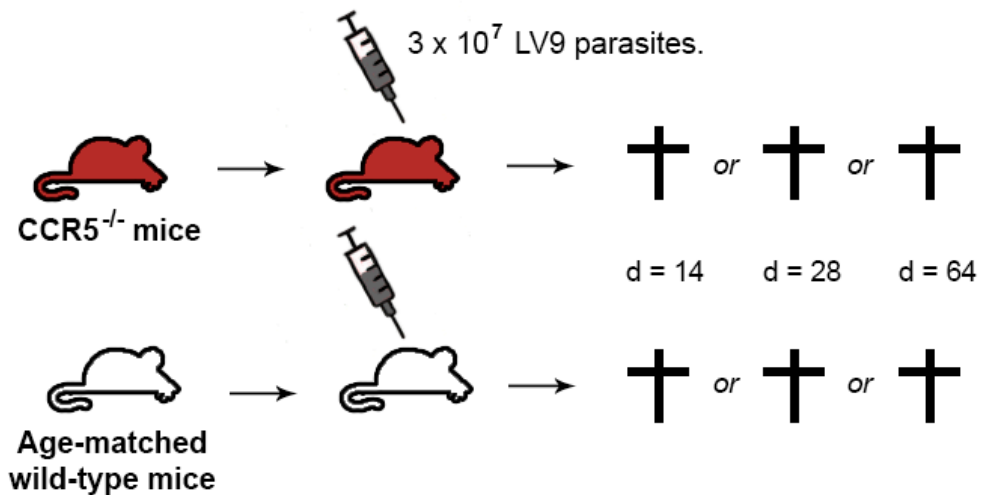
## 4.3 Results

### 4.3.1 Wild-type vs CCR5<sup>-/-</sup> experiments

Having confirmed the genotype of these mice (as shown previously in Section 3.3.2), one way to determine whether CCR5 had any effect on the course of *L. donovani* LV9 amastigote infection in our mouse model was to set up infections in wild-type vs CCR5<sup>-/-</sup> mice. Wild-type control (“CCR5<sup>+/+</sup>”) C57BL/6 mice and CCR5<sup>-/-</sup> mice were infected with *L. donovani* LV9 amastigotes by Dr Naj Brown (University of York) and left for up to 64 days (see **Figure 4.1** for experimental overview).

The first question we wanted to address was whether there were any differences in overall parasite burdens between the two mice strains. These data were measured for all mice for both spleen and liver by measuring the weight and LDU counts for each (see **Figures 4.2 and 4.3**). When analysing each time point individually, a significant difference was found between the CCR5<sup>-/-</sup> mice and wild-type mice at day 28 in the spleen for the first experiment but was not seen at the same time-point when the experiment was repeated. When the data were merged, there was no statistically significant difference seen at any time-point for either liver or spleen LDU counts (see **Figure 4.3**). In addition to LDU counts, at each time point the liver and spleen weights were calculated as a percentage of total body weight. As a normal response to the recruitment of immune cells and cellular exudate from inflamed tissue, the weight of these two organs increases during the course of infection. In our experiments, we showed this increase in organ weight and that there was no significant difference between wild-type or CCR5<sup>-/-</sup> mice (see **Figure 4.3**).

Another measure of *Leishmania* infection progression is to analyse the process of granuloma formation and maturation in these mice. Granulomas form as a result of the normal physiological response of the immune system to control and eventually resolve *L. donovani* hepatic infection. Even though there was no overall difference in organ weights or LDUs between wild-type and CCR5<sup>-/-</sup> mice, there might still have been a difference in granuloma stages between the two groups if only a small number of immune cells were



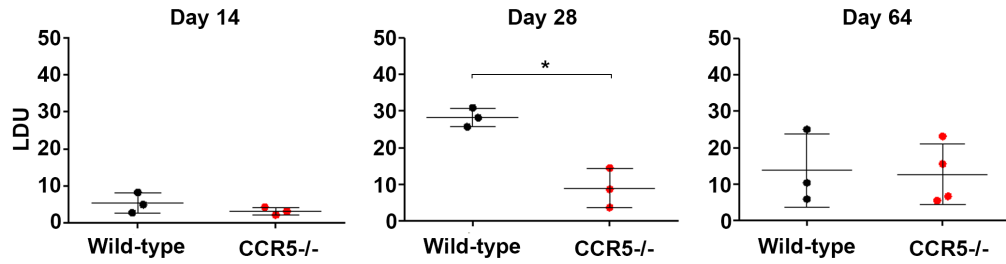
When mice were sacrificed, tissue was collected for the following purposes:

- **Leishman Donovan Unit (LDU) counting**  
Purpose: for a general assessment of overall parasite burden in both the spleen and liver.
- **Cryosectioning and immunohistochemistry**  
Purpose: to visualise the histological structure of liver tissue.
- **RNA extraction**  
Purpose: to quantitatively determine the relative amounts of CCR5 RNA present in infected wild-type spleen and liver tissue.

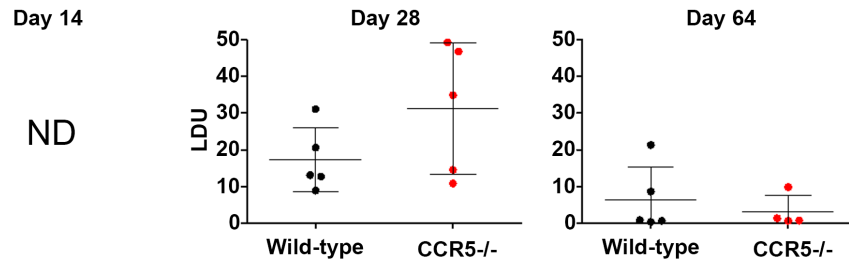
**FIGURE 4.1. Overview of CCR5<sup>-/-</sup> vs control wild-type (CCR5<sup>+/+</sup>) infection experiments.** Time-course experiments were performed using age-matched CCR5<sup>-/-</sup> and wild-type (CCR5<sup>+/+</sup>) mice. Mice were infected with  $3 \times 10^7$  *L. donovani* LV9 amastigote parasites and tissues harvested at day 14, 28 or 64. Liver and spleen slide impressions were made for LDU counting, and tissue pieces collected for cryosectioning and RNA extraction.

### SPLEEN LDUs:

#### EXPERIMENT 1:

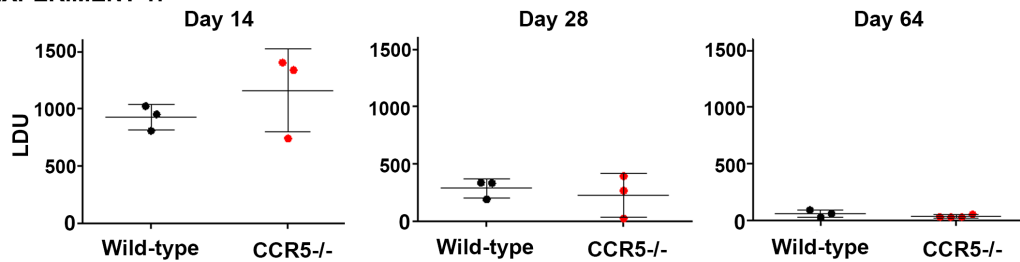


#### EXPERIMENT 2:

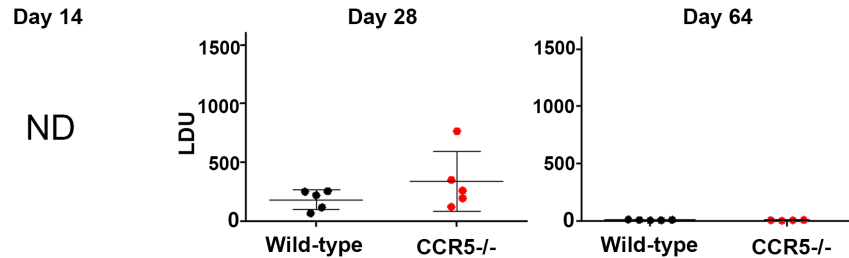


### LIVER LDUs:

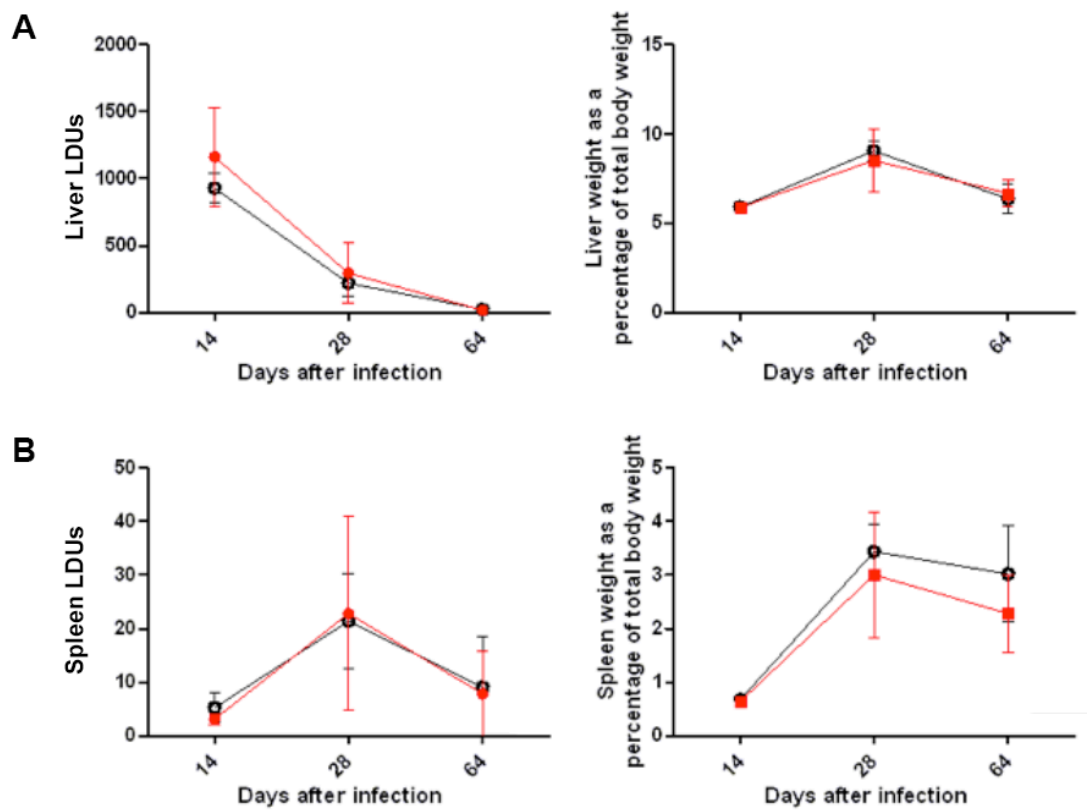
#### EXPERIMENT 1:



#### EXPERIMENT 2:



**FIGURE 4.2. Lack of CCR5 does not influence parasite burden during *in vivo* infection with *L. donovani* LV9 amastigotes.** CCR5<sup>-/-</sup> and wild-type mice were infected with *L. donovani* parasites and left for up to 64 days post-infection. Parasite burden was measured by calculating individual spleen and liver LDU counts for each mouse. Each data point represents a single mouse with between 3 and 5 mice used per time-point. Data shown as mean ± SD. \* = p < 0.05. ND = not determined.



**FIGURE 4.3. Overall time-course summaries of the LDU counts and organ weights in wild-type and CCR5<sup>-/-</sup> mice during *L. donovani* LV9 amastigote infection.** Time course of organ weights and LDU counts during *in vivo* infection for the target organs of infection: the liver (**A**) and the spleen (**B**). Data for each time-point is pooled from the experiments present in Figure 4.2, with at least 3 mice in each group for each time-point. Data shown as mean ± SD.

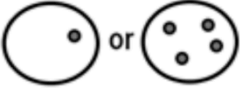
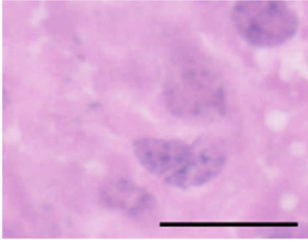


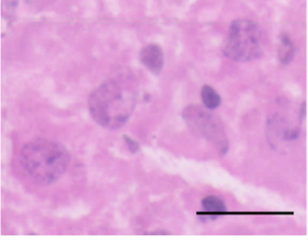
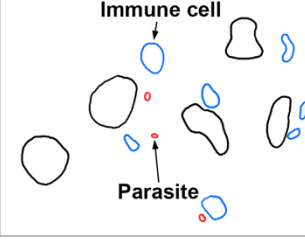

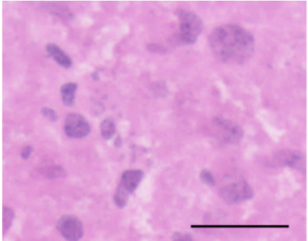
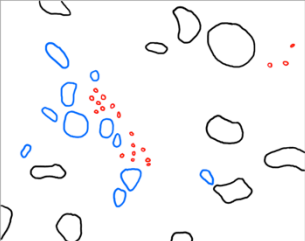

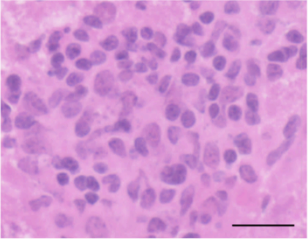
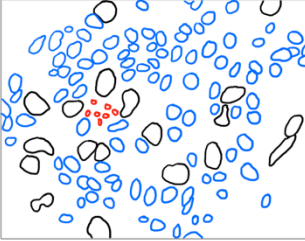

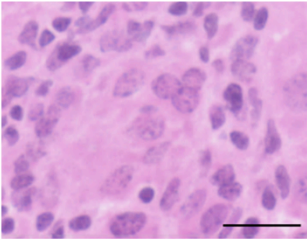
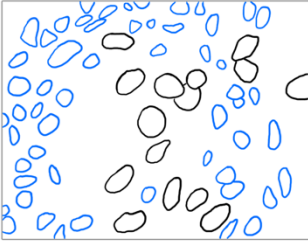
required to eliminate the parasite. We thus looked at haematoxylin and eosin stained liver cryosections and scored each infection foci using criteria adapted from Murphy *et al*, 1998, as summarised in **Figure 4.4**. When looking at the individual data for each time point, there was a slight but statistically significant difference between how advanced granulomas were in wild-type and CCR5<sup>-/-</sup> mice at day 28 post-infection (**Figure 4.5**). More specifically, CCR5<sup>-/-</sup> mice had lower scoring granulomas than wild-type mice. This trend was also apparent at day 64 although statistical significance was not reached. As the score assigned to infection foci is based upon the number of immune cells surrounding the infected cell, this suggests that CCR5<sup>-/-</sup> mice were able to recruit less immune cells to areas of infection.

#### **4.3.1.1 Repeating experiments with tdTomato *L. donovani* parasites**

To confirm the *in vivo* findings detailed thus far, *in vivo* experiments were repeated using a separate stock of tdTomato *L. donovani* amastigote parasites. It could not be assumed that the cellular progression of infection would be the same as with wild-type *L. donovani* amastigote parasites so the results are presented separately in **Figure 4.6**. As day 28 was the time-point that showed possible differences between wild-type and CCR5<sup>-/-</sup> mice when using wild-type parasites, this time-point was chosen to look at the effect of tdTomato parasites on parasite burden and granuloma progression. As before, there were no statistically significant differences between the groups for LDU counts and organ weights (**Figure 4.6A**). In addition, the granulomas present in the livers of infected CCR5<sup>-/-</sup> mice again scored less than those in wild-type mice (**Figure 4.6B**); when those granulomas scoring  $\geq 3$  were combined, there was a statistically significant difference between wild-type and CCR5<sup>-/-</sup> mice (**Figure 4.6C**), largely replicating the results obtained with wild-type parasites (**Figure 4.5**).

#### **4.3.1.2 Detailed screening of splenic cell populations**

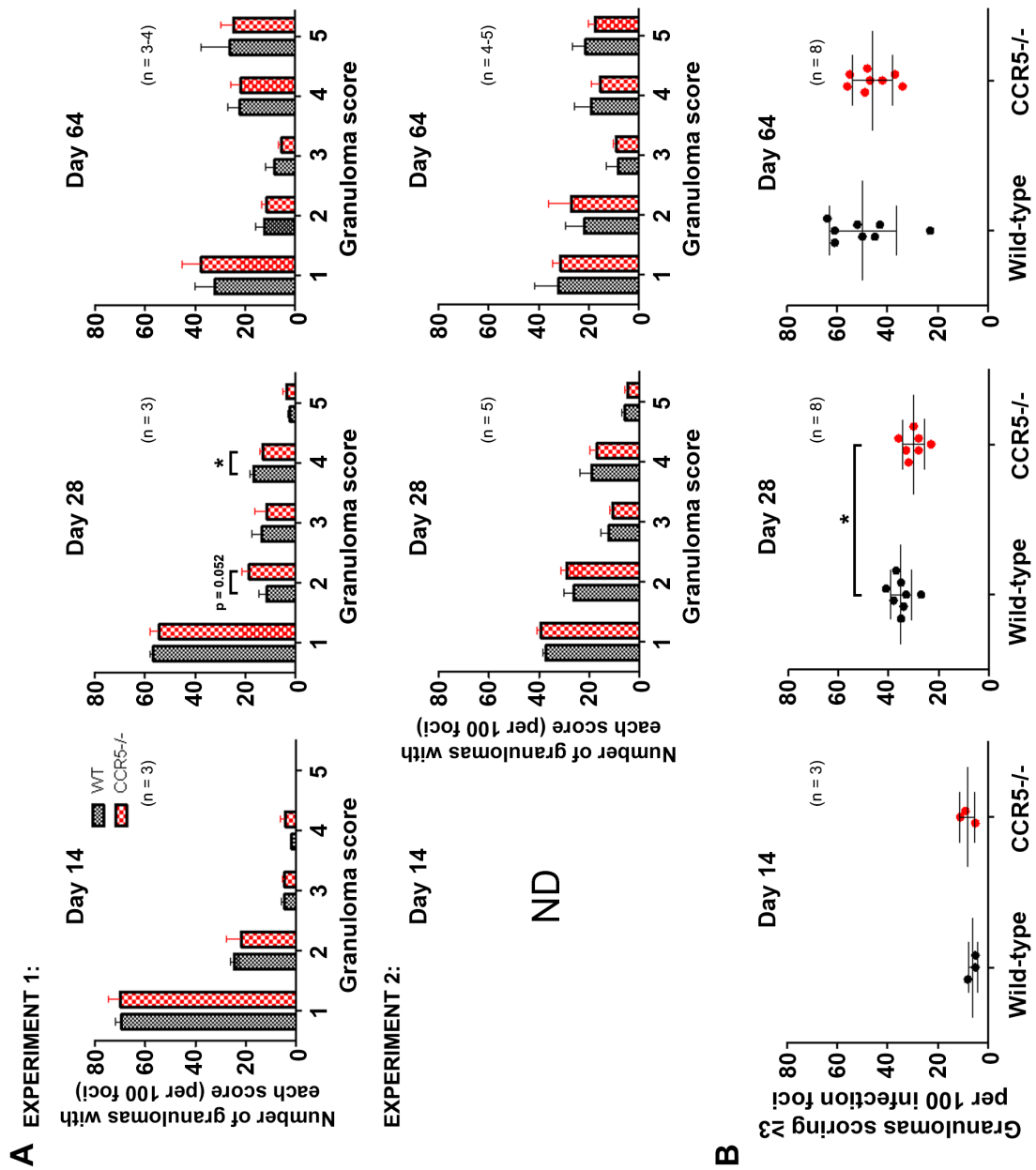
Dr James Hewitson, another researcher within the Centre for Immunology and Infection (University of York), had an established high-throughput protocol for screening splenic populations. To confirm that there were no subtle changes occurring in individual subpopulations of cells within the

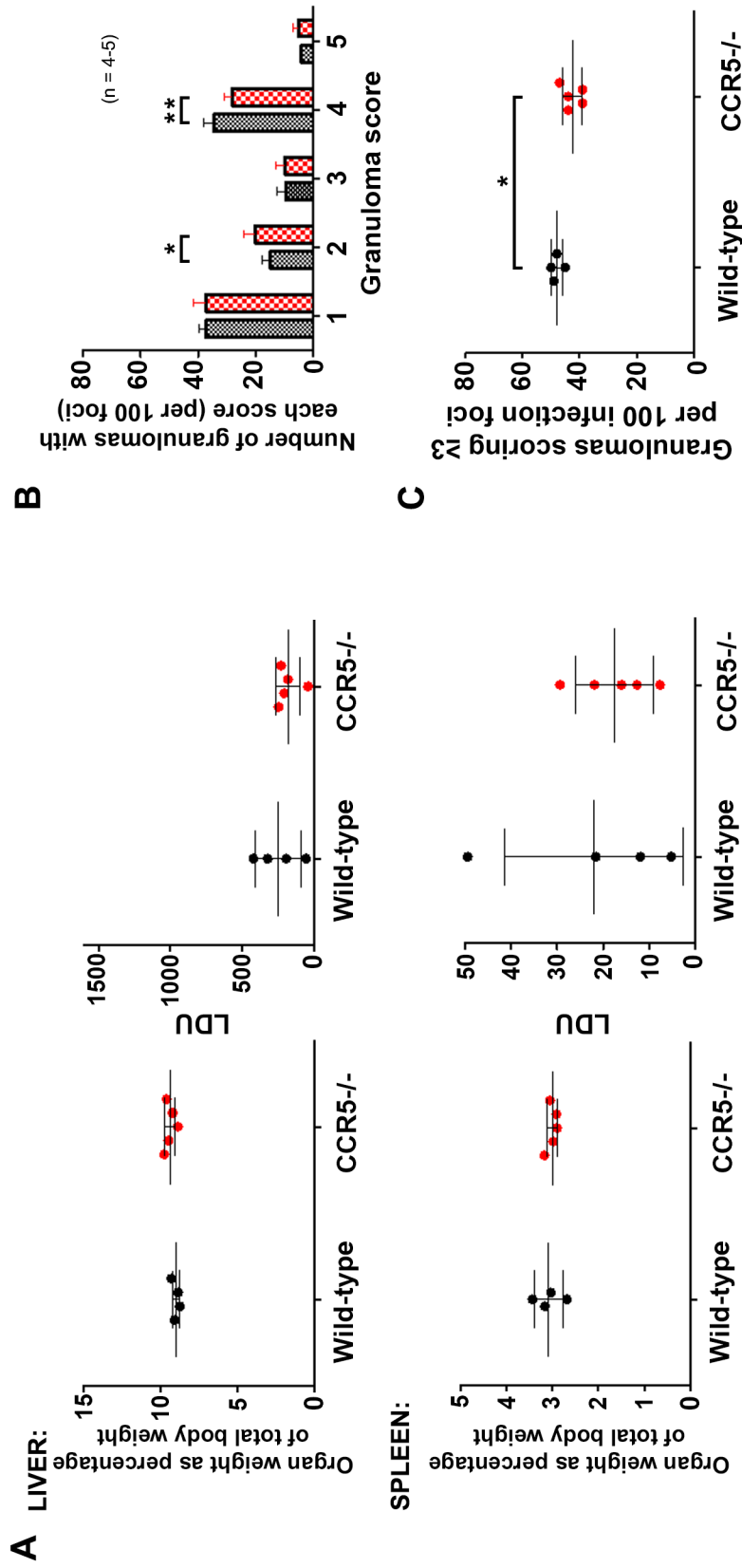
Score:	Criteria:	Example histological appearance:	
1	 <p>No immune cells around infection foci</p>		
2	 <p>&lt;5 immune cells around infection foci</p>		
3	 <p>5-10 immune cells around infection foci</p>		
4	 <p>&gt;10 immune cells around infection foci</p>		
5	 <p>Immune cells surrounding cell(s) with no visible parasite</p>		

**FIGURE 4.4. Method used for granuloma quantification.** Scoring criteria for granuloma analysis of infected tissue, adapted from Murphy et al. (1998). Cryosections were haematoxylin & eosin stained and infection foci identified by looking for parasites (dark purple staining). The number of immune cells (if any) surrounding infected cells was then counted. Black cell outline = liver cell; blue outline = immune cell; red outline = parasite. Scale bar = 20µm.



**FIGURE 4.5. CCR5<sup>-/-</sup> mice showed subtle differences in granuloma scores at day 28 post-infection. A)** Histograms showing the granuloma scores for infection foci present in either wild-type (WT) or CCR5<sup>-/-</sup> liver sections infected with *L. donovani*. One hundred infection foci were counted per mouse, with sections from at least 3 mice used per time-point. **B)** Summary of granulomas scoring  $\geq 3$  overall for both experiments combined. Data displayed as mean  $\pm$  SD; \* =  $p < 0.05$ . ND = not determined.





**FIGURE 4.6. The same results for organ weight, parasite burden and granuloma formation at day 28 were seen when infections used tdTomato *L. donovani* amastigotes.** Wild-type and CCR5<sup>-/-</sup> mice were infected at day 0 with 1x10<sup>8</sup> tdTomato *L. donovani* parasites. **A)** Graphs show individual liver or spleen weights and LDU counts for each mouse used in the CCR5<sup>-/-</sup> vs wildtype experiment when tdTomato parasites were used. Each data point represents a single mouse. **B)** Histogram shows the granuloma scores for infection foci present in either wild-type (grey bars) or CCR5<sup>-/-</sup> (red bars) liver sections infected with tdTomato parasites when one hundred infection foci were counted per mouse. **C)** Difference in number of granulomas scoring  $\geq 3$  in wild-type and CCR5<sup>-/-</sup> mice. Displayed as mean  $\pm$  SD; \* =  $p < 0.05$ ; \*\* =  $p < 0.01$ .

spleen during *L. donovani* infection, this screening procedure was applied to cells isolated from wild-type and CCR5<sup>-/-</sup> mice either immediately (day = 0) or 28 days post-infection. As cells were analysed by Dr Hewitson, the results from this analysis are presented in **Appendix B**. In brief, these analyses gated for cells that were live, intact, singlets and CD45<sup>+</sup> to ensure that only leukocytes were captured. These analyses showed that there might be a slight decrease in certain dendritic cell subpopulations within the spleen of CCR5<sup>-/-</sup> mice, both at day 0 and at day 28 post-infection, but statistical conclusions cannot be made because of the low sample number for day 0. All other major subpopulations, including CD4<sup>+</sup> and CD8<sup>+</sup> T cells, neutrophils and macrophages, showed no difference in either the absolute number or percentage of total cells present. This suggests that CCR5<sup>-/-</sup> does not have a major role in the recruitment of cells during *L. donovani* infection in the infected spleen, compared to the liver granuloma analyses reported in Section 4.3.1.

#### **4.3.2 Chimera experiments**

As no striking phenotype emerged from the wild-type vs CCR5<sup>-/-</sup> experiments, we instead moved on to determine whether there might be a more subtle effect at the cellular level. For example, if CCR5 was involved in either the entry or intracellular survival of *L. donovani* parasites, we may have seen differences in the number of parasites in wild-type and CCR5<sup>-/-</sup> macrophages if parasites were allowed to infect mixed populations of these cells. The proportion of wild-type and CCR5<sup>-/-</sup> immune cells within granulomas may also have been different if CCR5 was necessary for cellular recruitment to infection foci.

Chimeric mice generated from mixed bone marrow populations are often used for such experiments because cells are placed within the same cellular environment; thus any difference in infection of CCR5<sup>-/-</sup> macrophages was more likely to be due to the lack of CCR5 rather than inter-mouse variation. These chimeric mice exploit allelic variants of CD45, namely CD45.1 and CD45.2. CD45 is a phosphatase expressed in all nucleated haematopoietic cells and the two variants are considered to be broadly functionally

equivalent (Basu et al. 2013). The CD45 marker also has antibody tools readily available for differentially staining these variants to determine which genetic background individual cells are derived from, making it useful for exploring the effect that CCR5 had on *in vivo* *L. donovani* infection.

#### **4.3.2.1 Experimental overview**

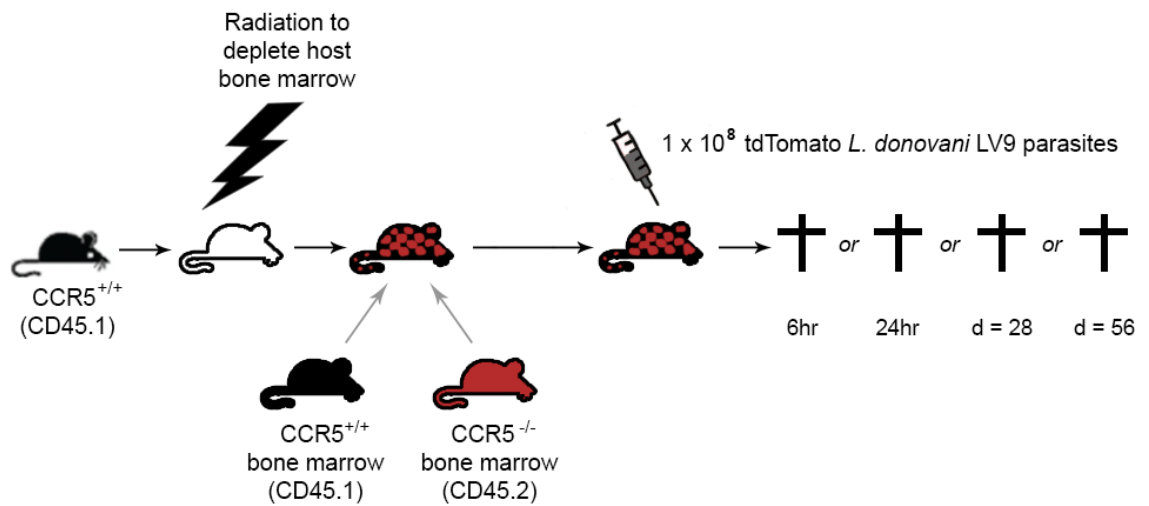
Mice with chimeric bone marrow populations were generated and infected by Dr Naj Brown (University of York) as summarised in **Figure 4.7**. Mice were then sacrificed at different time points: two early time points, 6hr and 24hr post-infection, were chosen to study the early entry and uptake of the parasite. Two later time points, 28 days and 56 days post-infection, were chosen to determine whether there might have been a longer-term effect.

#### **4.3.2.2 Weights and LDUs**

To confirm that mice had been infected, mice were weighed and the LDU counts calculated for each time point. As shown in **Figure 4.8**, all mice had LDUs greater than 0 indicating that they had been infected and by day 56 the vast majority of parasites had been cleared from all the mice used in the experiment. Of note, there was greater variation in LDU counts for each time point compared to the wild-type vs CCR5<sup>-/-</sup> experiments detailed in Section 4.3.1 above. Although this may be due to inter-mouse variation in the uptake of infection when administered with intravenous *L. donovani* parasites, it could also be due to other factors specific to chimeric mice. For example, one possible reason is that different mice may have different proportions of CCR5<sup>-/-</sup> macrophages compared to wild-type macrophages; it was therefore important to determine what the proportion of CD45.1 to CD45.2 phagocytes was for each mouse used.

#### **4.3.2.3 Immunofluorescent analyses**

As there may be inter-mouse variation in the CD45.1 to CD45.2 ratio for phagocytic cells present in this experiment, we first established whether there was a change in this ratio during the time-course of infection. After staining cryosections for CD45.2 and the phagocytic marker F4/80, the presence of these two cell populations could be visualised using confocal



**When mice were sacrificed, tissue was collected for the following purposes:**

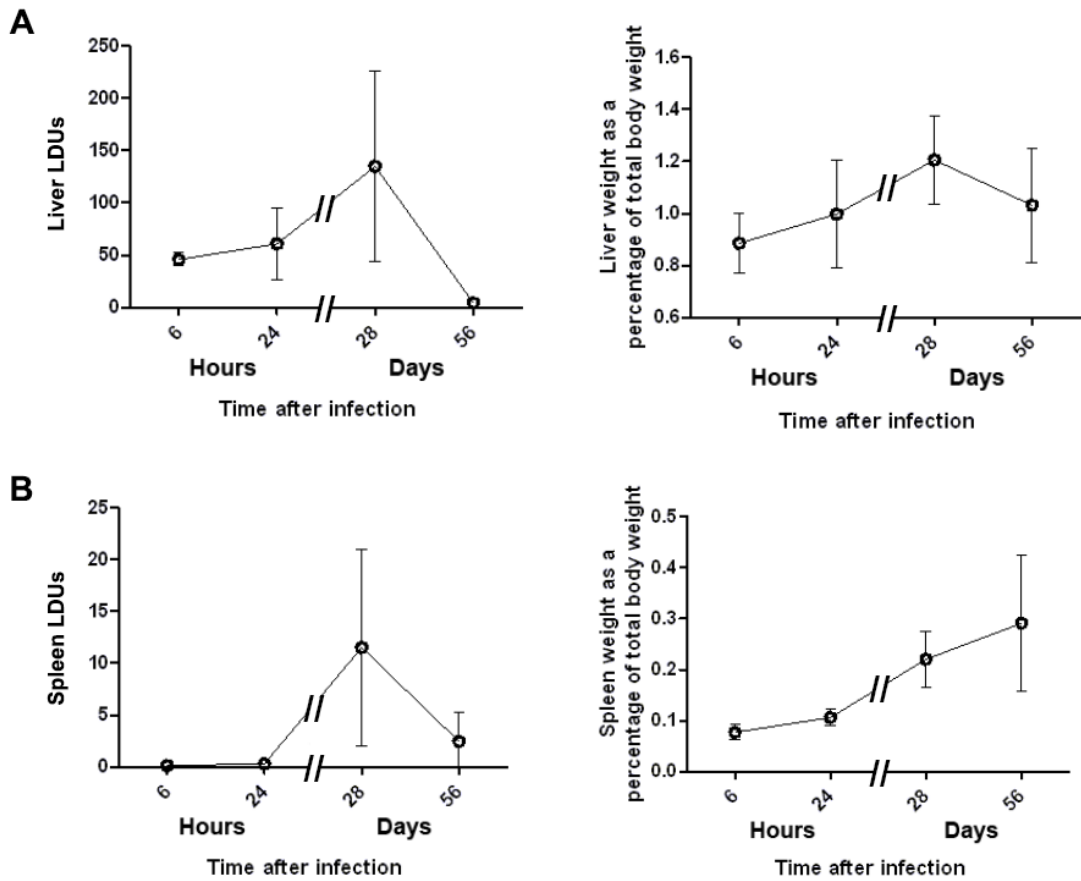
**- LDU counting**

Purpose: for a general assessment of overall parasite burden in both the spleen and liver.

**- Cryosectioning and immunofluorescent staining**

Purpose: to visualise where tdTomato parasites were in relation to CD45.1/2 phagocytes in liver sections.

**FIGURE 4.7. Overview of chimera experiments.** CD45.1 reporter mice that were CCR5<sup>+/+</sup> were irradiated to deplete bone marrow progenitor cells, which were replaced by adoptively transferring donor bone marrow cells 1:1 from either CCR5<sup>+/+</sup> (CD45.1) or CCR5<sup>-/-</sup> (CD45.2) mice. Chimeric mice were then infected with 1 x 10<sup>8</sup> tdTomato *L. donovani* LV9 amastigote parasites and tissues harvested at 6 hr, 24 hr, 28 days or 56 days. Liver and spleen slide impressions were made for LDU counting, and tissue pieces collected for cryosectioning and immunofluorescent staining.



**FIGURE 4.8. Overall summary of parasite burdens in chimeric mice.** Time course of organ weights and LDUs for both liver (**A**) and spleen (**B**) in chimeric mice during infection with tdTomato *L. donovani*. Data for each time-point from 1 experiment with at least 3 mice per group. Data shown as mean  $\pm$  SD.

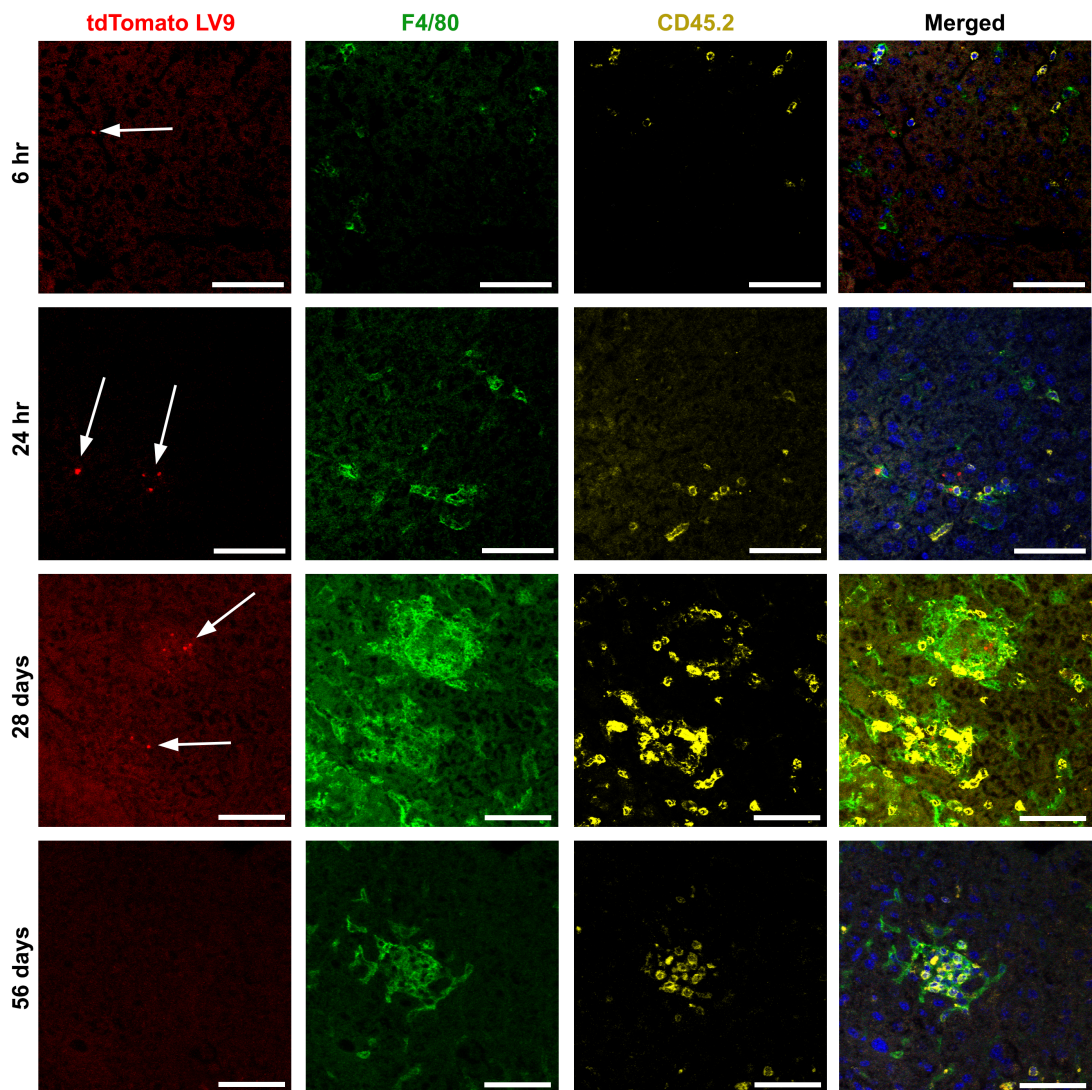
microscopy. As shown in **Figure 4.9**, both CD45.1<sup>+</sup> and CD45.2<sup>+</sup> phagocytes were present at all time-points. Both cell types were also present within granulomas, suggesting that immune cells lacking CCR5 could still be recruited to infection foci. Again, it is also important to note the relative absence of tdTomato parasites within tissue sections by day 56.

We then wanted to confirm that CCR5<sup>-/-</sup> macrophages could be infected by tdTomato parasites. As shown in **Figure 4.10A**, examples of infected F4/80<sup>+</sup> CD45.2<sup>+</sup> cells were readily available. This clearly shows that the CCR5<sup>-/-</sup> cells present within this chimera model can be infected with *L. donovani* parasites. Next, a quantitative analysis of CCR5<sup>-/-</sup> phagocytic cells was calculated for each time point using z-stacked confocal images. As shown in **Figure 4.10B**, the proportion of F4/80<sup>+</sup> cells that were also CD45.2<sup>+</sup> (and therefore CCR5<sup>-/-</sup>) was approximately 35% and remained the same for each time point. This provides further evidence that cells lacking CCR5 could still be recruited with the same efficiency as CCR5 positive phagocytes, suggesting that other non-CCR5-dependent mechanisms were in place to attract cells to infection sites.

In order to assess whether wild-type and CCR5<sup>-/-</sup> macrophages were able to take up *L. donovani* parasites with the same efficiency, tdTomato parasites within these same immunofluorescently-stained cryosections were analysed. Each parasite was first checked to see whether it was in an F4/80<sup>+</sup> phagocytic cell and then the presence or absence of co-localising CD45.2<sup>+</sup> signal was checked. As shown in **Figure 4.10C**, ~35% of the parasites that were present within an F4/80<sup>+</sup> cell were also in a cell that stained positive for CD45.2 for each time-point during infection. This suggests that there was no preferential infection of macrophages either lacking or possessing CCR5.

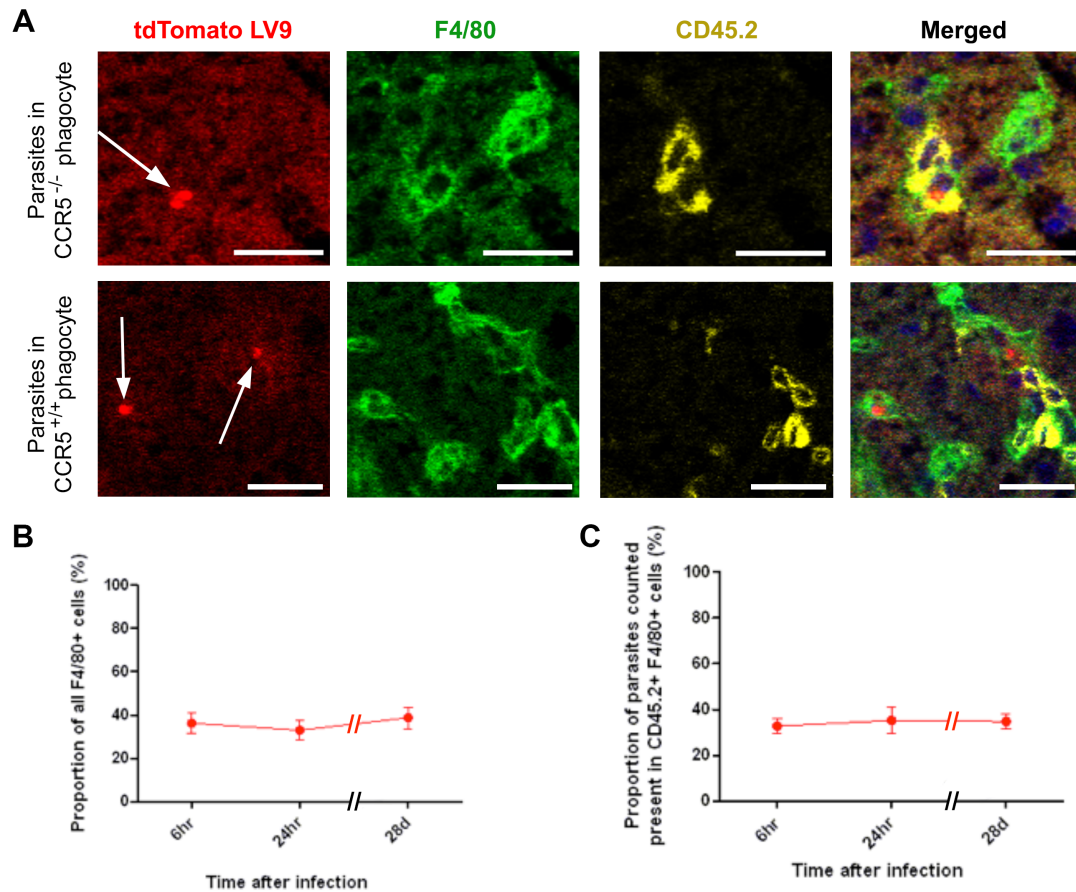
### **4.3.3 Wild-type vs CCR5<sup>-/-</sup> BMDM infection rates**

The *in vivo* findings presented here thus far suggested that CCR5 was not important for *L. donovani* infection. However, this differed from the findings from Bhattacharyya et al (2008) who found that knocking down the receptor using siRNA led to an approximate 60% decrease in intracellular parasites as counted inside *in vitro* BMDMs. We thus decided to replicate this same



**FIGURE 4.9. Appearance of infection foci in liver sections taken from chimeric mice.** Representative single section confocal images showing the differences in appearance between early infection (6 and 24 hr) and later infection (28 days and 56 days) time-points in chimeric mice. At 6 hr, parasites were typically in surrounding tissue having not yet been taken up by an F4/80<sup>+</sup> cell. By 24 hr, the majority of parasites were within F4/80<sup>+</sup> cells with few F4/80<sup>+</sup> or CD45.2<sup>+</sup> immune cells around infection foci. By 28 days post-infection, all parasites were now present within F4/80<sup>+</sup> cells and were typically surrounded by large granulomatous masses of immune cells, as shown by the accumulation of F4/80<sup>+</sup> and CD45.2<sup>+</sup> cells. By 56 days post-infection, the vast majority of parasites had been eliminated with granulomatous structures remaining. Scale bar = 50 $\mu$ m.

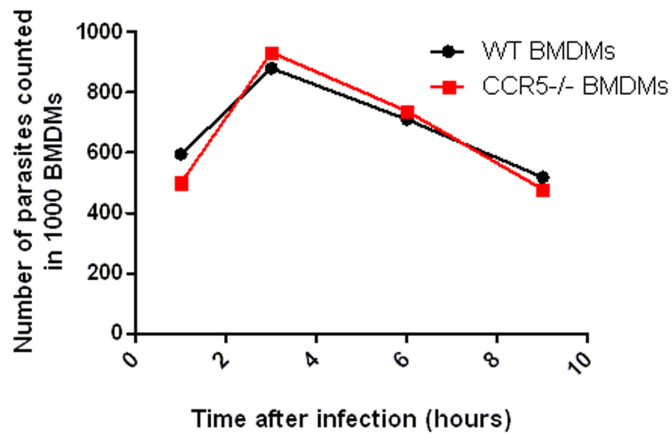




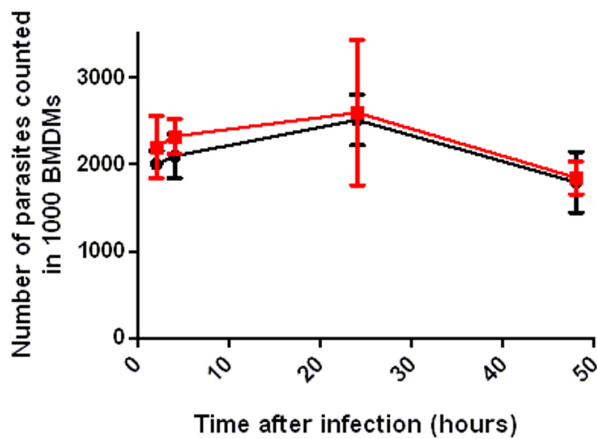
**FIGURE 4.10.** There was no difference in the uptake of *L. donovani* parasites by macrophages either possessing or lacking CCR5. The uptake of tdTomato *L. donovani* LV9 amastigotes by F4/80<sup>+</sup> cells was determined using chimeric mice with mixed CCR5<sup>-/-</sup> and CCR5<sup>+/+</sup> bone-marrow populations. **A)** Example confocal images of liver sections from chimeric mice. Single confocal image taken from a z stack; scale bar = 20µm. **B)** To determine whether parasites preferentially infected either CCR5<sup>+/+</sup> or CCR5<sup>-/-</sup> macrophages, the percentage of F4/80<sup>+</sup> cells that were CCR5<sup>-/-</sup> (CD45.2<sup>+</sup>) in infected chimera mice was calculated by analysing 100 F4/80<sup>+</sup> cells in random fields of view. **C)** 100 parasites were identified and checked to determine what percentage were in CCR5<sup>-/-</sup> (CD45.2<sup>+</sup>) phagocytes. At least 3 mice per group were analysed for each time-point; data shown as mean ± SD.

experiment using *in vitro* experimentation. Bone marrow cells from wild-type (“CCR5<sup>+/+</sup>”) and CCR5<sup>-/-</sup> mice were grown *in vitro* and differentiated into BMDMs (see Section 2.4.4 for method). After spinoculating *L. donovani* LV9 amastigote parasites onto cells, infections were left for 4 hr before washing off any unbound parasites. A time-course of up to 48 hr was set-up and at each time-point cells were fixed and processed for microscopy. As shown in **Figure 4.11**, there was no significant difference between CCR5<sup>-/-</sup> and CCR5<sup>+/+</sup> BMDMs for either early uptake (2 and 4 hr post-infection) or intracellular survival (9 hr post-infection) of amastigote parasites. To check whether there was a difference seen in infection rates if the promastigote form of the parasite was used instead, BMDMs derived from wild-type and CCR5<sup>-/-</sup> mice were infected with *L. donovani* LV9 promastigotes using the same experimental protocol detailed above for amastigotes. As shown in **Figure 4.11**, this again showed that there were no significant differences in infection uptake or intracellular survival between wild-type and CCR5<sup>-/-</sup> BMDMs.

### Amastigote



### Promastigote



**FIGURE 4.11. There was no difference in infection rates between wild-type and CCR5<sup>-/-</sup> BMDMs infected with *L. donovani*.** Amastigote and promastigote *L. donovani* LV9 parasites were used to infect wild-type (WT) or CCR5<sup>-/-</sup> BMDMs. Parasites were spinoculated and left exposed to cells for 4 hr before unattached parasites were washed away. Time-courses of infection were followed for up to 9 hr (amastigote) or 48 hr (promastigote) post-infection before cells were fixed, stained with DAPI and visualised on a fluorescence microscope. The number of parasite nuclei present per 1000 BMDM nuclei was counted.

## 4.4 Chapter-specific discussion

The *in vivo* models of infection presented in this chapter show no significant difference in parasite burden in CCR5<sup>-/-</sup> mice compared with age-matched C57BL/6 control mice during a typical 64 day time-course of infection. Furthermore, chimeric mice with adoptively transferred mixed populations of wild-type (CCR5<sup>+/+</sup>) and CCR5<sup>-/-</sup> macrophages showed no preferential infection by *L. donovani* LV9 amastigotes in either macrophage population at early (up to 24hr) or late (28 days) time-points. Despite this, the formation of granulomas in the liver was altered with a statistically significant reduction in the recruitment of immune cells to infection foci in CCR5<sup>-/-</sup> mice. These data suggest that although CCR5<sup>-/-</sup> may impede immune cell recruitment, there was no effect on the ability of parasites to infect macrophages or on the immune system's ability to clear *L. donovani* LV9 amastigotes in the absence of CCR5 in these models, as summarised in **Table 4.1**.

Days post-infection:	Day 14	Day 28	Day 64
Stage of infection:	Acute	Acute-chronic	Chronic
Combined number of mice:	3 wild-type 3 CCR5 <sup>-/-</sup>	12 wild-type 13 CCR5 <sup>-/-</sup>	8 wild-type 8 CCR5 <sup>-/-</sup>
Organ weights			
- Spleen:	N.s.d.	N.s.d.	N.s.d.
- Liver:	N.s.d.	N.s.d.	N.s.d.
LDUs			
- Spleen:	N.s.d.	N.s.d.	N.s.d.
- Liver:	N.s.d.	N.s.d.	N.s.d.
Liver granuloma analysis:	N.s.d.	CCR5 <sup>-/-</sup> have less immune cells surrounding foci	N.s.d.

**TABLE 4.1.** The overall effect of CCR5<sup>-/-</sup> on *L. donovani* LV9 amastigote infection *in vivo* was minimal with the only difference observed being a transient difference in liver granuloma progression. Overall combined descriptive summary from 2 experiments using wild-type *L. donovani* parasites and 1 experiment using tdTomato parasites. N.s.d. = no statistically significant difference observed between wild-type and CCR5<sup>-/-</sup> mice.

The only difference seen for parasite burden during these time-courses of infection was at day 28 for one experiment where the spleen LDU counts for CCR5<sup>-/-</sup> mice were lower. However, other repeats of this time-course experiment using either wild-type or tdTomato parasites failed to reproduce

this result. It could be argued that there was a trend towards lower LDU counts in CCR5<sup>-/-</sup> overall but statistical significance was not reached. It is possible that with further repeats of this time-course experiment this trend may become significant; however, any difference is likely to be small and minor differences are harder to reveal because of inherent variability between individual mice (Meyer et al. 2007). This would require experiments involving a substantial number of mice, the use of which may be questionable because there was no difference seen in disease progression or overall infection outcome.

The apparent disparity in results from the current study and from Sato et al. (1999) can be explained by several factors. Firstly, Sato et al. (1999) infect mice with promastigote parasites whereas amastigote parasites were used here; others have suggested that CCR5 may be important for promastigote parasites to initially attach to and enter target cells and establish infection (Bhattacharyya et al. 2008), and this necessity may be lost with the amastigote form. However, when *in vitro* time-courses of infection were performed using promastigote parasites, there was no difference between wild-type and CCR5<sup>-/-</sup> BMDMs in the ability of *L. donovani* to infect and survive intracellularly. As an alternative explanation, Sato et al. (1999) use the 1S strain of *L. donovani*; although having the same East African origin as LV9, there are distinct differences between individual strains of *L. donovani* that can change the overall infection kinetics and surface composition of parasites (Ghosh et al. 1998; El Tai et al. 2001; Basu et al. 2007). For the latter, this could result in differences in the receptors that the parasite interacts with. There are also differences in infection models, with Sato et al. (1999) using a model that had both spleen and liver LDUs steadily increasing over the time-course in wild-type C57BL/6J mice suggesting that the infection was not cleared. This was in stark contrast to our model of infection where LDU counts initially started high and decreased over time with the infection being effectively cleared by day 64 (LDUs < 10). This difference is relevant because the only difference that Sato et al (1999) found between parasite burdens in wild-type and CCR5<sup>-/-</sup> mice was in the liver at day 56, by which time the infection had been cleared in our model of infection. It may be that

CCR5 plays a larger role during persistent infection with *L. donovani*, as discussed later. Regardless, *in vivo* models of infection are inherently difficult to compare because of well established problems of backcrossing with knockouts (Flaherty 1981; Wolfer et al. 2002; Lusic et al. 2007; Vanden Berghe et al. 2015), intra-species variation (Zurita et al. 2011) and differences between animal houses (Beura et al. 2016), the latter of which is particularly relevant for infection studies.

The LDU counts that were obtained for each time-point during infection, particularly at day 28, were considerably lower than others have found even within the same laboratory (Beattie et al. 2011; Owens et al. 2012; Maroof et al. 2012). These low LDU counts make it harder to determine small changes in parasite burdens between the two mouse groups and were probably due to a general decrease in the 'quality' of the parasites. When parasites multiply and are serially passaged in RAG1<sup>-/-</sup> mice, the normal selective pressures applied by the immune system to destroy suboptimal parasites are lost. To address this, we repeated the *in vivo* time-course experiment using a separate population of tdTomato parasites that we hoped would achieve higher LDU counts but this was not the case. To increase the quality of the parasite stocks used for future experiments, it may be worthwhile passaging these parasites through an immunocompetent host such as an Armenian hamster.

The results from the chimera study demonstrated that there was no preference for parasites to infect either CCR5<sup>+/+</sup> or CCR5<sup>-/-</sup> macrophages. This correlated well with the findings seen during *in vitro* *L. donovani* infections using BMDMs and showed that the absence of CCR5 on macrophages did not inhibit parasite uptake or intracellular survival. These results are supported by others in the literature that have looked at the prevalence of the naturally occurring CCR5 $\Delta$ 32 mutant among patients with cutaneous or mucocutaneous forms of leishmaniasis (Brajão de Oliveira et al. 2007; Ribas et al. 2013; Sophie et al. 2016). Although all of these studies have relatively small sample group sizes, the results again suggest that a lack of CCR5 was not protective against *Leishmania* infection. However, one

caveat for all of these studies is that they do not use a visceralising form of *Leishmania* so the results are not directly comparable with the results presented in the current study or those from others (Bhattacharyya et al. 2008; Majumdar et al. 2014). Despite this, these findings support the results of the present study where CCR5<sup>-/-</sup> was found to have no influence on disease progression *in vivo* or the ability of macrophages to be infected *in vitro*. The only significant difference found between patients possessing or lacking CCR5 was based on whether patients had recurrence of the disease (Ribas et al. 2013). They found that the Δ32 mutation, with a lack of cell surface CCR5, was associated with a significantly reduced chance of disease recurrence, something that could not be tested with our self-resolving murine model of *L. donovani* infection.

The use of chimeric mice with mixed populations of CCR5<sup>+/+</sup> and CCR5<sup>-/-</sup> macrophages allowed us to recapitulate the findings that we have seen *in vitro* and helped in separating out the macrophage-specific role of CCR5 from that seen for the immune system overall. The finding that only ~35% of F4/80<sup>+</sup> cells were CD45.2<sup>+</sup> (CCR5<sup>-/-</sup>) was expected as others have shown that Kupffer cells are derived from two distinct locations, a radio-sensitive haematopoietic-derived population and radio-resistant yolk sac-derived population (Klein et al. 2007). Having macrophages derived from two different origins could be a potential issue when studying the differential ability of *L. donovani* parasites to be phagocytosed by and reside in Kupffer cells. However, Beattie et al. (2016) found that there was no difference in the ability of *L. donovani* LV9 amastigotes to be phagocytosed by or survive within these two macrophage populations. Furthermore, this same study also showed that although the transcriptomic signature may be unique to each population, the overall biological functions were comparable (Beattie et al. 2016).

Thus, confident that CCR5 had no effect on the ability of parasites to enter and survive within macrophages, we explored the effect that CCR5 had on the immune response to infection. In the liver, this was done by studying granuloma formation, with a slight and transient reduction in hepatic

granuloma progression seen in CCR5<sup>-/-</sup> mice. Mature granulomas provide the microenvironment needed for *L. donovani* destruction and are therefore a defence mechanism of benefit to the host to limit dissemination and ultimately eliminate the parasite, but at the cost of potential destruction of the local tissue micro-architecture (Murray 2001). Others have shown that these granulomas are composed of recruited CD4<sup>+</sup> and CD8<sup>+</sup> T cells along with activated mononuclear phagocytes that encircle a core of parasitised resident macrophages (Murray 2001). We have already demonstrated through our chimeric mouse study that there was no shift in the recruitment of phagocytes to the liver resulting from the lack of CCR5; thus, this difference could be accounted for by changes in T cell recruitment. Treg cells have been shown to express high levels of CCR5 and Vallejo et al. (2014) also noted that there was an up-regulation of the CCR5 present on CD8<sup>+</sup> Treg cells during *Leishmania* infection. CCR5 also plays a well-known role in T cell chemotaxis to areas of infection and this has also been demonstrated for *Leishmania* specifically (Yurchenko et al. 2006). By knocking out CCR5 these cells may have impaired recruitment to infection foci and this could help explain the delay seen in granuloma progression in the present study. Despite this, granuloma impairment had no significant effect on the outcome of the infection in the *in vivo* model used in the current study. Future experiments could test the effect T cell-associated CCR5 has on the structure of granulomas forming at hepatic infection foci. For example, T cells could be isolated from infected wild-type mice using a flow cytometer and then adoptively transferred into infected CCR5<sup>-/-</sup> mice. Once transferred, these T cells should undergo rapid clonal expansion. Unfortunately, because the model of *L. donovani* infection used here is one that is self-resolving, this same technique could not be used to check whether T cell-associated CCR5 is important for maintaining a persistent or relapsing infection without changing to a different model. However, others have shown that CCR5 plays a role in guiding nTreg cells to infection sites in the dermis during cutaneous *L. major* infection where they suppress CD4<sup>+</sup> T cell responses (Yurchenko et al. 2006), suggesting that further investigation into the role of T cell-associated CCR5 during a visceralising form of leishmaniasis would be valuable.



To study the general immune response to *L. donovani* infection in the spleen, we used flow cytometry screening of splenic cell populations and showed that although there was a slight decrease in dendritic cells within the spleen, all other major subpopulations showed no difference between wild-type and CCR5<sup>-/-</sup> mice. This suggested that, in contrast to the liver, the absence of CCR5 did not have a specific role in the recruitment of T cells to infection foci in the spleen. This may be due to the self-resolving model of infection used in our study, as in chronic diseases and infections T cell-associated CCR5 has been shown to play a role (Olive et al. 2011; Martin-Blondel et al. 2016).

Indeed, for *Leishmania* specifically others have suggested that T cells could play important roles during infection. Vallejo et al. (2014) compared the characteristics of T cell populations in patients co-infected with *Leishmania* and HIV-1, compared to patients with HIV-1 alone or healthy controls. They noticed that there were higher proportions of Treg cells in individuals co-infected with *Leishmania*; these cells are known to have high levels of CCR5 (reviewed by de Oliveira et al. 2014) and play a role in suppressing the local immune response to infection (Suffia et al. 2006). Furthermore, Yurchenko et al. (2006) suggest that CCR5 may play a role in guiding Treg cells to areas of *L. major* infection. Treg cells play a crucial role in dampening down the response by T effector cells, a role which is important to prevent pathological self-reactivity leading to autoimmune disease. However, it is becoming clear that they also play a role in persistent infections such as HIV, hepatitis C and malaria (Weiss et al. 2004; Cabrera et al. 2004; Hisaeda et al. 2004). The *in vivo* model of infection used in the current study is one that is self-resolving with the parasite effectively being eliminated by day 64. It may be that the role played by CCR5 in the Treg response may only be important during persistent infections rather than acute self-resolving infection courses. This would help explain why Sato et al (1999) see a possible role for CCR5 in their *in vivo* models of infection. Interestingly, they only observed an enhanced T cell-mediated immune response in CCR5<sup>-/-</sup> mice after 8 weeks of infection, which could explain why we see no difference in the CD4<sup>+</sup> and CD8<sup>+</sup> T cell populations within the spleen at day 28. It would also explain why

the only clinical effect on leishmaniasis seen with the naturally occurring  $\Delta 32$  mutant was a decrease in the recurrence of the disease (Ribas et al. 2013).

At the macrophage-level, no difference was seen in the ability of parasites to infect or survive within macrophages either possessing or lacking CCR5. In Chapter 3, data was shown to demonstrate that *in vitro* infection with *L. donovani* decreased the amount of CCR5 present at the cell surface and mRNA levels for the receptor. If this also occurred during the *in vivo* infections presented in this chapter, the macrophages present within wild-type mice would quickly have their CCR5 levels reduced. These cells would therefore more closely resemble the macrophages found in CCR5<sup>-/-</sup> mice, at least for expression of the receptor at the cell surface, and could offer one explanation as to why no difference was seen *in vivo*. An alternative experiment would be to determine if any effect is seen when CCR5 is overexpressed in mice. This could involve either a simple overexpression of CCR5 or could utilise a mutated receptor where the C terminal tail has been modified to inhibit activation of the intracellular signaling cascade upon receptor activation, thus leaving the receptor at the cell surface.

Altogether, our data show that CCR5 was not necessary for *L. donovani* LV9 amastigotes to gain entry to the macrophage. Furthermore, upon entry, there was no difference in the ability of the parasites to reside and survive within CCR5<sup>+/+</sup> or CCR5<sup>-/-</sup> macrophages. However, the parasite induces a down-regulation of CCR5, meaning that functionally these two populations of macrophages are likely to be similar. At the level of the immune system overall, we saw a transient decrease in the number of leukocytes recruited to infection foci in the liver but this had no impact in the outcome of infection using our self-resolving murine models of visceral leishmaniasis. Despite this, it is possible that CCR5 may play a more important role during chronic non-resolving cases of leishmaniasis by influencing the recruitment of Tregs, as has been suggested for many other forms of chronic infection (Weiss et al. 2004; Cabrera et al. 2004; Hisaeda et al. 2004) and future exploration into the role of CCR5 in chronic models of leishmaniasis infection may be useful.

# **5. Isolating intracellular *L. donovani*-containing compartments for qualitative proteomic membrane characterisation**

## **5.1 Chapter-specific background and rationale**

The decrease in cell surface CCR5 seen previously may be beneficial to the parasite and the parasite may have mechanisms to internalise the receptor directly. An obvious hypothesis for the decrease of CCR5 at the cell surface is that the receptor is being co-internalised within the parasite-containing compartment. This phenomenon has only recently been considered, with another member of the GPCR superfamily having been shown to co-internalise with Gram-negative bacteria (Billings et al. 2016). The lack of antibodies available to follow internalised CCR5, coupled with our interest in characterising the protein composition of this the *Leishmania*-containing intracellular compartment, meant that we then progressed on to developing a novel detergent-free method for isolating these compartments. This method required that isolated samples were exposed to minimal manipulation post-isolation because it is well established that GPCRs are inherently unstable (Hutchings et al. 2010).

*Leishmania* parasites are well adapted to being able to reside within the harsh intracellular phagolysosomal compartments that are normally catastrophic to most phagocytosed bacteria and parasites. As examples of these adaptive abilities, it has been shown that *Leishmania* contain high numbers of glycoinositol-phospholipids in their plasma membrane that protect against acidic conditions and hydrolases (McConville & Ralton 1997), while it has also been shown that *Leishmania* have amastigote stage-specific proton pumps and transporters to help them withstand and capitalise on the

acidic pH environment (Zilberstein & Shapira 1994). Additionally, it is also likely that the parasite can manipulate both the composition and the maturation of the host cell compartment to make its intracellular environment more favourable. The best documented example of this for *Leishmania* is the expression of LPG by the parasite, which is able to directly affect the progression of the parasite-containing compartment (Desjardins & Descoteaux 1997). More specifically, LPG, a complex glycosphosphatidylinositol-anchored phosphoglycan that is abundant on the surface of promastigote parasites from all *Leishmania* species (McMahon-Pratt & Alexander 2004), is thought to get passively transferred to the phagosome (Tolson et al. 1990) and restrict fusion of the parasite-containing compartment with late endosomal compartments (Desjardins & Descoteaux 1997; Scianimanico et al. 1999; Dermine et al. 2000). LPG is also thought to be involved in a number of virulence mechanisms, including dampening nitric oxide production (Proudfoot et al. 1996). Although LPG is commonly associated with the promastigote form of *Leishmania*, Turco & Sacks (1991) have shown that LPG is also found on amastigotes, albeit in lower amounts and as a structurally distinct form. However, unlike promastigotes, there is currently no evidence to suggest that this LPG alters the progression or fusibility of the amastigote-containing compartment.

Although this example of passive manipulation of the promastigote-containing compartment is well established, examples of active manipulation by the parasite are much less well understood. As one such example, it was shown that live parasites were able to avoid activation of CD4<sup>+</sup> cells and were thereby more readily able to establish infection (Nylén et al. 2003). This suggested that the parasite was able to actively manipulate its external environment, both for the parasite-containing compartment and the host cell in which it resides. However, the exact molecular mechanisms behind this are still unknown. Furthermore, this is only one such mechanism of active manipulation and it is likely that the live parasite is able to manipulate a plethora of proteins on the intracellular compartment to make its environment more amiable.

The parasite-containing compartment lies at the host-pathogen interface, acting as the first border that allows biochemical communication between organisms. It is clear that to get a better understanding of the parasite-containing compartment specifically, and thus the host-pathogen interaction in general, it would be advantageous to be able to isolate this parasite from infected cells and perform large-scale comprehensive studies of the protein composition of this compartment membrane. Attempts to do this so far have been limited due to the technical challenge of isolating these intracellular compartments without exposing the sample to a number of purification steps that can degrade the quality of the sample and remove potential proteins of interest (Li et al. 2010).

### **5.1.1 Objectives**

In order to characterise the proteomic composition of the parasite-containing compartment, we required a method that could isolate these compartments with minimal manipulation of isolated material. Within the Pryor lab, a method has already been developed to isolate and enrich for lysosomes from J774.2 cells (Rofe and Pryor, 2015). Here, we aimed to use this as a basis on which to develop a novel method to isolate *L. donovani*-containing compartments from infected J774.2 cells for qualitative and quantitative proteomic characterisation. The success of this method for isolating compartments would be assessed based on enrichment for LAMP1 and lysosomal enzymatic activity, and through LC-MS/MS assessment of the collected material. By using live and HI parasites, we could then determine whether the live parasite actively manipulated the compartment in which it resides.

## **5.2 Chapter-specific methods**

### **5.2.1 Assessing parasite viability**

The number of live parasites was determined using a Live/Dead Fixable Dead Cell Stain Kit (Molecular Probes, United States). Parasites were washed and re-suspended in 1mL PBS before being exposed to 1 $\mu$ L of dissolved dye for 30 mins at 22°C. Parasites were then fixed and analysed using a flow cytometer with an excitation wavelength of 405nm and emission wavelength 575nm. To determine whether *L. donovani* parasites retained the ability to transform into promastigotes, amastigote parasites were cultured in RPMI-1640 medium supplemented with 20% (v/v) FCS, 50U/mL penicillin/streptomycin and 25mM HEPES, pH 7.4, at 26°C for up to 7 days (Amit et al. 2014). The presence of promastigotes was checked every 2 days.

### **5.2.2 Colloidal iron dextran (FeDex) production**

FeDex was made as detailed by Rofe and Pryor (2015). In brief, at 22°C 5mL of 1.2M FeCl<sub>2</sub> was mixed with 5mL 1.8M FeCl<sub>3</sub>. Then 5mL of 28-30% (v/v) NH<sub>4</sub>OH was added while stirring, forming a Fe<sub>3</sub>O<sub>4</sub> precipitate. The precipitate was then held within a magnetic field by placing the beaker on a strong magnet. The remaining liquid was decanted and replaced with 5% (v/v) NH<sub>4</sub>OH, the magnet removed to re-suspend the precipitate, and then washed in this way twice more using distilled water. After the final wash, the precipitate was re-suspended in 40mL of 0.3M HCl and stirred for 30 mins. Next, 2g of 40,000MW dextran was added and stirred for 40 mins. The solution was then dialysed extensively in distilled water at 4°C for 48 hr using 10kDa MWCO dialysis tubing against 4L of deionised water with at least four changes of the dialysis bath. Large aggregates were removed by centrifuging at 47,800 x *g* (Sorvall SS-34 rotor) for 15 mins. After filtering through a 0.2 $\mu$ m filter for sterility, the resulting FeDex solution was stored at 4°C for up to 2 months.

### **5.2.3 Lysosome isolation**

Following the Rofe and Pryor (2015) protocol for isolating lysosomes using SPIONs, four 10cm dishes of J774.2 cells were seeded at a density of  $8 \times 10^6$  cells per dish and left to incubate overnight. The following day, cells were pulsed with FeDex (1:20 in complete DMEM) for 1 hr and then chased for 2 hr in complete DMEM. Previous results within the Pryor lab (Rofe and Pryor, 2015) have shown that longer pulse and chase durations led to diminishing lysosome recovery and latency. At 4°C throughout, cells that had been pulse-chased with FeDex were pelleted and re-suspended in 1mL STM buffer (250mM sucrose, 1mM MgCl<sub>2</sub>, 10mM TES, pH 7.4); cells were then lysed using nitrogen cavitation (model Q913534A, Parr Instrument Company, USA) at 250 PSI for 5 mins. A post nuclear supernatant (PNS) was made by centrifuging the lysate at 800 x g for 5 mins. A MACS large cell column (Miltenyi Biotech, UK) was held within a magnetic field and equilibrated with 3mL STM buffer. The PNS was then added to the column and the flow-through collected and applied twice more. After washing the column with 3mL of STM buffer, the column was removed from the magnetic field and lysosomes eluted in STM buffer. Lysosomes were pelleted by centrifugation at 37,500 x g for 15 mins and then re-suspended in 0.1-1mL STM buffer and subsequently characterised.

### **5.2.4 β-hexosaminidase assay**

Lysosome latency and enrichment were determined by assessing β-hexosaminidase activity. The standard reaction mixture contained 5μL of sample with 100μL of substrate solution (100mM citric acid, pH 5.0, 0.5mM 4-methylumbelliferyl-2-acetamido-2-deoxy-beta-D-glucopyranoside, 0.27M sucrose), with the reaction allowed to progress for exactly 3 mins. Reactions were terminated with the addition of 1mL of 1M Na<sub>2</sub>CO<sub>3</sub>. Fluorescence was measured using a Lumina fluorescence spectrometer (Thermo Scientific, USA) with an excitation wavelength of 360nm, emission wavelength of 445nm, and slit width of 10nm.

### **5.2.5 Protocol for parasite isolation**

To make magnetisable parasites, *L. donovani* amastigote parasites were left in complete RPMI and FeDex was added 1:20. Parasites were left in a humidified incubator (37°C, 5% CO<sub>2</sub>) for 1 hr before being washed three times in complete RPMI, each time centrifuging at 2000 x *g* for 10 mins to pellet parasites. Parasites were used immediately to infect J774.2 cells (MOI of 10) and were left on cells for 2 hr, at which point the cells were washed twice with complete DMEM and the infection allowed to progress for a further 2 hr. At 4°C throughout, cells were then pelleted and re-suspended in 1mL STM buffer; cells were then lysed using nitrogen cavitation (model Q913534A, Parr Instrument Company, USA) at 250 PSI for 5 mins. A PNS was made by spinning at 600 x *g* for 5 mins. A MACS large cell column (Miltenyi Biotech, UK) was held within a magnetic field and equilibrated with 3mL STM buffer. The PNS was then added to the column and the flow-through collected and applied twice more. After washing the column with 3mL of STM buffer, the column was removed from the magnetic field and parasite-containing phagolysosomes eluted in STM buffer. At this stage, parasites were HI for 30 mins at 56°C. Samples were then pelleted at 37,500 x *g* for 15 mins and re-suspended in 100µl of ddH<sub>2</sub>O. Samples were frozen at -80°C until further processing in preparation for LC-MS/MS analysis.

### **5.2.6 Nitric oxide production**

J774.2 cells were infected with either live or HI *L. donovani* parasites (MOI: 10). After 4 hr, cells were washed several times with complete DMEM and then exposed to complete DMEM supplemented with 1µg/mL LPS for a further 20 hr. Cells were then harvested and a Griess assay performed. This involved incubating 50µL of sample with 50µL of Griess reagent (1% (w/v) sulphanilamide in 5% (v/v) phosphoric acid) for 5 mins at 22°C before the addition of 50µL of N-1-naphthylethylenediamine dihydrochloride (NED). A spectrophotometric microplate reader was used to measure absorbance at 548nm.



### **5.2.7 Determining subcellular localisation of proteins**

The automatic assignment of gene ontology (GO) terminology to poorly characterised proteins using different annotation methods is often inaccurate, with figures of 65-70% accuracy reported (Khan et al. 2003; Martin et al. 2004; Conesa et al. 2005). To increase confidence that the proteins identified using LC-MS/MS (performed as described in Section 2.12) had a known localisation to the phagolysosome compartment, all proteins were manually checked via Google Scholar to determine whether there was experimental evidence in the literature to confirm a phagolysosomal localisation. Experimental evidence included all non-proteomic laboratory-based methods of identification, most commonly western blotting or immunofluorescence.

## 5.3 Results

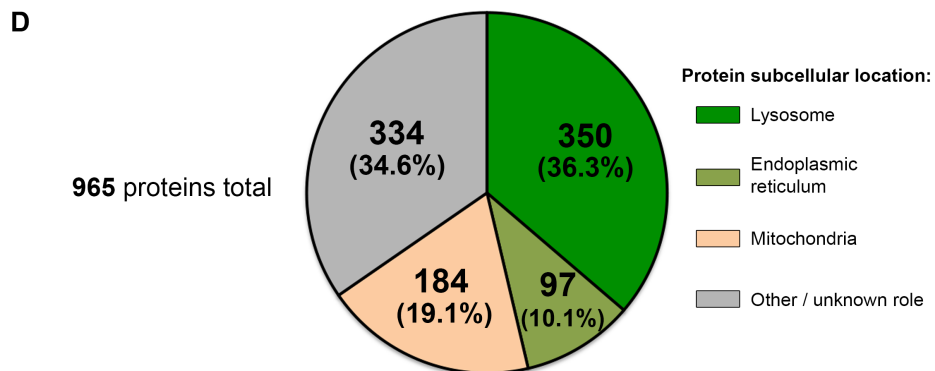
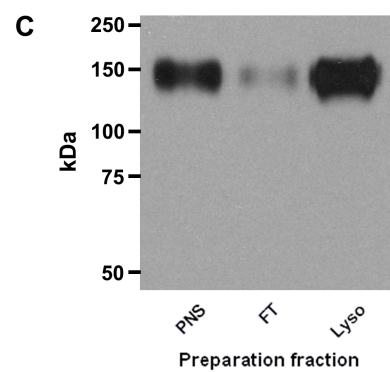
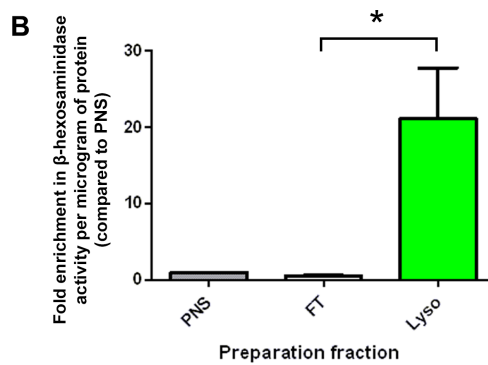
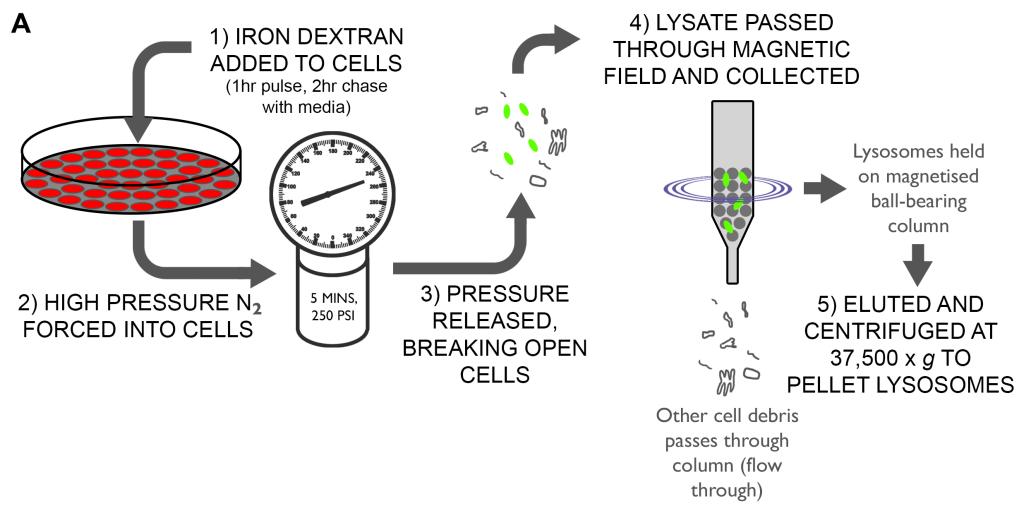
### 5.3.1 Isolating lysosomes from uninfected cells

#### 5.3.1.1 Isolation of lysosomes

As summarised in **Figure 5.1A**, J774.2 cells were processed using the method for lysosome isolation detailed in Section 5.2.3. After generating a post-nuclear supernatant (PNS), the lysed contents were passed through a column held within a magnetic field, with both the flow-through (FT) fraction and elution (Lyso) fraction from the column being collected for analysis. To confirm that the elution contained lysosomes, enrichment for the lysosomal enzyme  $\beta$ -hexosaminidase was assayed for. As shown in **Figure 5.1B**, there was an approximate 20-fold increase in the activity of this enzyme in the isolated lysosome fraction. Enrichment for lysosomal proteins was determined by western blotting each fraction for LAMP1, which has a predicted molecular mass of 38.3 kDa but appears at approximately 120 kDa because of extensive glycosylation (Carlsson et al. 1988). As shown in **Figure 5.1C**, there was high expression in the lysosomal fraction even though this fraction was loaded with 90% less protein than other fractions. Together, this suggested that this protocol had been successful in enriching for lysosomes.

#### 5.3.1.2 Proteomic data from isolated lysosomes

A lysosomal sample was generated as described above and then sent for qualitative LC-MS/MS. This dataset returned 965 proteins identified from 2897 peptide identifications and would provide a useful comparison to compare isolated phagolysosome samples with when collected from infected cells. To characterise the proteins in this sample, the subcellular location for each identified protein was checked and summarised in **Figure 5.1D**. This analysis revealed that 36.3% of identified proteins had known lysosomal subcellular localisations. Although the percentage of proteins classified as lysosomal may seem low, this was an underestimate because only proteins that had a literature-evidenced subcellular localisation to the lysosome were classified as being lysosomal. For example, the protein guanine nucleotide-binding protein G(I)/G(S)/G(T) subunit beta-1 (gi|6680045; gene name:



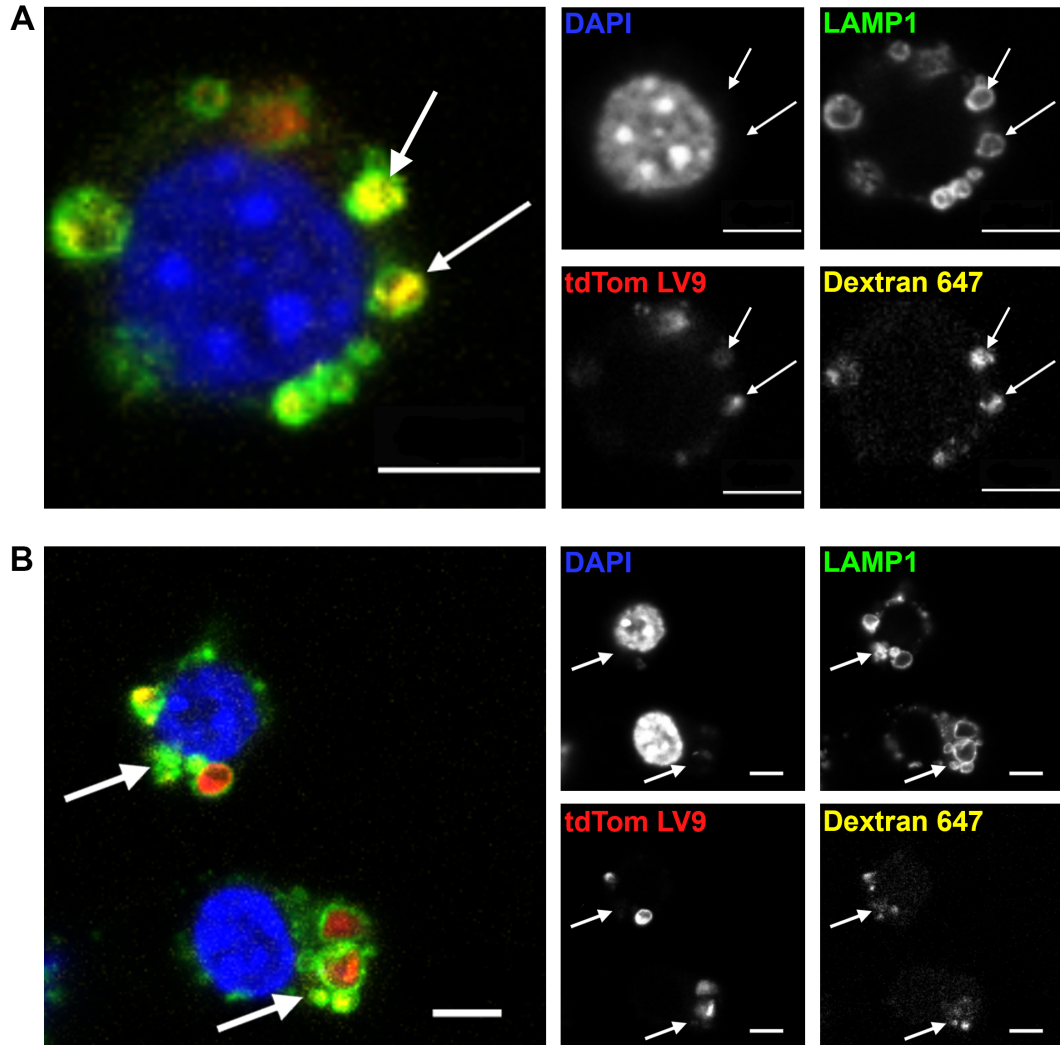
**FIGURE 5.1. Lysosomes can be isolated from J774.2 cells. A)** Summary of protocol used to isolate lysosomes from J774.2 cells. **B)**  $\beta$ -hexosaminidase activity in isolated post-nuclear supernatant (PNS), flow-through (FT) and eluted lysosomes (lyso). Data shown as mean  $\pm$  SEM from three independent experiments; \*  $p < 0.05$ . **C)** Western blot showing expression of LAMP1. Note that the lysosome fraction was loaded with 90% less total protein than other fractions. **D)** Subcellular location of proteins identified from LC-MS/MS analysis of isolated lysosome sample (proteins represented by any number of peptides).

Gnb1) was predicted on UniProt to be localised to the lysosome based on inference from sequence orthology. This was supported by the prominent identification of this protein in other lysosomal proteomic datasets (Nylandsted et al. 2011). However, this localisation has not yet been checked using non-proteomic methods of analysis and this protein was therefore categorised as “other/unknown”.

### **5.3.2 Isolating parasite-containing compartments from infected cells**

Success in isolating lysosomal compartments from J774.2 cells suggested that FeDex might also have been useful to isolate intracellular parasite-containing compartments from infected cells. As shown in **Figure 5.2**, *L. donovani* reached the same compartment as fluorescent dextran (10,000 MW). Thus, one method to isolate the parasite-containing compartment would be to pre-fill lysosomal compartments with FeDex and infect with parasites, collecting the lysosomal compartments as detailed previously. Others have shown that *Mycobacterium tuberculosis* mutants that were unable to arrest phagosome maturation could progress to these FeDex-filled lysosomes and could then be successfully isolated (Pethe et al. 2004).

However, the requirements for the study by Pethe et al (2004) were different to the study presented in this chapter; most notably, they did not require large numbers of pathogen-containing compartments to be isolated. In addition, as they were only interested in analysing the pathogen, they were able to isolate compartments that did not contain a pathogen without it affecting their desired results. Here, large numbers of purified parasite-containing compartments were needed and **Figure 5.2** helps highlight the problem with using this same technique. With an average of only one parasite per J774.2 cell, this method would isolate lysosomal compartments that were predominately free from parasites. This would dramatically interfere with the proteomic analyses of the parasite-containing compartment; it would therefore be advantageous to isolate only compartments with parasites in them.

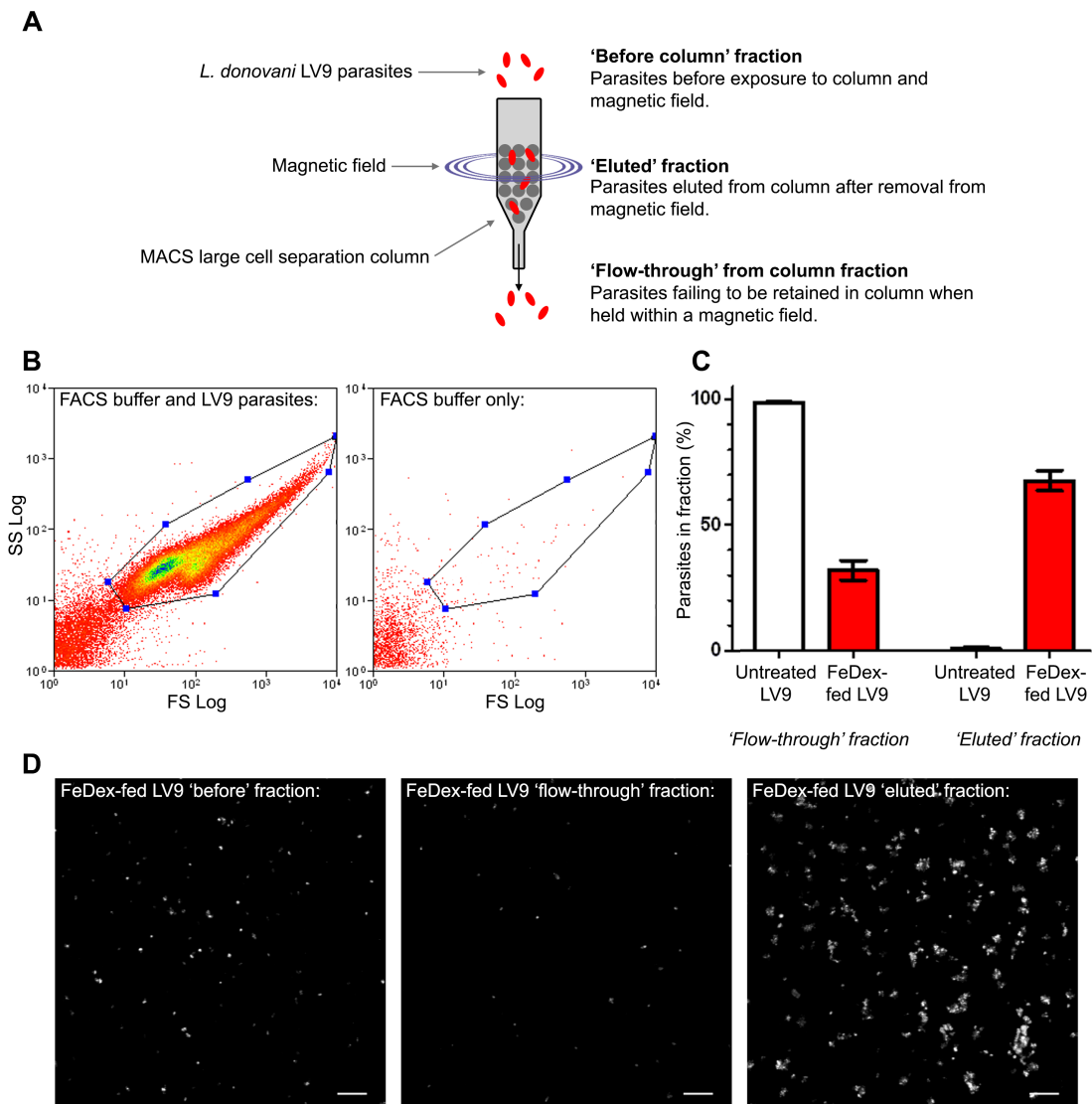


**FIGURE 5.2. Not all dextran-filled compartments contain *L. donovani* parasites.** J774.2 cells were pulse chased with 10,000MW fluorescent dextran (Alexa Fluor 647) and then infected with tdTomato *L. donovani* LV9 amastigotes for 4 hr. Two example images taken with a confocal microscope using the 63x oil immersion objective lens are shown. **A)** Arrows highlight a LAMP1-positive intracellular compartment that contains both fluorescent dextran and a parasite. **B)** Arrows highlight a LAMP1-positive compartment that contains fluorescent dextran but not a parasite. Figures show representative images from a single confocal section from a z-stack. Scale bars = 5µm.

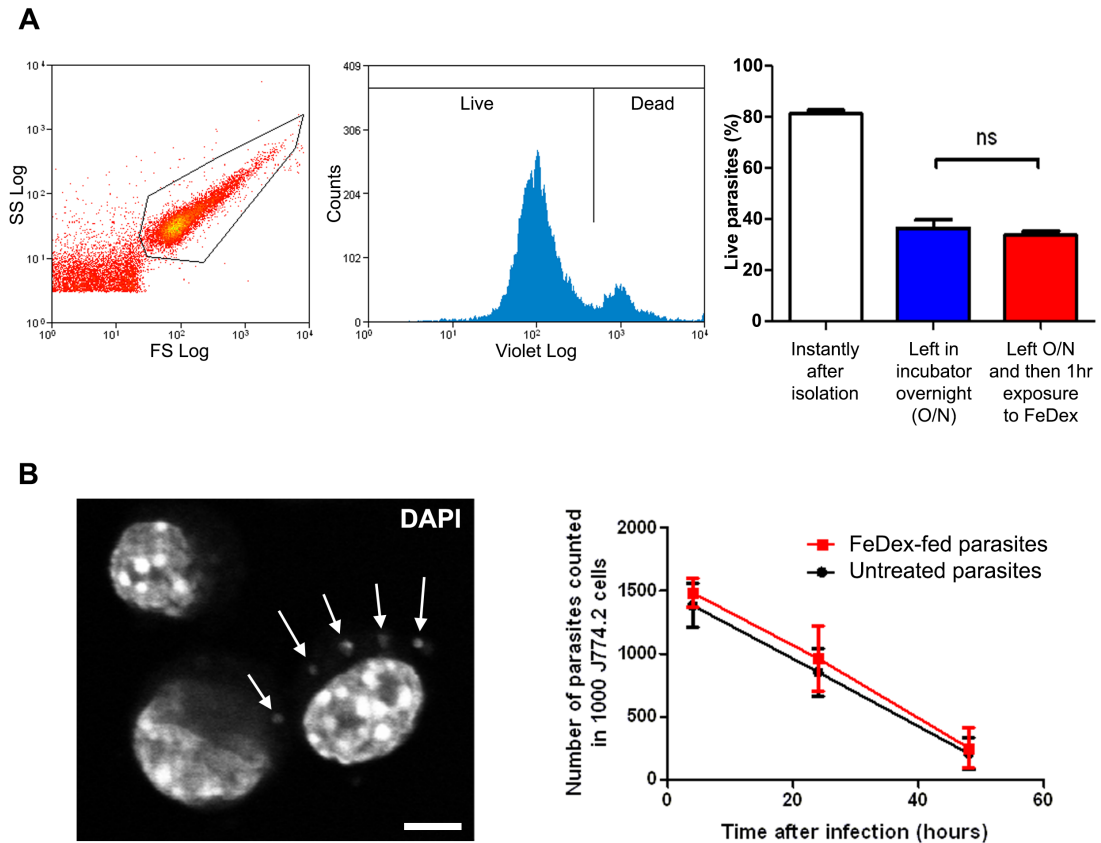
### 5.3.2.1 Making magnetisable *Leishmania* parasites

To isolate only parasite-containing compartments, parasites were made magnetisable by feeding with FeDex as detailed in Section 5.2.5. To determine whether these parasites could be subsequently retained within a magnetic field, both control (untreated) and FeDex-fed parasites were passed through a column suspended within a magnetic field. Three samples were collected: the fraction before being passed through the column (“Before column” fraction), the flow-through from the column (“Flow-through” fraction), and the fraction eluted from the column after removal from the magnetic field (“Eluted” fraction), as summarised in **Figure 5.3A**. The relative number of parasites present in either the flow-through or eluted fractions was then determined by analysing samples on a flow cytometer using gating on forward and side scatter histograms to identify parasites (**Figure 5.3B**). This demonstrated that approximately 70% of parasites can be held within the magnetic field (**Figure 5.3C**) and correlated well to confocal imaging of each of the fractions (**Figure 5.3D**). Encouragingly, the same percentage were retained when FeDex-fed parasites were left in an incubator for 4 hr and then passed through a magnetic field, suggesting that parasites can retain their magnetisable ability.

The potentially detrimental effect that FeDex has on the parasite’s normal physiological functioning was tested using a live/dead assay on *L. donovani* parasites present at different stages of the protocol. Although SPIONs are used clinically (Lin et al. 2008), others have suggested that SPIONs could have toxic effects on cells including membrane leakage, mitochondrial dysfunction and DNA damage (Singh et al. 2010). As shown in the bar graph in **Figure 5.4A**, exposure to FeDex did not result in a statistically significant difference in the percentage of live parasites. Furthermore, a time-course analysis up to 48 hr post-infection demonstrated that there was no statistically significant difference for the early uptake (4 hr post-infection) or longer-term survivability of FeDex-fed parasites compared to wild-type media control parasites in J774.2 cells (**Figure 5.4B**). FeDex-fed amastigote parasites were also able to transform into the promastigote form when cultured in appropriate media (method detailed in Section 2.4.6; data not



**FIGURE 5.3. Magnetisable *L. donovani* parasites can be retained within a magnetic field.** **A)** Diagram illustrating the setup of the column held within a magnetic field, with the corresponding fractions collected for analysis. **B)** Flow cytometry gating of parasites collected in fractions. **C)** The relative number of parasites collected in each fraction for untreated or FeDex-fed parasites; data shown as mean  $\pm$  SEM from 6 individual experiments. **D)** The presence of CFSE-labelled *L. donovani* parasites in equivalent volumes of each fraction visualised using confocal microscopy. Scale bar = 20 $\mu$ m.



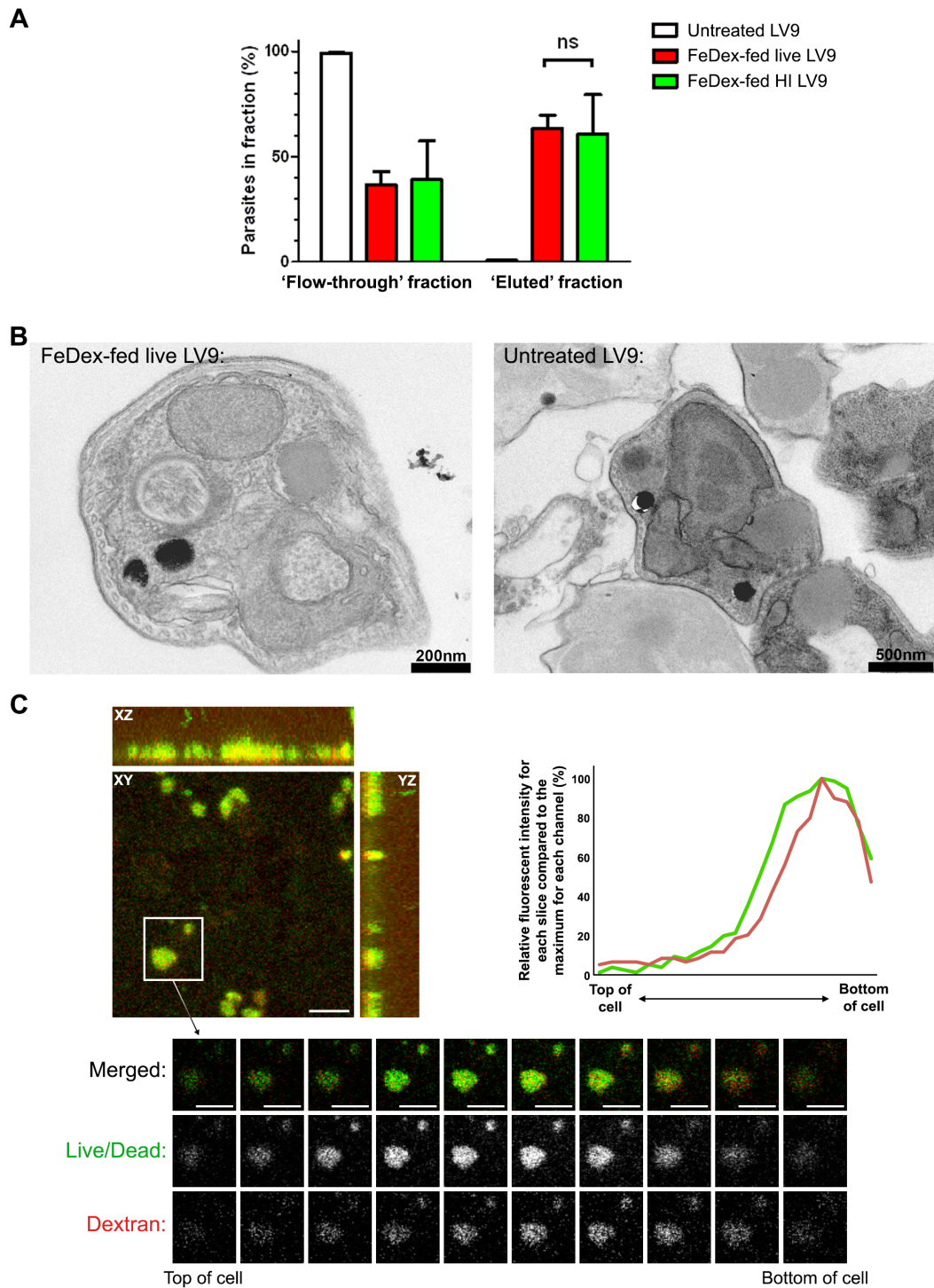
**FIGURE 5.4. Parasites survive exposure to FeDex and have unaltered infection uptake and intracellular survival. A)** Parasites were gated on a flow cytometer and their viability determined using a Live/Dead Fixable Dead Cell Stain Kit at different stages of the protocol. Graph shows mean  $\pm$  SEM from 3 independent experiments. **B)** *L. donovani* parasites were either FeDex-fed for 1hr or left untreated before being used to infect J774.2 cells. The infection was allowed to progress and parasite numbers were counted at 4hr, 24hr and 48hr post-infection by counting the number of parasite nuclei present in random fields of view until 1000 host cell nuclei had been counted. The micrograph is a representative image taken using a fluorescent microscope with a 100x oil immersion lens after DAPI-staining of cells, with arrows indicating the presence of parasites within J774.2 cells. Data on graph shown as mean  $\pm$  SD from 3 independent experiments.



shown). Together, these results suggested that the parasites were unaffected by FeDex treatment.

Although the data presented above suggest that parasites were able to associate with FeDex and that they remained infective, it was unclear whether parasites actively endocytosed FeDex or if instead FeDex was binding to the outer surface of the parasite. To this end, parasites were HI at 56°C for 30 mins and then processed to make magnetisable following the same protocol as previously described: exposure to FeDex for 1 hr and washed several times. There was no significant difference in the ability of these HI parasites to be subsequently retained within a magnetic field when compared with live FeDex-fed parasites (**Figure 5.5A**). This suggested that the uptake of FeDex was not an active process such as endocytosis. To attempt to visualise this, electron microscopy was performed on FeDex-fed parasites with the aim of locating electron-dense iron particles. Particular attention was paid to the outer surface of parasites to determine if FeDex was binding to the surface and to the flagellar pocket, as this is the only site for endocytosis in *Leishmania* amastigotes (Russell et al. 1992). Unfortunately, this analysis failed to identify observable differences between untreated and FeDex-fed parasites (**Figure 5.5B**); however, due to extensive wash steps involved in the processing protocol for TEM, any bound FeDex may have been washed off before it could be visualised.

To further clarify this, *L. donovani* parasites were exposed to fluorescent dextran (10,000MW) at the same concentration as used during FeDex-exposure. These parasites were then washed several times and left to settle on poly-D-lysine treated coverslips before being fixed and washed several times more. As shown in **Figure 5.5C**, these parasites were fluorescently labelled and the fluorescent signal was higher on the side of the parasite that was in direct contact with the poly-D-lysine coverslip. The most likely explanation for this was that the fluorescent dextran bound to the outer surface of the parasite and was subsequently washed off of the exposed side of the parasite to a certain extent, whereas the side in contact with coverslip was more protected from washing.



**FIGURE 5.5. FeDex likely binds to the outer surface of *L. donovani* amastigote parasites.** **A)** Live or heat-inactivated (HI) parasites were fed FeDex for 1 hr, or left untreated. The relative number of parasites collected in each fraction was counted using a flow cytometer with appropriate gating; data shown as mean  $\pm$  SEM from 3 individual experiments. **B)** Transmission electron microscopy images of unstained samples containing either FeDex-fed parasites (left) or untreated parasites (right). **C)** Parasites were incubated with 10,000MW fluorescent dextran (Alexa Fluor 647) for 1 hr and then washed several times. A Live/Dead Fixable Dead Cell Stain Kit was also used. Green = Live/Dead stain; red = fluorescent dextran; yellow = overlap. Individual images taken from a representative z-stack confocal image. Scale bar = 5  $\mu$ m.

In summary, we have shown that we can make magnetisable *L. donovani* parasites that can be retained within a magnetic field and were readily able to infect J774.2 cells with similar infection rates to control untreated parasites, and that this FeDex was likely to bind to the outside surface of the parasite.

### **5.3.2.2 Optimising the isolation of *L. donovani*-containing compartments**

The protocol already developed for isolating lysosomes was used as a foundation on which to isolate *L. donovani*-containing intracellular compartments. To comply with local safety rules for the safe handling of category 3 organisms, *L. donovani* parasites needed to be killed before being removed from the category 3 containment laboratories. Detergent-free methods of killing parasites were tested to ensure that phagosome membranes were not damaged and the efficacy of each treatment was judged by the ability of the parasites to subsequently transform into the promastigote form when cultured in appropriate medium (detailed in Section 2.4.6) at 26°C. As shown in **Table 5.1**, the most reliable method for killing parasites was to HI them at 56°C for 30 mins. Encouragingly, others have used this method previously to inactivate the parasite (e.g. Channon et al. 1984). Therefore, parasites were HI after eluting from a column so that samples could be centrifuged using the ultracentrifuge in a category 2 laboratory. To allow for spinoculation of the parasites onto cells, J774.2 cells were seeded onto 6-well plates rather than 10cm dishes. It was calculated that four 6-well plates would be of approximate equivalence to the four 10cm dishes used in the lysosome isolation protocol.

Having made these changes to the protocol, the first attempts to isolate parasite-containing compartments resulted in no pellets being produced at the ultracentrifugation stage of the protocol. This suggested that the amount of material being retained within the magnetic field was low. One potential reason for this was that the number of compartments with parasites in them was drastically lower in number than the number of lysosomes in a cell. The number of 6-well plates used was therefore increased to 6 plates per condition and the material produced from 2 separate experiments was pooled. This produced visible pellets and after qualitative LC-MS/MS

**TABLE 5.1. The only treatment found to fully inhibit the ability of amastigote *L. donovani* parasites to transform into promastigotes was heat inactivation at 56°C for 30 minutes.** Amastigote parasites were exposed to a number of different conditions: incubation in 5% FeDex-containing media for 1 hr, cell lysis using a N<sub>2</sub> cell cavitation device, increasing concentrations of sodium azide (NaN<sub>3</sub>; 0.1-5%), or heat inactivation (HI) at 56°C for 30 mins. The presence of promastigotes was checked at 3 and 6 days post-treatment using a light microscope.

<b>Treatment</b>	<b>Promastigotes present at day 3</b>	<b>Promastigotes present at day 6</b>
<b>Untreated</b>	Yes	Yes
<b>5% FeDex (1 hour)</b>	Yes	Yes
<b>N<sub>2</sub> cell cavitation device</b>	Yes	Yes
<b>0.1% NaN<sub>3</sub></b>	Yes	Yes
<b>1% NaN<sub>3</sub></b>	<b>No</b>	Yes
<b>5% NaN<sub>3</sub></b>	<b>No</b>	Yes
<b>HI at 56°C for 30 mins</b>	<b>No</b>	<b>No</b>

proteomic analysis, the dataset returned for this analysis (named 'Preliminary proteomics round A') identified 273 unique proteins across the live- and HI-parasite fed samples (hereon in referred to as 'live' and 'HI' preparations), as shown in **Figure 5.6**. This was lower than expected and significantly less than the 965 proteins identified in the lysosome preparation. Furthermore, several key proteins that are well established to be constitutive on the parasite-containing compartment, such as LAMP1, were absent and the only cathepsin present was cathepsin Z.

As a result, two changes were made to the protocol to increase the number of membrane-specific protein hits. Firstly, membrane preparations, rather than preparations consisting of the entire intraphagosomal contents, were made. This was done by using the combined material from three separate experiments, which were re-suspended in 3mL of ddH<sub>2</sub>O before being centrifuged at 596,000 x *g* for 15 mins. Centrifugation was repeated three times and samples were finally re-suspended in 100µL of ddH<sub>2</sub>O. Secondly, a deglycosylation step was added to the mass spectrometry processing to increase protein digest efficiency and therefore protein identifications for lysosomal proteins that are often highly glycosylated such as LAMP1 and LAMP2 (Kundra & Kornfeld 1999). Unfortunately, after making these changes the proteomic dataset returned (named 'Preliminary proteomics round B') contained a low number of identifications with peptide sequences for only 150 unique mouse proteins across the live and HI preparations, as shown in **Figure 5.6**. Furthermore, there was again a noticeable absence of LAMP1 within the dataset, even though the presence of this protein had been confirmed for these samples experimentally using western blotting (data not shown). The 10µg of protein for each sample should have been enough; over 2000 proteins are routinely identified from a 100ng lysed HeLa cell sample using the same experimental setup (Adam Dowle, University of York; informal communication). It was later discovered that the combination of deglycosylating samples in an iTRAQ-compatible buffer (triethylammonium bicarbonate; TEAB) had led to significantly reduced digestion yields.

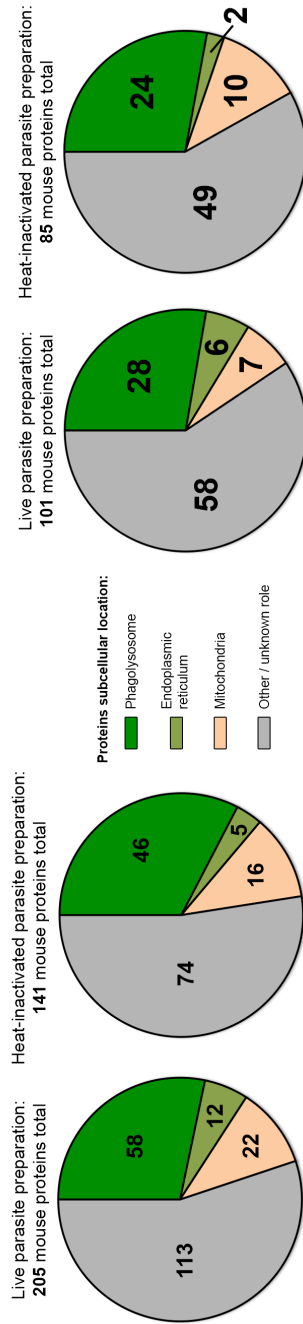
### Preliminary proteomics round A

Whole compartment proteomics with sample produced from  $1.32 \times 10^8$  J774.2 cells for each preparation (live or heat-inactivated). No deglycosylation step during mass spectrometry processing.

### Preliminary proteomics round B

Membrane proteomics with sample produced from  $2.88 \times 10^8$  J774.2 cells for each preparation (live or heat-inactivated). Deglycosylation step during mass spectrometry processing.

#### i) Subcellular location of mouse proteins identified:-

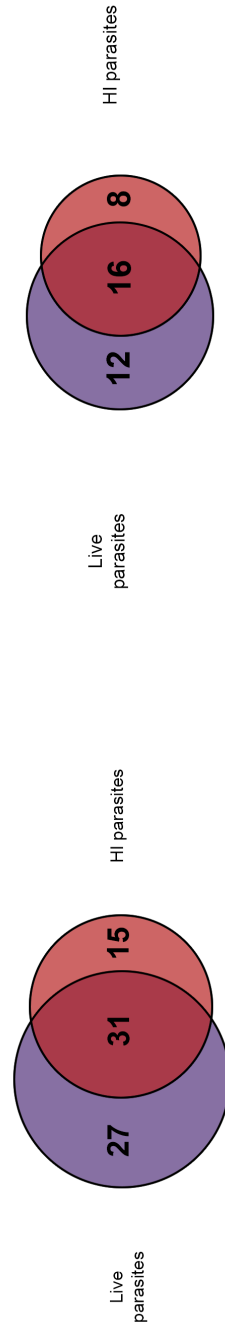


**FIGURE 5.6. Analysis of mouse proteins identified from each sample preparation for preliminary rounds of unlabelled LC-MS/MS.** Analyses include proteins identified by any number of peptide sequences. The subcellular location was identified for each protein by conducting a literature search (i) and the overall of distribution of proteins found between the heat-inactivated (HI) and live parasite-fed preparations determined (ii and iii).

#### ii) Overlap of proteins between the live and heat-inactivated preparations:-



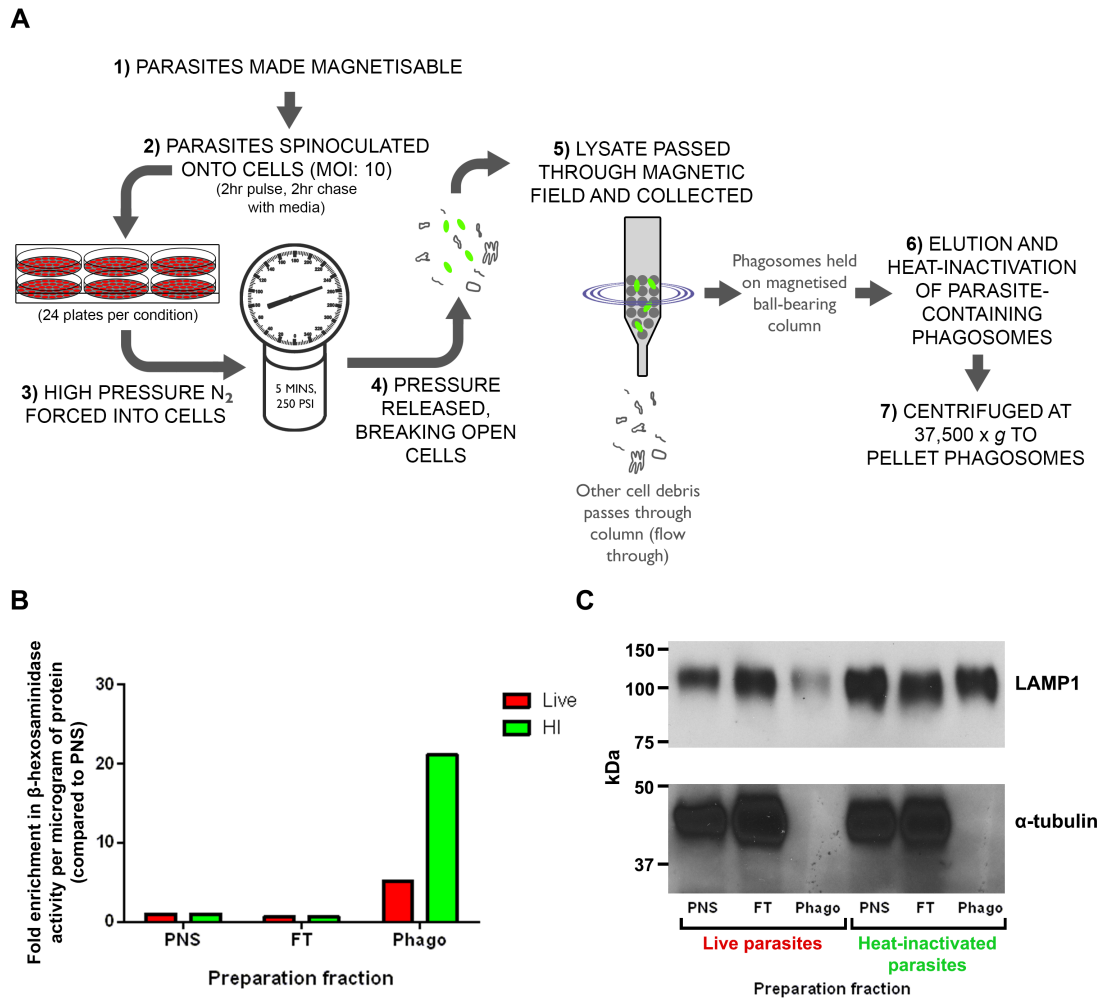
#### iii) Phagolysosomal proteins identified in each preparation:-



Thus, new membrane preparations were made and processed for mass spectrometry using the new buffer conditions detailed in Section 2.12.1. Each new final sample preparation was produced by combining material obtained from eight separate experiments using the protocol detailed in Section 5.2.5, as detailed in **Figure 5.7A**. Isolated parasite-containing compartments were assayed for lysosomal  $\beta$ -hexosaminidase activity (**Figure 5.7B**), which showed that enzymatic activity was enriched in phagolysosomal fractions for both live and HI samples. In addition, purification of LAMP1-positive compartments was confirmed by western blotting (**Figure 5.7C**), showing greatly enhanced levels compared to  $\alpha$ -tubulin. Interestingly, there was a reproducible trend for the live preparations to have less LAMP1 protein and lower  $\beta$ -hexosaminidase activity compared to HI preparations. When t-tests were performed to compare the  $\beta$ -hexosaminidase activity for lysosomes to the values for phagosomes from HI preparations, there was no significant difference between the two compartments suggesting that this may be a similar compartment being isolated. However, when the lysosome data were compared to phagosomes from live parasite-fed cells, there was a dramatic reduction in the enrichment of  $\beta$ -hexosaminidase activity in live phagosome preparations.

The qualitative proteomics data received back from these samples (named 'Preliminary proteomics round C') had many more protein identifications (1391 total mouse protein identifications) as shown in **Figure 5.8**. Of these proteins, 31.9% (live preparation) and 32.7% (HI preparation) have evidence in the literature demonstrating a known co-localisation with either endocytic organelles or phagosomes, which is comparable to the figure seen in isolated lysosomal compartments in Section 5.3.1. Importantly, proteins that have been well established as being present within the *L. donovani*-containing intracellular compartment, such as LAMP1 and cathepsins B, D, H and L (Lang et al. 1994), were all found within the samples.

Taken together, we have now defined the conditions needed experimentally and for mass spectrometry processing to successfully isolate and process phagosomal material from *L. donovani*-infected J774.2 cells.



**FIGURE 5.7. Alteration of the lysosome isolation technique can be used to isolate the parasite-containing compartment. A)** Summary of protocol used to isolate parasite-containing compartments from infected J774.2 cells. **B)**  $\beta$ -hexosaminidase activity in isolated post-nuclear supernatant (PNS), flow-through (FT) and eluted phagolysosomes (phago). Data shown as mean from two independent experiments. **C)** Western blotting for LAMP1 and  $\alpha$ -tubulin within each fraction.



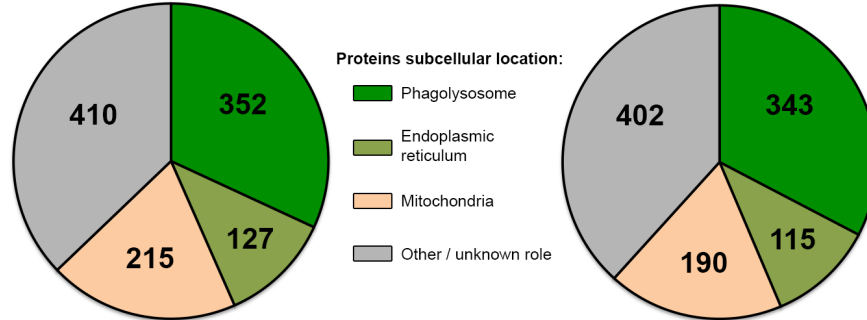
## Preliminary proteomics round C

Membrane proteomics with sample produced from  $2.3 \times 10^9$  J774.2 cells for each preparation (live or heat-inactivated). Deglycosylation step during mass spectrometry processing.

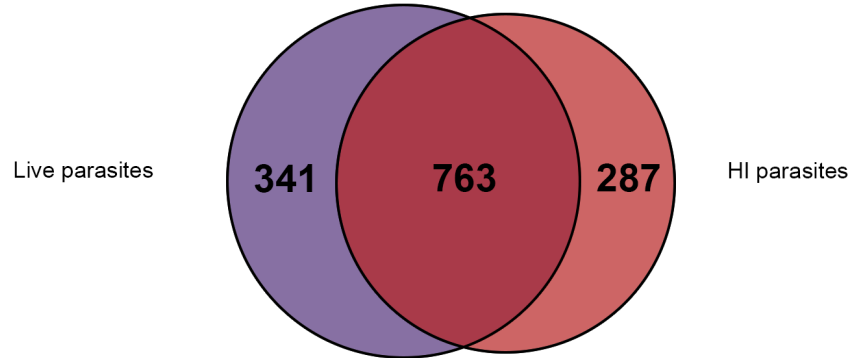
### i) Subcellular location of mouse proteins identified:-

Live parasite preparation:  
1104 mouse proteins total

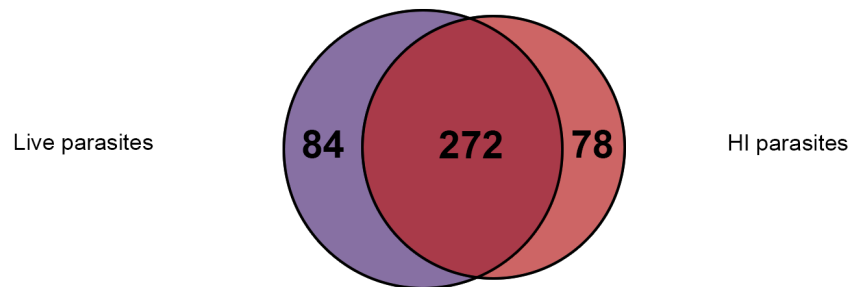
Heat-inactivated parasite preparation:  
1050 mouse proteins total



### ii) Overlap of proteins between the two preparations:-



### iii) Phagolysosomal proteins identified in each preparation:-



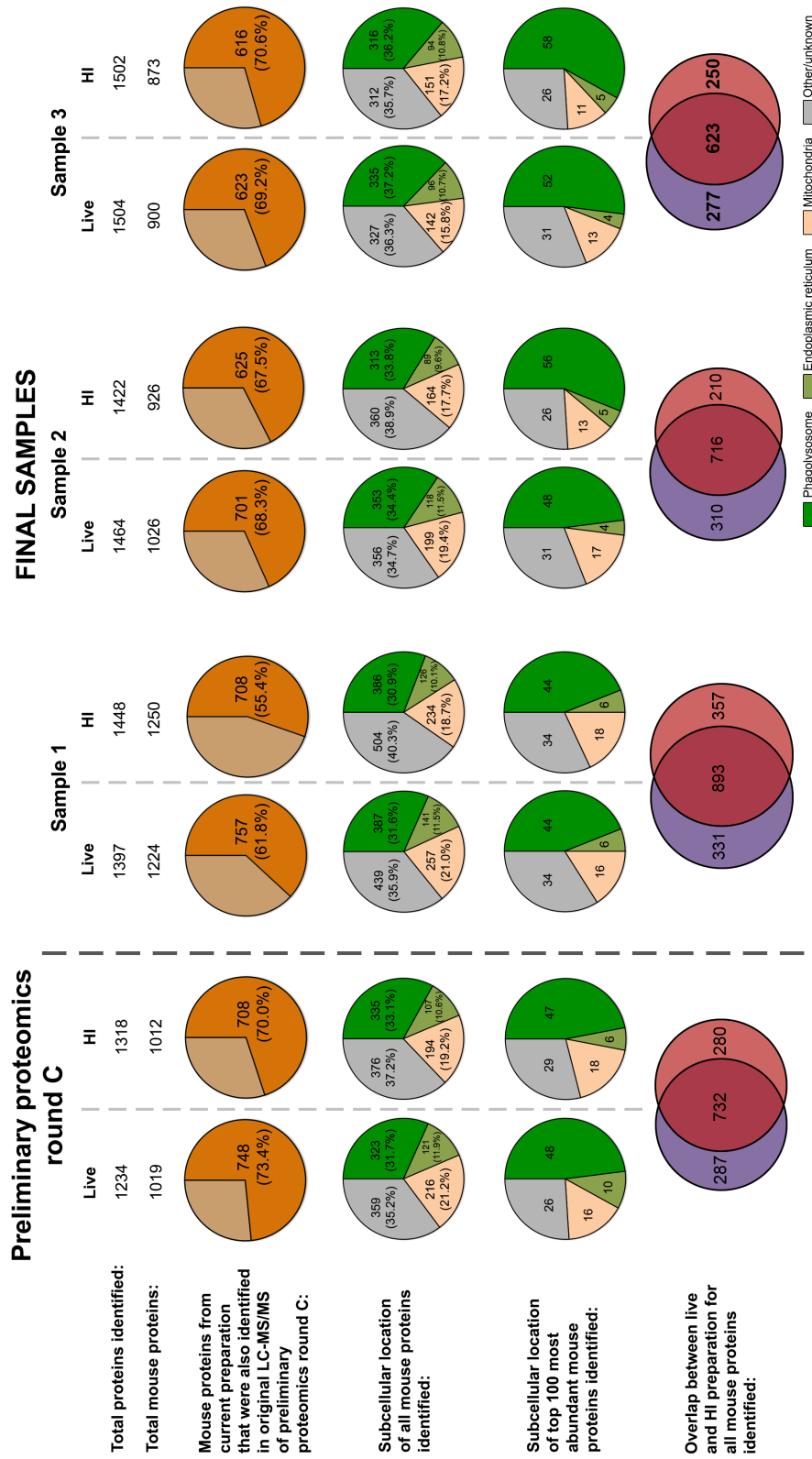
**FIGURE 5.8.** The total mouse proteins identified from each sample preparation (either using live or heat-inactivated parasites) for preliminary proteomics round C. Unlabelled LC-MS/MS, based on absolute protein numbers. Analyses include proteins identified by any number of peptide sequences. The subcellular location was identified for each protein by conducting a literature search (i) and the overall distribution of proteins found between the heat-inactivated (HI) and live parasite-fed preparations determined (ii and iii).

### 5.3.2.3 Qualitative proteomic characterisation of isolated parasite-containing compartments

The aim of this study was to compare, both qualitatively and quantitatively, the proteomic composition of phagosomal compartments obtained from cells fed either live or HI parasites. The preparation of samples was dictated by the more stringent requirements of quantitative MS, which is more technically demanding both in the quantity of material needed and the processing of samples compared to qualitative studies. It is well established that label-based methods of quantification increase the complexity of experimental methods, are more expensive, and require increased amounts of starting sample material (Bantscheff et al. 2007). More specifically, this meant that 100µg of material was needed per sample rather than the 1-10µg required for qualitative proteomics. Furthermore, the reagents used for quantitative proteomics allowed for up to 8 individual samples to be pooled and processed together. Thus, to fully utilise all available tracks, four live samples and four HI samples were made using the protocol detailed in Section 5.2.5.

Before moving on to labelled quantitative proteomics, all samples were first analysed using qualitative LC-MS/MS with the results summarised in **Figure 5.9**. This allowed for preliminary analyses of the samples before progressing to the more expensive labelled LC-MS/MS. Encouragingly, a mean of 1029 mouse proteins were detected in each sample (range: 873 – 1250 proteins). When the samples were taken together, there was a mean of 33.6% of proteins that had an evidence-based co-localisation to the phagolysosome. This percentage increased further still to a mean of 49.6% when the top 100 most abundant proteins identified (based on spectral count values) had their subcellular location classified.

The preliminary proteomics sample C that was produced in Section 5.3.2.2 above served as a useful comparison for the other three samples collected. Interestingly, when this sample was re-analysed by LC-MS/MS, 27.6% and 30.0% of proteins identified for the live and HI preparations, respectively, were not identified in the first LC-MS/MS run performed on this sample. This difference in datasets for the same sample is something that has been well

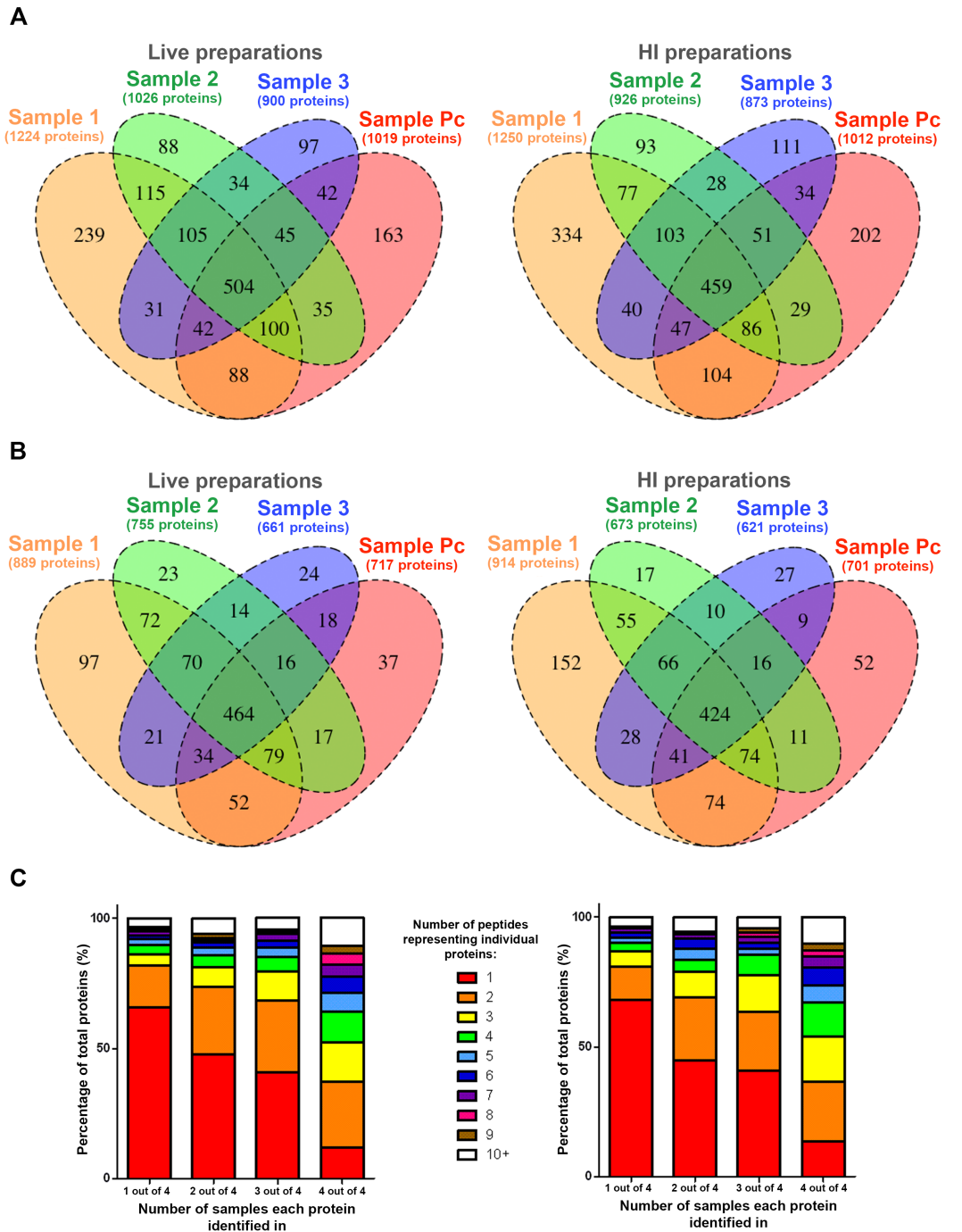


**FIGURE 5.9. Summary of proteins identified from four samples made using the final parasite-containing compartment isolation protocol.** Each sample has two separate preparations: a live and heat-inactivated (HI) preparation, made by feeding J774.2 cells live or HI *L. donovani* amastigote parasites, respectively. Unlabelled LC-MS/MS, based on absolute protein numbers. Most abundant mouse proteins calculated using EmpAI value.

reported (as discussed by Aebersold 2009), but due to the stochastic nature of peptide sampling is hard to eliminate without sampling each preparation multiple times with the associated significant investment in time and material.

Although unique proteins were identified in all of the samples, there was a common pool of 504 proteins or 459 proteins found in all four live or HI preparations, respectively, as shown in **Figure 5.10A**. This accounted for a mean of 49.0% (live) or 46.1% (HI) of all proteins identified for each sample; this increased to 62.2% (live) or 59.6% (HI) when only proteins represented by at least 2 peptides were included (**Figure 5.10B**). For proteins that were only found in one out of the four samples, 65.8% were represented by only 1 peptide (**Figure 5.10C**), which was in contrast to 12.1% for proteins that were found in all four samples. This illustrated that it was predominately low abundance proteins that were differentially identified in samples, suggesting that the compositions of the four samples for each preparation were broadly similar.

To perform a preliminary quantitative analysis of the samples, the label-free relative quantification method of spectral counting was performed. This technique is based on the observation that the tandem MS spectra for peptides of a particular protein correlate with its abundance (Bantscheff et al. 2007). In addition to providing preliminary analyses before going onto more expensive labelled techniques, it was a useful method to utilise to obtain very crude estimates for low abundance proteins that would not be picked up by iTRAQ-labelled proteomics (Li et al. 2012; Megger et al. 2014). As an early comparative analysis, proteins were analysed to determine which were found in all four live samples but either completely absent or only in one out of four of the HI samples, with only proteins represented by at least two peptides included in the analysis. As shown in **Table 5.2**, there was one solitary protein found in all live preparations but completely absent from all HI preparations (type II peroxiredoxin 1; gi|3603241). This protein was of potential interest because the *Leishmania* equivalent has been shown to be important in attenuating nitric oxide-mediated destruction of intracellular parasites by macrophages (Harder et al. 2006). The murine peptide



**FIGURE 5.10.** The majority of mouse proteins were found in all 4 samples for both live and heat-inactivated preparations, and those that were not were predominately low abundance proteins represented by a low number of peptide identifications. The overlap between mouse proteins identified in parasite-containing samples 1 to 3 and preliminary proteomics round C (“Sample Pc”) from cells fed either live (left) or heat-inactivated (right) parasites for proteins represented by either any number of peptides (**A**) or at least 2 peptides (**B**) was calculated. **C**) Graphs show the percentage of proteins that were represented by different numbers of peptide sequence identifications (1 peptide - 10+ peptides). Single run of LC MS/MS performed on each sample.

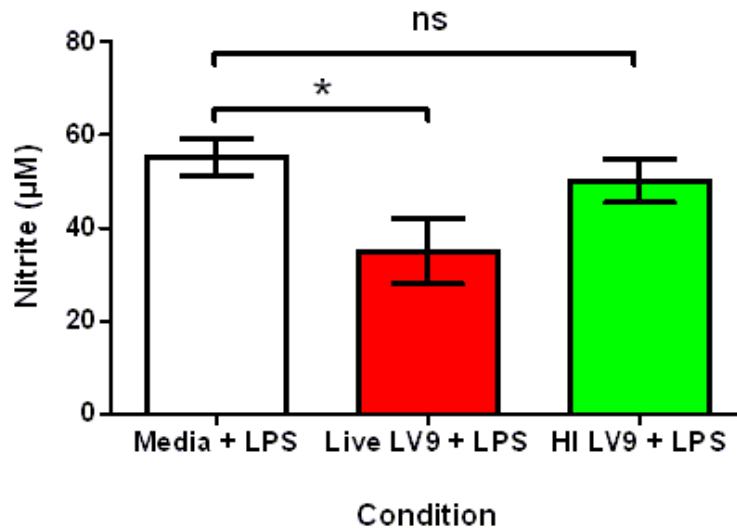
**TABLE 5.2. Proteins identified in all 4 live samples that were either entirely absent from heat-inactivated samples or only present in one sample.** Proteins represented by  $\geq 2$  peptides were included. Data on location and function were summarised from UniProt. HI1-3 and L1-3 refers to heat-inactivated parasite-fed proteomic preparations 1-3 and live parasite-fed proteomic preparations 1-3, respectively. HPC and LPC refers to preliminary proteomics round C, heat-inactivated and live preparations, respectively.

PROTEIN	Heat inactivated samples spectra				Live samples spectra			Total spectra	Location	Broad function	
	H1	H2	H3	HPC	L1	L2	L3				LPC
<b>ABSENT IN ALL 4 HI SAMPLES:</b>											
Type II peroxiredoxin 1 - gj 3603241					1	1	1	1	4	Cytoplasm, mitochondria	Anti-oxidant
<b>ABSENT IN 3 HI SAMPLES</b>											
V-type proton ATPase subunit A - gj 14919420	37				34	42	37	23	173	Lysosome	Vacuolar acidification mRNA processing/transcription regulation
p68 RNA helicase - gj 51263				6	11	11	8	5	41	Nucleus	Trafficking
Rab8b - gj 23463313		9			10	8	11	2	40	PM, phagosome, endosome	Trafficking
Phosphoglycerate kinase - gj 202423				6	3	2	3	3	17	Cytoplasm	ATP-/nucleotide-binding
Putative uncharacterised protein (gene: Sept7) - gj 26354124	3				3	3	3	4	16	Actin, PM, nucleus, cytoplasm	GTP-binding Aerobic respiration, electron transport chain
Pmpcb - gj 74151629	2				3	1	1	2	9	Mitochondria	
Probable phospholipid-transporting ATPase IH (Atp11a) - gj 7656914	1				2	1	1	2	7	Early endosome/recycling endosomes	Phospholipid translocation
Actin cross-linking family 7 (ACF7 neural isoform 1) - gj 1675222				1	1	1	1	2	6	Actin cytoskeleton, cytoplasm, membrane	Actin-binding/protein localisation
Endophilin-B1 isoform 2 - gj 9507097	1				2	1	1	1	6	Early endosome, cytoplasm, ER, Golgi, membrane, mito	Apoptosis/trafficking/membrane fusion/lipid-binding
Nucleoporin SEH1 isoform b - gj 20532338		1			1	1	1	1	5	Nucleus, GATOR2 complex	Cell cycle/cell division

sequence identified in this proteomic dataset was checked for homology to this *Leishmania* protein and it was found to be unique to the mouse. Experimentally, when J774.2 cells were infected with live *L. donovani* amastigotes for 4 hr and then LPS-stimulated, there was a reduction in nitrite production compared to cells infected with HI parasites (**Figure 5.11**), a finding that has been found by others (Channon et al. 1984). This may be due to parasite manipulation of the nitric oxide synthase enzyme (Perrella Balestieri et al. 2002) but the evidence provided here suggests that other mouse anti-oxidants, such as type II peroxiredoxin 1, may be contributing to this attenuation.

When proteins that were present in all live samples but only one out of four of the HI samples were analysed, there were a number of differentially represented proteins, for example: actin-binding proteins such as Sept7 (gi|26354124) and actin cross-linking family 7 (gi|1675222), along with several proteins that can be found in the pre-lysosomal endocytic pathway such as Atp11a (gi|7656914), endophilin-B1 isoform 2 (gi|9507097) and Rab8b (gi|23463313). Unexpectedly, one subunit of vATPase (subunit A; gi|14919420) was also found in only one of the HI samples; however, in this one sample it was present in relatively high abundance.

There were no proteins found in all HI samples while being completely absent from the live samples, as shown in **Table 5.3**. This was likely due to the live preparations also containing dead parasites in them as detailed in Section 5.3.2.1 above, further highlighting the importance of progressing on to quantitatively characterise the more subtle differences in protein composition between the two preparations. TGF- $\beta$  receptor II (gi|15430873), Ras-related GTP-binding protein A (gi|5729999) and integral membrane protein 2C (gi|7259292), all proteins with a role in cell death, were found in only one out of four of the live samples. This was of interest because others have shown infection with *Leishmania* parasites can inhibit macrophage apoptosis (Moore & Matlashewski 1994); the current data suggests that this effect was more pronounced for live rather than HI parasites, implying that it



**FIGURE 5.11. Live *Leishmania* parasites were able to attenuate nitric oxide production by J774.2 cells.** J774.2 cells were infected with either live or heat-inactivated (HI) *L. donovani* parasites (MOI: 10). After 4 hr, cells were washed several times and then exposed to complete DMEM supplemented with 1ug/mL LPS for a further 20 hr. Cells were then harvested and a Griess assay performed. Data shown as mean  $\pm$  SEM from one experiment performed in triplicate. \* p value < 0.05.



**TABLE 5.3. Proteins identified in all 4 heat-inactivated samples that were either entirely absent from live samples or only present in one sample.** Proteins represented by  $\geq 2$  peptides were included. Data on location and function were summarised from UniProt. H1-1-3 and L1-3 refers to heat-inactivated parasite-fed proteomic preparations 1-3 and live parasite-fed proteomic preparations 1-3, respectively. HPC and LPC refers to preliminary proteomics round C, heat-inactivated and live preparations, respectively.

PROTEIN	Heat inactivated samples spectra				Live samples spectra			Total spectra	Location	Broad function
	H1	H2	H3	HPC	L1	L2	L3			
<b>ABSENT IN ALL 4 LIVE SAMPLES:</b>										
None										
<b>ABSENT IN 3 LIVE SAMPLES</b>										
TGF-beta receptor II - gj 15430873	2	3	4	1	3			13	Caveola, plasma membrane, membrane raft	Apoptosis, differentiation
Ras-related GTP-binding protein A - gj 5729999	1	1	2	1	1	1		6	Lysosome, cytoplasm, nucleus	Apoptosis, host-virus interaction
SEC63-like - gj 18043928	1	1	1	1	1	1		5	ER	Protein transport
Integral membrane protein 2C (ltm2c) - gj 7259292	1	1	1	1	1			5	Lysosome, plasma membrane	May play a role in TNF-induced cell death

may be the result of active manipulation of the parasite-containing compartment rather than the mere presence of parasites.

## 5.4 Chapter-specific discussion

A novel protocol has been developed to make magnetisable parasites that can be successfully used to isolate *Leishmania*-containing phagolysosomal compartments from infected J774.2 cells. Using this powerful technique, *Leishmania*-containing compartments were then sent for qualitative proteomic analyses to determine the protein composition of the phagolysosome. By doing this, we have characterised the *L. donovani*-containing compartment in high resolution giving new insights into its composition. Furthermore, spectral counting has revealed a number of biologically relevant proteins that may be differentially expressed in live and HI parasite-containing compartments.

One reason for isolating *Leishmania*-containing intracellular compartments was the observation that *L. donovani*-infected cells had lower cell surface expression of CCR5 (see Chapter 3). It was therefore conceivable that the receptor may have been internalised with the parasite to form part of the parasite-containing compartment. In the proteomic datasets collected, CCR5 did not appear in any of the preparations and there was a general lack of any chemokine receptor and their associated G protein-related machinery. The absence of CCR5 could be due to: i) the receptor being degraded in the phagolysosome or pre-phagolysosomal compartment before analysis; ii) the receptor dissociating from the parasite-containing compartment prior to the phagolysosomal stage; iii) the receptor not being part of the *Leishmania*-containing compartment at any stage of parasite phagocytosis. Having a murine anti-CCR5 antibody that can be used for either western blotting or intracellular immunofluorescence could help to determine which of these options is correct.

Using the Rofe and Pryor (2015) method for isolating lysosomes, a lysosomal sample has been generated and sent for mass spectrometry analysis. Although FeDex has previously been used to isolate lysosomes from cells (Rodriguez-Paris et al. 1993; Diettrich et al. 1998), these early

studies were not able to subsequently perform proteomic analyses on these samples. Others have performed LC-MS/MS on isolated lysosomes using different methods of isolation (reviewed by Schröder et al. 2010); numbers of proteins identified from these studies have ranged from 109 proteins (Zhang et al. 2007) to over 1500 (Schröder et al. 2007). The lysosomal data presented here are an important addition to our understanding of the proteomic composition of the lysosome because different isolation methods introduce different methods of contamination, with slightly different proteins likely to be identified depending on the method used. Encouragingly, many of the main proteins listed in the review by Schröder et al. (2010) as being part of the lysosomal membrane were also identified here. Of note, only 36.3% of the proteins identified here were previously known to have an evidence-based localisation to the lysosome; this work therefore suggests that many more proteins not yet associated with the lysosome actually make up this compartment.

Although the process of using SPIONs to isolate lysosomes was not novel, this was the first time that SPIONs have been used to isolate parasite-containing compartments from cells. This required the technique to be adapted so that *L. donovani* amastigote parasites, rather than lysosomal compartments, were magnetisable. The resulting parasites do not have altered virulence characteristics nor reduced viability after exposure to FeDex. One disadvantage of this method of isolation was that there was no removal of the fraction of dying parasites contaminating the “live parasite” preparation as we wanted to keep manipulation of both parasites and cells to a minimum throughout the technique. As a result, the live parasite preparations had some dead parasites in them so any differences between live and HI preparations would be less apparent. This highlighted the importance of progressing to iTRAQ-labelling of samples so that the absolute quantity of proteins, rather than whether they are present or absent, can be compared making this less of a problem. Furthermore, although we had clear enrichment for phagolysosomal compartments as shown by increased lysosomal protein and enzymatic activity, the possibility of a small degree of contamination from other cellular debris cannot be excluded.

Early problems with the conditions used for processing samples for mass spectrometry analysis were overcome, allowing samples to be deglycosylated and processed for qualitative LC-MS/MS before later being buffer exchanged into an iTRAQ-compatible buffer. This allowed the novel isolation method developed to be coupled with high-throughput proteomics. With advancement in mass spectrometry sensitivity, increasing numbers of proteins can be identified; this is exemplified by only ~140 proteins being identified by Garin et al. in 2001 for phagosomal proteomics whereas Guo et al. (2015) identified more than 2500 proteins. To our knowledge, this is the first time that proteomic analyses have been performed on isolated *L. donovani*-containing intracellular compartments. In this study, each of the isolated phagosomal samples had approximately 1000 identified proteins in them with a common pool of either 504 or 459 proteins coming up repeatedly in all samples for live and HI parasite-containing compartments, respectively. Encouragingly, of the 140 proteins identified by Garin et al. (2001) for phagosomes, almost all were represented within these samples and greatly expanded upon. The differences seen were likely due to advancement in the sensitivity of mass spectrometry over the last 15 years but could also be due to using *Leishmania* parasites with their associated surface composition and morphology arguably providing a more physiologically relevant example of phagocytosis compared to latex beads (Li et al. 2010).

Although we have spectral count data for each protein in all of the samples, due to time constraints a more detailed analysis was not conducted to use these data to compare live and HI samples. This was because these samples would all be subsequently processed for iTRAQ-labelled quantitative LC-MS/MS. iTRAQ-labelled techniques are more accurate than spectral counting methods, particularly for lower molecular weight proteins and for measuring when equivalent amounts of a particular protein are in different samples (Schmidt et al. 2014). However, processing these samples for unlabelled LC-MS/MS was important to confirm that each had a similar composition and that there were no samples that were significantly different from the others before moving on to more expensive techniques. In addition, because labelling techniques, especially using iTRAQ 8-plex (Pichler et al.

2010), often reduce the number of peptide (and therefore overall protein) identifications, it was worthwhile comparing which proteins were completely represented by one condition (either live or HI parasites) while being absent from the other condition using unlabelled spectral counting. For live parasites, this revealed a number of actin- and phagolysosomal-associated proteins suggesting that the live parasites may be actively manipulating the actin cytoskeleton associated with the phagosome as well as phagolysosomal proteins directly. When this was done for proteins found in HI parasite preparations, the majority of proteins identified had a role in cell death. This was of interest because others have shown infection with *Leishmania* parasites can inhibit macrophage apoptosis (Moore & Matlashewski 1994); however, this provided the first evidence that this effect could be due to the live parasite actively manipulating its compartment by down-regulating or excluding these proteins.

The presence of proteins traditionally associated with other organelles within these phagosome samples is something that others have also observed in phagosome proteomics (Garin et al. 2001; Goyette et al. 2012; Guo et al. 2015). In particular, Goyette et al (2012) have noted that proteins related to the nucleus (such as histones), mitochondria and ribosomes were particularly well represented and it was these same protein groups that appear in our samples. They suggested that one potential explanation was that it could be due to contamination resulting from the flotation method of isolating latex beads (Goyette et al. 2012). However, since these same protein groups appeared in the samples from this study, which uses a completely different method of isolation, the probability that these are contaminants is lowered.

Alternatively, Goyette et al (2012) suggested that these other subcellular components could be explained by the lysosome's role as a degradative organelle meaning that proteins are continually being sorted to this compartment for degradation. This can be due to normal endocytosis where exogenous macromolecules can be endocytosed and reach the lysosomal compartment. It can also be due to autophagy. Autophagy, meaning 'eating of self' in Greek, is a cellular process for the degradation of cellular

constituents (Wang & Klionsky 2011). The term was first coined almost 50 years ago when it was noticed that mitochondria and other intracellular structures could be identified within lysosomes after glucagon challenge (Deter & De Duve 1967). Since then, it has been well established that autophagosomes target to lysosomes where their luminal contents, whether macromolecules or entire cellular components such as ribosomes and mitochondria, can be degraded either to recycle damaged organelles or to liberate amino acids during starvation conditions (Schröder et al. 2010). It was therefore not surprising that cellular components not traditionally associated with the lysosome were present within proteomic datasets derived from parasite-containing phagolysosomes. Although proteins transferred in this way should be luminal, and therefore removed during the membrane preparation process that was performed, incomplete breakage of some of the parasite-containing compartments cannot be excluded. Alternatively, during stress conditions the membranes from autophagosomes are partially derived from mitochondria (Hailey et al. 2010). This could account for some mitochondrial proteins being present on the parasite-containing compartment, although Hailey et al (2010) found that this transfer was predominately for lipids with the transfer of mitochondrial proteins being significantly lower. Furthermore, Goyette et al (2012) found that phagosomes isolated from cells with high autophagic activity levels had more proteins identified that were traditionally associated with the nucleus, mitochondria and ribosomes.

For *Leishmania* parasites specifically, there is evidence in the literature to demonstrate autophagous transfer into the parasite-containing compartment (Schaible et al. 1999). Schaible et al (1999) used immunoelectron microscopy to show that autophagosomes could fuse with *L. mexicana*-containing intracellular compartments and, in doing so, able to transfer their luminal contents. Some of the nutrients needed by *Leishmania* can only be obtained by collecting the products delivered to the lysosome via autophagy and endocytosis such as essential amino acids and heme (reviewed by McConville et al. 2015). It has been suggested that the parasite-containing compartment is able to influence intracellular trafficking and selectively allow

molecules into and out of the compartment (Harris et al. 1994). As well as the fusing of autophagosomes with the parasite-containing compartment, the compartment may change the way it interacts with mitochondria. For example, mitochondria have been found closely apposed to and in direct contact with the *Legionella pneumophila*-containing intracellular compartment, as shown by electron microscopy (Horwitz 1983). This has also been observed for *Chlamydial* inclusions (Matsumoto 1981) and *Toxoplasma* parasitophorous vacuoles (Jones et al. 1972) where it has been suggested to play a role in allowing pathogens access to specific mitochondrial functions or metabolites (recently reviewed by Dumoux & Hayward 2016). This same process may be occurring for *L. donovani* amastigote parasites.

A number of proteins identified within the parasite-containing compartment proteomic datasets were proteins traditionally associated with the ER. It is now well established that ER is likely involved in phagosome biogenesis and maturation (Li et al. 2010). Indeed, others have even used calnexin as a target for immunoaffinity selection of *Leishmania*-containing compartments (Kima & Dunn 2005) as discussed previously. The current datasets suggested that approximately 10% of the proteins present on the *Leishmania*-containing compartment were proteins that have traditionally been associated with the ER and do not yet have an established role in phagocytosis; this percentage was not significantly different between live and HI parasite-containing compartments discounting large-scale active recruitment of the ER.

There are a number of additional experiments that could be done in the future to expand upon the results detailed in this chapter. Firstly, only one time-point of 4 hr post-infection was used for this study. The reason that this time-point was chosen was from a careful balance between ensuring that the majority (>90%) of amastigotes were within their terminal LAMP1+ve compartment (Lang et al. 1994) and also that the HI parasites were not given enough time to be digested by the lysosome. A time-point of 4 hr post-infection was also well before the parasite's intracellular multiplication stage



which has been noted as appearing by day 3 post-infection with amastigotes (Chang & Dwyer 1978). It would be advantageous to give temporal resolution to the changing dynamics of the protein composition of the parasite-containing compartment; however, the time required to optimise the protocol and generate enough sample material for quantitative proteomics meant that additional time-points were not possible during the timeframe of this project. As another future experiment, FeDex-treated *L. donovani* amastigotes could be injected directly into a mouse. SPIONs are already used *in vivo* in applications such as magnetic drug delivery, magnetic resonance imaging and nanomedicine (Lin et al. 2008). The quantity of sample material required makes this experiment difficult but would give the most physiologically relevant results. Alternatively, as FeDex likely binds to the outside of the parasite, this isolation protocol could be adapted to be used with other intracellular microorganisms, either to study their intracellular compartment or properties of the microorganism itself.

To conclude, we have shown in this chapter data pertaining to the development of a novel method to isolate *L. donovani* amastigotes, and their associated phagolysosomal membrane, from infected J774.2 cells. This method has been used to generate four samples each from live or HI parasite-fed cells and used to characterise the *Leishmania*-containing intracellular compartment in high resolution. Importantly, CCR5 was not found to be associated with this compartment. The next chapter details the use of iTRAQ-labelling on these same samples to obtain precise quantification data for each protein, on which we could then perform comparative analyses to better determine which proteins were being actively manipulated by the live parasite.

# **6. iTRAQ-based quantitative proteomic analysis of the intracellular *L. donovani*-containing compartment**

## **6.1 Chapter-specific background and rationale**

There has been a shift in biology over the last decade away from mere protein identification towards quantifying the absolute and relative abundance of proteins present within a sample, helping to detail more subtle changes in protein expression. With technological advancement the datasets produced from such studies have become increasingly complex necessitating the use of statistical techniques other than those traditionally used in the field of biology. A range of the quantitative proteomic approaches available is discussed below together with subsequent analyses of acquired data.

### **6.1.1 Quantitative proteomics**

Quantitative proteomics aims to gain a better understanding of the underlying biology by determining whether proteins are differentially expressed between samples. Over the years, new methods of quantifying identified proteins have been developed allowing for increasingly accurate quantitative data to be produced from mass spectrometry (MS). These quantitative techniques include stable isotope labelling and label-free approaches, each having their own advantages and disadvantages. For stable isotope labelling, there are a number of different techniques: (i) chemical labelling, such as isobaric tags for relative and absolute quantification (iTRAQ) or tandem mass tag; (ii) metabolic labelling, such as stable isotope labelling by amino acids in cell culture (SILAC); (iii) enzymatic labelling; or (iv) the addition of other labelled peptides. Two of the most commonly used techniques are iTRAQ and SILAC. iTRAQ labelling, first described by Ross et al. (2004), is the process

of using isotope-labelled, chemically-identical molecules that covalently bond to N-terminal regions and amine side chains of proteins *in vitro* after samples have been generated. After LC-MS/MS, fragmentation data can be used for relative quantification of peptides and to determine from which sample the peptide originates. It provides an easy-to-use technique that allows up to 8 samples to be compared in one LC-MS/MS run, thus reducing reproducibility issues associated with multiple runs. In addition, it can more accurately quantify small differences in protein abundance between samples (Wang et al. 2012). However, the dynamic range is more limited with fold changes restricted to less than 2 orders of magnitude (Casado-Vela et al. 2010). Quantification ratios are often compressed particularly for high fold changes and the reagents are expensive (Wang et al. 2012). Additionally, it requires increased amounts of starting material compared to unlabelled techniques (Zhu et al. 2010). Alternatively, SILAC is an *in vivo* labelling technique that involves growing cells in medium containing amino acids labelled with stable isotopes, which are incorporated into the cells' proteins. Samples resulting from the use of these cells can then be mixed and analysed together in a single LC-MS/MS run and ratios of peak intensities compared between peptide pairs. SILAC has the disadvantage of requiring that all the cells used in our experiments were pre-labelled with expensive reagents; as our final sample would only be a tiny fraction of this, it would be better to label the sample at the end.

Unlabelled techniques also exist for quantifying relative protein abundance either using peptide peak intensities or spectral counting. Both of these methods involve performing separate LC-MS/MS runs on each sample and then making comparisons between different analyses. For the former, ion intensity changes such as peptide peak areas are measured (Zhu et al. 2010). This was first used as a method of quantification when it was noted that the peak areas increased with increasing concentrations of peptides belonging to specific proteins, even within complex sample preparations (Chelius & Bondarenko 2002). However, different LC-MS/MS runs can result in differences in peak intensities for peptides, even for the same sample, making normalisation and careful peak alignment essential to ensure validity

(Zhu et al. 2010). For the latter, post-MS/MS processing techniques are used for calculating relative quantification. The spectral count is defined as the total number of spectra identified for a particular protein and spectral counting, like peak area analyses, is easy to incorporate into existing proteomic workflows at no extra cost. Exponentially modified protein abundance index (emPAI) quantification is a modified form of spectral counting and was originally described as a method to quantify levels of proteins within the same sample (Ishihama et al. 2005). However, it has since been used to compare protein abundance between samples, despite a relative lack of validation for the accuracy of this technique for inter-sample quantification.

Direct comparisons between labelled and label-free quantitative proteomic approaches have been made by simultaneous processing of the same samples. For example, Wang et al. (2012) used two experimentally different samples, each with three replicates. They used iTRAQ-labelling along with unlabelled approaches and found that 558 and 921 total proteins were identified, respectively. They also found that a higher percentage of the identified proteins could be quantified using iTRAQ. Interestingly, when using sample triplicates, only 42-69% of proteins were found in all 3 samples, demonstrating the importance of multiple replicates to reduce sources of protein variation that are not treatment specific (Wang et al. 2012). Encouragingly, both approaches had a good correlation for protein ratios between the two experimental groups, suggesting that the overall picture for differentially expressed proteins was broadly similar for the two techniques. Others have found similar results with spectral counting offering the greatest proteome coverage for identifications, but at the cost of reduced quantification performance compared to labelled techniques (Li et al. 2012; Megger et al. 2014).

### **6.1.2 Exploring high dimensional proteomic datasets**

It has been over a decade since the first quantitative proteomic datasets were produced from LC-MS/MS. Since that time, advances in technology and

proteomic methodologies have led to ever-larger datasets that contain a plethora of increasingly precise quantitative information. However, proteomic datasets often demonstrate very high dimensionality making it difficult to ascertain which proteins are contributing most to the differences exhibited between datasets. In such situations, it is useful to complement traditional statistical techniques with machine learning algorithms. Indeed, there have been calls for a more standardised approach to be taken by researchers when analysing quantitative proteomic datasets (Karimpour-Fard et al. 2015).

Often, the first step in processing proteomic datasets is quality control and to make a general assessment of the dataset structure (Karimpour-Fard et al. 2015). For example, questions on whether the datasets require normalisation or whether the datasets can cluster according to initial experimental conditions should be asked at this stage in the process. Exploratory data analyses such as principal component analysis (PCA) can be used to identify any outliers and provide useful summaries of the main characteristics of the data. PCA is often used in proteomics to transform a set of potentially correlated protein quantities into a new set of uncorrelated variables, called principal components (PCs). As the components are obtained by a rotation of the coordinate axes, each principal component is a linear combination of the original variables, with coefficients (or loadings) chosen so that the first PC gives the direction of the maximum variance in the data. The second PC is orthogonal to the first and is in the direction of the next most variance, and so on. The goal is to reduce the dimensions of a  $d$ -dimensional dataset by projecting it into an  $e$ -dimensional subspace, where  $e < d$ , whilst keeping most of the information in the data. This is achieved by taking only the first few PCs, accounting for most of the variance in the data.

Relative quantification data for individual peptides or proteins from multiple experimental samples can be stored in a data matrix,  $\mathbf{X}$ , and the linear combinations that maximise the variance can be found by eigendecomposition of the covariance matrix,

$$\Sigma = \frac{1}{n-1} ((X - \bar{x})^T (X - \bar{x}))$$

where  $\bar{x}$  is the mean vector  $\bar{x} = \sum_{k=1}^n x_i$ . The eigenvectors trace the principal lines of force and the eigenvector with the highest eigenvalue corresponds to the first principal component (PC1), the eigenvector with the next highest to the second principal component (PC2), etc. As the eigenvalues decrease the amount of information that is lost when the corresponding component is removed decreases, allowing most of the variance in the data to be explained in fewer dimensions. Using matrix notation we can write

$$X = \mathbf{PT}' + \boldsymbol{\varepsilon}$$

where  $\mathbf{X}$  is the  $m \times d$  data matrix of  $d$  variables for each of  $m$  observations,  $\mathbf{P}$  is the  $m \times e$  matrix of principal components (with  $e < d$ ),  $\mathbf{T}$  is the  $e \times d$  loadings matrix relating the original variables to the principle components (and thus  $\mathbf{T}'$  the transformed  $\mathbf{T}$  matrix) and  $\boldsymbol{\varepsilon}$  is the matrix of residuals.

PCA is classified as an unsupervised technique, meaning that no class information is used in the analysis, i.e. there is no labelling of data by a human (or 'supervisor'). In addition to dimension reduction, PCA is a useful tool for data visualisation, quality control, and to identify potential outliers and patterns or clustering of the data (Karimpour-Fard et al. 2015). Often just the first two principal components (PC1 and PC2) of the newly projected data are plotted for easier visualisation and interpretation of data, allowing individual samples to be checked for clustering based on experimental conditions. The original variables contributing most to any PC of interest can be identified from the loadings as the coefficients of these variables in the linear combination will have the largest absolute values.

Cluster analysis is another exploratory data analysis tool that can be used to find clusters or patterns in datasets. It is a useful technique to visualise data and determine whether any grouping found in proteomic data matches the initial experimental conditions. Cluster analyses rely on being able to measure the similarity of objects using a distance metric such as the Euclidean distance:

$$d(X, Y) = \sqrt{(X_1 - Y_1)^2 + (X_2 - Y_2)^2 + (X_n - Y_n)^2}$$

This is used to produce a matrix that records the distance between every pair of observations. There are different types of cluster analyses but the most commonly used is hierarchical cluster analysis (HCA), which either uses agglomerative clustering (each observation starts as a separate entity which are then merged into groups until a single cluster is formed) or divisive clustering (a single cluster is split into groups based on levels of dissimilarity). Using the agglomerative method, the two observations that have the smallest distance cluster and a new distance matrix calculated. The smallest distance in this new matrix determines whether another observation joins the first cluster or forms a new cluster with some other observation. This process is repeated until all observations are merged to form a single cluster.

The distance between individual objects can be converted to a distance between clusters in several different ways such as: (i) single-linkage, where the distance between two clusters is calculated as the smallest distance between objects, from one each of the two clusters; (ii) complete-linkage, where the largest distance is used; (iii) average-linkage, where the average distance over all pairs of objects is used. All forms of HCA are able to display the results in dendrograms allowing for easy visualisation of data groupings.

After initial data exploration, more traditional univariate statistical techniques can be used to detect “low-hanging fruit” in the dataset (Karimpour-Fard et al. 2015). Student’s t-test is commonly used to test whether a single variable in two different datasets can be considered to come from the same underlying distribution. This uses the t-statistic:

$$t = \frac{\bar{x}_1 - \bar{x}_2}{SE}$$

to test whether the means of the two datasets are significantly different, taking into account the variance in the data. Here  $\bar{x}_1$  and  $\bar{x}_2$  are the means of the first and second datasets respectively and **SE** is the standard error. The value of **t** is compared to a critical value (that depends on the number of values) for a particular significance level to determine whether the null

hypothesis that there is no difference can be rejected. However, this test makes the assumption that data are normally distributed. Where this cannot be assumed, non-parametric tests such as Mann-Whitney U tests can be performed. For this test, the values from both datasets for a particular variable are given a rank from 1 for the lowest value up to  $x$  for the highest value, where  $x$  is the number of values. The sum of the ranks,  $S1$ , for dataset 1 with  $N1$  values, and  $S2$ , for dataset 2 with  $N2$  values, are then calculated and the test statistic,  $U$ , calculated as

$$U = N1 * N2 + NX * \frac{(NX + 1)}{2} - SX$$

where  $SX$  is the larger rank sum and  $NX$  is the number of values in the dataset with this rank sum. The  $U$  value can then be compared with a critical value for the numbers of values involved, with statistical significance achieved if the obtained  $U$  value  $\leq$  this critical value.

When using univariate techniques on each variable in a large dataset, we increase the probability of an apparently significant result happening simply by chance, and therefore multiple test correction using methods such as Bonferroni (Dunn 1961) or Benjamini-Hochberg correction (Benjamini & Hochberg 1995) need to be performed. Incredibly, despite the large number of proteins involved, this is something that the vast majority of quantitative proteomic studies were found to be missing (Diz et al. 2011). Benjamini-Hochberg correction is preferable for controlling multiple hypothesis testing in proteomics data because the high number of samples in proteomic analyses would lead to an extremely small p value with Bonferroni correction (Dunn 1961). In Benjamini-Hochberg correction, the smallest p value is given a rank of  $i=1$ , the second smallest  $i=2$ , and so on. Each individual p value is compared to its Benjamini-Hochberg critical value  $(i/m)Q$ , where  $i$  is the rank number,  $m$  is the total number of proteins, and  $Q$  is the false discovery rate (FDR). The largest p value where  $p < (i/m)Q$  is true is taken as the p value to test for significance.



The next step in the data analysis process is to use multivariate supervised machine learning to reveal any patterns related to the experimental conditions. Supervised algorithms learn to associate a particular output or response with the input variables using training data for which the responses have been assigned. It is reasonable to assume that proteins present in proteomic datasets are interconnected and, as a result, that groups of proteins may influence each other. There are many different machine learning techniques that can be used to consider combinations of variables rather than individual proteins, but possibly the most commonly used is partial least squares (PLS). This differs from PCA in that data is classified before analysis and only the variation due to class difference is considered in the analysis rather than all variance in the data as in PCA. This helps highlight key proteins that differ between descriptor groups, even if they have only a small contribution to the first principal components. PLS essentially performs PCA on the original data matrix  $\mathbf{X}$  whilst simultaneously relating the components to a matrix of response variables,  $\mathbf{Y}$ , to project  $\mathbf{X}$  onto  $e$ -dimensional subspace that explains as much of the covariance between  $\mathbf{X}$  and  $\mathbf{Y}$  as possible. As with any supervised technique, PLS is prone to over-fitting data and test data should be used to validate the results.

Finally, proteomic datasets can have functionally relevant biological information extracted from them using a suite of bioinformatics tools that range from relatively basic Gene Ontology (GO) category assignment to rich functional assessment of protein pathways and networks. For the latter, a variety of software packages exist, oftentimes using different databases of curated protein pathways and interactions. Ingenuity Pathway Analysis (IPA), arguably the most extensive package, compares proteins from proteomic datasets to corresponding gene objects in the Ingenuity Pathways Knowledgebase (IPKB), which uses published, peer reviewed experimental evidence of interactions between proteins. Pathway analyses can give the most complete picture of the biological implications of the dataset and can identify novel avenues for further research.

### 6.1.3 Objectives

Having developed a protocol to isolate *Leishmania*-containing phagolysosomes from infected J774.2 cells, these phagolysosomal samples were then iTRAQ-labelled for quantitative LC-MS/MS. iTRAQ has improved accuracy and precision over unlabelled techniques, particularly for proteins with quantitation ratios between samples close to 1. This was advantageous for the current investigation as it has already been established that the presence of dead parasites within the live parasite preparations would likely decrease the differences between the live and HI preparations; thus, a high sensitivity technique was required to detect subtle differences in protein abundances between live and HI parasite preparations.

We aimed to perform a variety of comparative analyses to determine whether live *L. donovani* LV9 amastigotes actively manipulated the protein composition of their intracellular compartment at a fixed 4 hr time-point post-infection. This involved traditional statistical methodologies combined with machine learning algorithms, pathway comparisons and network analyses, essentially following the workflow suggested by Karimpour-Fard et al. (2015) for proteomic data analysis.

## **6.2 Chapter-specific methods**

### **6.2.1 Gene Ontology annotation of biological processes**

Using GO tools available from AgBase (McCarthy et al. 2007), the biological processes associated with each protein were determined. Biological process annotations were then grouped to give more generalised categories using GO Slim viewer (McCarthy et al. 2006).

### **6.2.2 Statistics**

R (version 3.2.3, The R Foundation for Statistical Computing, Austria) was used for HCA, PCA and PLS analyses. The average-linkage, agglomerative clustering method was used for HCA. To control for multiple comparisons when using univariate tests, the Benjamini-Hochberg correction (Benjamini & Hochberg 1995) was applied. A more liberal FDR threshold of 25% was chosen to ensure that proteins of potential interest for further investigation were not missed, as suggested by Diz et al. (2011). Normalisation and variable scaling (detailed in Section 6.3.2) was carried out using C code written in-house (Dr Julie Wilson, University of York) that also allowed univariate tests to be performed for each identified protein. Log<sub>2</sub> fold changes were calculated for proteins by using the median peptide ratio values computed from preprocessed data across experiments 1 to 3.

### **6.2.3 Pathway and network analyses**

IPA (Ingenuity Systems, California) was used for pathway and network analyses, with no expression cut-off value selected. Text files containing protein GI numbers of iTRAQ-labelled LC-MS/MS identified proteins were uploaded onto the Ingenuity systems server and processed using the IPA software package. IPA compared proteins from proteomic datasets to corresponding gene objects in IPKB, which contains information on published, peer reviewed experimental evidence of interactions between proteins. For pathway analyses, IPA generates a p value for each canonical pathway in its database based on right-tailed Fisher's exact tests to calculate

the probability of the proteins in the pathway being present in the sample by chance, with a p value < 0.05 being significant.

For network analyses, IPA constructs dynamic networks of up to 35 proteins with networks ranked according to their assigned score. This score is calculated using right-tailed Fisher's exact tests to describe the probability of finding these selected proteins by random selection from all proteins in the IPKB database. Networks are then ranked based on their network score, which is calculated as:  $\text{score} = -\log_{10}(\text{p value})$ . IPA provides visual representations of these networks that can be exported from the software. Solid lines represent direct protein-protein interactions, whereas dotted lines represent indirect protein associations, both evidenced in the literature. A more detailed description of network generation is available from Deighton et al. (2010).

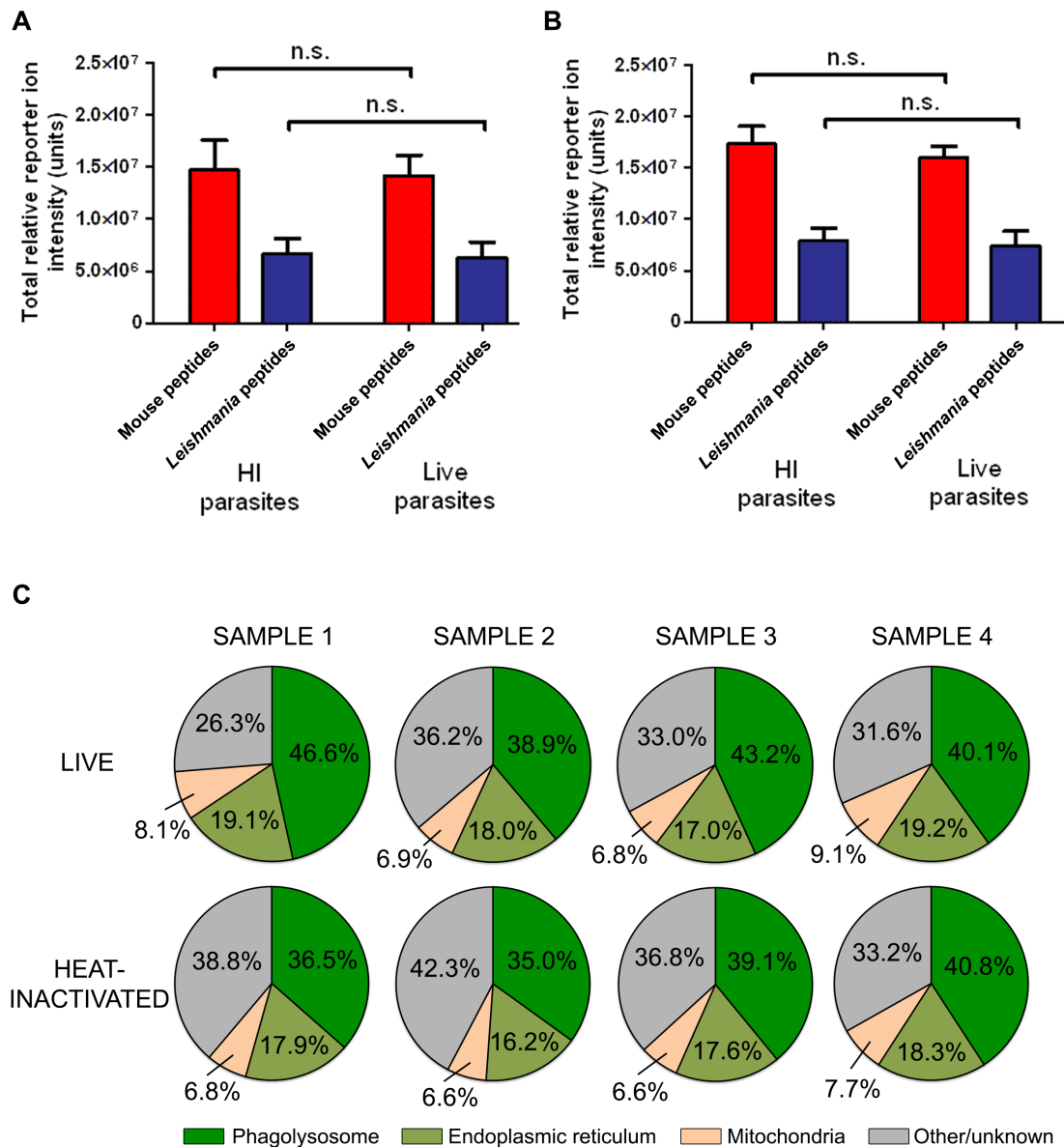
## 6.3 Results

### 6.3.1 Summary of iTRAQ-labelled samples

#### 6.3.1.1 iTRAQ-labelling of samples

The 4 live and 4 heat-inactivated (HI) samples detailed in Section 5.3.2 were iTRAQ-labelled as described in Section 2.12.2 and analysed by LC-MS/MS. The resulting dataset contained a total of 6189 peptide identifications representing 1088 different proteins, including *Leishmania*-specific peptides. As we were only initially interested in mouse proteins, *Leishmania*-specific peptides were removed from the dataset before further analyses. This gave a final dataset with 4425 peptides representing 777 mouse proteins. Although lower than the mean of 1029 proteins identified from the qualitative LC-MS/MS studies detailed in Section 5.3.2, this was expected due to the additional steps involved in iTRAQ-labelled proteomics (Wang et al. 2012). Of particular note, every peptide in the dataset had quantification values for at least 3 out of 4 samples for both of the preparation conditions studied (J774.2 cells fed either live or HI parasites). This meant that, in contrast to the qualitative datasets obtained in Section 5.3.2 where a number of proteins were exclusively found in one particular condition, no protein was present only in one condition and completely absent from the other. This was likely due to the differences in sensitivity between the two techniques, with lower abundance peptides that had accounted for preparation-specific proteins in qualitative analyses not being identified with iTRAQ. Interestingly, it was almost solely sample Pc (preliminary proteomics round C sample) for which quantitation data was missing for some peptides. To avoid later confusion when performing PCA, this sample was renamed sample 4.

We next compared the total relative reporter ion intensities for the different experimental conditions (**Figure 6.1A**), with no statistically significant differences found between the HI and live sample preparations. Sample 4 was noted to have much lower relative reporter ion intensities in comparison to the other samples and this sample was removed from later analyses. However, after removing sample 4, we again found no significant difference between the HI and live preparations for either mouse or *Leishmania*-specific



**FIGURE 6.1. Quantitative summary of the peptides identified using iTRAQ-labelled LC-MS/MS on 4 live and 4 heat-inactivated phagolysosome preparations. A)** The total relative reporter ion intensities for *Leishmania* peptides or mouse peptides, as output by iTRAQ-labelled LC-MS/MS, was calculated for all 4 sample preparations; n = 4, data shown as mean ± SEM. **B)** The total relative reporter ion intensities for *Leishmania* peptides or mouse peptides was calculated for samples 1 – 3 after removing sample 4; n = 3, data shown as mean ± SEM. **C)** The subcellular location was identified for each protein by conducting a literature search and the overall quantitative representation for each subcellular fraction calculated as a percentage of the total reporter ion intensity.

proteins (**Figure 6.1B**) demonstrating that the mouse:*Leishmania* protein ratio was maintained between live and HI preparations.

The subcellular location was classified for each identified protein by conducting a literature search (as detailed in Section 5.2.7). This was facilitated using Python code written in-house to allow proteins in new proteomic datasets to be assigned to previously identified subcellular locations and to subsequently check whether each protein was localised to the phagolysosome, ER, mitochondria, or none of these ('other') using in-house curated lists of proteins associated with each of these compartments. The percentage of the total reporter ion intensity for each subcellular fraction was calculated for each sample. For all samples, phagolysosomal-specific proteins accounted for between 35.0-46.6% of the total reporter ion intensity (as shown in **Figure 6.1C**) with no significant difference between live and HI preparations.

#### **6.3.1.2 Global analysis of identified proteins**

As the same proteins were present in both live and HI preparations, all proteins in the dataset were GO annotated and then processed through the generic GO Slim tool to identify the overall biological processes most represented within the parasite-containing compartment dataset (**Table 6.1**). This revealed that a number of highly represented biological processes were present within these samples, including those involved in transport, cellular nitrogen compound metabolic processing, and biosynthetic processing. The top represented biological process ('transport') included proteins involved in the direct movement of substances (such as ions) in addition to whole cellular components (such as organelles).

#### **6.3.2 Data pre-processing**

Data pre-processing was performed using an adaptation of the procedure described by Dowle et al. (2016). Peptide identifications and reporter ion intensities were exported from Mascot search results and individual ion intensities normalised against total ion intensity for each channel. To prevent

GO term	Description	Number of proteins
GO:0006810	Transport	331
GO:0034641	Cellular nitrogen compound metabolic process	256
GO:0009058	Biosynthetic process	241
GO:0048856	Anatomical structure development	216
GO:0007165	Signal transduction	213
GO:0006950	Response to stress	189
GO:0044281	Small molecule metabolic process	176
GO:0030154	Cell differentiation	163
GO:0016192	Vesicle-mediated transport	145
GO:0009056	Catabolic process	139
GO:0006464	Cellular protein modification process	125
GO:0002376	Immune system process	124
GO:0006412	Translation	119
GO:0061024	Membrane organization	108
GO:0042592	Homeostatic process	107

**TABLE 6.1. Overall biological processes of proteins represented within *L. donovani*-containing compartments.** Biological process gene ontology (GO) annotations of all proteins found in either live- or heat-inactivated parasite containing compartments. GO associations were determined using GO Slim and all biological processes represented by at least 100 proteins reported.



negative values affecting normalisation, any peptide with a negative reporter ion intensity was adjusted prior to normalisation by subtracting the most negative value from each intensity value for that peptide (**Figure 6.2A**). Missing reporter ion peaks that return a value of zero and later become negative after isotope purity correction could have caused these negative values. Despite the same equivalent amounts of protein being loaded for each sample, the total reporter ion intensity for each sample was slightly different. Thus, the next normalisation step was to make the sum of reporter ion intensities equal to 1000.0 for each sample; individual peptide intensity values were adjusted to a percentage of this total value (**Figure 6.2B**).

Due to considerable differences between experiments, particularly in sample 4, rather than calculating the percentage intensity of each reporter ion for each MS/MS spectrum over all channels, as in Dowle et al. (2016), pairwise proportions were calculated. That is, for each sample, the reporter ion intensities were rescaled so that the values for HI and live preparations within each sample summed to 1 (**Figure 6.2C**). This pairwise scaling is analogous to the common use of ratios in proteomics, but does not suffer from the problems introduced when dividing by very small numbers. The final stage of data pre-processing was to generate protein level data by calculating the mean value from all relevant peptide values (**Figure 6.2D**).

As one would expect, before normalisation high abundance proteins were represented by many more peptides and had a higher combined reporter ion intensity as shown in **Figure 6.3A**. The rescaling of peptide intensities ensured that these high abundance proteins did not dominate analyses and that any changes in lower abundance proteins might be identified. The method described by Dowle et al. (2016) in which the percentage intensity of each reporter ion for each MS/MS spectrum was calculated over all channels was also tested and gave similar results as to when data was scaled in pairs, but had the disadvantage of making it more difficult to isolate or exclude individual samples without renormalising the entire dataset.

**Raw peptide data:**

GI code	HI1	L1	HI2	L2	HI3	L3	HI4	L4
gi 19526814	11794.8	14488.9	7058.3	11070.9	9878.3	10401.3	4141.5	7438.9
gi 6753620	324.5	277.7	-33.5	484.5	557.4	620.0	-13.3	225.8
<b>Total</b>	20450611.7	18245206.1	14406234.4	15209989.9	17056917.4	14454197.2	6995180.8	8815029.9

↓ **A** Any peptide with a negative value in any sample has that value added to all samples to ensure all values are  $\geq 0$ .

GI code	HI1	L1	HI2	L2	HI3	L3	HI4	L4
gi 19526814	11794.8	14488.9	7058.3	11070.9	9878.3	10401.3	4141.5	7438.9
gi 6753620	358.0	311.2	0.0	518.0	590.9	653.5	20.2	259.3
<b>Total</b>	20456474.9	18251069.3	14412097.6	15215853.1	17062780.6	14460060.4	7001044.0	8820893.1

↓ **B** Samples normalised down column to ensure that all samples have the same total.

GI code	HI1	L1	HI2	L2	HI3	L3	HI4	L4
gi 19526814	0.576530	0.793847	0.489775	0.727580	0.578967	0.719354	0.591572	0.843348
gi 6753620	0.017499	0.017051	0.0	0.034043	0.034633	0.045196	0.002885	0.029397
<b>Total</b>	1000.0	1000.0	1000.0	1000.0	1000.0	1000.0	1000.0	1000.0

↓ **C** Peptides normalised in sample pairs to facilitate direct comparison between samples.

**Normalised peptide data:**

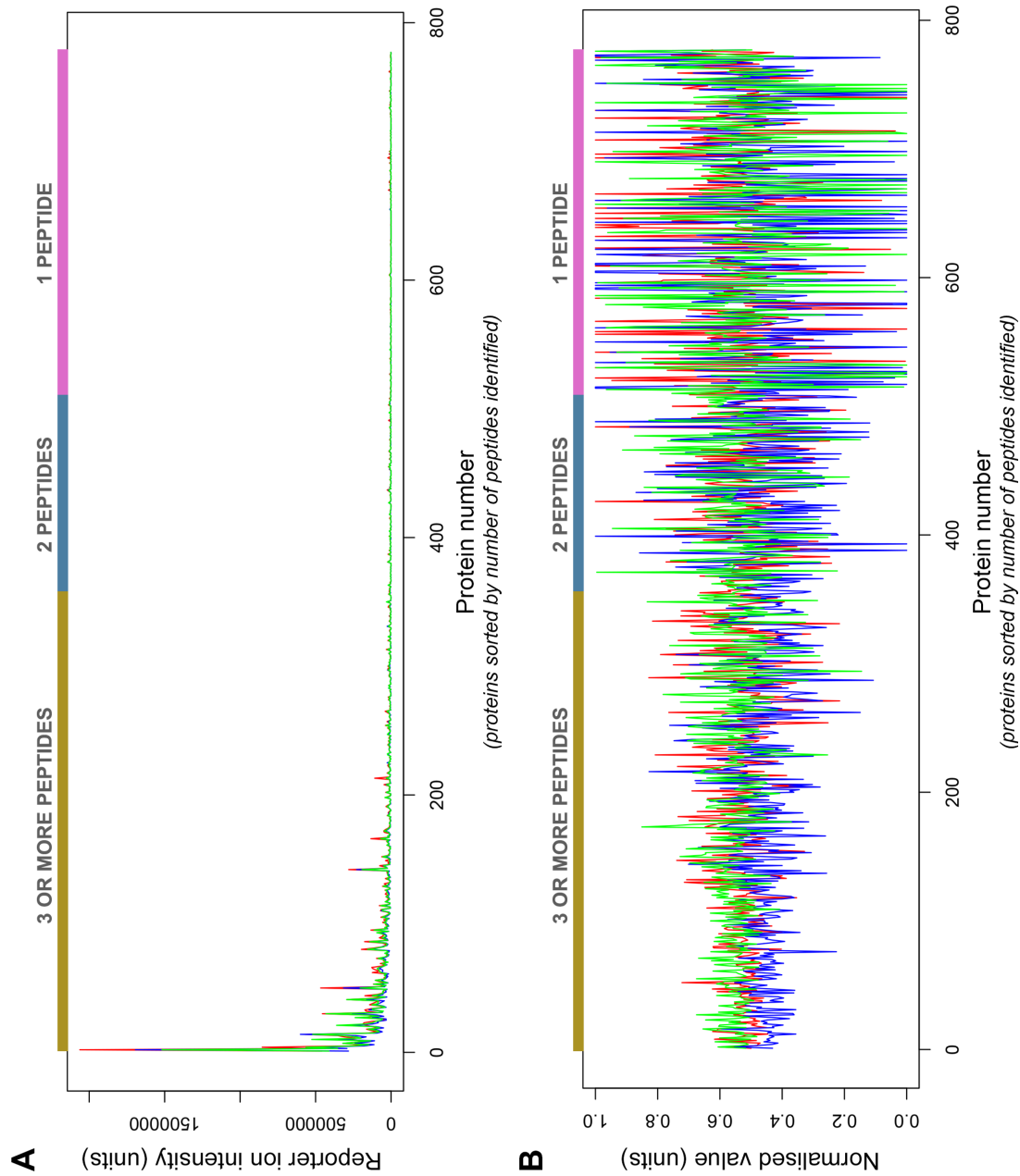
GI code	HI1	L1	HI2	L2	HI3	L3	HI4	L4
gi 19526814	0.4207	0.5793	0.4023	0.5977	0.4459	0.5541	0.4123	0.5877
gi 6753620	0.5065	0.4935	0.0	1.0	0.4338	0.5662	0.0894	0.9106

↓ **D** If more than one peptide is identified for a particular protein, the mean peptide value is used.

**Normalised protein data:**

GI code	HI1	L1	HI2	L2	HI3	L3	HI4	L4
gi 19526814	0.4207	0.5793	0.4023	0.5977	0.4459	0.5541	0.4123	0.5877
gi 6753620	0.4057	0.5943	0.4218	0.5782	0.3699	0.6301	0.0297	0.9703

**FIGURE 6.2. Summary of protocol used for data pre-processing to facilitate valid comparison between samples. A)** The raw peptide data output from the mass spectrometer was first corrected to ensure that no negative values existed in the dataset. **B)** Data were then normalised down columns to ensure that each sample had exactly the same quantity of protein. **C)** Within each sample, peptide pairs from each preparation were then scaled in pairs for each peptide in each sample, producing the final peptide data. **D)** If the protein was represented by more than one peptide then the mean peptide value was calculated to produce final protein-level data. HI1-4 = denotes heat-inactivated samples 1 to 4, L1-4 = denotes live samples 1 to 4.



**FIGURE 6.3. Data pre-processing was required to prevent high abundance proteins from dominating the samples. A)** Reporter ion intensities for individual proteins prior to normalisation and scaling were plotted with proteins sorted in descending order according to the number of peptides representing the protein. **B)** After the pre-processing procedure illustrated in Figure 6.2, values were plotted and proteins sorted in descending order according to number of peptides. Samples shown were from live parasitised samples: red = experiment 1, blue = experiment 2, green = experiment 3.

Although pre-processing allowed lower abundance proteins to be better visualised, **Figure 6.3B** shows that proteins represented by only one or two peptides were now more likely to be at the extremities of values (either 0 or 1). This was due to the lack of averaging the values across several different peptides to produce protein level data. To balance this effect, unless otherwise stated all further analyses were performed three times using datasets that included all proteins with  $\geq 1$ ,  $\geq 2$ , or  $\geq 3$  peptides to ensure that no information was lost.

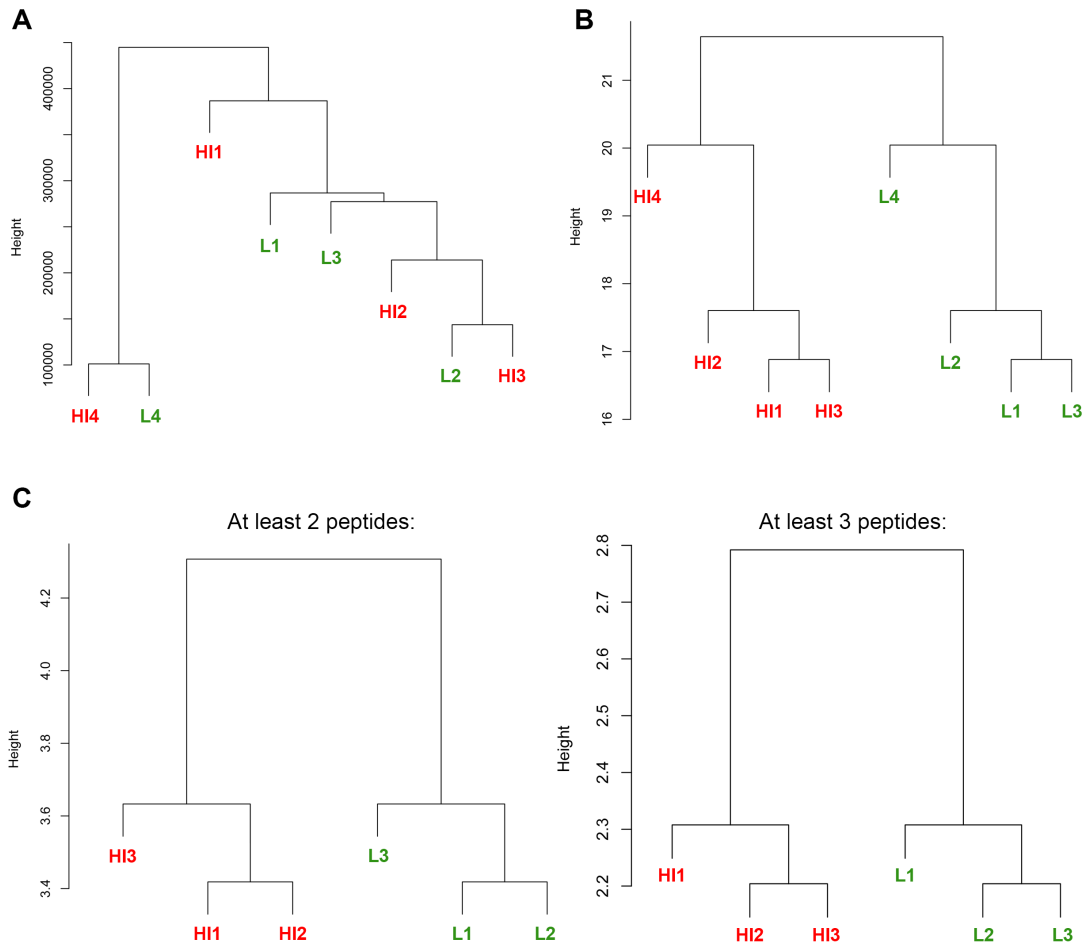
### **6.3.3 Hierarchical cluster analysis shows clear differentiation between live and heat-inactivated samples**

HCA is a useful statistical technique for proteomic analyses that is used to group samples based on their level of similarity and was performed on both raw (**Figure 6.4A**) and pre-processed (**Figure 6.4B**) data. This showed a clear separation between live and HI samples, suggesting that the differences between the samples were reproducible and preparation-specific. The analyses also suggest that sample 4 was most different in comparison to the other samples. This differentiation between samples was maintained when analysing only proteins represented by  $\geq 2$  or  $\geq 3$  peptides after leaving out sample 4, as shown in **Figure 6.4C**.

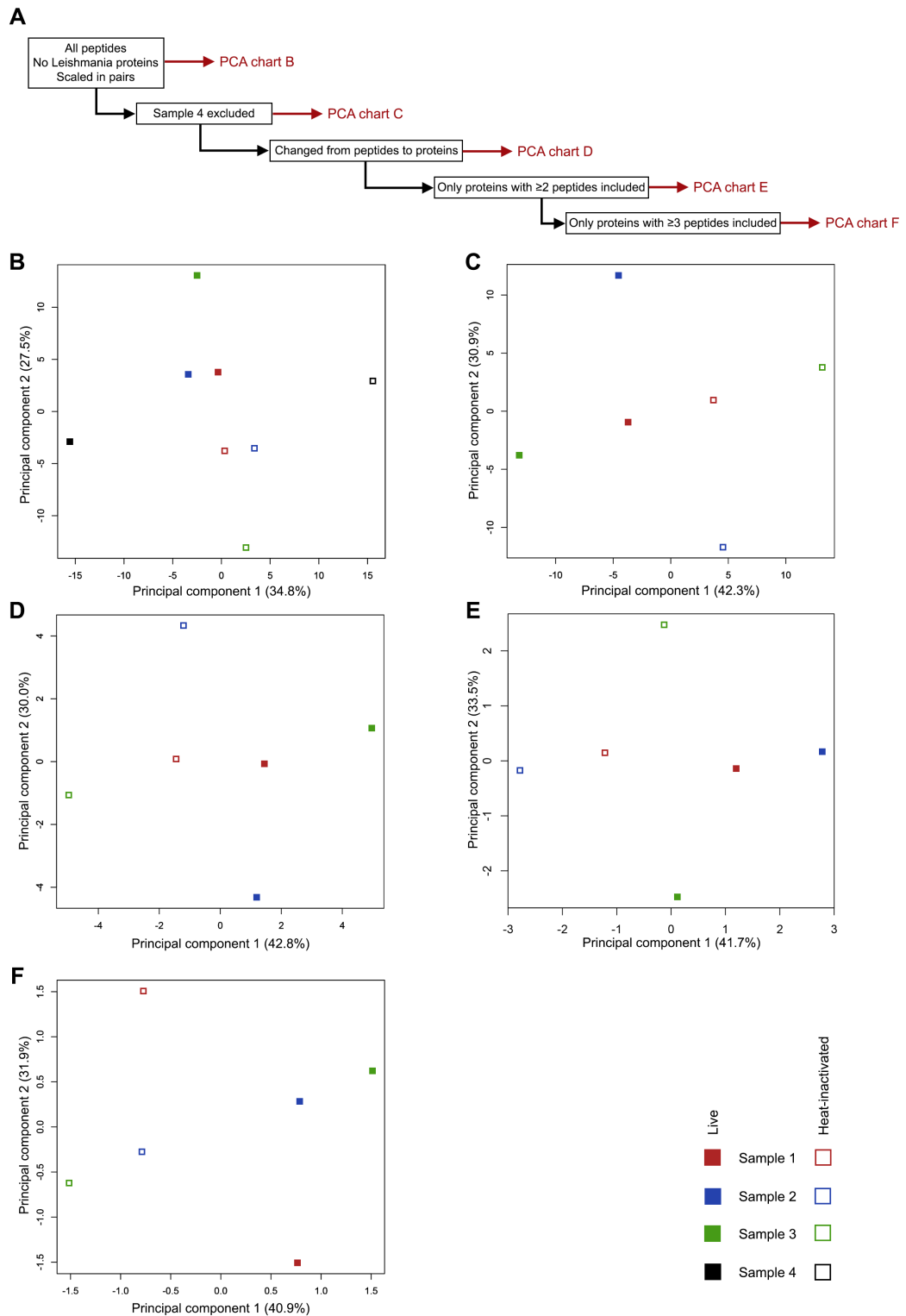
### **6.3.4 Initial exploration of datasets using principal component analysis**

PCA is a variance-based technique; the use of scaled data therefore prevented highly expressed proteins (with correspondingly large variances) obscuring differences caused by lower abundance proteins. The various PCA analyses conducted to investigate any differences between live- and HI-parasite fed preparations are shown in **Figure 6.5A**.

When all mouse peptides were included for all four experiments (**Figure 6.5B**), the biggest variation seen along PC1 was due to the difference between HI- and live-parasite preparations of sample 4, providing further evidence that this sample may be an outlier. After sample 4 was removed,



**FIGURE 6.4. After normalisation and scaling, live and heat-inactivated (HI) preparations differentiated into two distinct clusters. A)** Hierarchical cluster analyses (HCA) were performed on peptide-level data before data pre-processing. **B)** HCA performed on data after pre-processing. **C)** HCA performed on samples 1 – 3 using proteins represented by  $\geq 2$  or  $\geq 3$  peptides. L = live; HI = heat-inactivated.

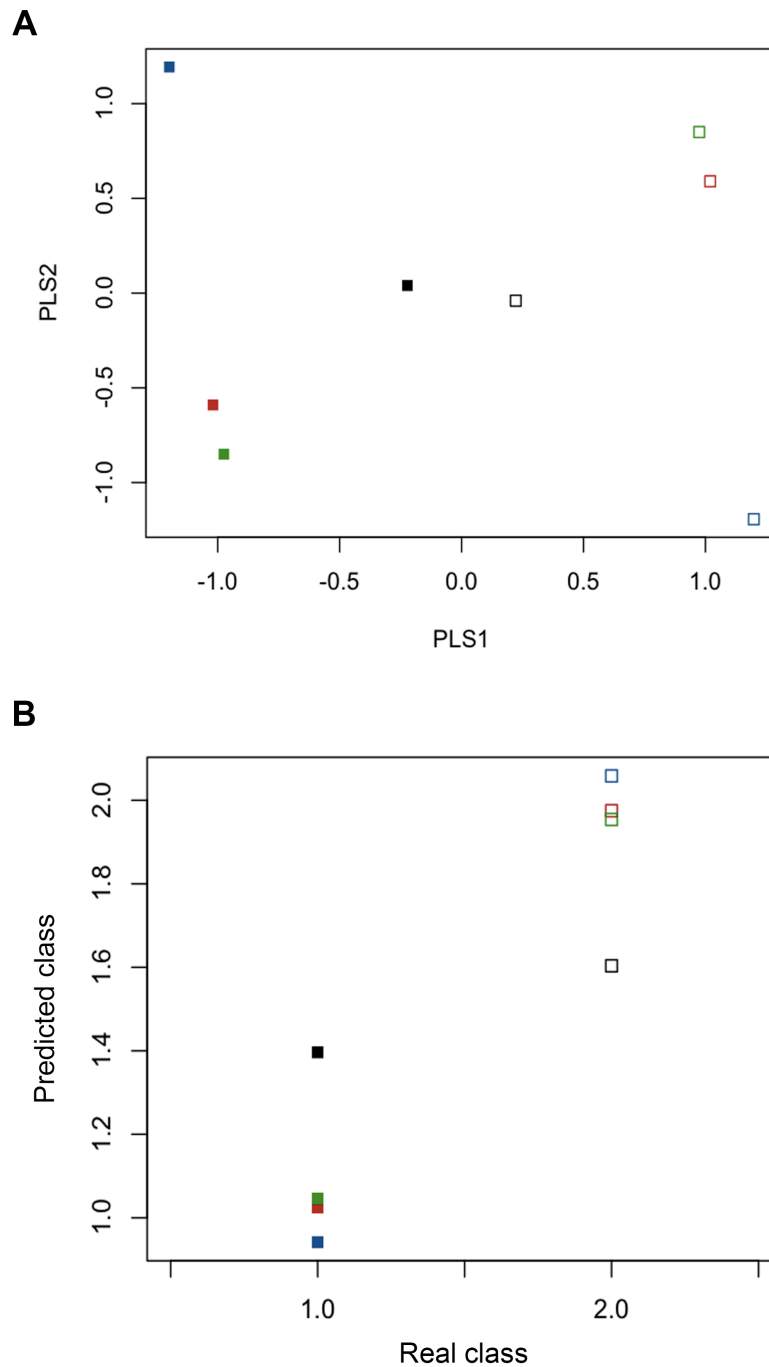


**FIGURE 6.5. Exploratory data analyses showed differentiation along principal component 1 for live and heat-inactivated samples. A) Diagram illustrating how data was handled for PCA. B)-F) Corresponding PCA graphs. Red = sample 1, blue = sample 2, green = sample 3; black = sample 4; closed boxes = live samples, open boxes = heat-inactivated samples. Percentage of variance accounted for with each principal component (PC) is shown in parentheses.**

there was a clear differentiation between HI- and live-parasite preparations along PC1 as shown in **Figure 6.5C**. This analysis used peptide-level data resulting in each protein being represented by several different peptides. This was problematic for data interpretation because peptides from the same protein were often differentially represented to varying degrees and, occasionally, some peptides would have opposite expression profiles for live or HI preparations. As an example, the protein radioprotective 105 (RP105; gi|761712) was represented by 4 peptide identifications; two of these peptides were slightly more differentially expressed within live preparations, whereas the other two were more differentially expressed within HI preparations.

To address this, protein level data was produced as the mean of the scaled data values for each peptide representing an individual protein. Encouragingly, the same differentiation along PC1 seen with peptide-level data was also evident at the protein-level as shown in **Figure 6.5D**. Each of the three HI and live samples were also similarly positioned in the PCA plot suggesting that a comparable picture was emerging from both peptide and protein analyses. When analyses were performed to include only proteins represented by at least 2 peptides (**Figure 6.5E**) or at least 3 peptides (**Figure 6.5F**), the separation between live and HI groups could still be seen.

It was encouraging to see that samples could be differentiated according to experimental conditions (live or HI preparations) even though PCA is an unsupervised statistical technique, based only on the variance in the data and not influenced by information such as experimental condition. However, the use of a supervised technique such as PLS could allow other proteins showing differences between live and HI preparations to be identified. A PLS model was constructed using samples 1-3 as training data and sample 4 as test data. **Figure 6.6A** shows the PLS scores plot for the first two latent variables (analogous to the principal components in PCA). The PLS model was used to correctly predict sample 4 (**Figure 6.6B**).



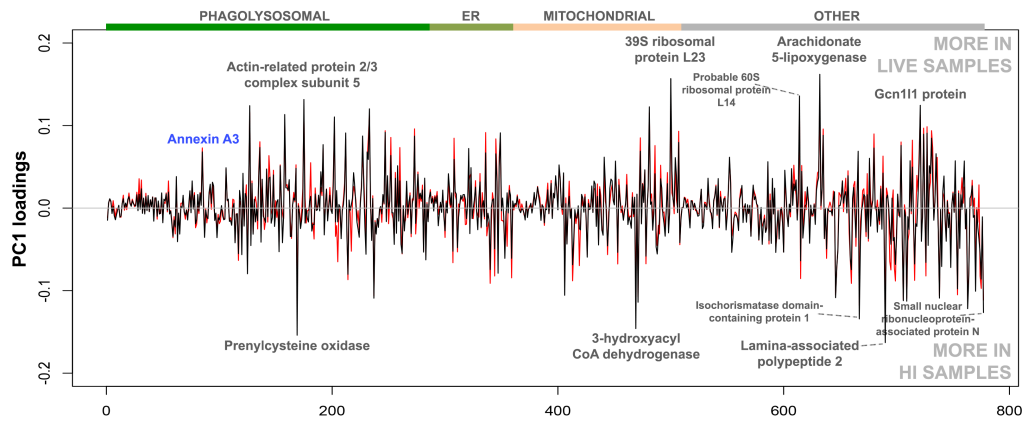
**FIGURE 6.6. The PLS model could correctly predict the class of the live and heat-inactivated preparation from sample 4. A)** The PLS scores plot for the first two latent variables, using samples 1-3 as training data and sample 4 as test data. **B)** The predicted classes for samples 1-3 and sample 4 when using the PLS, with class 1 being live preparations and class 2 being HI preparations. Red = sample 1, blue = sample 2, green = sample 3; black = sample 4; closed boxes = live samples, open boxes = heat-inactivated samples.



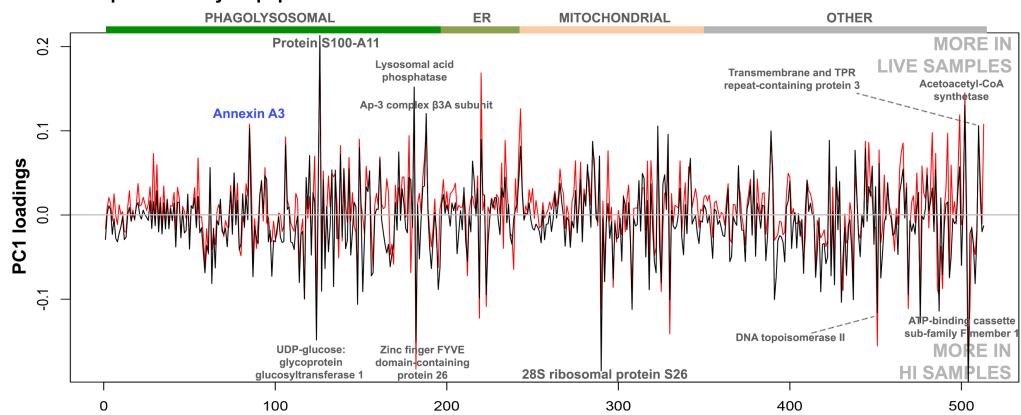
To visualise the individual contributions made by each protein during PCA to the overall PC1 loading, the PC1 loadings for each protein were extracted and plotted as shown in **Figure 6.7** (black line). This revealed several proteins that were most responsible for the variation seen between live and HI preparations. These proteins were from different subcellular locations, although those most important for the separation were proteins from the phagolysosomal and 'other' fractions. The aforementioned PLS analysis that was performed then had the loadings extracted and plotted on the same graphs as the PCA loadings to show the similarity (red line in **Figure 6.7**). Although the variance along the first principal component could have been from any source, the similarity of the loadings for the first latent projection in PLS showed that the proteins identified by PLS as responsible for the variance related to differences between HI and live preparations were largely the same proteins identified by PCA, i.e. that the variance seen in PCA was actually due to the difference in experimental conditions. In the analyses (both PCA and PLS) in which all proteins represented by at least 2 peptides were included, the separation between HI and live preparations for sample 3 is along the second component rather than the first, showing a different source of variance for this sample in this case. Considering the loadings for each protein also helped to illustrate the necessity for conducting separate analyses for proteins represented by  $\geq 1$ ,  $\geq 2$  or  $\geq 3$  peptides. As an example, Annexin A3 (shown in blue font in **Figure 6.7**) was the most differentially represented protein in live samples when looking at only proteins that had  $\geq 3$  peptides. However, these differences were masked when looking at proteins represented by  $\geq 1$  or  $\geq 2$  peptides.

When the proteins contributing to the greatest variation between the live and HI preparations were analysed (**Tables 6.2 and 6.3**), a number of proteins of potential biological interest were identified as being differentially expressed in live samples. For example, arachidonate 5-lipoxygenase (gi|886333) was identified as being the most differentially expressed in live samples by both PCA and PLS when analysing proteins with  $\geq 1$  peptide. This protein is involved in leukotriene biosynthesis and plays a role during inflammatory processes (Chen et al. 1995). A number of proteins with known interactions

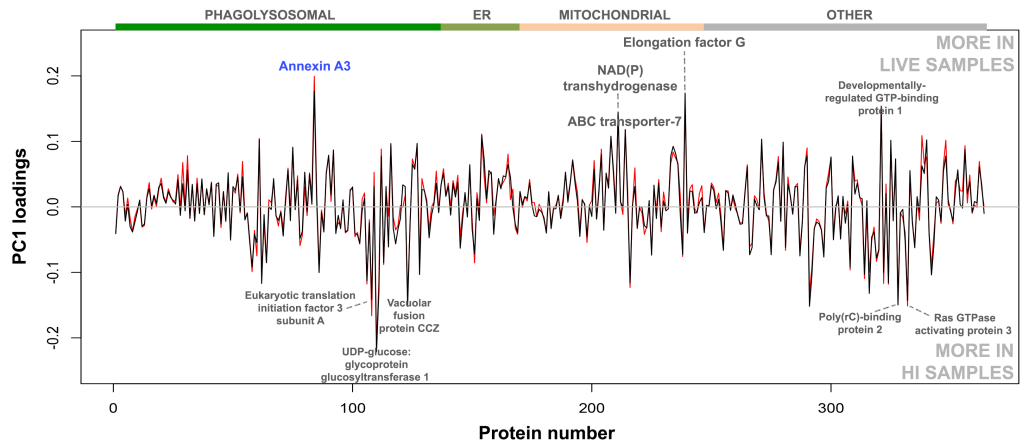
**Proteins represented by any number of peptides:**



**Proteins represented by  $\geq 2$  peptides:**



**Proteins represented by  $\geq 3$  peptides:**



**FIGURE 6.7. Several proteins disproportionately represented the variation seen between live and heat-inactivated (HI) parasite intracellular compartments.** The loadings for the first principal component (PC1) were plotted for each protein present in the samples, either using proteins represented by any number of peptides, or only those with at least 2 or 3 peptides. Lines indicate PC1 loadings from principal component analysis (black) and the first latent variable of partial least squares regression (red). The 5 top scoring proteins most represented in the live and HI samples for each graph are shown, along with the relative score for Annexin A3 for comparison.

**TABLE 6.2. Proteins (identified from either any number of peptides or at least 2 peptides) contributing to the greatest variation between the live and heat-inactivated parasite samples, as determined by principal component analysis (PCA). Partial least squares (PLS) loading scores and log<sub>2</sub> fold changes (FC) are also shown for each protein. Data shown to 2 decimal places. Black font = protein also in top 5 proteins contributing to differences seen in either live or HI samples as calculated by PLS; grey font = protein not found in top 5 proteins based on PLS.**

MORE REPRESENTED IN LIVE SAMPLE				MORE REPRESENTED IN HI SAMPLE			
PROTEIN	LOCATION AND FUNCTION	PCA/ PLS	LOG <sub>2</sub> FC	PROTEIN	LOCATION AND FUNCTION	PCA/ PLS	LOG <sub>2</sub> FC
<b>ANY NUMBER OF PEPTIDES:</b>							
Arachidonate 5-lipoxygenase - gj1886333	Cytoplasm / nucleus - catalyses leukotriene biosynthesis	0.13/ 0.16	6.78	Lamina-associated polypeptide 2 - gj1335849	Nucleus – involved in nuclear organisation	-0.13/ -0.16	-6.53
39S ribosomal protein L23, mitochondrial - gj16755352	Mitochondria – RNA binding / mitochondrial translation	0.13/ 0.16	4.31	Prenylcysteine oxidase - gj13385294	Lysosome / plasma membrane – degrades prenylated proteins	-0.12/ -0.15	-4.60
Probable 60S ribosomal protein L14 - gj12500362	Cytoplasm - translation	0.12/ 0.14	3.56	Isochorismatase domain-containing protein 1 - gj131541909	Peroxisome – catalytic activity	-0.12/ -0.13	-4.34
Actin-related protein 2/3 complex subunit 5-like protein - gj121312654	Cytoskeleton / cytoplasm - component of Arp2/3 complex, involved in regulation of actin polymerisation	0.12/ 0.13	3.76	Small nuclear ribonucleoprotein-associated protein N - gj14507135	Cytoplasm / nucleus – RNA binding / splicing	-0.11/ -0.13	-5.80
Protein S100-A11 - gj121886811	Cytoplasm / cytoskeleton - binds calcium ions, and helps regulate cell proliferation and control cytoskeleton assembly	0.12/ 0.12	4.18	Receptor-type tyrosine-protein phosphatase alpha - gj1198877	Membrane - protein tyrosine phosphatase activity	-0.11/ -0.12	-4.23
<b>AT LEAST 2 PEPTIDES:</b>							
Protein S100-A11 - gj121886811	Cytoplasm / cytoskeleton – binds calcium ions, and helps regulate cell proliferation and control cytoskeleton assembly	0.21/ 0.23	4.18	ATP-binding cassette sub-family F member 1 – gj139930335	Cytoplasm/nucleus – mRNA translation initiation	-0.19/ -0.20	-3.36
Extended synaptotagmin-2 – gj167782360	Plasma membrane / endoplasmic reticulum – found at sites where the ER and plasma membrane contact; involved in endocytosis and lipid transport	0.16/ 0.09	0.37	Zinc finger FYVE domain-containing protein 26 - gj126334653	Lysosome / cytoskeleton – metal ion / phosphatidylinositol-3-phosphate binding; plays a role in DNA repair	-0.19/ -0.16	-3.26
Acetoacetyl-CoA synthetase - gj121313520	Cytoplasm – ligase activity involved in fatty acid and lipid metabolism	0.15/ 0.14	2.84	Bifunctional purine biosynthesis protein PURH - gj112846177	Mitochondria – catalyst in purine biosynthesis	-0.15/ -0.12	-0.08
Lysosomal acid phosphatase - gj152871	Lysosome – acid phosphatase / hydrolase activity; plays a role in lysosome organisation	0.14/ 0.16	1.46	Phosphoenolpyruvate carboxykinase 2 - gj116307539	Mitochondria – catalyst in gluconeogenesis pathway	-0.14/ -0.10	-0.73
7-dehydrocholesterol reductase - gj16681179	Endoplasmic reticulum – involved in cholesterol biosynthesis	0.12/ 0.08	0.78	28S ribosomal protein S26 – gj146402169	Mitochondria – RNA binding / mitochondrial translation	-0.13/ -0.18	-2.49

**TABLE 6.3. Proteins (identified with 3 or more peptides) contributing to the greatest variation between the live and heat-inactivated parasite samples, as determined by PCA.** PLS loading scores and log<sub>2</sub> fold changes (FC) are also shown for each protein. Data shown to 2 decimal places. Black font = protein also in top 10 proteins contributing to differences seen in either live or HI samples as calculated by PLS; grey font = protein not found in top 10 proteins based on PLS.

MORE REPRESENTED IN LIVE SAMPLE				MORE REPRESENTED IN HI SAMPLE			
PROTEIN	LOCATION AND FUNCTION	PCA/ PLS	LOG <sub>2</sub> FC	PROTEIN	LOCATION AND FUNCTION	PCA/ PLS	LOG <sub>2</sub> FC
Annexin A3 - gj 2437840	Phagosome / cytoplasm / plasma membrane - inhibitor of phospholipase A2	0.20/ 0.18	0.49	UDP-glucose:glycoprotein glucosyltransferase 1 - gj 38566236	Phagosome / ER – a folding sensor in the calnexin/calreticulin quality control cycle; also involved in forming phagocytic cup	-0.21/ -0.22	-1.30
Elongation factor G, mitochondrial - gj 14285176	Mitochondria - GTPase	0.16/ 0.17	0.92	Eukaryotic translation initiation factor 3 subunit A - gj 1205976	Endosome / cytoplasm / nucleus – required for protein synthesis	-0.17/ -0.14	-0.56
Developmentally-regulated GTP-binding protein 1 - gj 6681225	Cytoplasm - regulates cell growth	0.15/ 0.15	0.85	Ras GTPase-activating protein 3 - gj 972944	Cytoplasm - inhibits the Ras-cyclic AMP pathway	-0.15/ -0.14	-0.81
NAD(P) transhydrogenase, mitochondrial - gj 840819	Mitochondria – functions as a proton pump; may play a role in ROS detoxification	0.14/ 0.14	0.44	Poly(rC)-binding protein 2 - gj 495128	Cytoplasm / nucleus – binds single-stranded nucleic acids	-0.14/ -0.15	-0.49
ABC transporter 7 - gj 1167982	Mitochondria – transport of haeme into the cytosol	0.12/ 0.11	0.66	Vacuolar fusion protein CCZ1 / Mon1b- gj 29244114	Lysosome – vesicle-mediated transport	-0.14/ -0.15	-0.47
Extended synaptotagmin-1 - gj 4200444	ER – binds glycerophospholipids and may be involved in lipid transport	0.11/ 0.11	0.68	Trifunctional enzyme subunit beta, mitochondrial - gj 21704100	Mitochondria – involved in fatty acid beta-oxidation	-0.12/ -0.12	-0.55
Heterogeneous nuclear ribonucleoproteins C1/C2 - gj 8393544	Nucleus – binds pre-mRNA	0.11/ 0.06	0.31	Splicing factor 3B subunit 3 - gj 19527174	Nucleus – involved in RNA binding and splicing	-0.12/ -0.12	-0.59
Peroxisomal multifunctional enzyme type 2 - gj 31982273	Mitochondria / peroxisome – acts on beta-oxidation pathway for fatty acids	0.11/ 0.10	0.74	CD180 antigen - gj 761712	Plasma membrane / phagosome- a TLR4 ligand mediating response to LPS	-0.11/ -0.11	-0.76
Beta-galactosidase - gj 22137334	Lysosome - hydrolyses beta-D-galactosides	0.10/ 0.10	0.52	Phenylalanine-tRNA ligase beta subunit - gj 4633656	Cytoplasm – protein biosynthesis	-0.12/ -0.10	-0.08
60S ribosomal protein L27a - gj 50321	Cytoplasm – binds RNA	0.10/ 0.08	0.40	Beta-hexosaminidase subunit beta - gj 6754186	Lysosome – degradation of GM2 gangliosides	-0.11/ -0.13	-0.69

with actin were also identified: Arp 2/3 complex subunit 5-like protein (gi|21312654), protein S100-A11 (gi|21886811) and annexin A3 (gi|2437840). Annexin A3 was found to be most important for separation when only proteins represented by at least 3 peptides were analysed. In addition, two proteins related to lysosome function (lysosomal acid phosphatase, gi|52871; beta-galactosidase, gi|22137334) were identified as being differentially expressed as well as a number of proteins relating to protein synthesis (39S ribosomal protein L23, gi|6755352; probable 60S ribosomal protein L14, gi|2500362; heterogeneous nuclear ribonucleoproteins C1/C2, gi|8393544; 60S ribosomal protein L27a, gi|50321), lipid metabolism/transport (acetoacetyl-CoA synthetase, gi|21313520; 7-dehydrocholesterol reductase, gi|6681179; extended synaptotagmin-1, gi|4200444) and enzymes and transporters traditionally associated with mitochondria (elongation factor G, gi|14285176; NAD(P) transhydrogenase, gi|840819; peroxisomal multifunctional enzyme type 2, gi|31982273).

There were also a number of proteins that were better represented in HI parasite-containing compartments, including a greater number of traditionally lysosomal-associated proteins such as vacuolar fusion protein Ccz1 (gi|29244114), prenylcysteine oxidase (gi|13385294), zinc finger FYVE domain-containing protein 26 (gi|26334653) and  $\beta$ -hexosaminidase subunit  $\beta$  (gi|6754186). The finding that  $\beta$ -hexosaminidase was differentially expressed in HI samples compared to live samples was interesting because a decrease in the activity of this enzyme with live parasites was found experimentally (see Section 5.3.2). The phagocytic protein UDP-glucose:glycoprotein glucosyltransferase 1 (gi|38566236), which is involved in forming the phagocytic cup, was more represented in HI samples along with RP105 (gi|761712) and eukaryotic translation initiation factor 3 subunit A (gi|1205976), both of which have an evidenced association with phagosomes (Moretti et al. 2010; Mantegazza et al. 2012). In addition, there were again proteins relating to protein synthesis (small nuclear ribonucleoprotein-associated protein N, gi|4507135; adenosine triphosphate (ATP)-binding cassette sub-family F member 1, gi|39930335; 28S ribosomal protein S26,

gi|46402169; poly(rC)-binding protein 2, gi|495128; slicing factor 3B subunit 3, gi|19527174; phenylalanine-tRNA ligase beta subunit, gi|4633656) and enzymes traditionally associated with mitochondria (bifunctional purine biosynthesis protein purH, gi|12846177; phosphoenolpyruvate carboxykinase 2, gi|16307539; trifunctional enzyme subunit beta, gi|21704100) identified as being differentially expressed between live and HI preparations.

Taken together, these data suggest parasite-containing compartments have complex compositions incorporating proteins that have not been traditionally associated with phagolysosomes.

### **6.3.5 Univariate comparisons between live- and heat-inactivated parasite-fed compartments**

The live- and HI compartments were also compared for individual proteins using two tailed, paired t tests on the values obtained for their peptide identifications. A total of 41 proteins with a statistically significant difference between the preparations were found. However, the large number of proteins in the datasets meant that there would be a high false discovery rate and therefore the Benjamini and Hochberg (1995) correction was applied and statistical significance re-tested. This reduced the number of statistically significant proteins to 19, as shown in **Table 6.4**. A statistically significant difference was found for LAMP2 and a subunit of vATPase (subunit d1) along with the lysosomal enzyme tripeptidyl peptidase 1. Two proteins from the ezrin, radixin and moesin (ERM) complex of proteins were also identified as being significantly different (radixin and moesin), both having higher expression in live samples. A number of endoplasmic reticulum proteins were also highlighted and, interestingly, there were also a number of histones in this list of proteins that were found to be significantly different.

The 22 proteins excluded by Benjamini and Hochberg correction included several lysosomal proteins:- type proton ATPase catalytic subunit B (gi|1184659;  $p = 0.015$ , higher in live),  $\beta$ -hexosaminidase subunit  $\beta$  (gi|6754186;  $p = 0.018$ , higher in HI), HSC70 (gi|13242237,  $p = 0.022$ , higher

**TABLE 6.4. Individual proteins with statistically significant differences between live and heat-inactivated (HI) parasite-fed compartments.** Paired T tests were performed for each protein, using multiple peptide data if the protein was represented by more than one peptide. Log<sub>2</sub> fold changes are also shown for each protein. Greyed out text indicates proteins that have a significant difference when checked by paired t test but not by Mann-Whitney U test. \* p < 0.05; \*\* p < 0.01; \*\*\* p < 0.001.

PROTEIN	SIGNIFICANT AFTER BENJAMINI-HOCHBERG CORRECTION	SAMPLE HIGHER IN	LOG <sub>2</sub> FOLD CHANGE	PAIRED T TEST P VALUE			MANN WHITNEY P-VALUE		LOCATION AND FUNCTION
				Exp. 1-3	Exp. 1	Exp. 2	Exp. 3	P-VALUE	
Histone H2B type 1-P - gj 556310		HI	-0.38	***	**	0.11	**	***	Nucleus – transcription regulation / DNA repair
Histone H4 - gj 4504301		HI	-0.52	***	**	***	***	***	Nucleus - transcription regulation / DNA repair
Histone H3.2 - gj 51301		HI	-0.66	***	***	**	***	***	Nucleus - transcription regulation / DNA repair
V-type proton ATPase subunit d 1 - gj 3955100		Live	0.24	***	0.76	*	0.59	**	Endosome/lysosome – acidifies the compartment
Radixin - gj 4388775		Live	0.54	**	*	*	0.36	***	Endosome/lysosomes – binds actin to endosomes and lysosomes.
BIP / 78kDa glucose-regulated protein - gj 2598562		Live	0.24	**	0.09	0.05	0.62	**	ER – likely helps with multimeric protein assembly
Protein disulfide-isomerase - gj 54777		Live	0.29	**	*	***	0.52	***	ER – catalyses the reformation of disulphide bonds
60S ribosomal protein L30 - gj 4506631		Live	0.45	**	*	0.50	0.16	0.09	Cytoplasm/nucleus – RNA binding
Endoplasmic / Hsp90b1 - gj 6755863		Live	0.18	**	0.45	0.12	0.14	*	ER – processes and transports secreted proteins
Tubulin alpha-1B chain - gj 34740335		Live	0.23	**	0.32	*	0.13	*	Cytoplasm – a major constituent of microtubules
Tripeptidyl peptidase 1 - gj 3766471		Live	0.21	**	**	*	0.46	**	Lysosome – a serine protease
Annexin A2 - gj 6996913		Live	0.16	**	*	*	0.85	***	Endosome/lysosome – involved in early to late endosome transport
60S ribosomal protein L12 - gj 398048		Live	0.21	**	0.22	0.07	0.13	**	Cytoplasm – binds to ribosomal RNA
Lamp2 - gj 12848716		HI	-0.09	**	0.10	0.38	0.71	*	Late endosome / lysosome – may help protect the lysosomal membrane from autolysis and helps to maintain an acidic environment
Protein disulfide-isomerase A4 - gj 49728		Live	0.33	**	0.29	0.03	0.17	*	ER – catalyses the rearrangement of SS bonds in proteins
Oligosaccharyltransferase - gj 2662377		Live	0.31	**	0.61	0.11	0.98	*	ER – catalyses high mannose oligosaccharide transfer
Msn protein - gj 116283288		Live	0.35	*	*	0.07	0.50	**	Cytoplasm – unknown
Cytochrome c oxidase subunit 6C - gj 16716343		Live	0.57	*	0.33	0.11	0.21	1	Mitochondria – terminal oxidase in mitochondrial electron transport
Histone H2A.V - gj 74207672		HI	-0.47	*	**	0.20	0.89	***	Nucleus - transcription regulation / DNA repair

in HI),  $\beta$ -galactosidase (gi|22137334,  $p = 0.026$ , higher in live), Ras-related protein Rap-1A (gi|4506413,  $p = 0.038$ , higher in live), and vacuolar protein sorting (Vps) 11 (gi|16740774,  $p = 0.048$ , higher in HI). Several of the excluded proteins were also involved in manipulating the actin cytoskeleton: coronin-1A (gi|4895037,  $p = 0.039$ , higher in live), T-complex protein 1 subunit  $\delta$  (gi|460317,  $p = 0.039$ , higher in HI), macrophage-capping protein / capg (gi|53018,  $p = 0.043$ , higher in live), myosin 9 (gi|17978023,  $p = 0.044$ , higher in HI), and cofilin-1 (gi|6680924,  $p = 0.046$ , higher in live). The former of these proteins was of interest because there is evidence to suggest that coronin-1A can inhibit fusion between phagosomes and lysosomes (Ferrari et al. 1999).

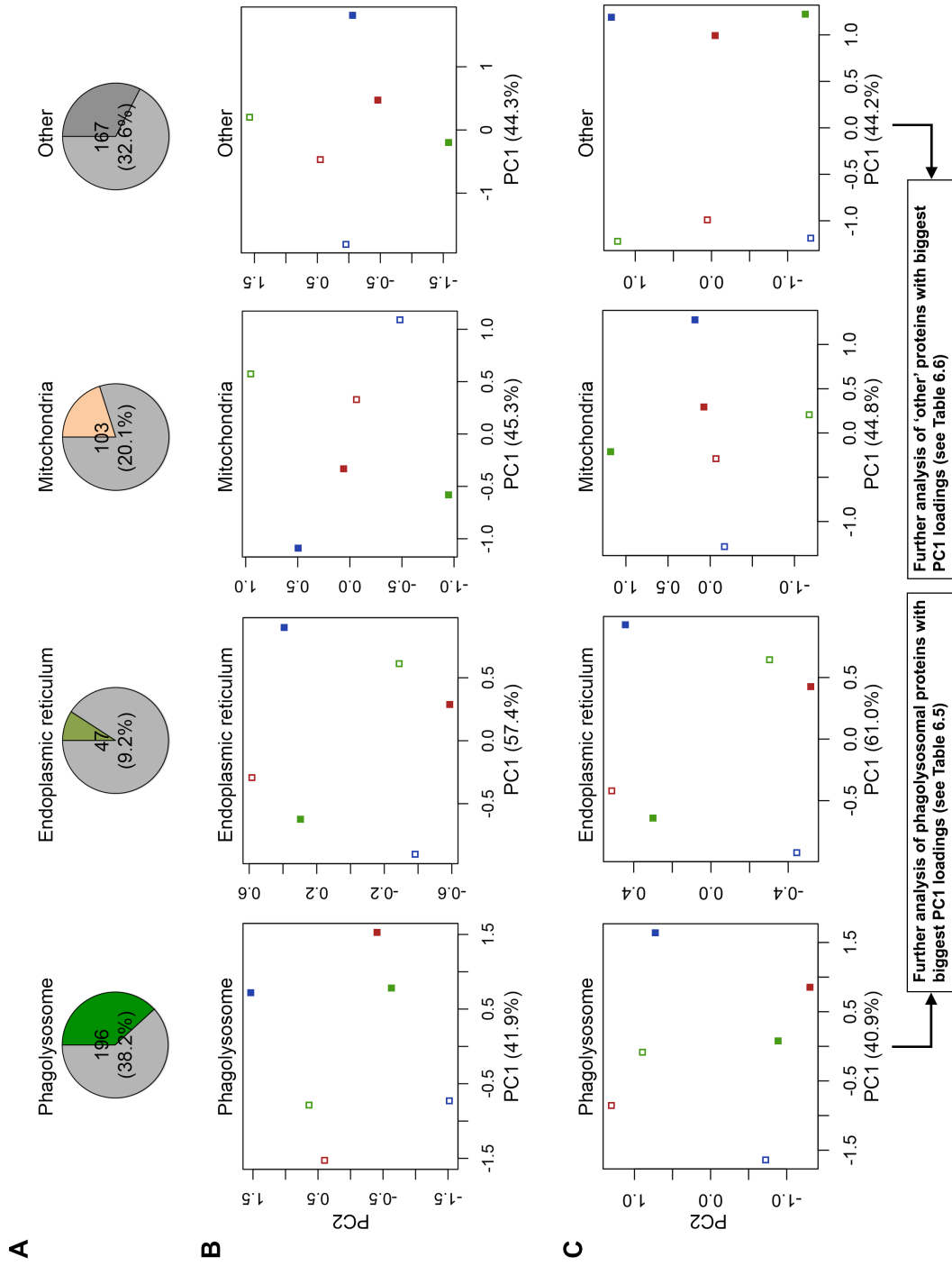
Although t-tests are quite robust to slightly skewed data, they can be affected by outliers, which we cannot rule out in the current proteomic dataset. Each protein shown to be significantly different by t-test was re-tested using the Mann-Whitney U test and the p values shown in **Table 6.4**. Reassuringly, all of the proteins that were originally shown to be statistically significant via paired t-tests were also significant using the Mann-Whitney U test, with the exception of cytochrome c oxidase subunit 6C (gi|16716343) for which there were only 3 peptide identifications, lower than the threshold needed for a test to be performed.

### **6.3.6 Analysing proteins based on subcellular location**

PCA of all proteins showed clear differentiation between live and HI preparations along PC1 meaning that the greatest source of variation between the samples was due to the parasite being alive or HI. The next question was whether this differentiation would exist when only proteins within a particular subcellular location were analysed, with the hypothesis that the greatest differences would be seen for the phagolysosomal fraction. The four subcellular categories (phagolysosomal, mitochondrial, endoplasmic reticulum and 'other') were analysed separately for all proteins represented by at least 2 peptides. The number of proteins identified for each subcellular fraction is shown in **Figure 6.8A** with the corresponding PCA plots shown in



**FIGURE 6.8. There was greater differentiation between samples when phagolysosomal and 'other' proteins were explored separately.** **A** The proportion of proteins identified as being localised to a particular subcellular location. **B** Organelle-specific proteins were extracted and analysed using principal component analysis (PCA). **C** To reduce the probability of an individual subcellular fraction being influenced by proteins from another fraction, proteins were re-normalised after extraction. Only proteins represented by at least 2 peptides were used for these analyses. Red = experiment 1, blue = experiment 2, green = experiment 3; closed boxes = live samples, open boxes = heat-inactivated samples. Percentage of variance accounted for with each principal component (PC) is shown in parentheses.



**Figure 6.8B.** Differentiation along PC1 can be seen for the phagolysosomal and mitochondrial fractions, and partially for proteins labelled as 'other'. Of particular significance, there was no such separation for proteins traditionally associated with the endoplasmic reticulum suggesting that this group of proteins was unaffected by the live parasite.

There was considerable inter-organelle dependency due to the normalisation process; a reduction for phagolysosomal proteins would need to be compensated for by proteins associated with other organelles in order to maintain the same total reporter ion intensity for an individual sample. To determine whether the normalisation process had introduced artifacts, proteins were normalised within each subcellular organelle and re-analysed. Raw peptide-level data were extracted from the dataset and normalised so that the total reporter ion intensity within a subcellular organelle was the same for each sample and PCA performed with each subset of data. Interestingly, as shown in **Figure 6.8C**, this had the effect of lowering the differentiation seen along PC1 for the phagolysosomal fraction but drastically increased it for the 'other' fraction.

The proteins that contributed the most to the differentiation along PC1 are shown in **Table 6.5** (for phagolysosomal proteins) and **Table 6.6** (for 'other' proteins). Encouragingly, many of the same proteins previously identified were still seen as the most differentially represented here. For example, protein S100-A11 still contributed most to PC1 for phagolysosomal proteins.

### **6.3.7 Global characterisation of the parasite-containing compartment**

When analysing these large proteomic datasets, it was important to study changes in the representation of individual proteins to ascertain whether any proteins were specifically targeted and actively manipulated by the parasite. The machine-learning techniques that we progressed on to after could unravel changes in groups of proteins considering the data as a whole. However, as the last step in proteomic analysis workflows suggested by

**TABLE 6.5. Phagolysosomal-specific proteins (identified with  $\geq 2$  peptides) contributing to the greatest variation between the live and heat-inactivated parasite samples, as determined by PCA. PLS loading scores and  $\log_2$  fold changes (FC) are also shown for each protein. Data shown to 2 decimal places. Black font = protein also in top 10 proteins contributing to differences seen in either live or HI samples as calculated by PLS; grey font = protein not found in top 10 proteins based on PLS.**

MORE REPRESENTED IN LIVE SAMPLE				MORE REPRESENTED IN HI SAMPLE			
PROTEIN	LOCATION AND FUNCTION	PCA/ PLS	LOG <sub>2</sub> FC	PROTEIN	LOCATION AND FUNCTION	PCA/ PLS	LOG <sub>2</sub> FC
Protein S100-A11 – gij 21886811	Cytoplasm / cytoskeleton – binds calcium ions, and helps regulate cell proliferation and control cytoskeleton assembly	0.31/ 0.35	4.13	Zinc finger FYVE domain-containing protein 26 - gij 263334653	Lysosome / cytoskeleton – metal ion / phosphatidylinositol-3-phosphate binding; plays a role in DNA repair	-0.31/ -0.26	-3.00
Lysosomal acid phosphatase - gj 52871	Lysosome – acid phosphatase / hydrolase activity; plays a role in lysosome organisation	0.24/ 0.25	1.51	UDP-glucose:glycoprotein glucosyltransferase 1 - gij 38566236	Phagosome / ER – a folding sensor in the calnexin/calreticulin quality control cycle; also involved in forming phagocytic cup	-0.19/ -0.23	-1.04
Ap-3 complex beta3A subunit - gj 3885988	Endosome / lysosome / trans-Golgi network – plays a role in protein sorting of transmembrane proteins targeted to the lysosome	0.20/ 0.21	2.98	Eukaryotic translation initiation factor 3 subunit A - gj 1205976	Endosome / cytoplasm / nucleus – required for protein synthesis	-0.15/ -0.13	-0.61
Annexin A3 – gj 2437840	Phagosome / plasma membrane / cytoplasm – phospholipase A2 inhibitor	0.18/ 0.16	0.32	Vacuolar fusion protein CCZ1 / Mon1b- gj 29244114	Lysosome – vesicle-mediated transport	-0.13/ -0.17	-0.52
Rab GDP dissociation inhibitor beta – gj 12841706	Endosome / plasma membrane / cytoplasm / Golgi – inhibits the dissociation of GDP from Rabs	0.17/ 0.15	1.19	Protein S100-A4 – gij 33859624	Cytoskeleton, cytosol, nucleus – binds calcium ions; reported to bind to actin filaments (Watanabe <i>et al.</i> , 1993).	-0.10/ -0.13	-0.97
Syntaxin 12 – gj 14715019	Endosome / Golgi - SNARE protein that regulates transport between late endosomes and trans-Golgi network	0.16/ 0.10	0.11	CD180 antigen - gj 761712	Plasma membrane / phagosome- a TLR4 ligand mediating response to LPS	-0.09/ -0.11	-0.61
Annexin A7 – gj 293294	Phagosome / plasma membrane / ER / nucleus - promotes membrane fusion, binds calcium/phospholipid; may inhibit phagosome fusion (Rogers <i>et al.</i> , 2007)	0.16/ 0.14	0.41	Ras-related protein Rab31 – gij 26341846	Early endosome / phagosome / trans-Golgi network – regulator of intracellular trafficking, has a role in the maturation of phagosomes containing pathogens	-0.09/ -0.09	-0.33
Rgs19 – gj 12834947	Endosome – GTPase-activating protein of the Gai subfamily (Berman <i>et al.</i> , 1996)	0.15/ 0.13	0.65	Ras-related protein Rap2c – gij 27369539	Recycling endosome / plasma membrane / cytosol – GTP-binding protein that may play a role in cytoskeletal rearrangements	-0.09/ -0.09	-0.19
H(+)/Cl(-) exchange transporter 7 – gj 6753436	Lysosome – voltage-gated chloride channel	0.12/ 0.09	0.86	Beta-hexosaminidase subunit beta - gj 6754186	Lysosome – degradation of GM2 gangliosides	-0.08/ -0.13	-0.86
Actin-related protein 3 – gij 5031573	Cytoskeleton / plasma membrane / cytosol – regulates actin polymerisation	0.12/ 0.10	0.80	T-complex protein 1 subunit delta – gj 460317	Cytoskeleton / cytoplasm – interacts with actin where it helps with actin folding	-0.08/ -0.11	-0.64

**TABLE 6.6. Proteins (identified with  $\geq 2$  peptides) categorised as ‘other’ for subcellular localisation contributing to the greatest variation between the live and heat-inactivated parasite samples, as determined by PCA. PLS loading scores and  $\log_2$  fold changes (FC) are also shown for each protein. Data shown to 2 decimal places. Black font = protein also in top 10 proteins contributing to differences seen in either live or HI samples as calculated by PLS; grey font = protein not found in top 10 proteins based on PLS.**

MORE REPRESENTED IN LIVE SAMPLE				MORE REPRESENTED IN HI SAMPLE			
PROTEIN	LOCATION AND FUNCTION	PCA/ PLS	LOG <sub>2</sub> FC	PROTEIN	LOCATION AND FUNCTION	PCA/ PLS	LOG <sub>2</sub> FC
Acetoacetyl-CoA synthetase - gjl21313520	Cytoplasm – ligase activity involved in fatty acid and lipid metabolism	0.17/ 0.17	2.58	ATP-binding cassette sub- family F member 1 – gjl39930335	Cytoplasm / nucleus – mRNA translation initiation	-0.30/ -0.30	-3.78
Transmembrane and TPR repeat-containing protein 3 – gjl26336877	Plasma membrane – involved in cell differentiation and development	0.13/ 0.13	0.31	DNA topoisomerase II – gjl220616	Nucleus – transiently breaks and rejoins DNA strands	-0.21/ -0.21	-1.61
Peptidyl-prolyl cis-trans isomerase – gjl12849271	Cytoplasm / nucleus - involved in protein folding	0.12/ 0.12	0.77	Phosphoglycerate mutase 2 – gjl9256624	Cytoplasm / nucleus – enzyme involved in glycolysis	-0.19/ -0.19	-0.92
Developmentally-regulated GTP-binding protein 1 - gjl6681225	Cytoplasm - regulates cell growth	0.11/ 0.10	0.53	Poly(rC)-binding protein 2 – gjl495128	Cytoplasm / nucleus – binds single- stranded nucleic acids	-0.17/ -0.17	-0.66
mCG141705 – gjl148665297	Unknown	0.09/ 0.09	0.71	Ras GTPase-activating protein 3 – gjl972944	Plasma membrane – GTPase activation	-0.16/ -0.16	-1.19
Importin subunit alpha-1 – gjl555823	Cytoplasm / nucleus – protein import into nucleus	0.08/ 0.08	-0.19	Oligosaccharyltransferase complex subunit OSTC – gjl13384930	Plasma membrane – enzymatic activity	-0.15/ -0.16	-1.04
ATPase / 26S protease regulatory subunit 6B – gjl1196528	Cytoplasm / nucleus – involved in ATP- dependent degradation of ubiquitinated proteins	0.07/ 0.06	0.42	60S ribosomal protein L31 – 4506633	Cytoplasm / membrane – binds to RNA	-0.15/ -0.15	-0.62
60S ribosomal protein L24 – gjl4506619	Cytoplasm / membrane – binds to RNA	0.06/ 0.06	0.07	Splicing factor 3B subunit 3 – gjl19527174	Nucleus – processes mRNA	-0.14/ -0.14	-0.82
60S ribosomal protein L13a – gjl31981945	Cytoplasm / nucleus / membrane – binds to RNA	0.06/ 0.06	0.51	Ribosomal protein L18 – gjl398050	Cytoplasm / nucleus / membrane – binds to RNA	-0.14/ -0.14	-0.86
60S ribosomal protein L30 – gjl4506631	Cytoplasm / nucleus / membrane – binds to RNA	0.06/ 0.06	0.16	Histone H3.2 – gjl51301	Nucleus – component of the nucleosome, binds DNA	-0.14/ -0.14	-1.06

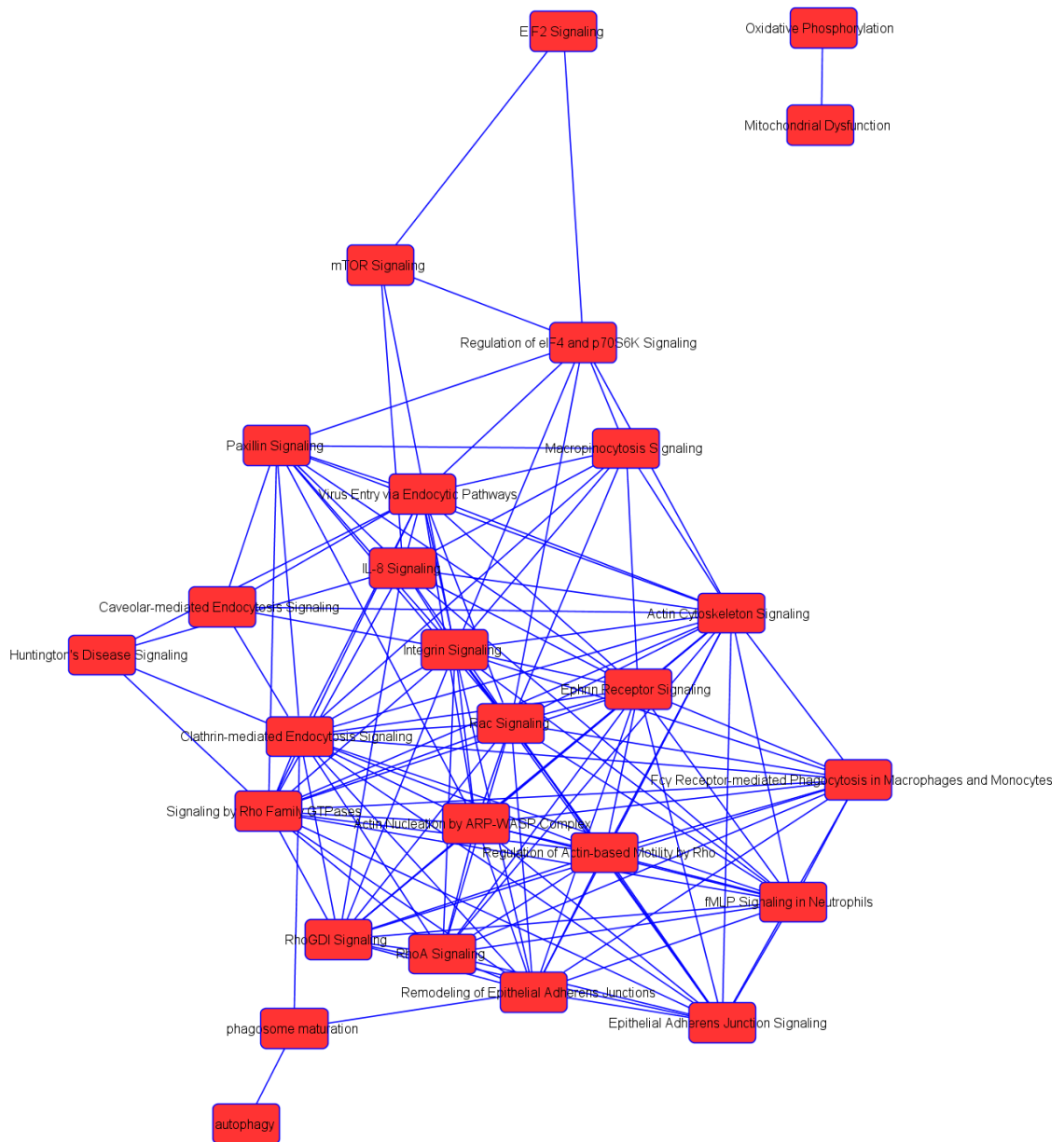
Karimpour-Fard et al. (2015), it was also important to take a global perspective on the data to assess the potentially more subtle effect that live parasites may have on groups of related proteins in protein complexes, biological networks and established canonical pathways.

#### **6.3.7.1 IPA analysis of proteins**

Initially IPA was used to look for well-represented canonical pathways within the overall proteomic dataset, regardless of individual protein expression levels. The entire mouse protein dataset was imported into IPA and, by exploiting extensive information maintained in the IPKB, right-tailed Fisher's exact tests were performed to determine whether a set of proteins related to a particular pathway were due to random chance or not. This analysis takes into consideration the number of proteins known to be in that pathway, the number of proteins present in the proteomic dataset relating to that pathway, and the total number of proteins within the sample. Thus, the more proteins present in the proteomic dataset relating to a particular pathway, the more statistically significant that over-representation becomes. IPA can use the overlap between these canonical pathways to determine whether there were pathway clusters within a dataset, thereby suggesting overall pathway themes. In the analysis of proteins present within isolated parasite-containing compartments, a number of interconnected themes arose: endocytosis/phagocytosis, actin cytoskeleton regulation, protein translation, and metabolism, as shown in **Figure 6.9**.

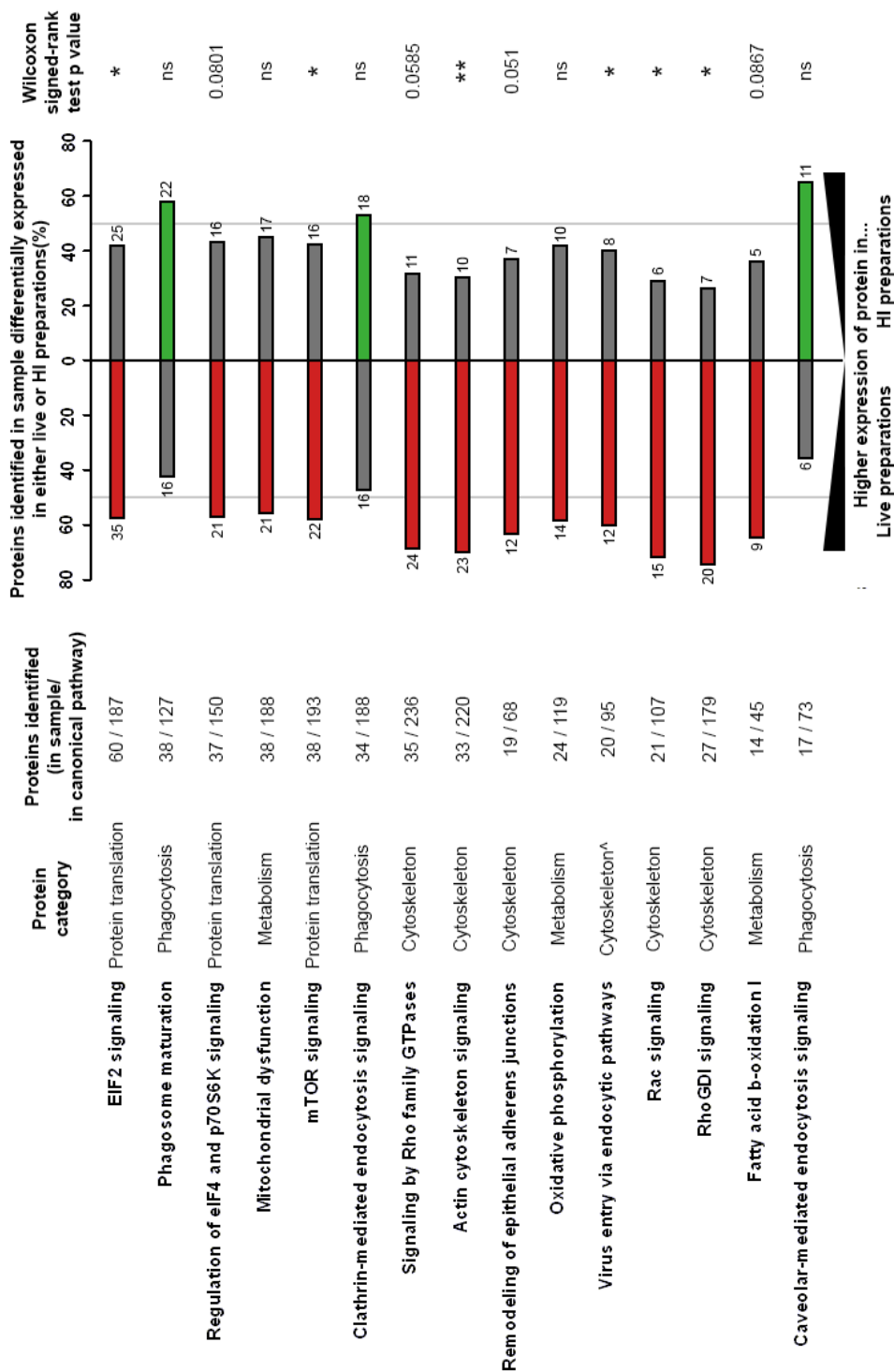
#### **6.3.7.2 Differentially expressed canonical pathways**

When quantitative data were added for each identified protein, a number of differentially expressed pathways were found using IPA as shown in **Figure 6.10**. The figure was constructed by taking the 15 best-represented pathways identified within the dataset (as determined using Fisher's exact test); the representation of all of these pathways was highly statistically significant ( $p < 0.001$ ). For each of these canonical pathways, the number of proteins that were preferentially found in either the live or HI sample was calculated. Where the number preferentially expressed in the live sample exceeded that in the HI sample, the bar indicating the number of proteins is coloured red,



**FIGURE 6.9. A number of interconnected canonical pathways were represented within the parasite-containing compartment samples. The overlapping canonical pathway analysis feature was used in IPA to generate an interconnected network of canonical pathways that share the same proteins.**

**FIGURE 6.10. Protein groups relating to phagocytosis, cytoskeleton signalling, protein translation and metabolism were well represented and differentially expressed between live and HI parasite-containing compartments. Canonical pathways produced in IPA were ordered by Fisher's exact test p value and identified proteins within each of these pathways were then checked for a preference for live- or HI-compartments. Red bar = pathway found more in live samples; green bar = pathway found more in HI samples. Wilcoxon signed-rank test was used to check significance. \* p < 0.05; \*\* p < 0.01; ^Although labelled as endocytosis, the identified proteins in this group were all related to the cytoskeleton.**

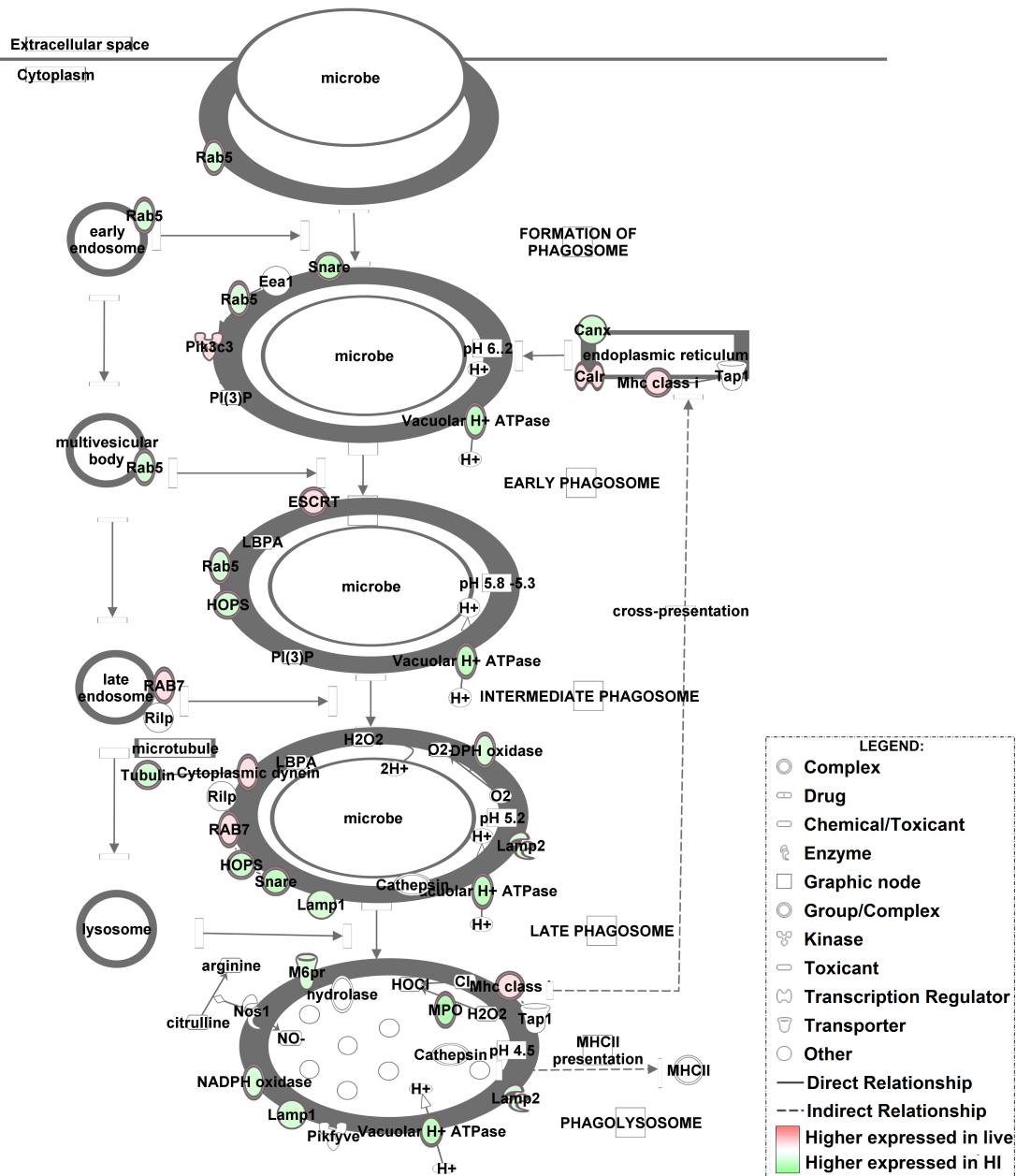


when the converse is true, the bar is coloured green. It was immediately obvious that all pathways strongly related to phagocytosis were better represented in the HI samples. This reinforced experimental observations and the results of the analyses described earlier. The pathways relating to the actin cytoskeleton, metabolism and protein translation were all preferentially expressed in live samples, with pathways relating to cytoskeletal dynamics among the most differentially expressed. The significance of this was tested by performing non-parametric Wilcoxon signed-rank tests on the data imported into IPA and it was found that a number of these pathways had statistically significant differential expression between preparations with the pathway relating to actin cytoskeleton signalling having the most significant difference ( $p = 0.0014$ ). Perhaps the most relevant pathway and one of the best represented in terms of protein coverage was that for phagosome maturation, as shown in **Figure 6.11**. As previously stated, a number of proteins were found to have lower representation in live samples, including lysosomal proteins LAMP1 and LAMP2, and this is reflected in this pathway analysis with other lysosomal proteins having overall lower expression in live preparations, such as vATPase and myeloperoxidase.

### **6.3.8 Relevant dynamic protein networks**

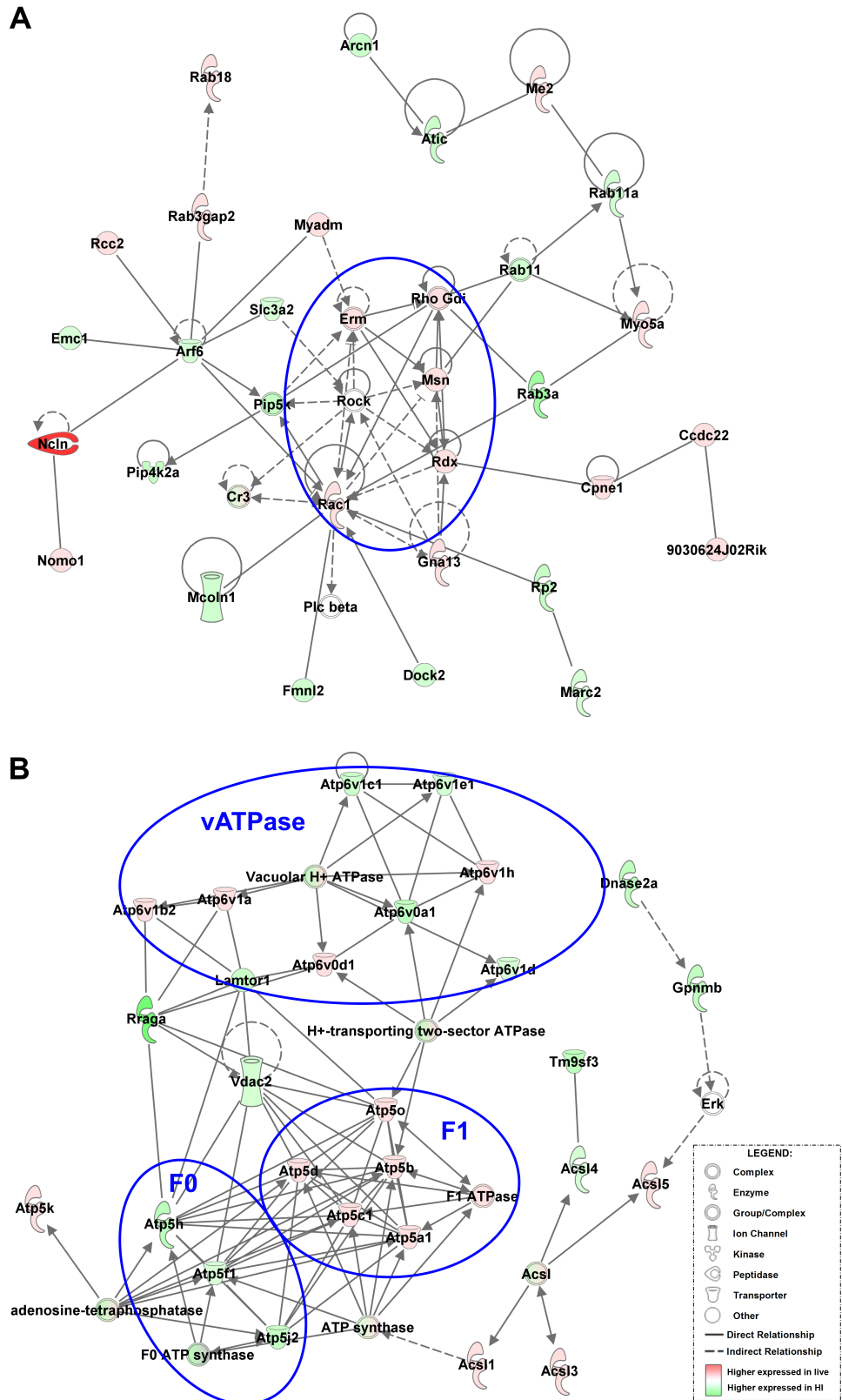
IPA uses known interactions listed in the IPKB to generate dynamic, interconnected networks that are not restricted to well established canonical pathways and often incorporate multiple subcellular locations. IPA generated protein networks as detailed in Section 6.2.3 and the highest scoring 25 networks were outputted. Importantly, the score assigned to a particular network does not reflect its biological relevance to a specific scientific question, nor does it make inferences on the network's quality. However, it is a useful tool to aid additional exploratory analyses and provide evidence for differential expression of interconnected protein groups. The top two scoring networks constructed were related to ribosomal proteins and protein translation. Network 3 had a number of nuclear proteins, such as histones, splicing factors and DNA topoisomerases, whereas network 4 was an eclectic mix of cytoskeletal and nuclear proteins. The highest scoring network





**FIGURE 6.11. Proteins related to phagosome maturation had lower expression in live parasite-containing compartment samples.** Diagram generated in IPA for the canonical pathway related to phagosome maturation, showing proteins represented by at least 2 peptides with no expression cut-off selected.

for the process of phagocytosis ('network 6') was related to cytoskeletal dynamics and is shown in **Figure 6.12A**. As well as radixin and moesin, which were already identified by t-tests as having a statistically significant difference between the conditions, a number of interacting proteins, such as copine 1, were also found to be increased in live samples. Another relevant network was 'network 9' (**Figure 6.12B**), which represented the interactions between several lysosomal and mitochondrial transporter proteins. The ten top scoring networks (excluding networks 6 and 9) are shown in **Appendix C**.



**FIGURE 6.12. The two most biologically relevant networks generated by IPA were related to actin cytoskeletal dynamics and transporters. A)** “Network 6” had several proteins that related to actin cytoskeletal dynamics, with the blue circle indicating a core of ERM proteins interacting with Rac1 and Rho signalling pathways. **B)** “Network 9” represented the interactions between several lysosomal and mitochondrial transporter proteins, with particularly relevant protein groups circled in blue. Proteins shown using their gene name.

## 6.4 Chapter-specific discussion

Our present understanding of how *Leishmania* parasites are able to survive in hostile phagolysosomes is hampered by a lack of information on the composition of this compartment. Furthermore, whether the parasite is actively manipulating the protein composition to aid its intracellular survival is currently unknown. Using iTRAQ-labelled quantitative LC-MS/MS, the present study has produced quantitative data for the proteins making up the intracellular *L. donovani*-containing compartment. By comparing phagolysosomal samples generated by feeding J774.2 cells either live or HI parasites, a number of protein groups, pathways and networks showing differential expression have been identified. Notably, these analyses have suggested that proteins involved in actin cytoskeletal manipulation and phagosome maturation may be actively manipulated by the live parasite.

Compared to the qualitative proteomic analyses detailed in Section 5.3.2, iTRAQ-labelled LC-MS/MS identified between 11.0 – 37.8% fewer proteins. This was expected and has been seen in other similar studies where labelled and unlabelled approaches were compared (Wang et al. 2012). There were two main reasons for this decrease in identifications: (i) there were additional steps involved in processing for iTRAQ-labelled proteomics, including labelling and desalting steps, and buffer exchange into an iTRAQ compatible buffer; (ii) as all samples were processed together in a single LC-MS/MS run, proteins specific to individual samples were diluted (Wang et al. 2012). With improving technologies, the number of proteins identified in association with the phagosome has steadily increased with some studies now finding over 2500 different proteins associated with the compartment (Guo et al. 2015). Although the number of proteins identified in this study was less than this, the use of a real pathogenic microorganism introduces increasing complexity into the methodology. Furthermore, the presence of proteins specific to *Leishmania* would dilute the murine specific proteins that we were interested in. When the proteins identified by Goyette et al. (2012) were checked using our curated lists of subcellular localisation, it was found that 38.8% of the

proteins had an evidence-based localisation to the phagolysosome; again, this is similar to the 38.2% found in the present study. Furthermore, the vast majority of proteins that had been previously associated with the parasite-containing compartment (Lang et al. 1994; Courret et al. 2002; Liévin-Le Moal & Loiseau 2016; and see Figure 1.5) were identified within the iTRAQ-labelled LC-MS/MS dataset.

Confident that iTRAQ-labelled LC-MS/MS had identified target proteins of interest, we progressed to further characterisation of the dataset. A three-pronged approach to data analysis, involving initial data observation, univariate and multivariate analyses, followed by pathway and network analyses, has been suggested (Karimpour-Fard et al. 2015) and this guided our proteomic analyses. The method of data pre-processing was chosen so that all proteins had an opportunity to influence the results, regardless of their overall abundance. Another common method in proteomic analyses is to normalise the data against a “house-keeping” protein, often actin (Griffin et al. 2010). However, for this study we decided not to take this approach since we were performing LC-MS/MS on subcellular compartments rather than whole cell preparations. In addition, we did not know what protein groups would be affected by the live parasite; it was later found that actin-related proteins were different between live and HI parasite preparations, which would have been missed had actin been used for data normalisation. After data pre-processing, the first stage of analysis was an initial exploration of the data; for this purpose, we chose the unsupervised techniques of HCA and PCA. These methods quickly identified sample 4 as an outlier sample that accounted for the most amount of variation seen within the dataset. This was the sample that was used to produce preliminary proteomics sample C (see Section 5.3.2) and therefore had pre-LC-MS/MS processing performed separately from the other samples. In contrast, the other three samples (HI/L1-3) were processed for mass spectrometry analysis at the same time. This highlights the experimental variation that can be introduced during pre-LC/MS-MS processing.

The exclusion of sample 4 from most analyses meant that this sample could be used for test data to validate the PLS. As the sample used to test the model was the most different compared to the other samples, we were making it harder for the model to correctly classify the data. However, we did not want to remove other samples from the model since we only had 4 replicates for each condition. Furthermore, it meant that we had more confidence that any proteins that were identified in PLS analyses were truly differentially expressed between the two samples, since we had made it harder for the model to identify these proteins. After sample 4 was removed, the samples divided into live and HI preparations both for PCA and HCA demonstrating that the biggest cause of variation was whether the preparation was from live or HI parasites. After initial exploration, PLS was used and univariate analyses were performed and confirmed many of the protein groups revealed by PCA. This was combined with pathway and network generation to get a global overview of the changes between the two preparations. IPA was chosen because it is widely regarded as having one of the most expansive databases of experimentally evidenced protein-protein interactions and has been used in many published proteomics studies. However, although there are examples of subcellular proteomic analyses using IPA in the literature (e.g. Yang et al. 2010), IPA is most often used for transcriptomic or proteomic datasets derived from whole cells or tissues rather than subcellular compartments. Another potential limitation with IPA is that the software was developed with an initial focus on cancer and drug discovery meaning that some pathways, for example that for phagosome maturation, may be relatively underrepresented compared to the large numbers of proteins likely to be found in these pathways (Griffiths & Mayorga 2007; Goyette et al. 2012). Regardless, the canonical pathways and networks identified by IPA had broadly similar themes compared to the protein groups identified from uni- and multi-variate analyses giving us confidence in the pathways identified. Together, these analyses revealed two strong features of the dataset: (i) there was actin cytoskeletal manipulation in live parasite preparations; (ii) there was altered phagosomal maturation in live parasite preparations.

For actin cytoskeletal manipulation, pathway analyses using IPA demonstrated that a number of cytoskeletal-related pathways were up-regulated in live parasite preparations. This was supported by findings from uni- and multivariate analyses that found actin-related proteins to be differentially expressed, with higher expression in live samples. For example, the proteins moesin and radixin, part of the ERM complex, were both found to have a statistically significant difference between live and HI preparations, as shown by t-tests. ERM proteins have a diverse range of functions involved in the recruitment, support, organisation and binding of F-actin (Fehon et al. 2010). Although these proteins have not previously been investigated in the context of *Leishmania* infection, they have been shown to play crucial roles during other infections. For example, during *Listeria monocytogenes* infection ezrin and radixin were found to localise around bacteria and along cellular protrusions (Temm-Grove et al. 1994). They suggested that ezrin and radixin might play a role in initiating the formation of surface protrusions that could help to infect adjacent cells. When coupled with the high-resolution time-lapse microscopy from Real et al. (2014) showing LAMP1+ve cellular protrusions transferring *Leishmania* parasites between cells, it is tempting to suggest that a similar ERM-mediated process may occur during infection with live *Leishmania* amastigotes. However, further experimental investigation into the roles these proteins play during *Leishmania* infection is necessary.

Rho/Rac proteins are part of the Ras superfamily of GTP hydrolases. Although implicated in a diverse array of cellular functions, they are perhaps best known for their roles in controlling cytoskeletal events (Bustelo et al. 2007). Rho GDP-dissociation inhibitors (RhoGDIs) play an important role in regulating these proteins and help maintain GTPases in an inactive state. Signalling components for Rho, Rac and RhoGDI pathways were all found significantly represented within the phagosomal proteomic dataset and were all increased in live parasite preparations. Network analyses also highlighted that ERM proteins interact extensively with Rac1, which was found to have a trend towards being higher expressed in live preparations, albeit not significant at the 95% confidence level. Rac1 has previously been shown to aid in non-opsonised *L. donovani* amastigote phagocytosis (Lodge &

Descoteaux 2006), which can avoid nicotinamide adenine dinucleotide phosphate (NADPH) oxidase activation and the resulting superoxide production. The parasites used in this study were from RAG1<sup>-/-</sup> mice lacking antibody-producing B cells; in addition, HI FCS was used throughout experiments meaning that complement would be absent and that the parasites used for this study would also be non-opsonised and likely enter the cell using similar mechanisms as to those described by Lodge & Descoteaux (2006). Interestingly, they found that Rac1 was able to associate with the parasite-containing compartment (Lodge & Descoteaux 2006), making it not surprising that this protein has been identified in the current proteomic dataset. However, this is the first time that the live parasite has been implicated in manipulating this pathway and the shift in this Rac1 signalling cascade could offer one explanation for the reduced nitric oxide production seen with live amastigote parasites, as shown in previous results in Chapter 5.

As another member of the Rho/Rac protein superfamily, components of Rho family GTPase signalling pathways were also differentially expressed in live *L. donovani* containing phagosomes. Rho family GTPases have previously been shown to play a crucial role in regulating phagocytosis during infection processes (Werner 2004), and they have also been shown to interact with ERM proteins (Fehon et al. 2010). They play a key role in regulating a number of dynamic cellular processes involving the actin cytoskeleton, such as morphogenesis, phagocytosis and cell migration (Fehon et al. 2010). They have also been directly linked to the uptake of *Leishmania* parasites, although for the promastigote form of the parasite (Lodge & Descoteaux 2005).

Protein S100-A11, a member of the S100 protein family, was found to be one of the most differentially expressed proteins in this study, as shown through PCA and PLS. This protein interacts principally with annexin A1 to form a Ca<sup>2+</sup> sensing system, although interactions with annexin A2 are likely (Rintala-Dempsey et al. 2006). In the current study, annexin A2, which binds to actin and interacts with the plasma membrane (reviewed by Grieve et al.



2012), was also found to have a statistically significant increase in its expression for live parasite preparations, even after multiple test correction. Through its interaction with annexin A2, S100-A11 has been shown to play an important role in regulating F-actin dynamics and repairing damaged regions of plasma membrane by facilitating F-actin polymerisation (Jaiswal et al. 2014). Although this process has been documented for membrane repair, it may reflect a more general role for this protein in controlling F-actin dynamics and linking the cytoskeleton with the plasma membrane. Others have shown that S100-A11 gene expression is greatly increased with infection of human monocyte-derived macrophages with *Leishmania major* metacyclic promastigotes (Guerfali et al. 2008). However, this is the first time that the protein has been found associated with the *Leishmania*-containing compartment and, again, the first time that active manipulation of this protein has been suggested for *Leishmania*.

Proteins relating to the Arp2/3 complex had higher expression in live preparations. This complex plays a crucial role in the formation of branched actin filament networks through the process of actin nucleation and is involved in the formation of protrusions (Rotty et al. 2013). In the current dataset, Arp2/3 complex subunit 5 and Arp3 were found to be contributing highly to the variation seen between live and HI preparations. However, it is well established that the Arp2/3 complex remains functionally inactive unless it is in the presence of nucleation promoting factors (NPFs), including proteins such as Wiskott-Aldrich syndrome protein (WASP) and WASP family verprolin-homologous protein (WAVE; also known as SCAR). These work in balance with branching inhibitors such as type 1 coronins and cofilin (Rotty et al. 2013). NPFs such as WASP and Scar homologue (WASH) were found within the proteomic dataset, while the inhibitors coronin-1A and cofilin-1 were both found to be differentially represented in live samples, albeit below the 95% confidence level after multiple test correction. The Arp2/3 complex has known roles in facilitating infections such as *E. coli*, *Salmonella*, *Shigella* and *Listeria*, where it has been shown to aid cell-to-cell transmission, phagocytosis, and intracellular pathogen motility (reviewed by Rotty et al. 2013). For *Leishmania* infections, less is known about the role of Arp2/3

proteins; Lodge & Descoteaux (2005) showed evidence to suggest that Arp2/3 and WASP were recruited to the *Leishmania* promastigote-containing compartment through an LPG-dependent mechanism. From our study, the presence of a number of differentially expressed Arp2/3 complex proteins and interacting proteins suggest that the live amastigote parasite was actively involved in manipulating F-actin dynamics.

In addition to its role in actin dynamics as a branching inhibitor, coronin-1A has also been implicated in aiding the survival of an intracellular pathogen. More specifically, others have found that this protein was actively recruited to the pathogen-containing phagosome during infection with live, but not dead, mycobacteria (Ferrari et al. 1999; Jayachandran et al. 2007). As part of this membrane, it acted to slow the phagosome maturation process, thereby increasing the survival of the pathogen. In our dataset, coronin-1A was found to have higher expression in live parasite preparations. When linked with the delay in phagosome maturation discussed later, it would be interesting to speculate as to whether the changes in the actin cytoskeleton induced by the live parasite have prompted the perturbation in phagosome maturation.

The results presented here for the actin cytoskeleton are important because others have shown that actin dynamics play a crucial role during *L. donovani* infection. F-actin is recruited to the *L. donovani* promastigote-containing compartment through Rac1- and RhoA-mediated mechanisms, both of which have been shown to be LPG-independent (Lodge & Descoteaux 2005). Furthermore, Roy et al. (2014) showed that the integrity of the host macrophage actin cytoskeleton was important during *L. donovani* promastigote infection, with lower F-actin levels associated with decreasing intracellular parasite load. This was specific to *Leishmania* as *E. coli* failed to reproduce this effect. However, most of the evidence so far has been related to the promastigote form of the parasite (Lodge & Descoteaux 2008), with the actin dynamics for the amastigote parasite only now starting to be explored in detail (Perrone Bezerra de Menezes et al. 2016). For the first time, we have detailed a number of actin cytoskeleton-related proteins that were differentially expressed on live parasite containing compartments for the

amastigote form of the parasite, demonstrating that the parasite actively manipulates proteins involved in periphagosomal F-actin recruitment to facilitate these Rac1- and RhoA-mediated mechanisms. This could be mediated by the parasite incorporating its proteins into the host cell phagosome in which it resides, as has been suggested for LPG (Winberg et al. 2009).

In addition to alterations in actin cytoskeleton dynamics, the analyses performed in this study identified differences in phagosome maturation between live and HI parasite phagosomes. During pathway analyses, it was noted that all pathways relating to phagosome maturation were more highly expressed in HI preparations, although to less than 95% significance. Performing Student's t-tests for many of the proteins relevant to this pathway revealed that there was a trend towards them being higher in HI preparations; LAMP2A was also found to have a statistically significant higher expression in HI parasite preparations, even after multiple test correction. A number of functions have been suggested for the protein, including a specific role in chaperone-mediated autophagy and in transporting substrate proteins into lysosomes (Cuervo & Dice 1996; Cuervo & Dice 1998). However, instead of being specifically targeted for down-regulation by the live parasite, the reduction in lysosomal-specific proteins may instead reflect a general delay in phagosome maturation and fusion with the terminal compartment of the endocytic pathway, the lysosome.

This delay in phagosome maturation would also explain why several lysosomal enzymes (such as prenylcysteine oxidase) were found to have higher expression in HI samples. Subunit  $\beta$  of  $\beta$ -hexosaminidase, another lysosomal enzyme, was found to be higher expressed in HI samples, as shown by PCA, PLS and t-tests. In conjunction with the cofactor GM2 activator protein, this enzyme helps to catalyse GM2 ganglioside degradation (Knapp et al. 1996). Experimentally, data was shown in Chapter 5 to demonstrate that live parasite-containing compartments have lower  $\beta$ -hexosaminidase activity. This helps support the validity of the proteins being identified from the proteomic analyses of these isolated parasite-containing

compartments. Interestingly, the  $\alpha$  subunit was not differentially expressed between live and HI preparations, suggesting that the reduction in  $\beta$ -hexosaminidase activity was due to a specific reduction in the  $\beta$  subunit. The zinc finger FYVE (Fab 1, YOTB, Vac 1 and EEA1) domain-containing protein 26, also known as spastizin, localises to the lysosome via its FYVE domain (Chang et al. 2014). Others have found that depletion of this protein using siRNA results in the accumulation of enlarged Lamp1-positive organelles and higher autophagosome accumulation within these compartments (Chang et al. 2014). Furthermore, Chang et al. (2014) demonstrated that spastizin was essential for the reformation of lysosomes after fusion with autophagosomes. It was interesting that this protein has one of the highest PC1 loadings, with levels higher in HI preparations than live preparations. This demonstrated that proteins involved in controlling autophagy were differentially expressed and may help account for some of the autophagy-related differences seen between the preparations. Thus far, this protein has not been associated with *Leishmania* specifically or infection in general; it would be premature to speculate about the exact roles of this protein during *Leishmania* infection, but its deficiency could reflect the active removal or degradation of this protein by the live amastigote parasite, thereby resulting in enlarged compartments with altered reformation and autophagic properties.

The Ccz1-Mon1 complex is normally recruited to the endosome by Rab5, whereby it functions as a Rab7 GEF and is needed for multiple intracellular trafficking pathways that converge at the lysosome (Hegedűs et al. 2016). In the current proteomic dataset, Ccz1 was found to be higher in HI parasite preparations as shown through PCA and PLS analyses. It has been shown that Ccz1 plays an important role in autophagy, with deletion of Ccz1 resulting in defective autophagy (Dong et al. 2015; Hegedűs et al. 2016). Again, like with spastizin, this would result in live parasite compartments with altered fusion and autophagic properties, although little is known about the role this protein plays during infection.

Together, these results provide evidence to suggest that the live amastigote parasite was able to actively manipulate phagosome maturation, both at the level of protein groups and pathways and through differential expression of specific lysosomal-associated proteins. Where the amastigote has been investigated previously, it was often compared to the promastigote form that has a more striking perturbation of phagosome maturation. Here, in combination with the experimental results from Chapter 5, we have shown that the live amastigote parasite was able to subtly alter its phagosomal compartment in such a way that its compartment had lower expression of lysosomal-associated proteins compared to HI parasite compartments. Thus, the HI parasite preparations more closely resembled the lysosomal compartments isolated, particularly with regards to  $\beta$ -hexosaminidase activity and the expression of lysosomal-associated proteins.

What could account for these differences seen with the live parasite? One possibility is LPG expression, as LPG-dependent disruption of phagosome progression has previously been documented for the promastigote form of the parasite (Lodge & Descoteaux 2005; Liévin-Le Moal & Loiseau 2016). Although possessing much less LPG than promastigotes, amastigote parasites still possess LPG on their surface, albeit at least 3 orders of magnitude less (Lodge & Descoteaux 2008) and as a structurally distinct form (Turco & Sacks 1991). Unfortunately, because LPG is not a protein, levels of LPG were not available as part of the proteomic data. However, others have shown that LPG-dependent mechanisms cause the parasite-containing compartment to be coated in F-actin, myosin and  $\alpha$ -actinin, and caused F-actin polymerisation factors such as Arp2/3 to be associated with the compartment (reviewed in Liévin-Le Moal & Loiseau 2016). Indeed, in LPG-defective promastigotes, this normal association of Arp2/3 to the parasite-containing compartment was lost (Lodge & Descoteaux 2005). In the current study, Arp2/3 was identified as a strong candidate that was preferentially represented in live preparations, as shown by PCA. This suggests that for the amastigote form, there may be an active role of the parasite in recruiting this protein to the parasite-containing compartment.

Alternatively, the live parasite may be manipulating non-actin related proteins to promote this delay in maturation. As discussed with Ccz1, spastizin and coronin-1A, a number of these lysosomal-associated proteins have known roles in altering the fusionability, reformation process and autophagic properties of incoming phagosomes. This explanation would also help to link the changes seen in ribosomal and mitochondrial proteins, as discussed later, with alterations in phagosome maturation.

In addition to manipulation of actin cytoskeleton dynamics and phagosome maturation by the live parasite, other themes arose within the dataset. For example, pathway analyses showed that there were a number of pathways related to protein translation within the dataset, such as eukaryotic initiation factor 2 (eIF2) signalling and mammalian target of rapamycin (mTOR) signalling, and that these were higher expressed in live parasite preparations. This was also representative of multivariate analyses that showed that a number of ribosomal proteins were higher in live preparations. Although the results from these analyses suggest that a diverse range of cellular processes can be affected by the live parasite, they all have the common underlying principal of changing intracellular signalling. This could provide the mechanism by which the parasite is able to affect processes remote from the immediate surroundings of its intracellular compartment. This was highlighted by a number of signalling-related pathways being well represented within our dataset, many of which were differentially expressed between live and HI parasite preparations. A comparison of *L. major* infected cells with non-infected control cells using whole cell-level proteomics suggested that the parasite may be able to manipulate intracellular signalling cascades (Menezes et al. 2013); our data suggests that many of these changes may be orchestrated at the level of the parasite-containing compartment.

In addition to differentially expressed pathways, the isolated *L. donovani*-containing compartments had several differentially expressed mitochondrial enzymes and transporters. Others have found that *Leishmania* infection can induce a cellular increase in autophagy activity (Frank et al. 2015) and, as

detailed in Chapter 5, there are well-established links between mitochondria and lysosomal compartments. Despite this, many of these proteins showed no overall pattern of expression, with both live and HI preparations having differential expression of a number of mitochondrial proteins. This was supported by the results of PCA performed on only a subset of mitochondrial proteins, showing that differentiation between the two experimental conditions was reduced. However, one observation for these current data was that all the proteins related to the multi-subunit mitochondrial transporter complex V (F1-F0 ATP synthase) were differentially expressed: proteins related to the F1 subgroup were increased in live preparations, whereas all the proteins related to the F0 subgroup were decreased (see Figure 6.12). F1-F0 ATP synthase uses a proton gradient across the inner mitochondrial membrane to generate the majority of the ATP used by the entire cell (reviewed by McStay 2016). Both F1 and F0 form a complex *in vivo*, with F0 being incorporated into the inner mitochondrial membrane and F1 remaining peripheral (Weber 2006). Whether the current finding of differential expression of the two subgroups has a functional relevance or is the indirect result of altered autophagy activity between the two preparations is unknown.

In addition to mitochondrial and ribosomal proteins, a number of proteins not traditionally associated with the phagolysosome were identified within isolated parasite-containing compartments. This was expected as qualitative LC-MS/MS analyses performed in Chapter 5 had already identified a wide-range of proteins associated with the compartment. However, when proteins from other subcellular compartments were analysed in isolation, there was still considerable differentiation between live and HI preparations (see Figure 6.8). This was found to be the case particularly for proteins that had been labelled as 'other' (i.e. not associated with the phagolysosome, mitochondria, or ER compartments). When PCA and PLS were performed on this subset, a number of cytoplasmic, plasma membrane and ribosomal proteins were identified. It would be interesting to subdivide this dataset further to identify whether proteins from each of those groups still retained a strong differentiation along PC1 for live and HI preparations. There was no differentiation for proteins associated with ER, suggesting that while the ER

is a major constituent of the phagolysosome, the live parasite does not actively manipulate its recruitment as a whole and instead only a small number of proteins may be actively manipulated as shown via t-tests.

After multiple test correction, there were relatively few proteins that were found to have a statistically significant difference between live and HI preparations. This suggests that active manipulation of the protein composition of the *Leishmania*-containing phagosome is subtle, with smaller changes in large protein groups rather than extreme changes in individual proteins. This may explain why other researchers have often overlooked the role that the amastigote plays in directing intracellular processes to aid its own survival. It also highlights the importance of using multivariate statistical methods to analyse large proteomic datasets where groups of proteins are often highly interdependent. Furthermore, the study presented here is one of only a limited number of studies that have directly compared live and dead parasites, even though such a comparison can prove fruitful (e.g. Nylen et al. 2003). Instead, most studies have compared the parasite-containing compartment with a normal phagosome, often using data derived from latex beads. Had latex beads been used as a comparison in the current study, it is likely that many more proteins would have been differentially expressed, because the passive effect made by surface morphology can have a significant role during phagocytosis (Li et al. 2010).

Indeed, much of our current understanding of the phagosome is derived from studies using latex beads (e.g. Garin et al. 2001; Trost et al. 2009; Goyette et al. 2012; Guo et al. 2015). These studies give important information on the process of phagocytosis and general features of the phagosome, but have the disadvantage that the morphology and surface markers specific to each pathogen cannot be accounted for. Latex beads also have a considerable advantage over pathogens in that isolation of purified compartments from pathogen-infected cells is challenging, particularly since they lack the significant density difference seen between latex beads and other subcellular organelles (Li et al. 2010). Most pathogen-containing compartment isolation protocols require multi-step purification methodologies involving sucrose



gradients that can be detrimental to isolated samples. Thus, by coupling LC-MS/MS with a novel parasite-containing compartment isolation protocol, the current study was able to produce proteomic datasets on the composition of this compartment and has shown that the live parasite is actively manipulating the protein composition of its intracellular compartment.

The validity of the results from these proteomic analyses relating to protein identification and differential expression of proteins was determined principally by comparing with existing data in the literature, as has been done by others (e.g. Latosinska et al. 2015). However, the perturbation of phagosome maturation with live compartments having lower quantities of lysosomal-associated proteins than HI compartments was also seen experimentally, as detailed in Chapter 5. More specifically, these samples had lower  $\beta$ -hexosaminidase activity, as shown by functional assay, and less LAMP1 protein, as shown by western blotting.

Despite this, future studies can now be performed to confirm and expand upon these results experimentally. In particular, it may be fruitful to concentrate on highly differentially expressed individual proteins that could have a relevant role during the infection process. To this end, S100-A11 may be a good target for follow-up experimentation. This protein was identified as a potential candidate of interest during *Leishmania* infection studies when gene expression profiling showed that this gene was elevated in human macrophages infected with *L. major* promastigotes (Guerfali et al. 2008); the findings in the current study showed that it is manipulated by the live parasite making this target even more interesting. Future studies should first confirm the localisation with the compartment through immunofluorescent staining and could then use siRNA knockdown or complete knockouts to determine whether its absence affects the normal pathogenesis of *L. donovani* amastigote infection. In addition, the zinc finger FYVE domain-containing protein 26, also known as spastizin, may be a suitable target based on it coming up high in PCA and PLS analyses and its known function in manipulating phagolysosomal properties. Future experiments can also concentrate on providing further experimental evidence for the active

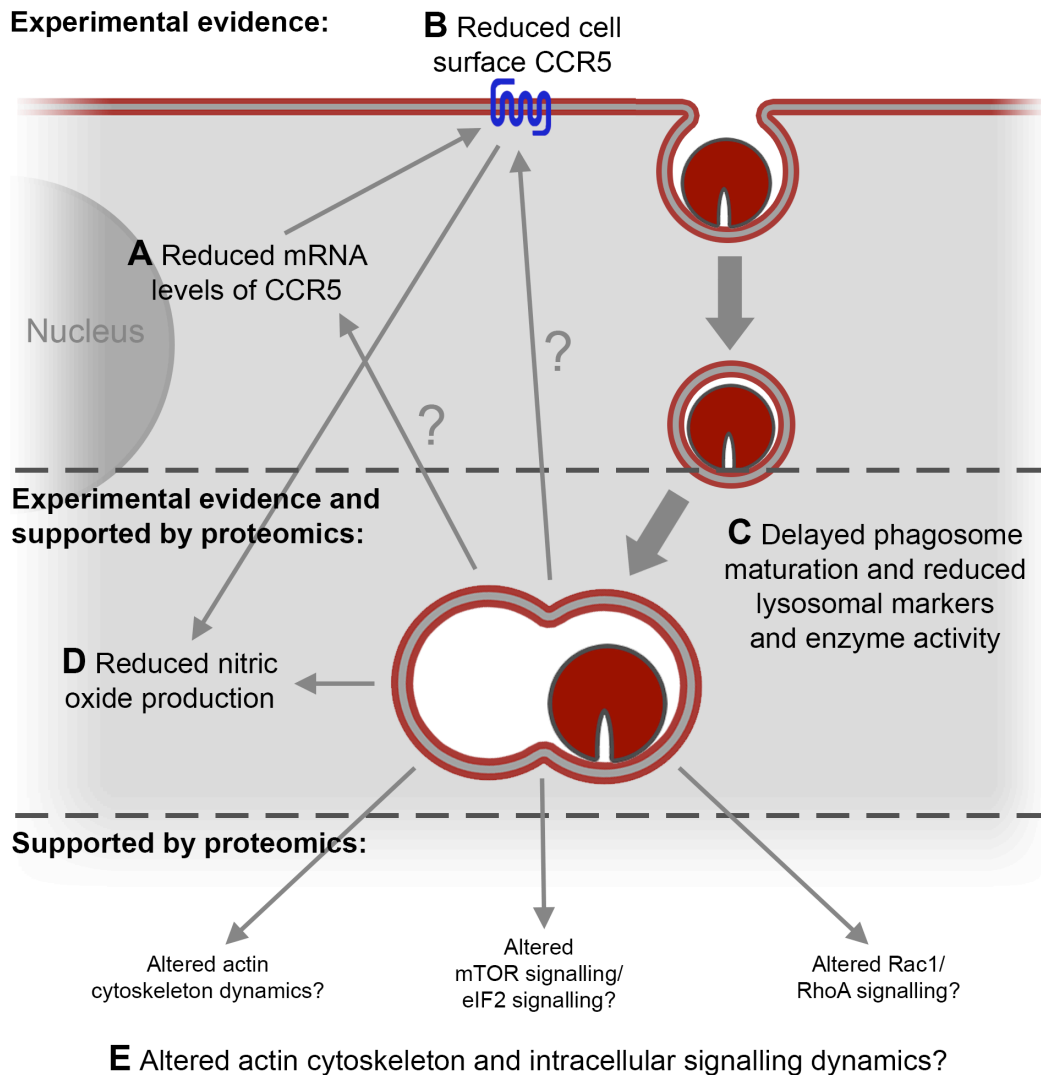
manipulation of actin cytoskeleton dynamics, principally through the use of immunofluorescence techniques to show recruitment to and association with the phagolysosomal compartment.

In summary, we have shown that a number of individual proteins and protein groups were actively manipulated by the live parasite during infection in J774.2 cells. Proteins relating to actin cytoskeleton dynamics and phagosome maturation were particularly different between live and HI parasite compartment preparations, suggesting that the parasite may manipulate the host cell cytoskeleton to change the composition of its intracellular environment. LPG-dependent delays in phagosome maturation have previously been observed for promastigote parasites (Lodge & Descoteaux 2008). However, this is the first time that perturbations in phagosome maturation and actin dynamics have been documented in as much detail for the amastigote form and also the first time that evidence has been provided to show that this is an active process orchestrated by the living parasite, rather than the normal host cell response to proteins present on the parasite's surface.

## 7. General discussion

This thesis explored ways in which the live *L. donovani* amastigote was able to actively exploit a number of intracellular processes (**Figure 7.1**), an aspect of research that has been relatively neglected within the *Leishmania*-field. We have detailed the protein composition of the parasite-containing compartment for *L. donovani* LV9 amastigotes and have shown that a number of key pathways were differentially regulated by the live parasite. This work also provided new insights into the protein composition of the phagosome using a clinically-relevant pathogen, building on the work of others using latex beads to help proteomically define this intracellular compartment (Garin et al. 2001; Goyette et al. 2012; Guo et al. 2015). Furthermore, we have developed a novel phagosome isolation method that will provide a useful platform on which to perform future pathogen-containing compartment studies, either using different forms of the parasite, specific time-points, other host cells, or completely new pathogens.

In addition to this, we have shown that although there is an association between CCR5 and *L. donovani* LV9 amastigote infection, CCR5 was not present on the membrane of the parasite-containing compartment. Absence of the receptor does not influence the ability of parasites to infect macrophages or be cleared from mice, but may influence the recruitment of leukocytes to infection foci. We show that *L. donovani* LV9 amastigotes down-modulate CCR5 at the cell surface by an indirect mechanism of cross regulation likely through down-regulation of transcription of the receptor. Together, these new insights greatly expand our understanding of how live *Leishmania* LV9 amastigotes are able to manipulate their host cell to survive intracellularly. These findings also suggest a new role of the parasite-containing compartment as a signalling platform, and how the live parasite is able to exploit this to fine-tune the host cell's response to infection.



**FIGURE 7.1. Schematic representation of the overall effects that infection with live *L. donovani* LV9 amastigotes had on J774.2 cells.** Combined summary of the main results from my thesis on the effect of live *L. donovani* LV9 amastigote infection compared to infection with heat-inactivated (HI) parasites. **A**) Reduced CCR5 mRNA levels were found with live parasites (see Figure 3.13). **B**) A greater decrease in CCR5 cell surface expression was seen using live parasites compared with HI parasites throughout a 48 hr time-course of infection (see Chapter 3). **C**) Pathways and proteins relating to phagosome maturation were reduced in live parasite preparations (see Chapter 6). There was also reduced LAMP1 western blotting and  $\beta$ -hexosaminidase activity (see Figure 5.7). **D**) There was reduced nitric oxide production in J774.2 cells infected with live parasites (see Figure 5.11) and an anti-oxidant was found to be differentially expressed in live parasite compartments as shown by unlabelled LC-MS/MS spectral counting (see Table 5.2). **E**) A number of pathways relating to altered actin cytoskeleton dynamics and intracellular signalling had higher expression in live parasite preparations, as shown by univariate and multivariate analyses of iTRAQ-labelled LC-MS/MS data (see Chapter 6).

## 7.1 The parasite-containing compartment as a signalling platform

A role for the lysosome as a signalling hub that can control metabolism and homeostasis at the cellular level is starting to emerge (Ballabio 2016). Signalling pathways are usually coordinated by the formation of specific signalling complexes, recruited to the required location by adaptor and scaffold proteins. As a relevant example, mTOR exists as two functionally distinct complexes, with mTOR complex 1 (mTORC1) having been shown to associate with the lysosomal membrane where it is activated and can regulate autophagy at a transcriptional level by responding to lysosomal nutrient content (Zoncu et al. 2011). In our proteomic dataset, several of the components of this lysosomal signalling hub were present such as mTOR itself and a number of interacting proteins, such as the adaptor protein called late endosomal/lysosomal adaptor, MAPK and MTOR activator 2 (LAMTOR2), which acts as a scaffold for the recruitment and activation of mTORC1 to the lysosome (Martina et al. 2012). Several of these proteins had higher expression in live preparations for iTRAQ-labelled LC-MS/MS (see Chapter 6). When mTORC1 dissociates from the lysosome, it phosphorylates transcription factor 'EB' (TFEB), which prevents TFEB from translocating into the nucleus and causing an up-regulation of lysosomal-autophagic gene expression (Martina et al. 2012). Thus, to confirm perturbation of this pathway by *L. donovani*, future experiments could determine the levels of TFEB in cells infected with *L. donovani* LV9 amastigotes to determine whether the differential expression of mTOR components seen in our proteomic dataset influences this transcription factor. Through the mTOR signalling pathway, *L. donovani* parasites have a mechanism by which they can regulate autophagy and the current data suggest that the parasite may be inhibiting this process. Although this may reduce the delivery of some nutrients to the compartment, it would also restrict transfer of mitochondria-derived reactive oxygen species into the parasite-containing compartment.

As well as this established lysosomal-associated signalling pathway, components of many other signalling pathways came up in the proteomics dataset, several of which have not yet been characterised as having a phagolysosomal association. As an example, components of the eIF2 signalling pathway were well represented in the dataset and had higher expression in live parasite preparations (see Figure 6.10). This is one of the main pathways by which eukaryotic cells can regulate protein translation in response to stress and may have anti-bacterial properties (Shrestha et al. 2012). This highly conserved signalling pathway has previously been shown to be disrupted by certain pathogenic agents (Shrestha et al. 2012), so the finding that it is actively manipulated by *Leishmania* may not be surprising. However, what is perhaps more unexpected is that a number of the components of this pathway were present as part of the parasite-containing compartment. When these compartments were annotated with GO biological processes, one of the most represented categories of proteins was that for signal transduction. Altogether, this suggests that there may be many more signalling pathways related to diverse cellular processes such as metabolism, autophagy and protein translation that are influenced by the phagolysosomal compartment remaining to be discovered. Although the lysosome is starting to be acknowledged as a signalling compartment (Ballabio 2016), our results suggest that this property can also be extrapolated to phagolysosomes and could be targeted by live *Leishmania* parasites.

In Chapter 3, the data presented demonstrate that there was an association, albeit indirect, between CCR5 cell surface expression and *L. donovani* LV9 amastigotes that was greatest for the live parasite. Downstream effectors of chemokine receptors are known to include signalling pathways of small G proteins, several of which had higher expression in live parasite-containing compartments. Although CCR5 was not found to be a component of the parasite-containing compartment and there was an absence of other chemokine receptors and GPCR-related machinery, several components downstream of CCR5 were found associated with the compartment. While the decrease of CCR5 was associated with a corresponding decrease in

CCR5 mRNA levels, it does not exclude the possibility that CCR5 expression at the cell surface might also be altered by the parasite through other mechanisms. Others have shown that the parasite can reduce cell surface expression of receptors by inducing production of receptor ligands from the host cell (Cortez et al. 2011); we have shown that a similar mechanism is not modulating CCR5 expression during *L. donovani* infection because down-modulation remains when the receptor is blocked using an antagonist. It has also been shown that *Leishmania* parasites can regulate the activity of PKC (Olivier et al. 2012), a kinase that can influence CCR5 internalisation (Oppermann et al. 1999) and thus we cannot exclude that we are also seeing a novel mechanism for down-modulating CCR5 induced by the parasite. Regardless, these data provide one of the first examples of a pathogen down-regulating CCR5 at the gene level, showing that the live parasite can have wide-ranging effects and can alter both proteins and gene transcription to modulate intracellular signalling cascades. This would likely be beneficial to the parasite because it would dampen chemokine-induced nitric oxide production, with its associated clearance of parasites, by reducing the amount of chemokine receptor available for activation (Bhattacharyya et al. 2002), in addition to altering cell migration. It would also help to explain why the results from our *in vivo* CCR5<sup>-/-</sup> mice time-course experiment did not deviate from the wild-type (CCR5<sup>+/+</sup>) controls. To test this, future studies could utilise a mutated receptor where the C terminal tail has been modified to inhibit  $\beta$ -arrestin-mediated recruitment of CCR5 but not activation of the intracellular signalling cascade.

Thus, we have seen large-scale manipulation of a number of diverse intracellular signalling events by the live parasite, suggesting active manipulation of the compartment by *L. donovani* LV9 amastigotes.

## **7.2 Active manipulation of intracellular processes by the live parasite**

Consistently throughout this work, there have been differences in the results gained from live and HI parasites suggesting that the live parasite is able to

induce different cellular responses from its host. This was seen for nitric oxide production, CCR5 down-regulation and proteomic characterisation of the parasite-containing compartment. This active manipulation by the live parasite during infection is an aspect of *Leishmania*-related research that has often been understudied. It is known that the live parasite is able to differentially activate a number of leukocytes and initiate different cytokine secretion profiles compared to HI parasites (Nylen et al. 2003). Live parasites can also functionally alter key killing mechanisms as shown by live *L. donovani* L82 amastigotes' ability to considerably lower expression of reactive oxygen species compared to HI parasites (Channon et al. 1984); similarly, we found that live *L. donovani* LV9 amastigotes had lower levels of nitric oxide production (see Figure 5.11). Furthermore, when others have exposed J774A.1 cells to live or HI *L. amazonensis* amastigotes, subsequent western blotting analysis revealed significant differences in the tyrosine-phosphorylation of proteins in cell lysates suggesting that the live parasite may have wide-spread functional effects on a number of host proteins (Love et al. 1998), although the numbers of proteins affected and what these proteins related to was not determined. To build on this further, the data presented in this thesis demonstrated that 19 proteins identified from iTRAQ-labelled LC-MS/MS had a statistically significant difference between live and HI preparations even after multiple test correction, whilst many more proteins had more subtle differences between the preparations as revealed using multivariate and pathway analyses. This suggests that live *L. donovani* LV9 amastigotes actively manipulate the protein composition of their intracellular compartment.

Earlier studies often portray the parasite as being an inactive participant relying on normal host processes and responses for the delivery of nutrients that the parasite needs to survive, perhaps initiated by factors present on the surface of the parasite. Although the *Leishmania* field is starting to appreciate that the live parasite is able to respond to and manipulate external cues (Podinovskaia & Descoteaux 2015; Liévin-Le Moal & Loiseau 2016), there is currently a lack of experimental evidence to portray the role of the active parasite. We have shown through our proteomic analyses that the live



parasite was able to affect phagosome maturation, actin cytoskeleton dynamics and intracellular signalling cascades. In addition to changing the composition of the parasite-containing compartment, the live parasite was able to have wide-ranging effects on the cell as demonstrated by the down-regulation of CCR5 and reduced nitric oxide production (**Figure 7.1**). These changes are likely to have functional consequences both for the parasite and the host cell in which it resides.

### **7.3 Balance at the host-pathogen interface**

The other partner in these orchestrated changes induced by live parasites is the host cell and, specifically, the mechanisms that it has in place to respond to intracellular infection. The phagosomes from IFN- $\gamma$ -activated RAW 267.4 cells have previously been isolated by floatation on a sucrose gradient and their proteome characterised (Trost et al. 2009). Interestingly, it was found that IFN- $\gamma$  activation induced a delay in phagosome maturation and induced changes in actin cytoskeleton elements associated with the phagosome. We observed similar changes in the proteomes of intracellular compartments isolated from live parasite infection, suggesting that the live parasite may be activating the macrophage. Others have shown that live, but not HI, *L. donovani* promastigotes were able to activate primary human natural killer cells, thereby causing them to produce IFN- $\gamma$  (Nylen et al. 2003). However, our results can only be partially explained by macrophage activation. For example, the down-modulation of CCR5 seen at the cell surface is in contrast to the increased expression at the cell surface that has been seen with IFN- $\gamma$ -induced activation in a number of different cell types (Hariharan et al. 1999; Mantovani et al. 2004). IFN- $\gamma$ -induced activation of J774.2 cells has also been demonstrated to increase nitric oxide production (Mulero & Brock 1999); in contrast to this, we see a decrease in nitric oxide production in live parasites compared to HI parasites. Furthermore, our proteomic dataset does not show the large scale IFN- $\gamma$ -induced differential expression of proteins involved in the immune response, as seen by Trost et al. (2009), suggesting that the parasite is actively fine-tuning this cellular response to infection. This is exemplified by the finding that the parasite was able to

down-regulate CCR5, whereas it might be expected to increase based on the increased cytokine secretion alone (Takayama et al. 2001).

Others have previously performed whole cell proteomic studies of *Leishmania*-infected cells. Menezes et al. (2013) found that, compared to non-infected murine macrophages, macrophages infected with either *L. amazonensis* or *L. major* stationary-phase promastigotes differentially expressed a number of proteins involved in cell metabolism, cellular detoxification and cell signalling. Although whole cell analyses are looking at multiple events and different levels of integration, it is interesting that these themes were also largely mirrored in our qualitative and quantitative data using *L. donovani* amastigotes, suggesting that the pathways modulated at the level of the parasite-containing compartment may cascade out to influence whole cell processes. Alternatively, it may be that the differences others have seen at the whole cell-level were due to changes at the level of the parasite-containing compartment; indeed, when Menezes et al. (2013) confirmed the differential expression of hypoxia-inducible factor 1- $\alpha$  in infected cells using immunofluorescent imaging, a punctate appearance for the protein was seen that may correspond to the parasite-containing compartment. Transcriptomics performed on macrophages infected with *L. donovani* amastigotes has previously found that pathways involved in cell signalling, immune cell trafficking, cell death, and lipid metabolism, among others, were differentially modulated by the parasite (Beattie et al. 2013) compared to non-infected cells that were exposed to inflammatory mediators, again suggesting that the response seen is partially mediated by the cell and partially by the parasite. In this project, we have shown that many of these pathways were differentially expressed at the level of the parasite-containing compartment and that they are mediated by active processes from the live parasite, rather than resulting from the normal cellular response to *Leishmania* parasite phagocytosis. Thus, our data suggest that the host cell is responding to infection but the parasite is combating and dampening down some of these responses.

## 7.4 Fine-tuning, rather than dramatic shifts, in host cell processes

Several other pathogens are known to survive within macrophages and have mechanisms to alter host membrane trafficking to aid their survival (reviewed by Asrat et al. 2014). Some pathogens have factors that target specific host proteins to achieve this. As an example, *Legionella pneumophila* creates a specialised intracellular compartment that resembles the ER by using the bacterial-derived 'Recruitment of Arf1 to Legionella phagosome' (RalF) protein to target ADP-ribosylation factor-1 (Arf1) to its compartment. Arf1 stimulates the recruitment of ER-derived coat protein I (COPI)-coated vesicles to the *Legionella*-containing phagosome, thereby creating a hybrid organelle that is conducive to pathogen replication and avoids lysosomal destruction (Kagan & Roy 2002). In contrast, *Mycobacterium tuberculosis* resides in an intracellular compartment that is able to arrest phagosome maturation and acidification through the effects of a small number of bacterial factors, each with specific target host proteins; for example, protein tyrosine phosphatase A (PtpA) excludes host vATPase machinery thereby inhibiting phagosome acidification (Wong et al. 2011). Rather than complete diversions of the intracellular trafficking of the parasite-containing compartment or wholesale exclusion of specific proteins, our data suggest that the effects that *Leishmania* had on its intracellular compartment were more subtle and wide-ranging.

This suggests that, in contrast to these aforementioned pathogens, the *Leishmania* parasite is well adapted to survive within the hostile environment found in these compartments, as has been suggested previously (McConville & Ralton 1997). However, this does not mean that the parasite is a passive bystander during the intracellular trafficking process. Recent shifts in our understanding of the lysosome could offer an explanation to the differences observed in phagosome maturation for live parasite compartments. Bright et al. (2016) have demonstrated that the newly defined site of active degradation, the endolysosome, with its corresponding high hydrolase activity and acidic pH, continuously undergoes fusion events with late

endosomes and terminal lysosomal storage compartments in a dynamic cycling process. It has previously been shown that *L. donovani* amastigotes were within an intracellular compartment that was acidic and contained a number of active acidic hydrolases (Antoine et al. 1998). Our data suggest that, compared to HI parasites, live parasites receive less cargo from the terminal lysosomal compartment and more from the late endosome/MVB. More specifically, the live *Leishmania*-containing compartment may be at a different stage of this dynamic cycling process. This would explain the low levels of lysosomal markers and enzymes such as LAMP2A and  $\beta$ -hexosaminidase, and the higher expression of late endosomal markers such as Rab7. It would be interesting to determine the exact pH and hydrolase activity of the live parasite compartment compared to those formed with HI parasites; our data suggest that there could be subtle differences that may help the parasite's intracellular survival.

These findings of subtle differences between live and HI parasite compartments are important because it suggests that, unlike *L. pneumophila* and *M. tuberculosis*, it is unlikely that there is a single key host protein that is actively targeted during infection. This helps to explain why such proteins have been difficult to identify for *Leishmania* infection. Alternatively, it could suggest that any important changes made to the phagolysosomal compartment are mediated by the surface architecture of the parasite and can therefore be induced by a HI parasite. This was seen for the down-modulation of CCR5, albeit with the live parasite being able to decrease CCR5 more and for longer. Despite this, it would be interesting to analyse the *Leishmania*-specific proteomic data collected during this project to see whether any of the changes in the host cell response could be explained by the differential expression of certain proteins of the *Leishmania* parasite.

## **7.5 Future directions**

There are many avenues of potential future research that could build on the results collected during this project. An essential next step to facilitate much of this work would be the development of a specific antibody against murine

CCR5 suitable for a variety of techniques. Although we produced GST-CCR5 fusion proteins to help assist with this, the resulting rabbit sera did not contain antibodies against the full length *in situ* receptor. CCR5 has several post-translational modifications that may alter target epitopes making antibody production difficult (Mack et al. 2001; Bernstone et al. 2012; Ford et al. 2013). However, a validated antibody would be useful to determine whether the receptor co-localises with the parasite-containing compartment during early stages of entry. If this co-localisation exists, a time-course of infection could be performed to determine at what stage the receptor dissociates with the compartment, since we know that CCR5 was not present on the phagolysosomal membrane. Furthermore, the antibody would be useful to determine whether total cell quantities of CCR5 are changing during the time-course of infection as has been suggested by others using a different model of infection (Bhattacharyya et al. 2008; Majumdar et al. 2014), and as the decreasing mRNA levels of CCR5 would suggest. Alternatively, as *L. donovani* down-regulates CCR5, we could use gene knock-in technology to replace CCR5 with a form of the receptor that has a mutated GRK or PKC phosphorylation site, thereby inhibiting the removal of CCR5 from the cell surface without disabling intracellular signalling cascades, as has been done for other GPCRs (e.g. Morgan et al. 2014).

The J774.2 cell-line was used to generate parasite-containing compartment material for proteomic analyses. A cell-line was used rather than primary cells because of the large number of cells needed to generate the required quantity of sample; this issue was particularly acute during the method development period. However, future studies could replicate this study using primary cells from the mouse, likely BMDMs. It has been shown that proteomic data generated from phagosomes isolated from either the RAW 264.7 cell-line or primary BMDMs have significant differences in the proteins that were identified and the relative quantity of proteins in each sample (Guo et al. 2015). Of particular interest, Guo et al. (2015) found that a number of ribosomal and translation-related proteins had higher expression on phagosomes from RAW 264.7 cells compared to those from BMDMs. With a number of proteins relating to these protein groups identified as being

differentially regulated in our dataset in response to live *L. donovani* infection, it would be interesting to determine whether these same results are observed for BMDMs. In addition, BMDM-derived phagosomes were found to have many more receptors related to the immune response present on them (Guo et al. 2015); whether CCR5 might appear as a component of the phagosomal membrane if primary cells are used remains to be explored. Although the number of primary cells needed to generate sufficient phagosomal material makes this challenging, it is encouraging that others have found that phagocytosis is significantly more efficient in primary cells suggesting that fewer cells could be used (Guo et al. 2015).

The process of phagolysosome biogenesis is a dynamic and evolving process that has temporal resolution (Goyette et al. 2012). The fluidity of this process has been recently highlighted by Bright et al. (2016), showing that the endolysosomal compartment undergoes continuous fusion and fission events with late endosomes and terminal lysosomes. In the context of *Leishmania* infection, there have been temporal changes documented for the parasite-containing compartment (Antoine et al. 1998). It would be valuable to use proteomic characterisation to document these changes in phagosome composition, particularly for the pathways and functional protein groups that were identified as differentially expressed. However, the protocol may need to be further refined for this use because it is likely that HI parasites will be fully degraded by later time-points. A later time-point post-infection may be particularly fruitful for investigation because maximum down-modulation of CCR5 was seen at 6 hr and 24 hr post-infection for BMDMs and J774.2 cells, respectively, suggesting that the parasite may have maximal influence over intracellular processes and signalling cascades during this time-frame. Furthermore, Menezes et al. (2013) found that proteins were most differentially expressed at 24 hr post-infection in whole infected cell proteomics.

By combining LC-MS/MS proteomics with mathematical and statistical techniques, this study could readily identify the presence or absence of proteins, changes in the relative abundance of proteins, and possible

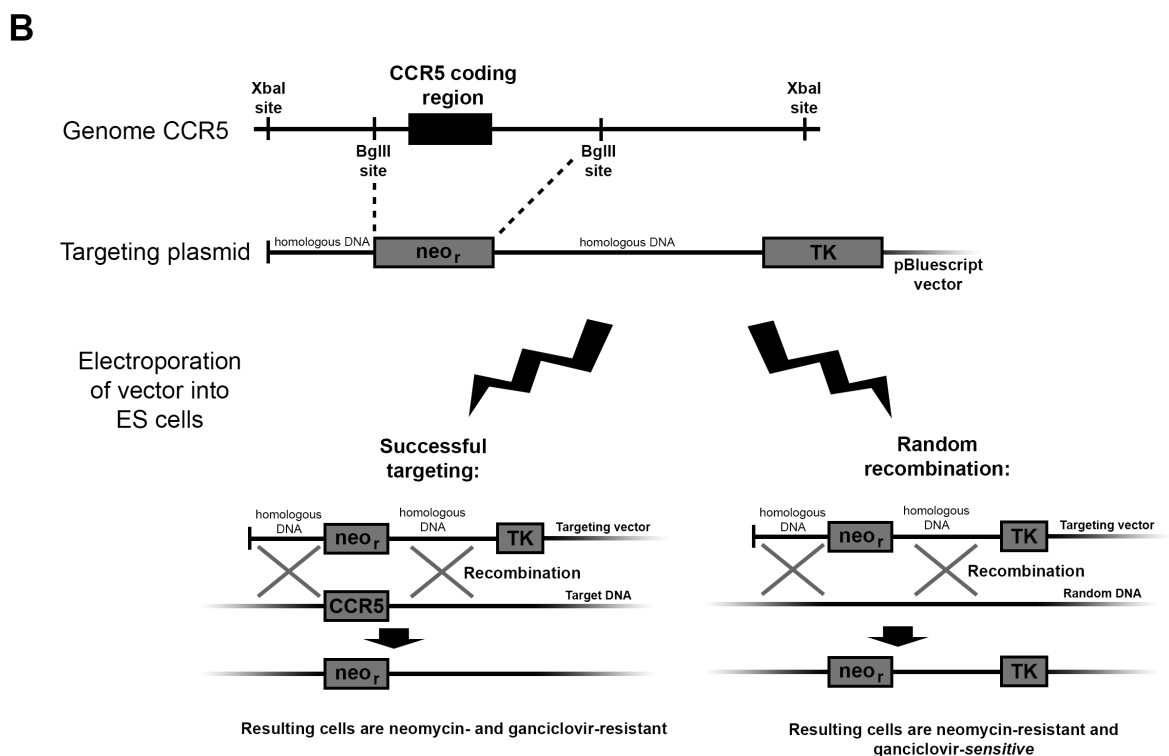
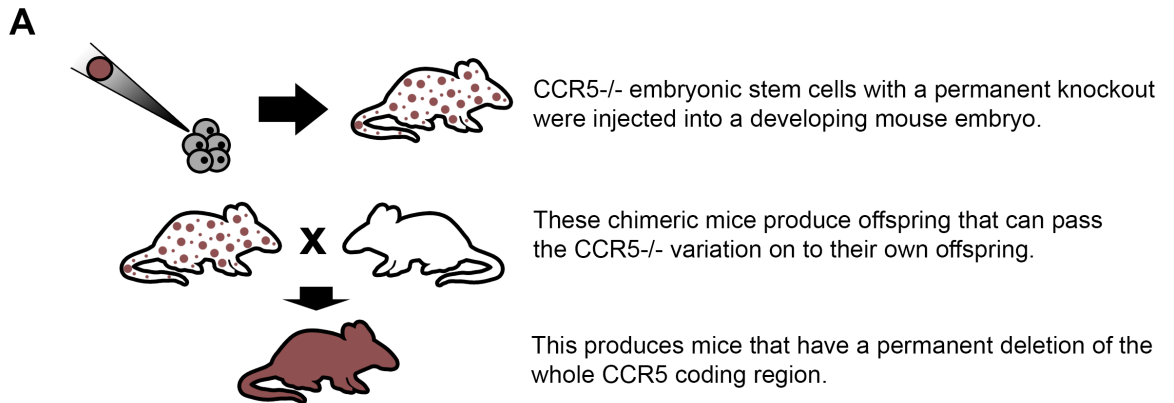
fluctuations in protein binding. However, there are many post-translational modifications, such as phosphorylation, that can alter the function and activity of proteins that our proteomics study was unable to assess. As a number of signalling transduction pathways were identified as being differentially expressed in our dataset, there may be widespread changes in the phosphorylation of proteins induced by the parasite. Indeed, it has been found that the majority of proteins involved in signalling pathways can be phosphorylated, with some proteins often having multiple sites of phosphorylation (Humphrey et al. 2015), highlighting the importance of this mechanism for controlling trafficking and intracellular signalling cascades. *L. amazonensis* amastigote-mediated phosphorylation from the parasite-containing compartment has been recently documented for extracellular signal-regulated kinase (ERK) causing a reduction in parasite clearance from infected DCs (Boggiatto et al. 2014); this was shown to be an active process because HI parasites were unable to phosphorylate the kinase to the same level. Although this is one of the only examples of protein phosphorylation orchestrated by the parasite from the intracellular compartment so far, there are likely many other proteins either directly or indirectly phosphorylated by or in response to the parasite. Thus, coupling the isolation method developed in Chapter 5 with quantitative phosphoproteomic MS-based approaches is essential future work to provide useful information on additional changes that the parasite is making to its compartment, in addition to helping to explain some of the mechanisms by which the parasite was able to bring about those changes. This could be combined with whole-cell infection phosphoproteomics to provide a complete picture of the cellular changes occurring during *L. donovani* infection. There have been several studies that have intricately mapped out intracellular signalling dynamics using this approach (e.g. Humphrey et al. 2015); in particular, this approach may be particularly applicable since others have used it to successfully detail mTORC1-dependent phosphorylation patterns resulting from external stimuli (Hsu et al. 2011). This would add an additional dimension to the work that we have performed thus far in helping to characterise the multifaceted changes that the live parasite induces at the host-pathogen interface.

## 7.6 Concluding remarks

The work presented in this thesis has shown several examples of active manipulation by the live parasite. Although we have shown that CCR5 was not required for *L. donovani* LV9 amastigote infection, it was down-regulated by the live parasite and may play a role in directing the subsequent immune response. We have also characterised the protein composition of the parasite-containing compartment by developing a novel protocol to isolate intracellular *L. donovani* amastigotes from infected J774.2 cells for iTRAQ-labelled LC-MS/MS. Univariate and multivariate statistical analyses of the resulting dataset have revealed a number of proteins that were differentially expressed on compartments from cells infected with live parasites compared with HI parasites, many of which were involved in actin cytoskeleton dynamics, phagosome maturation and signalling networks. This work gives us new insights into what defines the parasite-containing compartment and suggests that the live parasite is able to exploit its compartment to fine-tune the host cell's response to infection.



## Appendix A: CCR5<sup>-/-</sup> mice



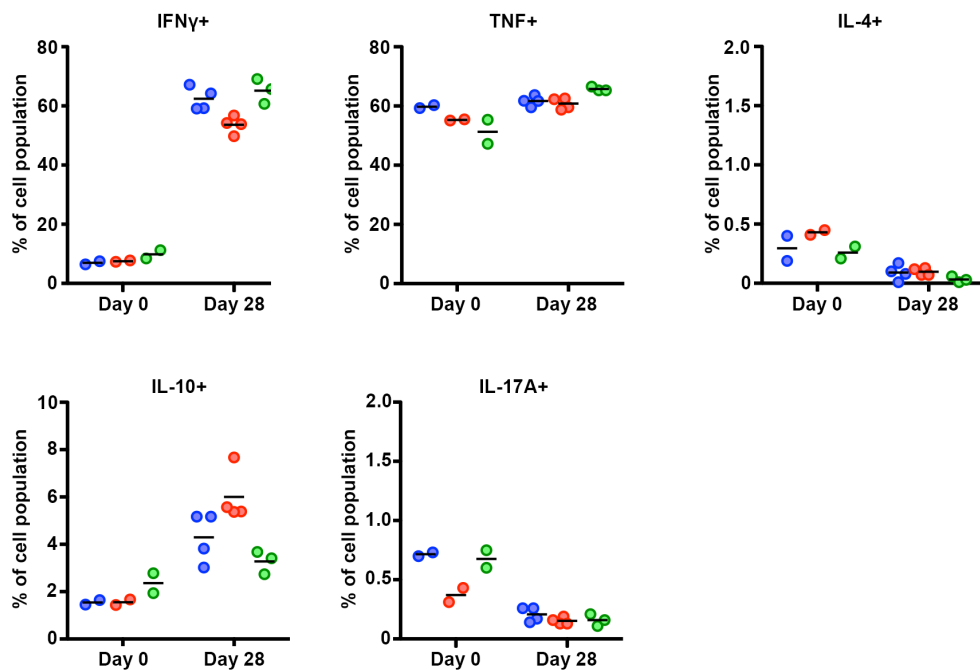
**FIGURE A1. Strategy adopted by Kuziel et al. 2003 to make CCR5<sup>-/-</sup> mice. A)** CCR5<sup>-/-</sup> embryonic stem (ES) cells were injected into a developing mouse embryo. The offspring of these chimeric mice can then pass on the CCR5<sup>-/-</sup> variation on to their own offspring to produce mice that have a permanent deletion of the whole CCR5 coding region. **B)** Summary of plasmid design and incorporation into embryonic stem (ES) cells. A 9.0kbp XbaI restriction fragment containing the gene for CCR5 was inserted into the XbaI site of the pBluescript vector, which also contains a gene for ganciclovir sensitivity (TK). The entire coding region of CCR5, ~550bp of the preceding intron and ~1.1kbp of DNA downstream of the translation stop codon were removed using BglIII and replaced with a 1.8kbp neomycin resistance gene in the opposite transcriptional orientation. ES cells that had successfully incorporated the vector could then be selected by treating cells with media containing neomycin and ganciclovir antibiotics.

## Appendix B: Detailed analysis of splenic populations from infected mice

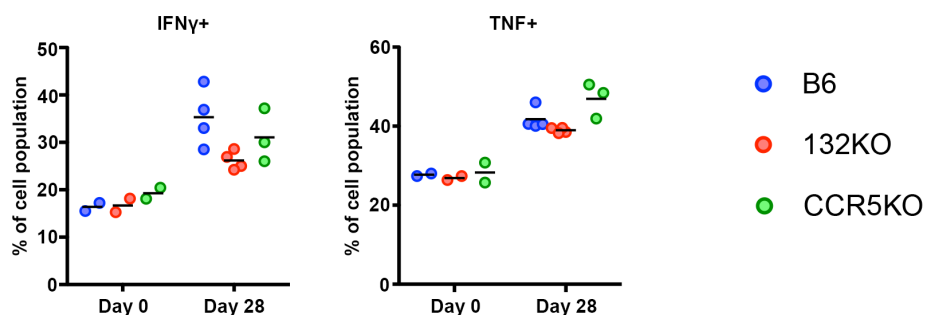
This assay was performed by Dr James Hewitson (University of York) on splenic cells isolated from infected wild-type ('B6') and CCR5<sup>-/-</sup> mice. Data are also shown for another knockout mouse for comparison (miR-132 microRNA knockout).

### Splenic T cells – intracellular cytokine profiles:

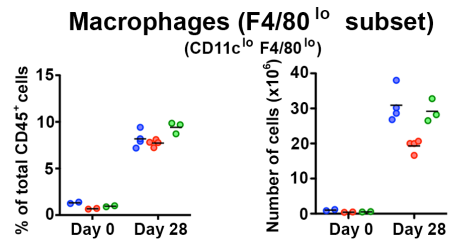
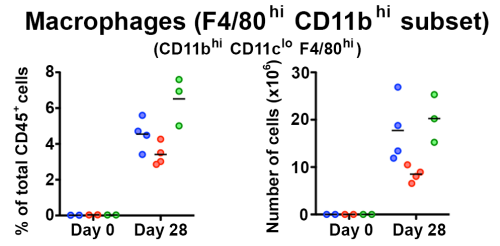
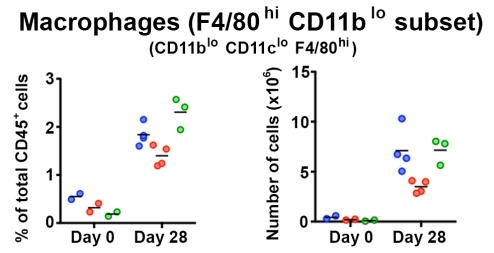
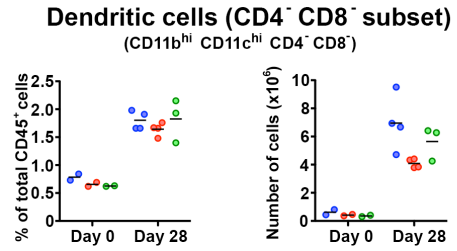
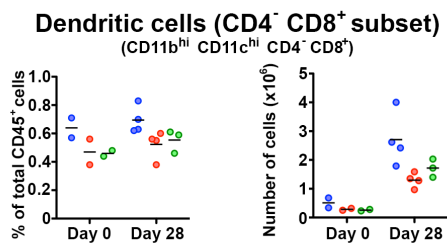
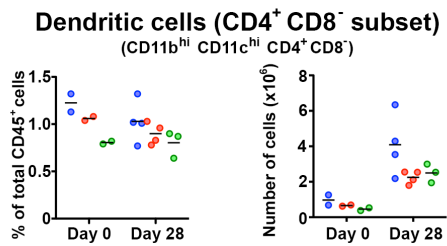
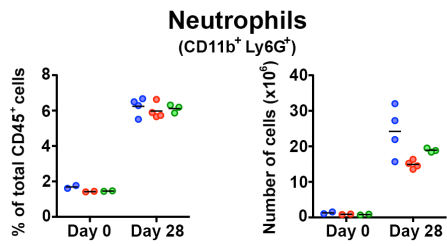
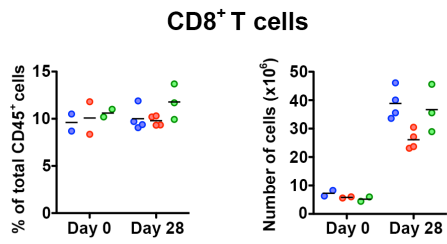
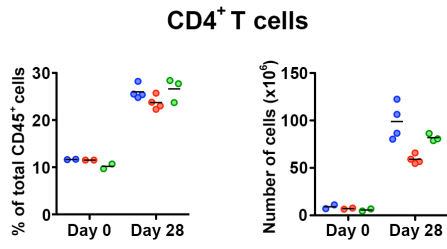
#### CD4<sup>+</sup> T cells:



#### CD8<sup>+</sup> T cells:



## Splenic CD45<sup>+</sup> cell populations:

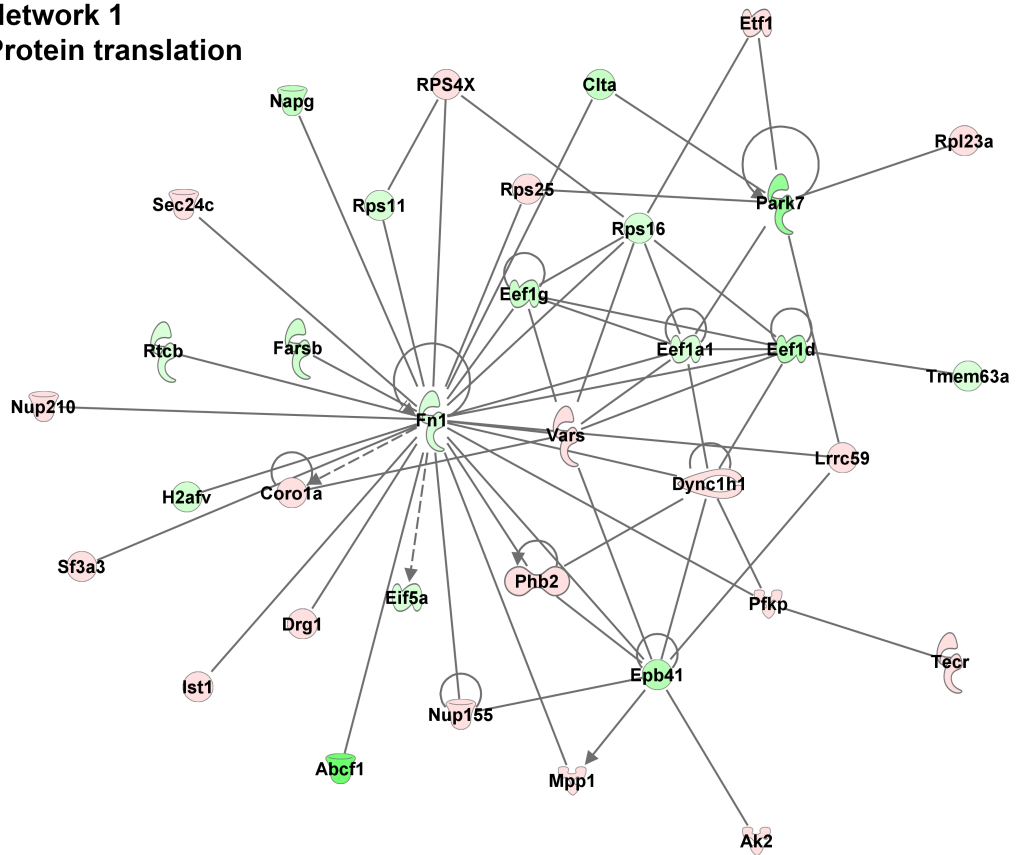


● B6 ● 132KO ● CCR5KO

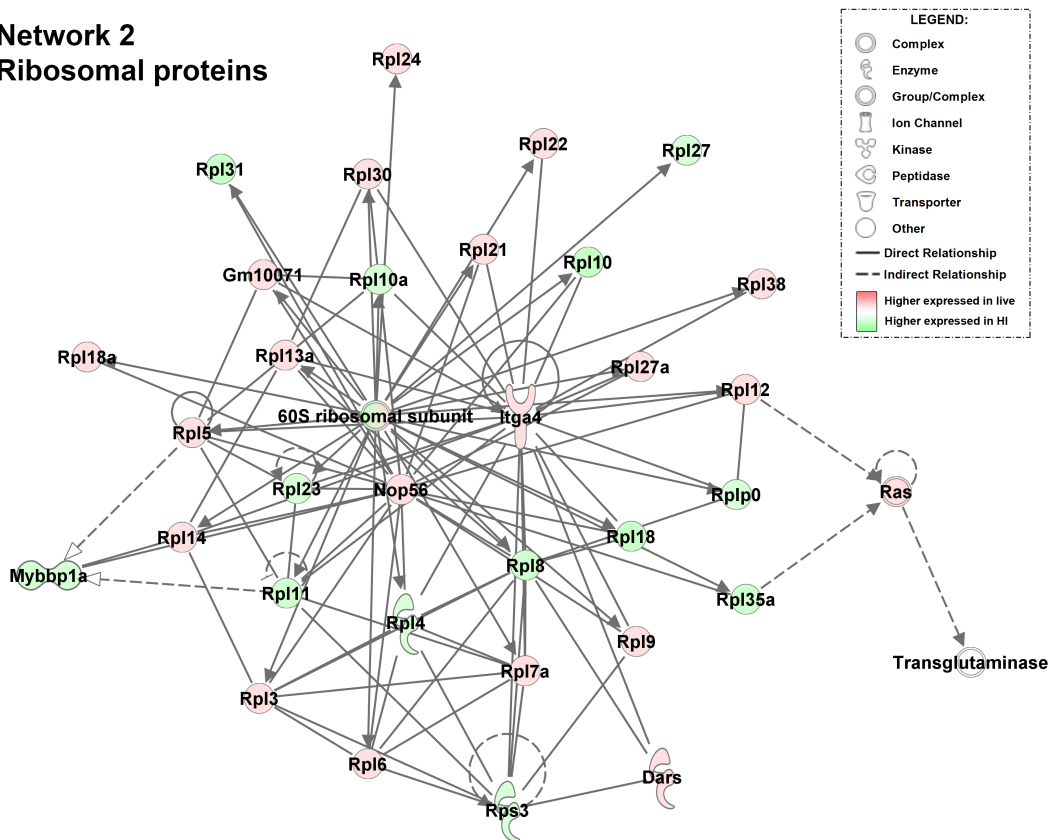
## Appendix C: Dynamic networks generated by IPA

The top 10 scoring networks generated by IPA for proteins present within isolated *Leishmania*-containing phagolysosomal samples are shown below, excluding network 6 and network 9 which are shown in **Figure 6.12**.

**Network 1  
Protein translation**



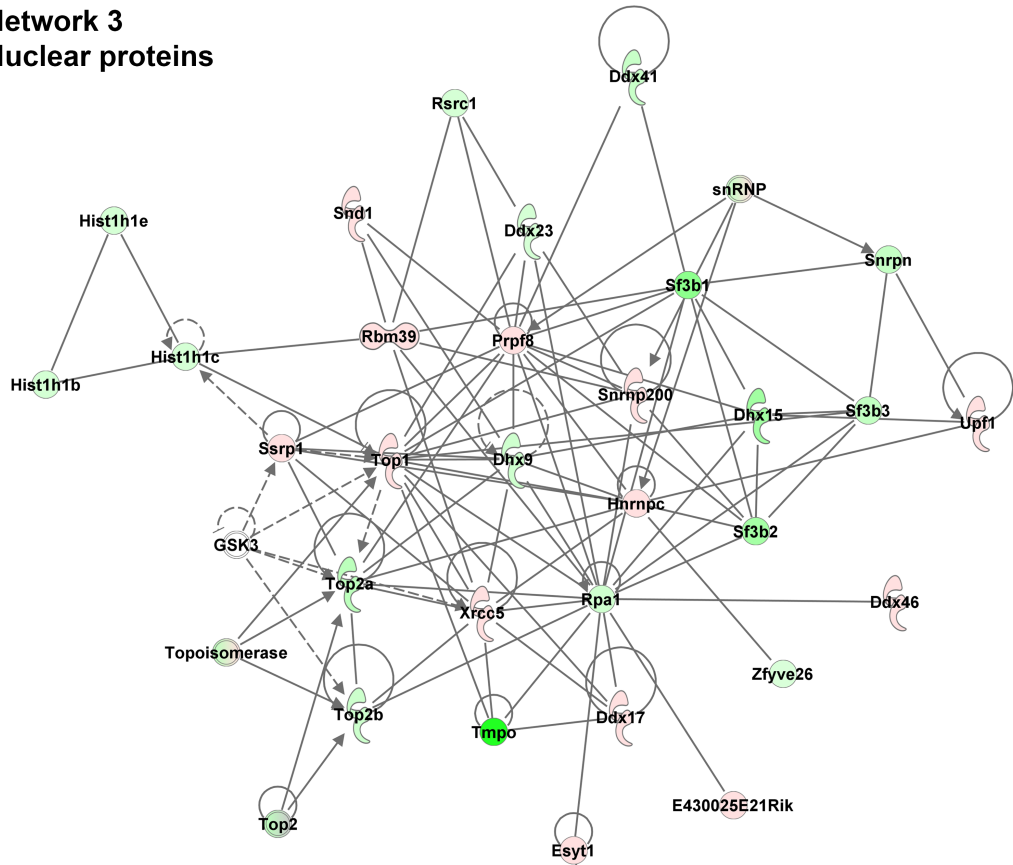
**Network 2  
Ribosomal proteins**



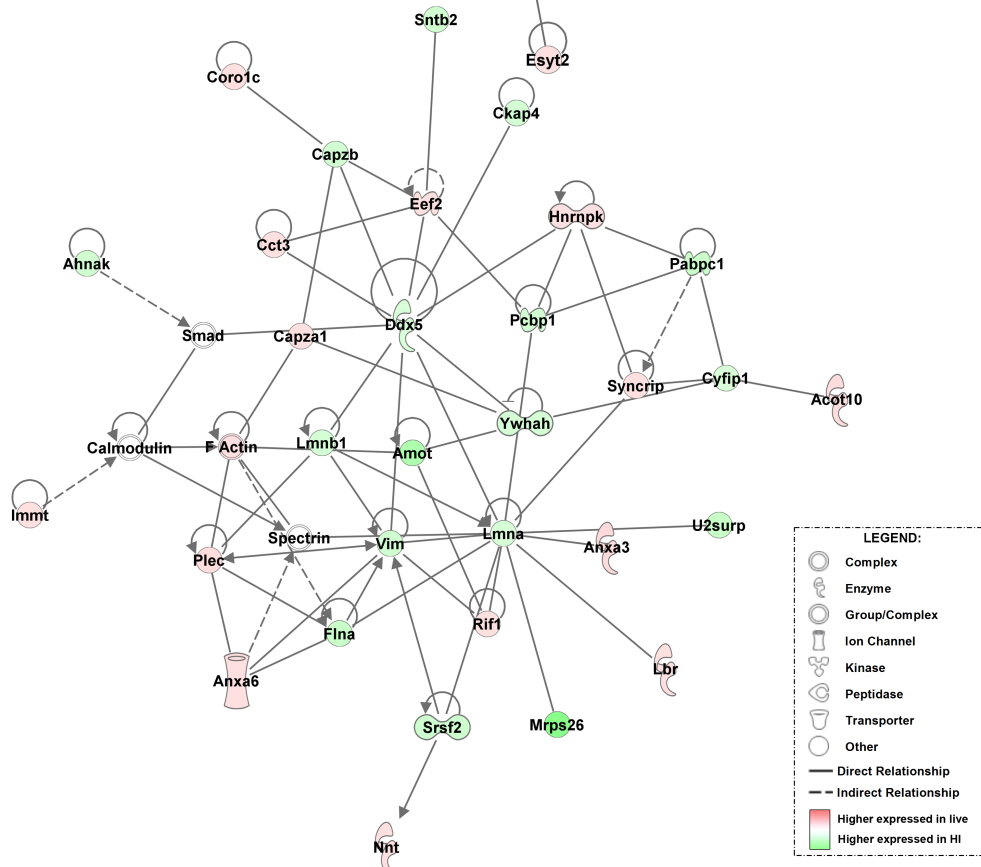
**LEGEND:**

- Complex
- Enzyme
- Group/Complex
- Ion Channel
- Kinase
- Peptidase
- Transporter
- Other
- Direct Relationship
- Indirect Relationship
- Higher expressed in live
- Higher expressed in HI

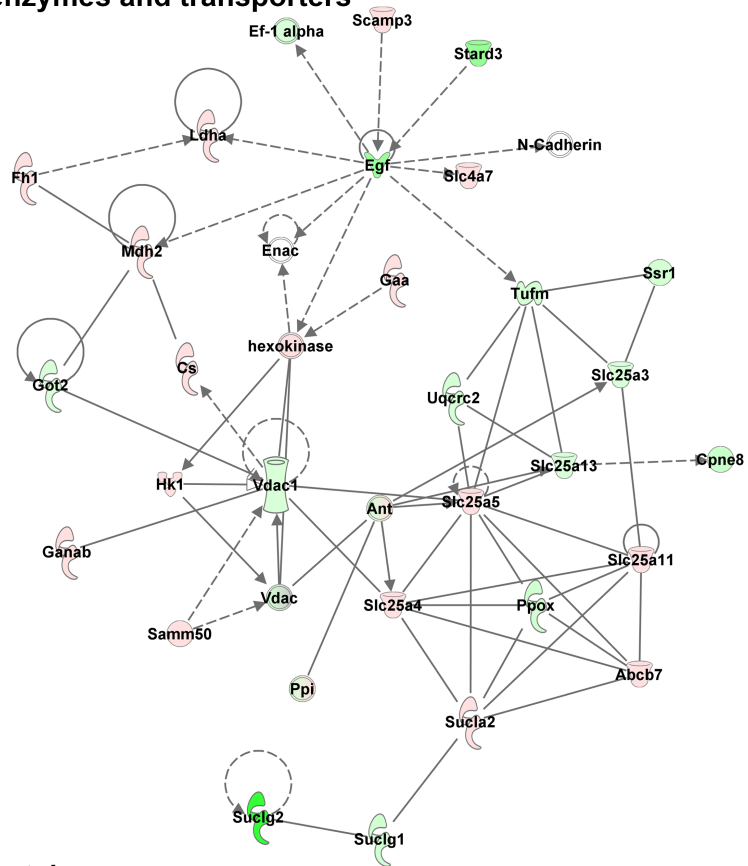
### Network 3 Nuclear proteins



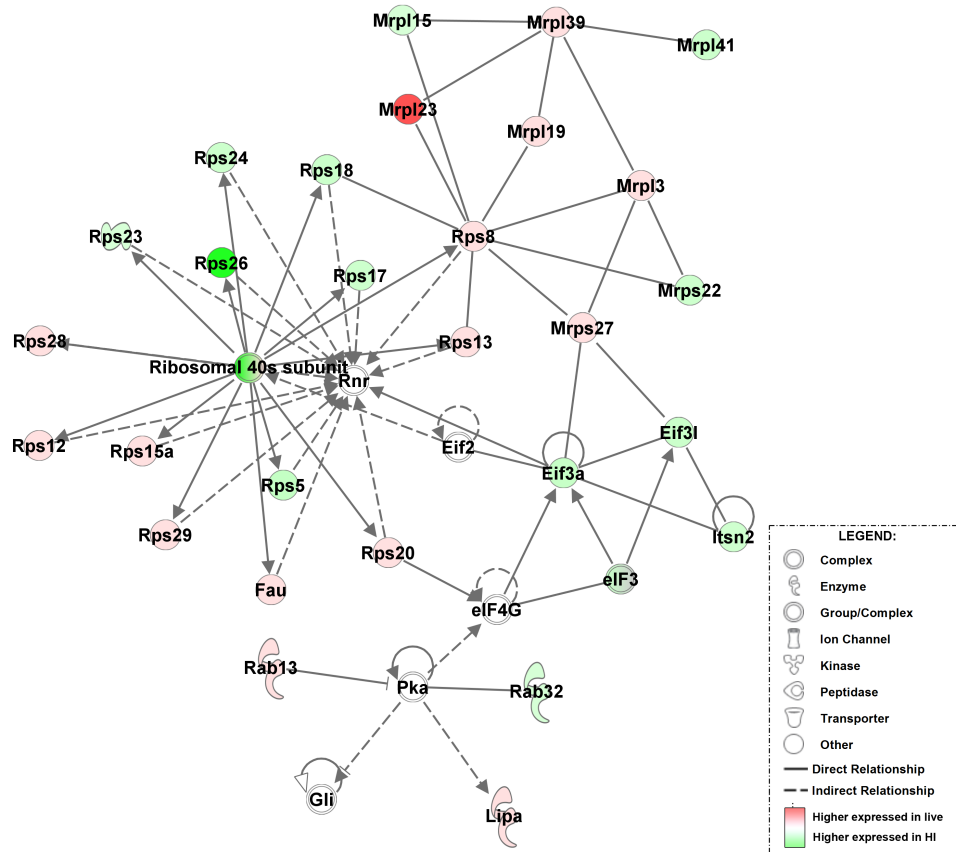
### Network 4 Actin-related and nuclear proteins



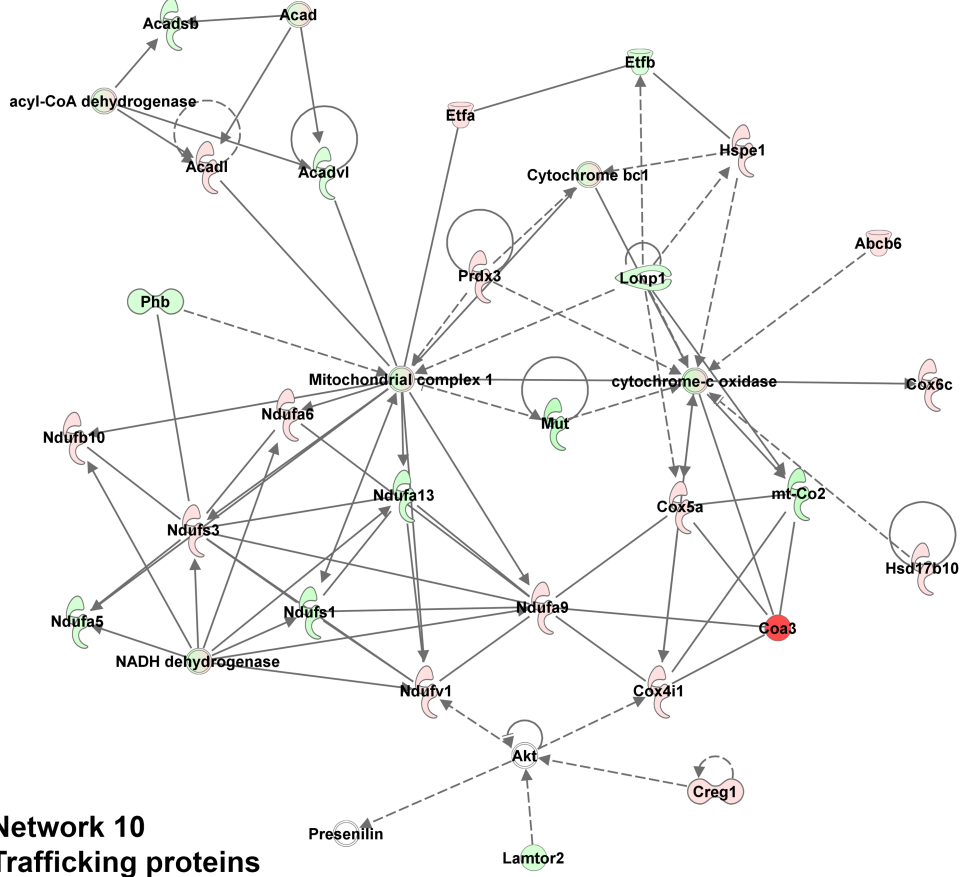
**Network 5**  
**Metabolism enzymes and transporters**



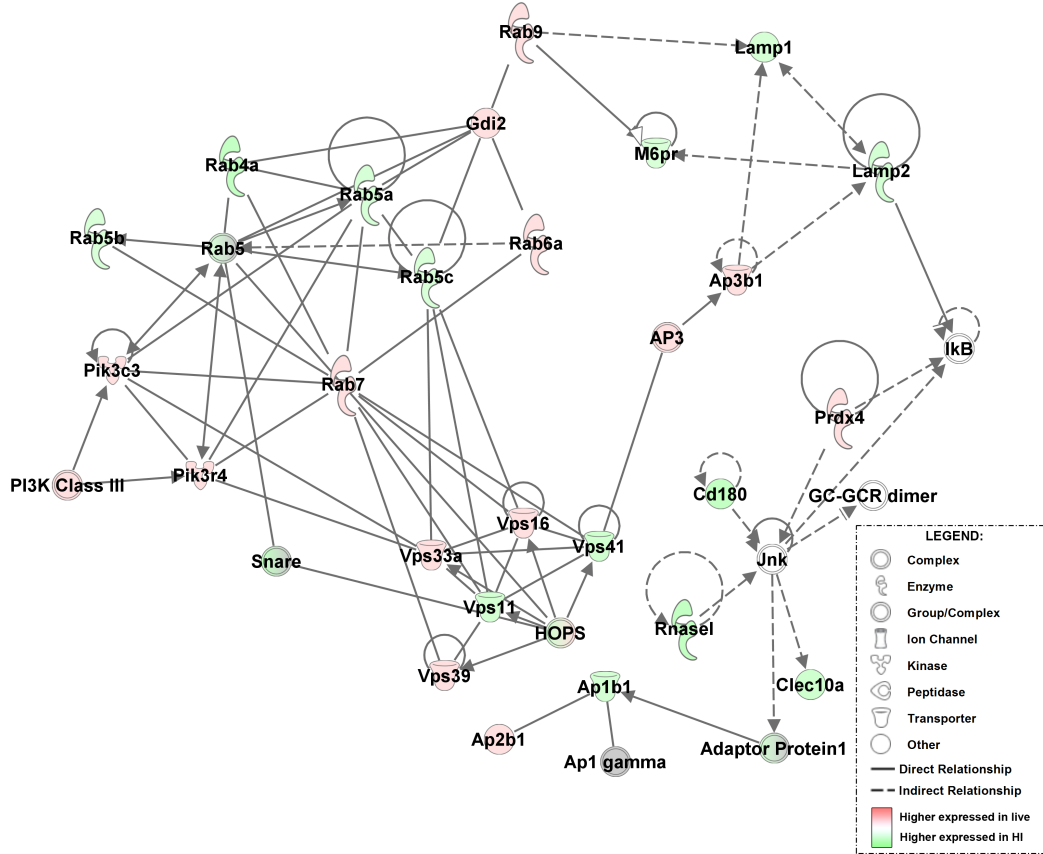
**Network 7**  
**Ribosomal proteins**



**Network 8  
Mitochondrial proteins**



**Network 10  
Trafficking proteins**



**LEGEND:**

- Complex
- Enzyme
- Group/Complex
- Ion Channel
- Kinase
- Peptidase
- Transporter
- Other
- Direct Relationship
- Indirect Relationship
- Higher expressed in live
- Higher expressed in HI



# Abbreviations

<b>AA</b>	Amino acid
<b>AOP</b>	Aminooxypentane
<b>Arf1</b>	Adenosine diphosphate-ribosylation factor 1
<b>Arp</b>	Actin-related protein
<b>ATP</b>	Adenosine triphosphate
<b>BCA</b>	Bicinchoninic acid
<b>BMDM</b>	Bone marrow-derived macrophage
<b>BME</b>	Basal medium Eagle
<b>BSA</b>	Bovine serum albumin
<b>CCD</b>	Charge-coupled device
<b>CCL</b>	C-C chemokine ligand
<b>CCR</b>	C-C chemokine receptor
<b>CD</b>	Cluster of differentiation
<b>Cdc42</b>	Cell division control protein 42 homolog
<b>CFDA-SE</b>	Carboxyfluorescein diacetate succinimidyl ester
<b>CL</b>	Cutaneous leishmaniasis
<b>CNS</b>	Central nervous system
<b>COPI</b>	Coat protein I
<b>CXCL</b>	C-X-C chemokine ligand
<b>CXCR</b>	C-X-C chemokine receptor
<b>DAPI</b>	4'-6' diamidine-2-phenylindole
<b>DNA</b>	Deoxyribonucleic acid
<b>DC</b>	Dendritic cell
<b>ddH<sub>2</sub>O</b>	Double distilled H <sub>2</sub> O
<b>DMEM</b>	Dulbecco's Modified Eagle's medium
<b>DMSO</b>	Dimethyl sulphoxide
<b>DRY</b>	Aspartate-arginine-tyrosine
<b>DTE</b>	Dithioerythritol
<b>ECL</b>	Extracellular loop
<b>EDTA</b>	Ethylenediaminetetraacetic acid
<b>EEA</b>	Early endosome antigen 1

<b>eIF2</b>	Eukaryotic initiation factor 2
<b>ELISA</b>	Enzyme-linked immunosorbent assay
<b>emPAI</b>	Exponentially modified protein abundance index
<b>ER</b>	Endoplasmic reticulum
<b>ERK</b>	Extracellular signal-regulated kinase
<b>ERM</b>	Ezrin, radixin and moesin
<b>ES</b>	Embryonic stem
<b>ESCRT</b>	Endosomal sorting complexes required for transport
<b>EV</b>	Extracellular vesicle
<b>FACS</b>	Fluorescence-activated cell sorting
<b>FC</b>	Flow cytometry
<b>FCS</b>	Foetal calf serum
<b>FDR</b>	False discovery rate
<b>FeDex</b>	Colloidal iron dextran
<b>FT</b>	Flow-through
<b>FYVE</b>	Fab 1, YOTB, Vac 1 and early endosome antigen 1
<b>g</b>	Grams
<b>GAP</b>	GTPase-activating protein
<b>GEF</b>	Guanine nucleotide exchange factor
<b>GPCR</b>	G protein-coupled receptor
<b>GRK</b>	G protein receptor kinase
<b>GDP</b>	Guanosine diphosphate
<b>GO</b>	Gene ontology
<b>GP</b>	Glycoprotein
<b>GST</b>	Glutathione S-transferase
<b>GTP</b>	Guanosine triphosphate
<b>HCA</b>	Hierarchical cluster analysis
<b>HI</b>	Heat inactivated
<b>HIV</b>	Human immunodeficiency virus
<b>HOPS</b>	Homotypic fusion and vacuole protein sorting
<b>HPRT</b>	Hypoxanthine guanine phosphoribosyl transferase
<b>hr</b>	Hour
<b>HRP</b>	Horseradish peroxidase

<b>ICL</b>	Intracellular loop
<b>IF</b>	Immunofluorescence
<b>IFN</b>	Interferon
<b>IgG</b>	Immunoglobulin G
<b>IL</b>	Interleukin
<b>IPA</b>	Ingenuity Pathway Analysis
<b>IPKB</b>	Ingenuity Pathways Knowledgebase
<b>IPTG</b>	Isopropyl $\beta$ -D-1-thiogalactopyranoside
<b>kDa</b>	Kilodaltons
<b>iTRAQ</b>	Isobaric tag for relative and absolute quantitation
<b>L</b>	Litre
<b>LAMP</b>	Lysosome-associated membrane protein
<b>LAMTOR2</b>	Late endosomal/lysosomal adaptor, mitogen-activated protein kinases and mammalian target of rapamycin activator 2
<b>LB</b>	Liquid broth
<b>LC-MS</b>	Liquid chromatography-mass spectrometry
<b>LC-MS/MS</b>	Liquid chromatography-tandem mass spectrometry
<b>LDS</b>	Lithium dodecyl sulphate
<b>LDU</b>	Leishman Donovan unit
<b>LPG</b>	Lipophosphoglycan
<b>LPS</b>	Lipopolysaccharide
<b>LTA</b>	Lipoteichoic acid
<b>m</b>	Metre
<b>M6PR</b>	Mannose-6-phosphate receptor
<b>m-CSF</b>	Macrophage colony stimulating factor
<b>MFI</b>	Mean fluorescence intensity
<b>mins</b>	Minutes
<b>MOI</b>	Multiplicity of infection
<b>mRNA</b>	Messenger ribonucleic acid
<b>MS</b>	Mass spectrometry
<b>MS/MS</b>	Tandem mass spectrometry
<b>mTOR</b>	Mammalian target of rapamycin

<b>mTORC1</b>	Mammalian target of rapamycin complex 1
<b>MVB</b>	Multivesicular body
<b>MWCO</b>	Molecular weight cut-off
<b>NADPH</b>	Nicotinamide adenine dinucleotide phosphate
<b>NED</b>	N-1-naphthylethylenediamine dihydrochloride
<b>NK</b>	Natural killer
<b>NPF</b>	Nucleation promoting factors
<b>N.s.d.</b>	No statistically significant difference
<b>nTreg</b>	Natural T regulatory
<b>OD</b>	Optical density
<b>OCT</b>	Optimal cutting temperature
<b>PBS</b>	Phosphate-buffered saline
<b>PC</b>	Principal component
<b>PCA</b>	Principal component analysis
<b>PCR</b>	Polymerase chain reaction
<b>PDZ</b>	Post synaptic density protein 95, Drosophila disc large tumor suppressor 1, and zonula occludens-1 protein
<b>pH</b>	Power of hydrogen
<b>PKC</b>	Protein kinase C
<b>PLS</b>	Partial least squares
<b>PNS</b>	Post-nuclear supernatant
<b>PS</b>	Phosphatidylserine
<b>psi</b>	Pounds per square inch
<b>PtpA</b>	Protein tyrosine phosphatase A
<b>PVDF</b>	Polyvinylidene difluoride
<b>qRT-PCR</b>	Quantitative real-time polymerase chain reaction
<b>Rac1</b>	Ras-related C3 botulinum toxin substrate 1
<b>RAG1</b>	Recombination activating gene 1
<b>RaLF</b>	Recruitment of adenosine diphosphate-ribosylation factor-1 to Legionella phagosome
<b>RANTES</b>	Regulated on activation, normal T cell expressed and secreted

<b>RhoA</b>	Ras homolog gene family member A
<b>RhoGDI</b>	Rho guanosine diphosphate-dissociation inhibitor
<b>RNA</b>	Ribonucleic acid
<b>RP105</b>	Radioprotective 105
<b>RPMI</b>	Roswell Park Memorial Institute
<b>siRNA</b>	Short interfering ribonucleic acid
<b>SDS-PAGE</b>	Sodium dodecyl sulphate polyacrylamide gel electrophoresis
<b>SILAC</b>	Stable isotope labelling by amino acids in cell culture
<b>SNARE</b>	Soluble N-ethylmaleimide-sensitive factor-attachment protein receptor
<b>SNP</b>	Single nucleotide polymorphism
<b>SPF</b>	Specific pathogen free
<b>SPION</b>	Supraparamagnetic iron oxide nanoparticle
<b>Spp.</b>	Species
<b>TAE</b>	Tris base, acetic acid and ethylenediaminetetraacetic acid
<b>TBS</b>	Tris-buffered saline
<b>TCA</b>	Trichloroacetic acid
<b>TEAB</b>	Triethylammonium bicarbonate
<b>TEM</b>	Transmission electron microscopy
<b>TEMED</b>	Tetramethylethylenediamine
<b>TFEB</b>	Transcription factor 'EB'
<b>TGF-<math>\beta</math></b>	Transforming growth factor $\beta$
<b>Th1</b>	Type 1 T helper
<b>Th2</b>	Type 2 T helper
<b>TLR</b>	Toll-like receptor
<b>TNF</b>	Tumour necrosis factor
<b>Treg</b>	T regulatory
<b>vATPase</b>	V-type vacuolar H <sup>+</sup> adenosine triphosphatase
<b>VPS</b>	Vacuolar protein sorting
<b>WASH</b>	Wiskott-Aldrich syndrome protein and Scar

	homologue
<b>WASP</b>	Wiskott-Aldrich syndrome protein
<b>WAVE</b>	Wiskott-Aldrich syndrome protein family verprolin-homologous protein
<b>WB</b>	Western blotting

## References

- Abe C, Tanaka S, Nishimura M, Ihara F, Xuan X & Nishikawa Y, 2015. Role of the chemokine receptor CCR5-dependent host defense system in *Neospora caninum* infections. *Parasit Vectors*, 8(1):1–12.
- Aebersold R, 2009. A stress test for mass spectrometry – based proteomics. *Nat Methods*, 6(6):411–2.
- Afonso LCC, Schariton TM, Vieira LQ, Wysocka M, Trinchieri G & Scott P, 1994. The adjuvant effect of interleukin-12 in a vaccine against *Leishmania major*. *Science*, 263(5144):235–7.
- Aliberti J, Reis e Sousa C, Schito M, Hieny S, Wells T, Huffnagle G & Sher A, 2000. CCR5 provides a signal for microbial induced production of IL-12 by CD8 alpha+ dendritic cells. *Nat Immunol*, 1(1):83–7.
- Alvar J, Vélez ID, Bern C, Herrero M, Desjeux P, Cano J, Jannin J & de Boer M, 2012. Leishmaniasis worldwide and global estimates of its incidence. *PLoS ONE*, 7(5).
- Amit A, Chaudhary R, Yadav A, Suman SS, Narayan S, Das VNR, Pandey K, Singh SK, Singh BK, Ali V, Das P & Bimal S, 2014. Evaluation of *Leishmania donovani* disulfide isomerase as a potential target of cellular immunity against visceral leishmaniasis. *Cell Immunol*, 289(1-2):76–85.
- Antoine JC, Prina E, Lang T & Courret N, 1998. The biogenesis and properties of the parasitophorous vacuoles that harbour *Leishmania* in murine macrophages. *Trends Microbiol*, 6(10):392–401.
- Asrat S, De Jesus DA, Hempstead AD, Ramabhadran V & Isberg RR, 2014. Bacterial pathogen manipulation of host membrane trafficking. *Annu Rev Cell Dev Biol*, 30:79–109.
- Atayde VD, Hassani K, da Silva Lira Filho A, Borges AR, Adhikari A, Martel C & Olivier M, 2016. *Leishmania* exosomes and other virulence factors: impact on innate immune response and macrophage functions. *Cell Immunol*, 309:7-18.
- Ato M, Stäger S, Engwerda CR & Kaye PM, 2002. Defective CCR7 expression on dendritic cells contributes to the development of visceral leishmaniasis. *Nat Immunol*, 3(12):1185–91.
- Bachelier F, Ben-Baruch A, Burkhardt AM, Combadiere C, Farber JM, et al., 2014. International Union of Pharmacology. LXXXIX. Update on the extended family of chemokine receptors and introducing a new nomenclature for atypical chemokine receptors. *Pharmacol Rev*, 66(1):1–79.
- Ballabio A, 2016. The awesome lysosome. *EMBO Mol Med*, 8(2):73–76.
- Bantscheff M, Schirle M, Sweetman G, Rick J & Kuster B, 2007. Quantitative mass spectrometry in proteomics: A critical review. *Anal Bioanal Chem*, 389(4):1017–31.
- Barashi N, Weiss ID, Wald O, Wald H, Beider K, Abraham M, Klein S, Goldenberg D, Axelrod J, Pikarsky E, Abramovitch R, Zeira E, Galun E & Peled A, 2013. Inflammation-induced hepatocellular carcinoma is dependent on CCR5 in mice. *Hepatology*, 58(3):1021-30.
- Barmania F & Pepper MS, 2013. C-C chemokine receptor type five (CCR5): An emerging target for the control of HIV infection. *Appl Transl Genom*, 2:3–16.
- Basu R, Bhaumik S, Halder AK, Naskar K, De T, Dana SK, Walden P & Roy S, 2007. Hybrid cell vaccination resolves *Leishmania donovani* infection by eliciting a strong CD8+ cytotoxic T-lymphocyte response with concomitant suppression of interleukin-10 (IL-10) but not IL-4 or IL-13. *Infect Immun*, 75(12):5956–66.
- Basu S, Ray A & Dittel BN, 2013. Differential representation of B cell subsets in mixed bone marrow chimera mice due to expression of allelic variants of CD45 (CD45.1/CD45.2). *J Immunol Methods*, 396(1-2):163–7.

- Beattie L, D'El-Rei Hermida M, Moore JWJ, Maroof A, Brown N, Lagos D & Kaye PM, 2013. A transcriptomic network identified in uninfected macrophages responding to inflammation controls intracellular pathogen survival. *Cell Host and Microbe*, 14(3):357–368.
- Beattie L, Evans KJ, Kaye PM & Smith DF, 2008. Transgenic Leishmania and the immune response to infection. *Parasite Immunol*, 30(4):255–66.
- Beattie L, Phillips R, Brown N, Owens BMJ, Chauhan N, Dalton JE & Kaye PM, 2011. Interferon regulatory factor 7 contributes to the control of Leishmania donovani in the mouse liver. *Infect Immun*, 79(3):1057–66.
- Beattie L, Sawtell A, Mann J, Frame T, Teal B, de Labastida Rivera F, Brown N, Walwyn-Brown K, Moore J, MacDonald S, Lim E, Dalton J, Engwerda C, MacDonald K & Kaye P, 2016. Bone marrow-derived and resident macrophages display unique transcriptomic signatures but similar biological functions. *J Hepatol*, 65(4):758–68.
- Benchimol M & de Souza W, 1981. Leishmania mexicana amazonensis: attachment to the membrane of the phagocytic vacuole of macrophages in vivo. *Z Parasitenkd*, 66(1):25–9.
- Benjamini Y & Hochberg Y, 1995. Controlling the false discovery rate: a practical and powerful approach to multiple testing. *J R Statist Soc*, 57(1):289–300.
- Benkirane M, Jin D, Chun R, Koup R & Jeang K, 1997. Mechanism of transdominant inhibition of CCR5-mediated HIV-1 infection by ccr5 $\Delta$ 32. *JBC*, 272(49):30603–6.
- Bennett LD, Fox JM & Signoret N, 2011. Mechanisms regulating chemokine receptor activity. *Immunology*, 134(3):246–56.
- Vanden Berghe T, Hulpiau P, Martens L, Vandenbroucke RE, Van Wonterghem E, Perry SW, Bruggeman I, Divert T, Choi SM, Vuylsteke M, Shestopalov VI, Libert C & Vandenabeele P, 2015. Passenger mutations confound interpretation of all genetically modified congenic mice. *Immunity*, 43(1):200–9.
- Bernstone L, van Wilgenburg B & James W, 2012. Several commercially available anti-CCR5 monoclonal antibodies lack specificity and should be used with caution. *Hybridoma*, 31(1):7–19.
- Beura LK, Hamilton SE, Bi K, Schenkel JM, Odumade OA, Casey KA, Thompson EA, Fraser KA, Rosato PC, Filali-Mouhim A, Sekaly RP, Jenkins MK, Vezys V, Haining WN, Jameson SC & Masopust D, 2016. Normalizing the environment recapitulates adult human immune traits in laboratory mice. *Nature*, 532(7600):512–6.
- Bhattacharyya S, Dey R, Majumder N, Bhattacharjee S & Majumdar S, 2008. A novel approach to regulate experimental visceral leishmaniasis in murine macrophages using CCR5 siRNA. *Scand J Immunol*, 67(4):345–53.
- Bhattacharyya S, Ghosh S, Dasgupta B, Mazumder D, Roy S & Majumdar S, 2002. Chemokine-induced leishmanicidal activity in murine macrophages via the generation of nitric oxide. *J Infect Dis*, 185(12):1704–8.
- Billings EA, Lee CS, Owen KA, Souza RSD, Ravichandran KS & Casanova JE, 2016. The adhesion GPCR BAI1 mediates macrophage ROS production and microbicidal activity against Gram-negative bacteria. *Sci Signal*, 9(413):ra14.
- Boggiatto PM, Martinez PA, Pullikuth A, Jones DE, Bellaire B, Catling A & Petersen C, 2014. Targeted extracellular signal-regulated kinase activation mediated by Leishmania amazonensis requires MP1 scaffold. *Microbes Infect*, 16(4):328–36.
- Brajão de Oliveira K, Reiche EMV, Kaminami Morimoto H, Pelegrinelli Fungaro MH, Estevão D, Pontello R, Franco Nasser T & Watanabe MAE, 2007. Analysis of the CC chemokine receptor 5 delta32 polymorphism in a Brazilian population with cutaneous leishmaniasis. *J Cutan Pathol*, 34(1):27–32.
- Bright NA, Davis LJ & Luzio JP, 2016. Endolysosomes are the principal intracellular sites of acid hydrolase activity. *Curr Biol*, 26(17):2233–45.



- Bustelo X, Sauzeau V & Berenjeno I, 2007. GTP-binding proteins of the Rho/Rac family: regulation, effectors and functions in vivo. *Bioessays*, 29(4):356–70.
- Cabrera R, Tu Z, Xu Y, Firpi RJ, Rosen HR, Liu C & Nelson DR, 2004. An immunomodulatory role for CD4+CD25+ regulatory T lymphocytes in hepatitis C virus infection. *Hepatology*, 40(5):1062–71.
- Callahan JW, Bagshaw RD & Mahuran DJ, 2009. The integral membrane of lysosomes: Its proteins and their roles in disease. *J Proteomics*, 72(1):23–33.
- Campbell-Valois FX, Trost M, Chemali M, Dill BD, Laplante A, Duclos S, Sadeghi S, Rondeau C, Morrow IC, Bell C, Gagnon E, Hatsuzawa K, Thibault P & Desjardins M, 2012. Quantitative proteomics reveals that only a subset of the endoplasmic reticulum contributes to the phagosome. *Mol Cell Proteomics*, 11(7):M111.016378.
- Canton J, Ndjamen B, Hatsuzawa K & Kima PE, 2012. Disruption of the fusion of Leishmania parasitophorous vacuoles with ER vesicles results in the control of the infection. *Cell Microbiol*, 14(6):937–48.
- Carlsson SR, Roth J, Piller F & Fukuda M, 1988. Isolation and characterization of human lysosomal membrane glycoproteins, h-lamp-1 and h-lamp-2. Major sialoglycoproteins carrying polylectosaminoglycan. *J Biol Chem*, 263(35):18911–9.
- Carmo CR, Esteves PJ, Ferrand N & Van Der Loo W, 2006. Genetic variation at chemokine receptor CCR5 in leporids: alteration at the 2nd extracellular domain by gene conversion with CCR2 in *Oryctolagus*, but not in *Sylvilagus* and *Lepus* species. *Immunogenetics*, 58(5-6):494–501.
- Casado-Vela J, Martínez-Esteso MJ, Rodríguez E, Borrás E, Elortza F & Bru-Martínez R, 2010. iTRAQ-based quantitative analysis of protein mixtures with large fold change and dynamic range. *Proteomics*, 10(2):343–7.
- Casciola-Rosen LA, Renfrew CA & Hubbard AL, 1992. Lumenal labeling of rat hepatocyte endocytic compartments: Distribution of several acid hydrolases and membrane receptors. *J Biol Chem*, 267(17):11856–64.
- Centers for Disease Control and Prevention Division of Parasitic Diseases, 2015. Leishmaniasis. Available at: <http://www.dpd.cdc.gov/dpdx/HTML/leishmaniasis.htm> [Accessed June 2, 2016].
- Chang J, Lee S & Blackstone C, 2014. Spastic paraplegia proteins spastizin and spatascin mediate autophagic lysosome reformation. *J Clin Invest*, 124(12):5249–62.
- Chang K & Dwyer D, 1978. Hamster macrophage interactions in vitro: cell entry, intracellular survival, and multiplication of amastigotes. *J Exp Med*, 147(2):515–30.
- Channon JY, Roberts MB & Blackwell JM, 1984. A study of the differential respiratory burst activity elicited by promastigotes and amastigotes of *Leishmania donovani* in murine resident peritoneal macrophages. *Immunology*, 53(2):345–55.
- de Chastellier C & Thilo L, 1997. Phagosome maturation and fusion with lysosomes in relation to surface property and size of the phagocytic particle. *Eur J Cell Biol*, 74(1):49–62.
- Chavier P, Parton RG, Hauri HP, Simons K & Zerial M, 1990. Localization of low molecular weight GTP binding proteins to exocytic and endocytic compartments. *Cell*, 62(2):317–29.
- Chelius D & Bondarenko PV, 2002. Quantitative profiling of proteins in complex mixtures using liquid chromatography and mass spectrometry. *J Proteome Res*, 1(4):317–323.
- Chen XS, Naumann TA, Kurre U, Jenkins NA, Copeland NG & Funk CD, 1995. cDNA cloning, expression, mutagenesis, intracellular localization, and gene chromosomal assignment of mouse 5-lipoxygenase. *J Biol Chem*, 270(30):17993–9.

- Chen Z, Yu S, Bakhiet M, Winblad B & Zhu J, 2003. The chemokine receptor CCR5 is not a necessary inflammatory mediator in kainic acid-induced hippocampal injury: Evidence for a compensatory effect by increased CCR2 and CCR3. *J Neurochem*, 86(1):61–8.
- Christmann BS, Moran JM, McGraw J a, Buller RML & Corbett J a, 2011. Ccr5 regulates inflammatory gene expression in response to encephalomyocarditis virus infection. *Am J Pathol*, 179(6):2941–51.
- Coelho-Finamore JM, Freitas VC, Assis RR, Melo MN, Novozhilova N, Secundino NF, Pimenta PF, Turco SJ & Soares RP, 2011. Leishmania infantum: Lipophosphoglycan intraspecific variation and interaction with vertebrate and invertebrate hosts. *Int J Parasitol*, 41(3):333–42.
- Conesa A, Gotz S, Garcia-Gomez J, Terol J, Talon M & Robles M, 2005. Blast2GO: A universal tool for annotation, visualization and analysis in functional genomics research. *Bioinformatics*, 21(18):3674–6.
- Cortez M, Huynh C, Fernandes MC, Kennedy K a, Aderem A & Andrews NW, 2011. Leishmania promotes its own virulence by inducing expression of the host immune inhibitory ligand CD200. *Cell Host Microbe*, 9(6):463–71.
- Courret N, Fréhel C, Gouhier N, Pouchelet M, Prina E, Roux P & Antoine JC, 2002. Biogenesis of Leishmania-harboring parasitophorous vacuoles following phagocytosis of the metacyclic promastigote or amastigote stages of the parasites. *J Cell Sci*, 115(11):2303–16.
- Cronemberger-Andrade A, Aragão-França L, de Araujo CF, Rocha VJ, Borges-Silva M da C, Figueiras CP, Oliveira PR, de Freitas LAR, Veras PST & Pontes-de-Carvalho L, 2014. Extracellular vesicles from Leishmania-infected macrophages confer an anti-infection cytokine-production profile to naïve macrophages. *PLoS Negl Trop Dis*, 8(9):e3161.
- Cuervo A & Dice J, 1996. A receptor for the selective uptake and degradation of proteins by lysosomes. *Science*, 273(5274):501–3.
- Cuervo A & Dice J, 1998. Lysosomes, a meeting point of proteins, chaperones, and proteases. *J Mol Med*, 76(1):6–12.
- Das S, Banerjee S, Majumder S, Paul Chowdhury B, Goswami A, Halder K, Chakraborty U, Pal NK & Majumdar S, 2014. Immune subversion by Mycobacterium tuberculosis through CCR5 mediated signaling: Involvement of IL-10. *PLoS ONE*, 9(4):1–11.
- Dasgupta B, Roychoudhury K, Ganguly S, Akbar MA, Das P & Roy S, 2003. Infection of human mononuclear phagocytes and macrophage-like THP1 cells with Leishmania donovani results in modulation of expression of a subset of chemokines and a chemokine receptor. *Scand J Immunol*, 57(4):366–74.
- Dean M, Carrington M, Winkler C, Huttley G, Smith M, Allikmets R, Goedert J, Buchbinder S, Vittinghoff E, Gomperts E, Donfield S, Vlahov D, Kaslow R, Saah A, Rinaldo C, Detels R & O'Brien S, 1996. Genetic restriction of HIV-1 infection and progression to AIDS by a deletion of the CKR5 structural gene: Hemophilia Growth and Development Study, Multicenter AIDS Cohort Study, Multicenter Hemophilia Cohort Study, San Francisco City Cohort, ALIVE Study. *Science*, 273(5283):1856–62.
- Deighton RF, Kerr LE, Short DM, Allerhand M, Whittle IR & McCulloch J, 2010. Network generation enhances interpretation of proteomic data from induced apoptosis. *Proteomics*, 10(6):1307–15.
- Delhaye M, Gravot A, Ayinde D, Niedergang F, Alizon M & Brelot A, 2007. Identification of a postendocytic sorting sequence in CCR5. *Mol Pharmacol*, 72(6):1497–1507.
- Dermine J, Goyette G, Houde M, Turco S & Desjardins M, 2005. Leishmania donovani lipophosphoglycan disrupts phagosomal microdomains in J774 macrophages. *Cell Microbiol*, 7(9):1263–70.
- Dermine JF, Scianimanico S, Privé C, Descoteaux A & Desjardins M, 2000.

- Leishmania promastigotes require lipophosphoglycan to actively modulate the fusion properties of phagosomes at an early step of phagocytosis. *Cell Microbiol*, 2(2):115–26.
- Desjardins BM & Descoteaux A, 1997. Inhibition of phagolysosomal biogenesis by the Leishmania lipophosphoglycan. *J Exp Med*, 185(12):2061–8.
- Desjardins M, 2003. ER-mediated phagocytosis: a new membrane for new functions. *Nat Rev Immunol*, 3(4):280–91.
- Desjardins M, Huber LA, Parton RG & Griffiths G, 1994. Biogenesis of phagolysosomes proceeds through a sequential series of interactions with the endocytic apparatus. *J Cell Biol*, 124(5):677–88.
- Deter R & De Duve C, 1967. Influence of glucagon, an inducer of cellular autophagy, on some physical properties of rat liver lysosomes. *J Cell Biol*, 33(2):437–49.
- Dey R, Sarkar A, Majumder N, Bhattacharyya SM, Roychoudhury K, Bhattacharyya S, Roy S & Majumdar S, 2005. Regulation of impaired protein kinase C signaling by chemokines in murine macrophages during visceral leishmaniasis. *Infect Immun*, 73(12):8334–44.
- Diettrich O, Mills K, Johnson AW, Hasilik A & Winchester BG, 1998. Application of magnetic chromatography to the isolation of lysosomes from fibroblasts of patients with lysosomal storage disorders. *FEBS letters*, 441(3):369–72.
- Diz AP, Carvajal-Rodríguez A & Skibinski DOF, 2011. Multiple hypothesis testing in proteomics: a strategy for experimental work. *MCP*, 10(3):M110.004374.
- Doeing DC, Borowicz JL & Crockett ET, 2003. Gender dimorphism in differential peripheral blood leukocyte counts in mice using cardiac, tail, foot, and saphenous vein puncture methods. *BMC Clin Pathol*, 3(1):3.
- Dong Y, Yu Q, Chen Y, Xu N, Zhao Q, Jia C, Zhang B, Zhang K, Zhang B, Xing L & Li M, 2015. The Ccz1 mediates the autophagic clearance of damaged mitochondria in response to oxidative stress in *Candida albicans*. *Int J Biochem Cell Biol*, 69:41–51.
- Dostálová A & Volf P, 2012. Leishmania development in sand flies: parasite-vector interactions overview. *Parasit Vectors*, 5(276):1–12.
- Dumoux M & Hayward RD, 2016. Membrane contact sites between pathogen-containing compartments and host organelles. *Biochim Biophys Acta*, 1861(8):895–9.
- Dunn OJ, 1961. Multiple comparisons among means. *Journal of the American Statistical Association*, 56(293):52–64.
- Dwinell MB, Eckmann L, Leopard JD, Varki NM & Kagnoff MF, 1999. Chemokine receptor expression by human intestinal epithelial cells. *Gastroenterology*, 117(2):359–67.
- Eden ER, 2016. The formation and function of ER-endosome membrane contact sites. *Biochim Biophys Acta*, 1861(8):874–9.
- Edinger AL, Mankowski JL, Doranz BJ, Margulies BJ, Lee B, Rucker J, Sharron M, Hoffman TL, Berson JF, Zink MC, Hirsch VM, Clements JE & Doms RW, 1997. CD4-independent, CCR5-dependent infection of brain capillary endothelial cells by a neurovirulent simian immunodeficiency virus strain. *Proc Natl Acad Sci U S A*, 94(26):14742–7.
- Elkin SR, Lakoduk AM & Schmid SL, 2016. Endocytic pathways and endosomal trafficking: a primer. *Wien Med Wochenschr*, 166(7-8):196-204.
- Engwerda CR, Murphy ML, Cotterell SEJ, Smelt SC & Kaye PM, 1998. Neutralization of IL-12 demonstrates the existence of discrete organ-specific phases in the control of *Leishmania donovani*. *Eur J Immunol*, 28(2):669–80.
- Escola J-M, Kuenzi G, Gaertner H, Foti M & Hartley O, 2010. CC chemokine receptor 5 (CCR5) desensitization: cycling receptors accumulate in the trans-Golgi network. *J Biol Chem*, 285(53):41772–80.
- Feasey N, Wansbrough-Jones M, Mabey DCW & Solomon AW, 2010. Neglected

- tropical diseases. *B Med Bull*, 93(1):179–200.
- Fehon RG, McClatchey AI & Bretscher A, 2010. Organizing the cell cortex: the role of ERM proteins. *Nat Rev Mol Cell Biol*, 11(4):276–87.
- Ferrari G, Langen H, Naito M & Pieters J, 1999. A coat protein on phagosomes involved in the intracellular survival of mycobacteria. *Cell*, 97(4):435–447.
- Flaherty L, 1981. *Congenetic strains* 1st ed., NY: Academic Press.
- Ford L, Hansell C & Nibbs R, 2013. Using fluorescent chemokine uptake to detect chemokine receptors by fluorescent activated cell sorting. *Methods Mol Biol*, 1013:203–14.
- Forgac M, 2007. Vacuolar ATPases: rotary proton pumps in physiology and pathophysiology. *Nat Rev Mol Cell Biol*, 8(11):917–29.
- Fox JM, Letellier E, Oliphant CJ & Signoret N, 2011. TLR2-dependent pathway of heterologous down-modulation for the CC chemokine receptors 1, 2, and 5 in human blood monocytes. *Blood*, 117(6):1851–60.
- Frank B, Marcu A, de Oliveira Almeida Petersen AL, Weber H, Stigloher C, Mottram JC, Scholz CJ & Schurigt U, 2015. Autophagic digestion of *Leishmania major* by host macrophages is associated with differential expression of BNIP3, CTSE, and the miRNAs miR-101c, miR-129, and miR-210. *Parasit Vectors*, 8(1):404.
- Freeman SA & Grinstein S, 2014. Phagocytosis: Receptors, signal integration, and the cytoskeleton. *Immunol Rev*, 262(1):193–215.
- de Freitas Balanco JM, Moreira ME, Bonomo A, Bozza PT, Amarante-Mendes G, Pirmez C & Barcinski MA, 2001. Apoptotic mimicry by an obligate intracellular parasite downregulates macrophage microbicidal activity. *Curr Biol*, 11(23):870–3.
- Gagnon E, Bergeron J & Desjardins M, 2005. ER-mediated phagocytosis: myth or reality. *J Leukoc Biol*, 77(6):843–5.
- Gagnon E, Duclos S, Rondeau C, Chevet E, Cameron PH, Steele-Mortimer O, Paiement J, Bergeron JJM & Desjardins M, 2002. Endoplasmic reticulum-mediated phagocytosis is a mechanism of entry into macrophages. *Cell*, 110(1):119–31.
- Galasso JM, Harrison JK & Silverstein FS, 1998. Excitotoxic brain injury stimulates expression of the chemokine receptor CCR5 in neonatal rats. *Am J Pathol*, 153(5):1631–40.
- Garin J, Diez R, Kieffer S, Dermine JF, Duclos S, Gagnon E, Sadoul R, Rondeau C & Desjardins M, 2001. The phagosome proteome: insight into phagosome functions. *J Cell Biol*, 152(1):165–80.
- Gerdes JM, Davis EE & Katsanis N, 2009. The vertebrate primary cilium in development, homeostasis, and disease. *Cell*, 137(1):32–45.
- Ghosh SS, Mukerjee S & Adhya S, 1998. Chromosome profile of *Leishmania donovani*: Interstrain and interspecific variations. *J Biosoc Sci*, 23(3):247–54.
- Glass WG, McDermott DH, Lim JK, Lekhong S, Yu SF, Frank WA, Pape J, Cheshier RC & Murphy PM, 2006. CCR5 deficiency increases risk of symptomatic West Nile virus infection. *J Exp Med*, 203(1):35–40.
- Glueck E, Hoog J, Smith A, Dawe H, Shaw M & Gull K, 2010. Beyond 9+0: noncanonical axoneme structures characterize sensory cilia from protists to humans. *FASEB J*, 24(9):3117–21.
- Golding H, Khurana S, Yarovinsky F, King LR, Abdoulaeva G, Antonsson L, Owman C, Platt EJ, Kabat D, Andersen JF & Sher A, 2005. CCR5 N-terminal region plays a critical role in HIV-1 inhibition by *Toxoplasma gondii*-derived cyclophilin-18. *J Biol Chem*, 280(33):29570–7.
- Gomez M, Contreras I, Halle M, Tremblay M, McMaster R & Olivier M, 2009. *Leishmania* GP63 alters host signaling through cleavage-activated protein tyrosine phosphatases. *Sci Signal*, 2(90):ra58.
- Goyette G, Boulais J, Carruthers NJ, Landry CR, Jutras I, Duclos S, Dermine JF,

- Michnick SW, LaBoissière S, Lajoie G, Barreiro L, Thibault P & Desjardins M, 2012. Proteomic characterization of phagosomal membrane microdomains during phagolysosome biogenesis and evolution. *Mol Cell Proteomics*, 11(11):1365–77.
- Gregory DJ, Sladek R, Olivier M & Matlashewski G, 2008. Comparison of the effects of *Leishmania major* or *Leishmania donovani* infection on macrophage gene expression. *Infect Immun*, 76(3):1186–92.
- Grieve AG, Moss SE & Hayes MJ, 2012. Annexin A2 at the interface of actin and membrane dynamics: A focus on its roles in endocytosis and cell polarization. *Int J Cell Biol*:852430.
- Griffin NM, Yu J, Long F, Oh P, Shore S, Li Y, Koziol JA & Schnitzer JE, 2010. Label-free, normalized quantification of complex mass spectrometry data for proteomic analysis. *Nat Biotechnol*, 28(1):83–9.
- Griffiths G & Mayorga L, 2007. Phagosome proteomes open the way to a better understanding of phagosome function. *Genome Biol*, 8(3):207.
- Gueirard P, Laplante A, Rondeau C, Milon G & Desjardins M, 2008. Trafficking of *Leishmania donovani* promastigotes in non-lytic compartments in neutrophils enables the subsequent transfer of parasites to macrophages. *Cell Microbiol*, 10(1):100–11.
- Guerfali FZ, Laouini D, Guizani-Tabbane L, Ottones F, Ben-Aissa K, Benkahla A, Manchon L, Piquemal D, Smandi S, Mghirbi O, Commes T, Marti J & Dellagi K, 2008. Simultaneous gene expression profiling in human macrophages infected with *Leishmania major* parasites using SAGE. *BMC Genomics*, 9:238.
- Guo M, Hartlova A, Dill BD, Prescott AR, Gierlinski M & Trost M, 2015. High-resolution quantitative proteome analysis reveals substantial differences between phagosomes of RAW 264.7 and bone marrow derived macrophages. *Proteomics*, 15(18):3169–74.
- Gupta N, Goyal N & Rastogi AK, 2001. In vitro cultivation and characterization of axenic amastigotes of *Leishmania*. *Trends Parasitol*, 17(3):150–3.
- Hailey DW, Rambold AS, Satpute-Krishnan P, Mitra K, Sougrat R, Kim PK & Lippincott-Schwartz J, 2010. Mitochondria supply membranes for autophagosome biogenesis during starvation. *Cell*, 141(4):656–667.
- Harder S, Bente M, Isermann K & Bruchhaus I, 2006. Expression of a mitochondrial peroxiredoxin prevents programmed cell death in *Leishmania donovani*. *Eukaryot Cell*, 5(5):861–70.
- Hariharan D, Douglas SD, Lee B, Lai JP, Campbell DE & Ho WZ, 1999. Interferon-gamma upregulates CCR5 expression in cord and adult blood mononuclear phagocytes. *Blood*, 93(4):1137–44.
- Harris R, Dwyer D & Kaye P, 1994. Characterisation of the site of antigen processing in *Leishmania* infected macrophages. *J Cell Biochem*, 56(18A):57.
- Hassani K, Shio MT, Martel C, Faubert D & Olivier M, 2014. Absence of metalloprotease GP63 alters the protein content of leishmania exosomes. *PLoS ONE*, 9(4):e95007.
- Hazan U, Romero IA, Canello R, Valente S, Perrin V, Mariot V, Dumonceaux J, Gerhardt CC, Strosberg AD, Couraud P & Pietri-rouxel F, 2002. Human adipose cells express CD4, CXCR4, CCR5 and receptors: a new target cell type for the immunodeficiency virus-1? *Faseb J*, 16:1254–6.
- Hegedus K, Takats S, Boda A, Jipa A, Nagy P, Varga K, Kovacs A & Juhasz G, 2016. The Ccz1-Mon1-Rab7 module and Rab5 control distinct steps of autophagy. *Mol Biol Cell*, 27(20):3132–42.
- Henne WM, 2016. Organelle remodeling at membrane contact sites. *J Struct Biol*, 196(1):15–9.
- Hirst J, Futter CE & Hopkins CR, 1998. The kinetics of mannose 6-phosphate receptor trafficking in the endocytic pathway in HEp-2 Cells: the receptor enters and rapidly leaves multivesicular endosomes without accumulating in a

- prelysosomal compartment. *Mol Biol Cell*, 9(4):809–16.
- Hisaeda H, Maekawa Y, Iwakawa D, Okada H, Himeno K, Kishihara K, Tsukumo S & Yasutomo K, 2004. Escape of malaria parasites from host immunity requires CD4+ CD25+ regulatory T cells. *Nat Med*, 10(1):29–30.
- Horwitz MA, 1983. The Legionnaires' disease bacterium (*Legionella pneumophila*) inhibits phagosome-lysosome fusion in human monocytes. *J Exp Med*, 158(6):2108–26.
- Hsu PP, Kang SA, Rameseder J, Zhang Y, Ottina KA, Lim D, Peterson TR, Choi Y, Gray NS, Yaffe MB, Marto JA & Sabatini DM, 2011. The mTOR-regulated phosphoproteome reveals a mechanism of mTORC1-mediated inhibition of growth factor signaling. *Science*, 332(6035):1317–22.
- Hsu VW, Bai M & Li J, 2012. Getting active: protein sorting in endocytic recycling. *Nat Rev Mol Cell Biol*, 13(5):323–8.
- Humphrey SJ, Azimifar SB & Mann M, 2015. High-throughput phosphoproteomics reveals in vivo insulin signaling dynamics. *Nat Biotechnol*, 33(9):990–5.
- Hutchings CJ, Koglin M & Marshall FH, 2010. Therapeutic antibodies directed at G protein-coupled receptors. *MAbs*, 2(6):594–606.
- Ishihama Y, Oda Y, Tabata T, Sato T, Nagasu T, Rappsilber J & Mann M, 2005. Exponentially Modified Protein Abundance Index (emPAI) for Estimation of Absolute Protein Amount in Proteomics by the Number of Sequenced Peptides per Protein. *Mol Cell Proteomics*, 4(9):1265–72.
- Isnard A, Christian JG, Kodiha M, Stochaj U, McMaster WR & Olivier M, 2015. Impact of *Leishmania* infection on host macrophage nuclear physiology and nucleopore complex integrity. *PLoS Pathog*, 11(3):1–26.
- Ivens AC, Peacock CS, Worthey EA, Murphy L, Aggarwal G, et al., 2005. The genome of the kinetoplastid parasite, *Leishmania major*. *Science*, 309(5733):436–42.
- Jain K & Jain NK, 2014. Vaccines for visceral leishmaniasis: A review. *J Immunol Methods*, 422:1–12.
- Jaiswal JK, Lauritzen SP, Scheffer L, Sakaguchi M, Bunkenborg J, Simon SM, Kallunki T, Jäättelä M & Nylandsted J, 2014. S100A11 is required for efficient plasma membrane repair and survival of invasive cancer cells. *Nat Commun*, 5:3795.
- Jayachandran R, Sundaramurthy V, Combaluzier B, Mueller P, Korf H, Huygen K, Miyazaki T, Albrecht I, Massner J & Pieters J, 2007. Survival of mycobacteria in macrophages is mediated by coronin 1-dependent activation of calcineurin. *Cell*, 130(1):37–50.
- Ji J, Sun J & Soong L, 2003. Impaired expression of inflammatory cytokines and chemokines at early stages of infection with *Leishmania amazonensis*. *Infect Immun*, 71(8):4278–88.
- Johnson DE, Ostrowski P, Jaumouillé V & Grinstein S, 2016. The position of lysosomes within the cell determines their luminal pH. *J Cell Biol*, 212(6):677–92.
- Jones KL, Maguire JJ & Davenport AP, 2011. Chemokine receptor CCR5: From AIDS to atherosclerosis. *Br J Pharmacol*, 162(7):1453–69.
- Jones TC, Yeh S & Hirsch JG, 1972. The interaction between *Toxoplasma gondii* and mammalian cells. *J Exp Med*, 136:1157–72.
- Kagan JC & Roy CR, 2002. *Legionella* phagosomes intercept vesicular traffic from endoplasmic reticulum exit sites. *Nat Cell Biol*, 4(12):945–54.
- Kaplan G, Mathur N, Job C, Nath I & Cohn ZA, 1989. Effect of multiple interferon gamma injections on the disposal of *Mycobacterium leprae*. *Proc Natl Acad Sci U S A*, 86(20):8073–7.
- Karimpour-Fard A, Epperson LE & Hunter LE, 2015. A survey of computational tools for downstream analysis of proteomic and other omic datasets. *Hum Genomics*, 9:28.

- Kassi M, Kassi M, Afghan AK, Rehman R & Kasi PM, 2008. Marring leishmaniasis: The stigmatization and the impact of cutaneous leishmaniasis in Pakistan and Afghanistan. *PLoS Negl Trop Dis*, 2(10):e259.
- Kaye P & Scott P, 2011. Leishmaniasis: complexity at the host-pathogen interface. *Nat Rev Microbiol*, 9(8):604–15.
- Kaye PM, Curry AJ & Blackwell JM, 1991. Differential production of Th1- and Th2-derived cytokines does not determine the genetically controlled or vaccine-induced rate of cure in murine visceral leishmaniasis. *J Immunol*, 146(8):2763–70.
- Kershaw T, Wavre-Shapton ST, Signoret N & Marsh M, 2009. Analysis of chemokine receptor endocytosis and intracellular trafficking. *Methods Enzymol*, 460(9):357–77.
- Khan IA, Thomas SY, Moretto MM, Lee FS, Islam SA, Combe C, Schwartzman JD & Luster AD, 2006. CCR5 is essential for NK cell trafficking and host survival following *Toxoplasma gondii* infection. *PLoS Pathog*, 2(6):484–500.
- Khan S, Situ G, Decker K & Schmidt C, 2003. GoFigure: automated Gene Ontology annotation. *Bioinformatics*, 19(18):2484–5.
- Kima PE & Dunn W, 2005. Exploiting calnexin expression on phagosomes to isolate *Leishmania* parasitophorous vacuoles. *Microb Pathog*, 38(4):139–45.
- Klein I, Cornejo JC, Polakos NK, John B, Wuensch SA, Topham DJ, Pierce RH & Crispe IN, 2007. Kupffer cell heterogeneity: functional properties of bone marrow-derived and sessile hepatic macrophages. *Blood*, 110(12):4077–85.
- Knapp S, Vocadlo D, Gao Z, Kirk B, Lou J, Withers SG, 1996. NAG-thiazoline, an N-acetyl-hexosaminidase inhibitor that implicates acetamido participation. *J Am Chem Soc*, (10):6804–5.
- Kumar Y & Valdivia RH, 2009. Leading a sheltered life: intracellular pathogens and maintenance of vacuolar compartments. *Cell Host Microbe*, 5(6):593–601.
- Kundra R & Kornfeld S, 1999. Asparagine-linked oligosaccharides protect Lamp-1 and Lamp-2 from intracellular proteolysis. *J Biol Chem*, 274(43):31039–46.
- Kuziel WA, Dawson TC, Quinones M, Garavito E, Chenuaux G, Ahuja SS, Reddick RL & Maeda N, 2003. CCR5 deficiency is not protective in the early stages of atherogenesis in apoE knockout mice. *Atherosclerosis*, 167(1):25–32.
- Lang T, Hellio R, Kaye PM & Antoine JC, 1994. *Leishmania donovani*-infected macrophages: characterization of the parasitophorous vacuole and potential role of this organelle in antigen presentation. *J Cell Sci*, 107(8):2137–50.
- Latosinska A, Vougas K, Makridakis M, Klein J, Mullen W, Abbas M, Stravodimos K, Katafigiotis I, Merseburger AS, Zoidakis J, Mischak H, Vlahou A & Jankowski V, 2015. Comparative analysis of label-free and 8-plex iTRAQ approach for quantitative tissue proteomic analysis. *PLoS ONE*, 10(9):1–25.
- Leary O, Labeling S, Fadok VA, Bratton DL, Rose DM, Pearson A, Ezekewitz RAB & Henson PM, 2000. A receptor for phosphatidylserine-specific clearance of apoptotic cells. *Nature*, 260(1996):85–90.
- Li Q, Jagannath C, Rao PK, Singh CR & Lostumbo G, 2010. Analysis of phagosomal proteomes: From latex-bead to bacterial phagosomes. *Proteomics*, 10(22):4098–116.
- Li Z, Adams RM, Chourey K, Hurst GB, Hettich RL & Pan C, 2012. Systematic comparison of label-free, metabolic labeling, and isobaric chemical labeling for quantitative proteomics on LTQ orbitrap velos. *J Proteome Res*, 11(3):1582–90.
- Liévin-Le Moal V & Loiseau PM, 2016. *Leishmania* hijacking of the macrophage intracellular compartments. *FEBS Journal*, 283(4):598–607.
- Lin MM, Kim DK, El Haj AJ & Dobson J, 2008. Development of superparamagnetic iron oxide nanoparticles (SPIONS) for translation to clinical applications. *IEEE Trans Nanobioscience*, 7(4):298–305.
- Liu J, Louie S, Hsu W, Yu KM, Nicholas HB & Rosenquist GL, 2008. Tyrosine

- sulfation is prevalent in human chemokine receptors important in lung disease. *Am J Respir Cell Mol Biol*, 38(6):738–43.
- Livak KJ & Schmittgen TD, 2001. Analysis of relative gene expression data using real-time quantitative PCR and the 2(-Delta Delta C(T)) method. *Methods*, 25:402–8.
- Lodge R & Descoteaux A, 2005. Leishmania donovani promastigotes induce periphagosomal F-actin accumulation through retention of the GTPase Cdc42. *Cell Microbiol*, 7(11):1647–58.
- Lodge R & Descoteaux A, 2008. Leishmania invasion and phagosome biogenesis. *Subcell Biochem*, 47:174–81.
- Lodge R & Descoteaux A, 2006. Phagocytosis of Leishmania donovani amastigotes is Rac1 dependent and occurs in the absence of NADPH oxidase activation. *Eur J Immunol*, 558:2735–44.
- Long GS, Bryant JM, Taylor PW & Luzio JP, 1995. Complete nucleotide sequence of the gene encoding bacteriophage E endosialidase: implications for K1E endosialidase structure and function. *Biochem J*, 309(2):543–50.
- Lorenz MC, Bender JA & Fink GR, 2004. Transcriptional response of Candida albicans upon internalization by macrophages. *Eukaryot Cell*, 3(5):1076–87.
- Love DC, Mentink Kane M & Mosser DM, 1998. Leishmania amazonensis: the phagocytosis of amastigotes by macrophages. *Exp Parasitol*, 88(3):161–71.
- Lusis AJ, Yu J & Wang SS, 2007. The problem of passenger genes in transgenic mice. *Arterioscler Thromb Vasc Biol*, 27(10):2100–3.
- Luzio JP, Gray SR & Bright NA, 2010. Endosome–lysosome fusion. *Biochem Soc Trans*, 38(6):1413–6.
- Luzio JP, Pryor PR & Bright NA, 2007. Lysosomes: fusion and function. *Nat Rev Mol Cell Biol*, 8(8):622–32.
- Lynne AM, Foley SL & Nolan LK, 2006. Immune response to recombinant Escherichia coli Iss protein in poultry. *Avian Dis*, 50(2):273–6.
- Mack M, Brühl H, Gruber R, Jaeger C, Cihak J, Eiter V, Plachý J, Stangassinger M, Uhlig K, Schattenkirchner M & Schlöndorff D, 1999. Predominance of mononuclear cells expressing the chemokine receptor CCR5 in synovial effusions of patients with different forms of arthritis. *Arthritis Rheuma*, 42(5):981–8.
- Mack M, Cihak J, Simonis C, Luckow B, Proudfoot AE, Plachý J, Brühl H, Frink M, Anders HJ, Vielhauer V, Pfirstinger J, Stangassinger M & Schlöndorff D, 2001. Expression and characterization of the chemokine receptors CCR2 and CCR5 in mice. *J Immunol*, 166(7):4697–704.
- Mack M, Luckow B, Nelson P, Cihak J, Simmons G, Clapham P, Signoret N, Marsh M, Borlat F, Stangassinger F, Wells T, Schlöndorff D & Proudfoot A, 1998. AOP-RANTES prevents CCR5 recycling: a novel inhibitory mechanism of HIV infectivity. *J Exp Med*, 187(8):1215–24.
- Majumdar SB, Bhattacharya P, Bhattacharjee S, Majumder S, Banerjee S & Majumdar S, 2014. Toll like receptor 2 and CC chemokine receptor 5 cluster in the lipid raft enhances the susceptibility of Leishmania donovani infection in macrophages. *Indian J Exp Biol*, 52(1):17–29.
- Makino Y, Cook DN, Smithies O, Hwang OY, Neilson EG, Turka LA, Sato H, Wells AD & Danoff TM, 2002. Impaired T cell function in RANTES-deficient mice. *Clin Immunol*, 102(3):302–309.
- Mantegazza AR, Guttentag SH, El-Benna J, Sasai M, Iwasaki A, Shen H, Laufer TM & Marks MS, 2012. Adaptor protein-3 in dendritic cells facilitates phagosomal Toll-like receptor signaling and antigen presentation to CD4+ T cells. *Immunity*, 36(5):782–94.
- Mantovani A, Sica A, Sozzani S, Allavena P, Vecchi A & Locati M, 2004. The chemokine system in diverse forms of macrophage activation and polarization. *Trends Immunol*, 25(12):677–86.



- Marchese A, Paing MM, Temple BRS & Trejo J, 2008. G protein-coupled receptor sorting to endosomes and lysosomes. *Annu Rev Pharmacol Toxicol*, 48:601–29.
- Maroof A, Brown N, Smith B, Hodgkinson MR, Maxwell A, Losch FO, Fritz U, Walden P, Lacey CNJ, Smith DF, Aebischer T & Kaye PM, 2012. Therapeutic vaccination with recombinant adenovirus reduces splenic parasite burden in experimental visceral leishmaniasis. *J Infect Dis*, 205(5):853–63.
- Martin DMA, Berriman M & Barton GJ, 2004. GOtcha: a new method for prediction of protein function assessed by the annotation of seven genomes. *BMC Bioinformatics*, 5:178.
- Martin-Blondel G, Brassat D, Bauer J, Lassmann H & Liblau RS, 2016. CCR5 blockade for neuroinflammatory diseases — beyond control of HIV. *Nat Rev Neurol*, 12(2):95–105.
- Martina JA, Chen Y, Gucek M & Puertollano R, 2012. MTORC1 functions as a transcriptional regulator of autophagy by preventing nuclear transport of TFEB. *Autophagy*, 8(6):903–914.
- Martinez FO, Helming L, Milde R, Varin A, Melgert BN, Draijer C, Thomas B, Fabbri M, Crawshaw A, Ho LP, Hacken NH Ten, Jimenez VC, Kootstra NA, Hamann J, Greaves DR, Locati M, Mantovani A & Gordon S, 2013. Genetic programs expressed in resting and IL-4 alternatively activated mouse and human macrophages: Similarities and differences. *Blood*, 121(9):57–70.
- Maspi N, Abdoli A & Ghaffarifar F, 2016. Pro- and anti-inflammatory cytokines in cutaneous leishmaniasis: a review. *Pathog Glob Health*, 110(6):247–60.
- Matsumoto A, 1981. Isolated and electron microscopic observations of intracytoplasmic inclusions containing *Chlamydia psittaci*. *J Bacteriol*, 145(1):605–12.
- Matte C & Olivier M, 2002. Leishmania-induced cellular recruitment during the early inflammatory response: modulation of proinflammatory mediators. *J Infect Dis*, 185(5):673–81.
- McCall LI, Zhang WW & Matlashewski G, 2013. Determinants for the development of visceral leishmaniasis disease. *PLoS Pathog*, 9(1):e1003053.
- McCarthy FM, Bridges SM, Wang N, Magee GB, Williams WP, Luthe DS & Burgess SC, 2007. AgBase: A unified resource for functional analysis in agriculture. *Nucleic Acids Res*, 35(SUPPL. 1):599–603.
- McCarthy FM, Wang N, Magee GB, Nanduri B, Lawrence ML, Camon EB, Barrell DG, Hill DP, Dolan ME, Williams WP, Luthe DS, Bridges SM & Burgess SC, 2006. AgBase: a functional genomics resource for agriculture. *BMC Genomics*, 7:229.
- McConville M & Ralton J, 1997. Developmentally regulated changes in the cell surface architecture of *Leishmania* parasites. *Behring Inst Mitt*, (99):34–43.
- McConville MJ, Saunders EC, Kloehn J & Dagley MJ, 2015. *Leishmania* carbon metabolism in the macrophage phagolysosome- feast or famine? *F1000Research*, 4(F1000 Faculty Rev):938.
- McMahon-Pratt D & Alexander J, 2004. Does the *Leishmania* major paradigm of pathogenesis and protection hold for New World cutaneous leishmaniasis or the visceral disease? *Immunol Rev*, 201:206–24.
- McStay GP, 2016. Complex formation and turnover of mitochondrial transporters and ion channels. *J Bioenerg Biomembr*:1–11.
- van Meel E & Klumperman J, 2008. Imaging and imagination: understanding the endo-lysosomal system. *Histochem Cell Biol*, 129(3):253–66.
- Megger DA, Pott LL, Ahrens M, Padden J, Bracht T, Kuhlmann K, Eisenacher M, Meyer HE & Sitek B, 2014. Comparison of label-free and label-based strategies for proteome analysis of hepatoma cell lines. *Biochim Biophys Acta*, 1844(5):967–76.
- Mellman I, 1996. Endocytosis and Molecular Sorting. *Annu Rev Cell Dev Biol*,

12(1):575–625.

- Menezes JPB, Almeida TF, Petersen ALOA, Guedes CES, Mota MS V, Lima JGB, Palma LC, Buck GA, Krieger MA, Probst CM & Veras PST, 2013. Proteomic analysis reveals differentially expressed proteins in macrophages infected with *Leishmania amazonensis* or *Leishmania major*. *Microbes Infect*, 15(8-9):579–91.
- Menezes-Souza D, Guerra-Sá R, Carneiro CM, Vitoriano-Souza J, Giunchetti RC, Teixeira-Carvalho A, Silveira-Lemos D, Oliveira GC, Corrêa-Oliveira R & Reis AB, 2012. Higher expression of CCL2, CCL4, CCL5, CCL21, and CXCL8 chemokines in the skin associated with parasite density in canine visceral leishmaniasis. *PLoS Negl Trop Dis*, 6(4).
- Meyer CW, Elvert R, Scherag A, Ehrhardt N, Gailus-Durner V, Fuchs H, Schäfer H, Hrabé De Angelis M, Heldmaier G & Klingenspor M, 2007. Power matters in closing the phenotyping gap. *Naturwissenschaften*, 94(5):401–6.
- Moore KJ & Matlashewski G, 1994. Intracellular infection by *Leishmania donovani* inhibits macrophage apoptosis. *J Immunol*, 152(6):2930–7.
- Moradin N & Descoteaux A, 2012. *Leishmania* promastigotes: building a safe niche within macrophages. *Front Cell Infect Microbiol*, 2:121.
- Moretti J, Chastagner P, Gastaldello S, Heuss SF, Dirac AM, Bernards R, Masucci MG, Israel A & Brou C, 2010. The translation initiation factor 3f (eIF3f) exhibits a deubiquitinase activity regulating notch activation. *PLoS Biol*, 8(11):e1000545.
- Morgan DJ, Davis BJ, Kearn CS, Marcus D, Cook AJ, Wager-miller J, Straiker A, Myoga MH, Karduck J, Leishman E, Sim-selley LJ, Czyzyk TA, Bradshaw HB, Selley DE & Mackie K, 2014. Mutation of putative GRK phosphorylation sites in the cannabinoid receptor 1 (CB1R) confers resistance to cannabinoid tolerance and hypersensitivity to cannabinoids in mice. *J Neurosci*, 34(15):5152–63.
- Mueller A, Mahmoud NG, Goedecke MC, Mckeating JA & Strange PG, 2002. Pharmacological characterization of the chemokine, CCR5. *Br J Pharmacol*, 135(4):1033–43.
- Mueller A & Strange PG, 2004. The chemokine receptor, CCR5. *Int J Biochem Cell Biol*, 36(1):35–8.
- Mulero V & Brock JH, 1999. Regulation of iron metabolism in murine J774 macrophages: role of nitric oxide-dependent and -independent pathways following activation with gamma interferon and lipopolysaccharide. *Blood*, 94(7):2383–9.
- Muñoz-Eliás EJ & McKinney JD, 2005. Mycobacterium tuberculosis isocitrate lyases 1 and 2 are jointly required for in vivo growth and virulence. *Nat Med*, 11(6):638–44.
- Murray H, Luster A, Zheng H & Ma X, 2017. Gamma interferon-regulated chemokines in *Leishmania donovani* infection in the liver. *Infect Immun*, 85(1):e00824–16.
- Murray HW, 2001. Tissue granuloma structure-function in experimental visceral leishmaniasis. *Int J Exp Pathol*, 82(5):249–67.
- Naderer T, Ellis M a, Sernee MF, De Souza DP, Curtis J, Handman E & McConville MJ, 2006. Virulence of *Leishmania major* in macrophages and mice requires the gluconeogenic enzyme fructose-1,6-bisphosphatase. *Proc Natl Acad Sci U S A*, 103(14):5502–7.
- Ndjamen B, Kang BH, Hatsuzawa K & Kima PE, 2010. *Leishmania* parasitophorous vacuoles interact continuously with the host cell's endoplasmic reticulum; parasitophorous vacuoles are hybrid compartments. *Cell Microbiol*, 12(10):1480–94.
- Neel NF, Schutyser E, Sai J, Fan GH & Richmond A, 2005. Chemokine receptor internalization and intracellular trafficking. *Cytokine Growth Factor Rev*, 16:637–58.

- Nogueira CV, Zhang X, Giovannone N, Sennott EL & Starnbach MN, 2015. Protective immunity against *Chlamydia trachomatis* can engage both CD4+ and CD8+ T cells and bridge the respiratory and genital mucosae. *J Immunol*, 194:2319–29.
- Nomiyama H, Osada N & Yoshie O, 2011. A family tree of vertebrate chemokine receptors for a unified nomenclature. *Dev Comp Immunol*, 35(7):705–15.
- Nylandsted J, Becker AC, Bunkenborg J, Andersen JS, Dengjel J & Jäättelä M, 2011. ErbB2-associated changes in the lysosomal proteome. *Proteomics*, 11(14):2830–8.
- Nylen S, Maasho K, Soderstrom K, Ilg T & Akuffo H, 2003. Live *Leishmania* promastigotes can directly activate primary human natural killer cells to produce interferon-gamma. *Clin Exp Immunol*, 131(3):457–67.
- Oghumu S, Lezama-Dávila CM, Isaac-Márquez AP & Satoskar AR, 2010. Role of chemokines in regulation of immunity against leishmaniasis. *Exp Parasitol*, 126(3):389–96.
- Ohya T, Miaczynska M, Coskun U, Lommer B, Runge A, Drechsel D, Kalaidzidis Y & Zerial M, 2009. Reconstitution of Rab- and SNARE-dependent membrane fusion by synthetic endosomes. *Nature*, 459(7250):1091–7.
- Olive AJ, Gondek DC & Starnbach MN, 2011. CXCR3 and CCR5 are both required for T cell-mediated protection against *C. trachomatis* infection in the murine genital mucosa. *Mucosal Immunol*, 4(2):208–16.
- de Oliveira C, Oda M, Losi Guembarovski R, de Oliveira K, Ariza C, Neto J, Banin Hirata B & Watanabe M, 2014. CC chemokine receptor 5: the interface of host immunity and cancer. *Dis Markers*, 2014:126954.
- Olivier M, Atayde VD, Isnard A, Hassani K & Shio MT, 2012. *Leishmania* virulence factors: Focus on the metalloprotease GP63. *Microbes Infect*, 14(15):1377–89.
- Oppermann M, Mack M, Proudfoot AEI & Olbrich H, 1999. Differential effects of CC chemokines on CC chemokine receptor 5 (CCR5) phosphorylation and identification of phosphorylation sites on the CCR5 carboxyl terminus. *J Biol Chem*, 274(13):8875–85.
- Owens BMJ, Beattie L, Moore JWJ, Brown N, Mann JL, Dalton JE, Maroof A & Kaye PM, 2012. IL-10-producing Th1 cells and disease progression are regulated by distinct CD11c+ cell populations during visceral leishmaniasis. *PLoS Pathog*, 8(7):e1002827.
- De Pablos L, Ferreira T & Walrad P, 2016. Developmental differentiation in *Leishmania* lifecycle progression: post-transcriptional control conducts the orchestra. *Curr Opin Microbiol*, 34:82–9.
- Pace D, 2014. Leishmaniasis. *J Infect*, 69(S1):S10–S18.
- Panaro M, Spinelli R, Lisi S, Sisto M, Acquafredda A, Fumarola L, Mitolo V & Brandonisio O, 2004. Reduced expression of the chemokine receptor CCR1 in human macrophages and U-937 cells in vitro infected with *Leishmania infantum*. *Clin Exp Med*, 3(4):225–30.
- Perrella Balestieri FM, Pires Queiroz AR, Scavone C, Assis Costa VM, Barral-Netto M & Abrahamsohn Ide A, 2002. *Leishmania* (*L.*) *amazonensis*-induced inhibition of nitric oxide synthesis in host macrophages. *Microbes Infect*, 4(1):23–29.
- Perrone Bezerra de Menezes J, Koushik A, Das S, Guven C, Siegel A, Laranjeira-Silva M, Losert W & Andrews N, 2016. *Leishmania* infection inhibits macrophage motility by altering F-actin dynamics and the expression of adhesion complex proteins. *Cell Microbiol*, doi: 10.1111/cmi.12668.
- Pethe K, Swenson DL, Alonso S, Anderson J, Wang C & Russell DG, 2004. Isolation of *Mycobacterium tuberculosis* mutants defective in the arrest of phagosome maturation. *Proc Natl Acad Sci U S A*, 101(37):13642–7.
- Pichler P, Köcher T, Holzmann J, Mazanek M, Taus T, Ammerer G & Mechtler K, 2010. Peptide labeling with isobaric tags yields higher identification rates using

- iTRAQ 4-plex compared to TMT 6-plex and iTRAQ 8-plex on LTQ orbitrap. *Anal Chem*, 82(15):6549–58.
- Pinheiro NF, Hermida MDR, Macedo MP, Mengel J, Bafica A & dos-Santos WLC, 2006. Leishmania infection impairs beta 1-integrin function and chemokine receptor expression in mononuclear phagocytes. *Infect Immun*, 74(7):3912–21.
- Podinovskaia M & Descoteaux A, 2015. Leishmania and the macrophage: a multifaceted interaction. *Future Microbiol*, 10(1):111–29.
- Proudfoot L, Nikolaev A V, Feng GJ, Wei WQ, Ferguson MA, Brimacombe JS & Liew FY, 1996. Regulation of the expression of nitric oxide synthase and leishmanicidal activity by glycoconjugates of Leishmania lipophosphoglycan in murine macrophages. *Proc Natl Acad Sci U S A*, 93(20):10984–9.
- Pryor P & Rofe A, 2015. Isolating phagosomes from tissue culture cells. In *Subcellular Fractionation: A Laboratory Manual*. 55–8.
- Rabinowitz S, Horstmann H, Gordon S & Griffiths G, 1992. Immunocytochemical Characterization of the Endocytic and Phagolysosomal Compartments in Peritoneal Macrophages. *J Cell Biol*, 116(1):95-112.
- Ralph P, Prichard J & Cohn M, 1975. Reticulum cell sarcoma: an effector cell in antibody-dependent cell-mediated immunity. *J Immunol*, 114(2):898–905.
- Real F, Florentino PTV, Reis LC, Ramos-Sanchez EM, Veras PS, Goto H & Mortara RA, 2014. Cell-to-cell transfer of Leishmania amazonensis amastigotes is mediated by immunomodulatory LAMP-rich parasitophorous extrusions. *Cell Microbiol*, 16(10):1549-64.
- Ribas AD, Ribas RC, Da Silva WV, Aristides SMA, Lonardoni MVC, Watanabe MAE, Borelli SD & Silveira TGV, 2013. Effect of the chemokine receptor CCR5 in the development of American cutaneous leishmaniasis in a Southern Brazilian population. *Mol Med Rep*, 8(1):189–94.
- Rintala-Dempsey AC, Santamaria-Kisiel L, Liao Y, Lajoie G & Shaw GS, 2006. Insights into S100 target specificity examined by a new interaction between S100A11 and annexin A2. *Biochemistry*, 45(49):14695–705.
- Rodriguez-Paris JM, Nolte K V & Steck TL, 1993. Characterization of lysosomes isolated from Dictyostelium discoideum by magnetic fractionation. *J Biol Chem*, 268(12):9110–6.
- Rodriguez-Sosa M, Rosas LE, Terrazas LI, Lu B, Gerard C & Satoskar AR, 2003. CC chemokine receptor 1 enhances susceptibility to Leishmania major during early phase of infection. *Immunol Cell Biol*, 81(2):114–20.
- Rofe A & Pryor P, 2015. Purification of lysosomes using supraparamagnetic iron oxide nanoparticles (SPIONs). In *Subcellular Fractionation: A Laboratory Manual*. 72–6.
- Ross P, Huang Y, Marchese J, Williamson B, Parker K, Hattan S, Khainovski N, Pillai S, Dey S, Daniels S, Purkayastha S, Juhasz P, Martin S, Bartlet-Jones M, He F, Jacobson A & Pappin D, 2004. Multiplexed protein quantitation in Saccharomyces cerevisiae using amine-reactive isobaric tagging reagents. *Mol Cell Proteomics*, 3(12):1154–69.
- Rotty JD, Wu C & Bear JE, 2013. New insights into the regulation and cellular functions of the ARP2/3 complex. *Nat Rev Mol Cell Biol*, 14(1):7–12.
- Rougerie P, Miskolci V & Cox D, 2013. Generation of membrane structures during phagocytosis and chemotaxis of macrophages: Role and regulation of the actin cytoskeleton. *Immunol Rev*, 256(1):222–39.
- Roy S, Kumar GA, Jafurulla M, Mandal C & Chattopadhyay A, 2014. Integrity of the actin cytoskeleton of host macrophages is essential for Leishmania donovani infection. *Biochim Biophys Acta*, 1838(8):2011–8.
- Roychoudhury K, Dasgupta B, Sen P, Laskay T, Solbach W, De T & Roy S, 2006. Evidence of direct interactions between the CC-chemokines CCL3, CCL4 and CCL5 and Leishmania promastigotes. *Mol Biochem Parasitol*, 150(2):374–7.
- Rubin-Bejerano I, Fraser I, Grisafi P & Fink GR, 2003. Phagocytosis by neutrophils

- induces an amino acid deprivation response in *Saccharomyces cerevisiae* and *Candida albicans*. *Proc Natl Acad Sci U S A*, 100(19):11007–12.
- Russell DG, Xu S & Chakraborty P, 1992. Intracellular trafficking and the parasitophorous vacuole of *Leishmania mexicana*-infected macrophages. *J Cell Sci*, 103:1193–210.
- Sacks D & Noben-Trauth N, 2002. The immunology of susceptibility and resistance to *Leishmania major* in mice. *Nat Rev Immunol*, 2:845–858.
- Saftig P & Klumperman J, 2009. Lysosome biogenesis and lysosomal membrane proteins: trafficking meets function. *Nat Rev Mol Cell Biol*, 10(9):623–35.
- Samson M, Larosa G, Libert F, Paindavoine P, Detheux M, Vassart G & Parmentier M, 1997. The second extracellular loop of CCR5 is the major determinant of ligand specificity the second extracellular loop of CCR5 is the major determinant of ligand specificity. *J Biol Chem*, 272(40):24934–41.
- Samson M, Libert F, Doranz B, Rucker J, Liesnard C, et al., 1996. Resistance to HIV-1 infection in caucasian individuals bearing mutant alleles of the CCR-5 chemokine receptor gene. *Nature*, 382:722.
- Sapir Y, Vitenshtein A, Barsheshet Y, Zohar Y, Wildbaum G & Karin N, 2010. A fusion protein encoding the second extracellular domain of CCR5 arrests chemokine-induced cosignaling and effectively suppresses ongoing experimental autoimmune encephalomyelitis. *J Immunol*, 185(4):2589–99.
- Sato BN, Ahuja SK, Quinones M, KostECKI V, Reddick RL, Melby PC, Kuziel WA & Ahuja SS, 2000. CC chemokine receptor (CCR) 2 is required for Langerhans cell migration and localization of T helper cell type 1 (Th1)-inducing dendritic cells: absence of CCR2 shifts the *Leishmania major* – resistant phenotype to a susceptible state dominated by Th2 cytokines, B cell outgrowth, and sustained neutrophilic inflammation. *J Exp Med*, 192(2):205–18.
- Sato N, Kuziel WA, Melby PC, Reddick RL, KostECKI V, Zhao W, Maeda N, Ahuja SK & Ahuja SS, 1999. Defects in the generation of IFN- $\gamma$  are overcome to control infection with *Leishmania donovani* in CC chemokine receptor (CCR) 5-, macrophage inflammatory protein-1 $\alpha$ -, or CCR2-deficient Mice. *J Immunol*, 163(10):5519–25.
- Savoia D, 2015. Recent updates and perspectives on leishmaniasis. *J Infect Dev Ctries*, 9(6):588–96.
- Schaible UE, Schlesinger PH, Steinberg TH, Mangel WF, Kobayashi T & Russell DG, 1999. Parasitophorous vacuoles of *Leishmania mexicana* acquire macromolecules from the host cell cytosol via two independent routes. *J Cell Sci*, 112(5):681–93.
- Schechter a D, Calderon TM, Berman a B, McManus CM, Fallon JT, Rossikhina M, Zhao W, Christ G, Berman JW & Taubman MB, 2000. Human vascular smooth muscle cells possess functional CCR5. *J Biol Chem*, 275(8):5466–71.
- Schmidt C, Grønberg M, Deckert J, Bessonov S, Conrad T, Luhrmann R, Urlaub H, 2014. Mass spectrometry-based relative quantification of proteins in precatalytic and catalytically active spliceosomes by metabolic labeling (SILAC), chemical labeling (iTRAQ), and label-free spectral count. *RNA*, 20(6):406–20.
- Schröder BA, Wrocklage C, Hasilik A & Saftig P, 2010. The proteome of lysosomes. *Proteomics*, 10(22):4053–76.
- Schröder B, Wrocklage C, Pan C, Jäger R, Kosters B, Schäfer H, Elsasser HP, Mann M & Hasilik A, 2007. Integral and associated lysosomal membrane proteins. *Traffic*, 8(12):1676–86.
- Scianimanico S, Desrosiers M, Dermine JF, Méresse S, Descoteaux a & Desjardins M, 1999. Impaired recruitment of the small GTPase rab7 correlates with the inhibition of phagosome maturation by *Leishmania donovani* promastigotes. *Cell Microbiol*, 1(1):19–32.
- Shrestha N, Bahnan W, Wiley DJ, Barber G, Fields KA & Schesser K, 2012.

- Eukaryotic Initiation Factor 2 (eIF2) signaling regulates proinflammatory cytokine expression and bacterial invasion. *J Biol Chem*, 287(34):28738–44.
- Signoret N, Christophe T, Oppermann M & Marsh M, 2004. pH-independent endocytic cycling of the chemokine receptor CCR5. *Traffic*, 5(7):529–43.
- Signoret N, Hewlett L, Wavre S, Pelchen-Matthews A, Oppermann M & Marsh M, 2005. Agonist-induced endocytosis of CC chemokine receptor 5 is clathrin dependent. *Mol Biol Cell*, 16(2):902–17.
- Signoret N, Pelchen-Matthews A, Mack M, Proudfoot AE & Marsh M, 2000. Endocytosis and recycling of the HIV coreceptor CCR5. *J Cell Biol*, 151(6):1281–94.
- Simpson J, Newcombe J, Cuzner M & Woodroffe M, 1998. Expression of monocyte chemoattractant protein-1 and other  $\beta$ -chemokines by resident glia and inflammatory cells in multiple sclerosis lesions. *J Neuroimmunol*, 84(2):238–49.
- Singh N, Jenkins GJ, Asadi R & Doak SH, 2010. Potential toxicity of superparamagnetic iron oxide nanoparticles (SPION). *Nano Rev*, 1:1–15.
- Smelt SC, Engwerda CR, Mccrossen M & Kaye PM, 1997. Destruction of follicular dendritic cells during chronic visceral leishmaniasis'. *J Immunol*, 158(8):3813–21.
- Somanna A, Mundodi V & Gedamu L, 2002. Functional analysis of cathepsin B-like cysteine proteases from *Leishmania donovani* complex: Evidence for the activation of latent transforming growth factor ? *J Biol Chem*, 277(28):25305–12.
- Sophie M, Hameed A, Muneer A, Samdani AJ, Saleem S & Azhar A, 2016. CC chemokine receptor 5 (CCR5) 32 polymorphism: association analysis and allele distribution among cutaneous leishmaniasis patients from Pakistan. *J Cutan Pathol*, 43:564–570.
- Stauber L, 1955. Leishmaniasis in the hamster. In W. Cole, ed. *Some Physiological Aspects and Consequences of Parasitism*. New Brunswick, New Jersey: Rutgers University Press, 76–90.
- Steigerwald M & Moll H, 2005. *Leishmania major* modulates chemokine and chemokine receptor expression by dendritic cells and affects their migratory capacity. *Infect Immun*, 73(4):2564–7.
- Storrie B & Desjardins M, 1996. The biogenesis of lysosomes: is it a kiss and run, continuous fusion and fission process? *Bioessays*, 18(11):895–903.
- Suffia IJ, Reckling SK, Piccirillo CA, Goldszmid RS & Belkaid Y, 2006. Infected site-restricted Foxp3<sup>+</sup> natural regulatory T cells are specific for microbial antigens. *J Exp Med*, 203(3):777–88.
- El Tai NO, El Fari M, Mauricio I, Miles M a, Oskam L, El Safi SH, Presber WH & Schönian G, 2001. *Leishmania donovani*: intraspecific polymorphisms of Sudanese isolates revealed by PCR-based analyses and DNA sequencing. *Exp Parasitol*, 97(1):35–44.
- Takayama T, Morelli AE, Onai N, Hirao M, Matsushima K, Tahara H & Thomson AW, 2001. Mammalian and viral IL-10 enhance C-C chemokine receptor 5 but down-regulate C-C chemokine receptor 7 expression by myeloid dendritic cells: impact on chemotactic responses and in vivo homing ability. *J Immunol*, 166(12):7136–43.
- Teixeira MJ, Fernandes JD, Teixeira CR, Andrade BB, Pompeu ML, Barral-netto M & Barral A, 2005. Distinct *Leishmania braziliensis* isolates induce different paces of chemokine expression patterns. *Infect Immun*, 73(2):1191–5.
- Temm-Grove CJ, Jockusch BM, Rohde M, Niebuhr K, Chakraborty T & Wehland J, 1994. Exploitation of microfilament proteins by *Listeria monocytogenes*: microvillus-like composition of the comet tails and vectorial spreading in polarized epithelial sheets. *J Cell Sci*, 107(1):2951–60.
- Thapa M, Kuziel W a & Carr DJJ, 2007. Susceptibility of CCR5-deficient mice to genital herpes simplex virus type 2 is linked to NK cell mobilization. *J Virol*,

81(8):3704–13.

- Tolson DL, Turco SJ & Pearson TW, 1990. Expression of a repeating phosphorylated disaccharide lipophosphoglycan epitope on the surface of macrophages infected with *Leishmania donovani*. *Infect Immun*, 58(11):3500–7.
- Touret N, Paroutis P & Grinstein S, 2005. The nature of the phagosomal membrane: endoplasmic reticulum versus plasmalemma. *J Leukoc Biol*, 77(6):878–85.
- Tripathi P, Singh V & Naik S, 2007. Immune response to leishmania: Paradox rather than paradigm. *FEMS Immunol Med Microbiol*, 51(2):229–42.
- Trost M, English L, Lemieux S, Courcelles M, Desjardins M & Thibault P, 2009. The phagosomal proteome in interferon- $\gamma$ -activated macrophages. *Immunity*, 30(1):143–54.
- Tuon FF, Amato VS, Bacha H a, Almusawi T, Duarte MI & Amato Neto V, 2008. Toll-like receptors and leishmaniasis. *Infect immun*, 76(3):866–72.
- Turco SJ & Sacks DL, 1991. Expression of a stage-specific lipophosphoglycan in *Leishmania major* amastigotes. *Mol Biochem Parasitol*, 45(1):91–9.
- Ueno N & Wilson ME, 2012. Receptor-mediated phagocytosis of *Leishmania*: Implications for intracellular survival. *Trends Parasitol*, 28(8):335–44.
- Vallejo A, Abad-Fernandez M, Moreno S, Moreno A, Perez-Elias MJ, Drona F & Casado JL, 2014. High levels of CD4+ CTLA-4+ Treg cells and CCR5 density in HIV-1-infected patients with visceral leishmaniasis. *Eur J Clin Microbiol Infect Dis*, 34(2):267–75.
- Venkatesan S, Rose JJ, Lodge R, Murphy PM & Foley JF, 2003. Distinct mechanisms of agonist-induced endocytosis for human chemokine receptors CCR5 and CXCR4. *Mol Biol Cell*, 14(8):3305–24.
- Veras BPST, De Chastellier C & Rabinovitch M, 1992. Transfer of zymosan (yeast cell walls) to the parasitophorous vacuoles of macrophages infected with *Leishmania amazonensis*. *J Exp Med*, 176:639–46.
- Walters SB, Kieckbusch J, Nagalingam G, Swain A, Latham SL, Grau GER, Britton WJ, Combes V & Saunders BM, 2013. Microparticles from mycobacteria-infected macrophages promote inflammation and cellular migration. *J Immunol*, 190:669–77.
- Walz D, Wu V, de Lamo R, Dene H & McCoy L, 1977. Primary structure of human platelet factor 4. *Thromb Res*, 11(6):893–8.
- Wanderley JLM, Moreira MEC, Benjamin A, Bonomo AC & Barcinski M a, 2006. Mimicry of apoptotic cells by exposing phosphatidylserine participates in the establishment of amastigotes of *Leishmania (L) amazonensis* in mammalian hosts. *J immunol*, 176(3):1834–9.
- Wang H, Alvarez S & Hicks LM, 2012. Comprehensive comparison of iTRAQ and label-free LC-based quantitative proteomics approaches using two *Chlamydomonas reinhardtii* strains of interest for biofuels engineering. *J Proteome Res*, 11(1):487–501.
- Wang K & Klionsky DJ, 2011. Mitochondria removal by autophagy. *Autophagy*, 7(3):297–300.
- Weber C, Weber KSC, Klier C, Gu S, Wank R, Horuk R & Nelson PJ, 2001. Specialized roles of the chemokine receptors CCR1 and CCR5 in the recruitment of monocytes and TH1-like/CD45RO+ T cells. *Blood*, 97(4):1144–46.
- Weber J, 2006. ATP synthase: subunit-subunit interactions in the stator stalk. *Biochim Biophys Acta*, 1757(9-10):1162–1170.
- Weiss L, Donkova-Petrini V, Caccavelli L & Levy Y, 2004. Human immunodeficiency virus – driven expansion of CD4+ CD25+ regulatory T cells which suppress HIV-specific CD4 T-cell responses in HIV-infected patients. *Blood*, 104(10):3249–3256.
- Werner E, 2004. GTPases and reactive oxygen species: switches for killing and signaling. *J Cell Sci*, 117(2):143–53.

- Wheeler RJ, Gluenz E & Gull K, 2015. Basal body multipotency and axonemal remodelling are two pathways to a 9+0 flagellum. *Nat Commun*, 6:8964.
- Winberg ME, Holm A, Sarndahl E, Vinet AF, Descoteaux A, Magnusson KE, Rasmusson B & Lerm M, 2009. Leishmania donovani lipophosphoglycan inhibits phagosomal maturation via action on membrane rafts. *Microbes Infect*, 11(2):215–22.
- Wolfer DP, Crusio WE & Lipp HP, 2002. Knockout mice: Simple solutions to the problems of genetic background and flanking genes. *Trends Neurosci*, 25(7):336–40.
- Wong D, Bach H, Sun J, Hmama Z & Av-Gay Y, 2011. Mycobacterium tuberculosis protein tyrosine phosphatase (PtpA) excludes host vacuolar-H<sup>+</sup>-ATPase to inhibit phagosome acidification. *Proc Natl Acad Sci U S A*, 108(48):19371–6.
- Wu Y, Li Y-Y, Matsushima K, Baba T & Mukaida N, 2008. CCL3-CCR5 axis regulates intratumoral accumulation of leukocytes and fibroblasts and promotes angiogenesis in murine lung metastasis process. *J Immunol*, 181(9):6384–93.
- Yan M, Collins R, Grinstein S & Trimble W, 2005. Coronin-1 function is required for phagosome formation. *Mol Biol Cell*, 16(8):3077–87.
- Yang W, Di Vizio D, Kirchner M, Steen H & Freeman M, 2010. Proteome scale characterization of human S-acylated proteins in lipid raft-enriched and non-raft membranes. *Mol Cell Proteomics*, 9(1):54–70.
- Yurchenko E, Tritt M, Hay V, Shevach EM, Belkaid Y & Piccirillo C a, 2006. CCR5-dependent homing of naturally occurring CD4<sup>+</sup> regulatory T cells to sites of Leishmania major infection favors pathogen persistence. *J Exp Med*, 203(11):2451–60.
- Zamilpa R, Kanakia R, Iv JC, Dai Q, Escobar GP, Martinez H, Jimenez F, Ahuja SS & Lindsey ML, 2011. CC chemokine receptor 5 deletion impairs macrophage activation and induces adverse remodeling following myocardial infarction. *Am J Physiol Heart Circ Physiol*, 300(4):1418–26.
- Zhang H, Fan X, Bagshaw RD, Zhang L, Mahuran DJ & Callahan JW, 2007. Lysosomal membranes from Beige mice contain higher than normal levels of endoplasmic reticulum proteins. *J Proteome Res*, 6(1):240–9.
- Zhou Y, Kurihara T, Ryseck RP, Yang Y, Ryan C, Loy J, Warr G & Bravo R, 1998. Impaired macrophage function and enhanced T cell-dependent immune response in mice lacking CCR5, the mouse homologue of the major HIV-1 coreceptor. *J Immunol*, 160(8):4018–25.
- Zhu W, Smith JW & Huang CM, 2010. Mass spectrometry-based label-free quantitative proteomics. *J Biomed Biotechnol*:840518.
- Zilberstein D & Shapira M, 1994. The role of pH and temperature in the development of Leishmania parasites. *Annu Rev Microbiol*, 48:449–70.
- Zlotnik A & Yoshie O, 2012. The chemokine superfamily revisited. *Immunity*, 36(5):705–12.
- Zoncu R, Bar-Peled L, Efeyan A, Wang S, Sancak Y & Sabatini D, 2011. mTORC1 senses lysosomal amino acids through an inside-out mechanism that requires the vacuolar H<sup>+</sup>-ATPase. *Science*, 344:678–83.
- Zurita E, Chagoyen M, Cantero M, Alonso R, González-Neira A, López-Jiménez A, López-Moreno JA, Landel CP, Benítez J, Pazos F & Montoliu L, 2011. Genetic polymorphisms among C57BL/6 mouse inbred strains. *Transgenic Res*, 20(3):481–9.
- Zwaal R & Schroit A, 1997. Pathophysiologic implications of membrane phospholipid asymmetry in blood cells. *Blood*, 89(4):1121–31.